NASA Contractor Report 4737

Cost Optimization Software for Transport Aircraft Design Evaluation (COSTADE)

Design Cost Methods

L. B. Ilcewicz, G. E. Mabson, S. L. Metschan, G. D. Swanson, M. R. Proctor, D. K. Tervo, H. G. Fredrikson, T. G. Gutowski, E. T. Neoh, and K. C. Polgar

Contracts NAS1-18889 and NAS1-20013
Prepared for Langley Research Center

August 1996

NASA Contractor Report 4737

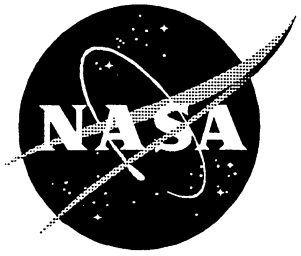

Cost Optimization Software for Transport Aircraft Design Evaluation (COSTADE)

Design Cost Methods

L. B. Ilcewicz, G. E. Mabson, S. L. Metschan, G. D. Swanson, M. R. Proctor, D. K. Tervo, and H. G. Fredrikson
The Boeing Company • Seattle, Washington

T. G. Gutowski, E. T. Neoh, and K. C. Polgar
Massachusetts Institute of Technology • Cambridge, Massachusetts

National Aeronautics and Space Administration
Langley Research Center • Hampton, Virginia 23681-0001

Prepared for Langley Research Center
under Contracts NAS1-18889 and NAS1-20013

August 1996

Printed copies available from the following:

NASA Center for AeroSpace Information
800 Elkridge Landing Road
Linthicum Heights, MD 21090-2934
(301) 621-0390

FOREWORD

This document is one of four complementary final technical reports on the development of a design cost model. The design cost model was part of a larger effort focused on composite technology development for transport fuselage structure. Therefore, most of the applications documented in this report relate to advanced composite designs and processes. The four reports comprising final documentation for the design cost model include:

Cost Optimization Software for Transport Aircraft Design Evaluation (COSTADE)

- **Overview** (CR 4736). *Synopsis of COSTADE initiative, including integration of cost, weight, manufacturing, design, structural analysis, load redistribution, optimization, and blending.*
- **Design Cost Methods** (CR 4737). *Components of cost analysis and their interactions. Theoretical framework for process-time prediction. Methods for developing and maintaining cost equations. Applications to ATCAS quadrant designs.*
- **User's Manual** (CR 4738). *COSTADE user instructions, including hardware requirements and installation procedures. Program structure, capabilities, and limitations. Basis of cost model and structural analysis routines. Example problems.*
- **Process Cost Analysis Database** (CR 4739). *Rationale for database framework. Database user's guide, including capabilities and limitations. ATCAS process step equations.*

Work described in these reports was sponsored by the National Aeronautics and Space Administration, Langley Research Center (NASA-LaRC) as a part of the contracts NAS1-18889 and NAS1-20013, Task 2. The Boeing Commercial Airplane Group, Seattle, Washington, was prime for these contracts, which were performed from May 1989 through December 1995. Both contracts were funded by the Advanced Composite Technology (ACT) program. Boeing's ACT program was called Advanced Technology Composite Aircraft Sructures (ATCAS). Direction from NASA-LaRC specific to ATCAS design cost model development was provided by J.G. Davis, and W.T. Freeman.

At completion of these contracts, Boeing program management included Bjorn Backman as Program Manager, Peter Smith as Technical Manager, and Larry Ilcewicz as Principal Investigator. Authors listed for this contractor report prepared portions of the document. The members (past and present) of the Boeing ACT contract team who contributed to the work described in this document include:

Program Management:
Phil Whalley
Ron Johnson
Ray Horton
Jordan Olson
Bjorn Backman

Technical Management:
Peter Smith

Principal Investigators:
Randy Coggeshall
Larry Ilcewicz

Structural Design:
George Truslove
Chris Hanson
Ken Griess
Mike Schram
Stephen Metschan
Mike Morris
Tuan Le

Computing Support:
Bob Lundquist
Bill Koch
Sterling Johnston

Structural Analysis:
Tom Walker
Ernie Dost
Gary Swanson
Blake Flynn
Gerald Mabson
David Carbery
Scott Finn
Dan Murphy
Bernhard Dopker
David Polland
William Avery
Jerry Bodine
Doug Graesser
Andre Williams
Mark Fedro
Peter Grant
Adam Sawicki
Pierre Minguet

Technical Aide:
Bill Waltari

Materials and Processes:
Dodd Grande
David Scholz
Karl Nelson
Tony Falcone
Brian Perkins

Manufacturing Technology:
Tom May
Kurtis Willden
Val Starkey
Tim Davies
Mark Gessel
Joe Hafenrichter
Bob Matetich
Ken Goodno
Dick Curran
Ken Dull
Rob Biornstad
Peter Lohr
Stan Stawski
Chris Harris
Greg Bell
Jan Koontz
Rob Synder
Tom Cundiff
Gary Moon

Cost Analysis:
Kent Venters
Will Gaylord
Cal Pfahl
David Tervo
Len Witonsky
Odo Bormke
Robert Humphrey
Michael Proctor
Hans Fredrikson
Dennis Stogin

Fire Worthiness:
Jim Peterson
Thomas Murray

Developmental Manufacturing:
Jose Valdez
Ponci Puzon
Bonnie Luck

Test Laboratories:
Ron Slaminko
John Schneider
Carl Preuss
Joan Dufresne
Tony Phillips
Dan Moreillon
Bill Hardrath

Business Management:
Jeff Heineman
Marge Apeles
Kira Goerlich

QC and NDE Development:
Ken Mackey
Brian Lempriere
Bill Fortig
John Linn

Weights:
Glenn Parkan

Repair Development:
Bert Bannink
Mike Evens
Sherry Marrese

Customer Support:
Dave Berg
Jeff Kollgaard

Materiel:
Maureen Hughes
Mark Jones
Steve Ruth
Doug Wood
Christal Tyson-Winston
Howard Lanie
Mark McConnell
Tom Hesketh

Industry And University Design-Build-Team Members

University of Washington:
Kuen Y. Lin
James Seferis
Zelda Zabinsky
Mark Tuttle

Stanford University:
Fu-Kuo Chang

Oregon State University:
Tim Kennedy

M.I.T:
Paul Lagace
Tim Gutowski
David Hoult
Greg Dillon
Hugh McManus

Drexel University:
Jonathan Awerbuch
Albert Wang
Alan Lau
Frank Ko

University of Iowa:
Roderic Lakes

University of Utah:
William Bascom
John Nairn

University of Wyoming:
Donald Adams
Rhonda Coguill
Scott Coguill

U. of Cal. Santa Barbara:
Keith Kedward

Univ. of British Columbia:
Anoush Poursartip

Brigham Young University:
Ken Chase

San Jose State University:
Robert Anderson

Dow-UT:
Rich Andelman
Douglas Hoon

Sikorsky Aircraft:
Christos Kassapoglou

Northrop/Grumman:
Ravi Deo
Steve Russell
Bob Ley
Ram Vastava
Ram Ramkumar

McDonnell Douglas:
Benson Black

Lockheed Aero. Systems:
Tony Jackson
Ron Barrie
Bob Chu
Dan Skolnik
Jay Shukla
Bharat Shah
Lowell Adams
Lisa Ott

Fiber Innovations:
Steve Goodwin
Garrett Sharpless

Hercules Materials Co.:
Doug Cairns
David Cohen
Roger Stirling
Lynn Muir
Will McCarvill
Yas Tokita

Alliant Techsystems:
Carroll Grant
George Walker
Tammy Harris
Todd Brown
Mark Wheeler
Jon Poesch
Vern Benson

American Airlines:
Jim Epperson
Marcus Peter

Northwest Airlines:
Jim Oberg
Erik Restad
Mark Wolf

United Airlines:
Bob Bernicchi
John Player

Cherry Textron:
Howard Gapp

Sunstrand:
Glen Smith
Hossein Saatchi
Bill Durako

ICI Fiberite:
Erinann Corrigan
Russ Holthe

G.M.I:
Roland Chemana

Intec:
Brian Coxon
Chris Eastland
Rod Wishart
Shreeram Raj
Don Stobbe

Zetec:
Chuck Fitch
Gregg Colvin

Draper Laboratory:
Ed Bernardon

Hexcel:
Stacy Biel
Julaine Nichols
Kevin Marshal

E. I. Du Pont De Nemours:
Jim Pratte
Hal Loken
Ginger Gupton

Materials Science Corp.:
Walt Rosen
Anthony Caiazzo

Structural Consultant:
John McCarty

EBCO Tooling:
Rich Roberts

TABLE OF CONTENTS

1.0 ABSTRACT

Multi-functional teams are vital to accurately predict the manufacturing time and associated costs to fabricate and assemble aircraft structure. The task becomes particularly manpower intensive when it involves an assessment of advanced technologies that have little or no production database. For example, the author list for this document represents a small fraction of the work force contributing to the developments described in this document.

A theoretical framework for design cost analyses and guidelines to support such team efforts have been developed in the Advanced Technology Composite Aircraft Structures (ATCAS) program. The recommended framework was applied and updated during the course of ATCAS as a major part of the program's design build team approach used to select and develop cost-effective concepts. These developments were also an integral part of the initiative to create Cost Optimization Software for Transport Aircraft Design Evaluation (COSTADE) discussed in ref. 1. The framework is linked to the contention that predictions of process times are not only essential to estimating the costs of labor, but also are crucial to assessing other cost centers (e.g., tooling and equipment quantities, and manufacturing facilities).

All facets of a theoretical framework developed in ATCAS to predict the costs of new or existing technologies are presented in this report. This includes an analytical basis for predicting process times and recommended steps and procedures for establishing credible cost predictions. To date, the primary application has been in guiding the development of composite designs and manufacturing processes for transport fuselage shell structure. Recommended procedures have been identified for extending the analysis to applications in new product and factory definition, and production design.

A number of theoretical equations were formulated with a physical basis in relating manufacturing process times to key design variables. Size scaling for extensive processes constitutes much of the theory that was developed and applied during ATCAS. The summation of equations for multiple process steps and a grouping of the terms involving common design variables helped to simplify some of the equations. Analytical formulations were also established for material handling tasks such as the transport and positioning of objects. Preliminary efforts with complexity scaling and other simplifying analyses were performed in hopes of minimizing the data requirements needed to characterize coefficients used in design cost analyses.

Results from analytical formulations compared favorably with traditional empirical methods used for design cost predictions in the industry. Evolving composite processes under development in the ATCAS program (e.g., automated fiber placement, preform braiding) were used to demonstrate the formulation and application of cost analyses. Steps to create and update cost equations as the manufacturing database expands for these processes are shown. Finally, the current status of cost equation developments for ATCAS applications to composite fuselage structure are presented and reviewed. This includes discussions of selected process steps and design variables critical to cost.

2.0 INTRODUCTION

Manufacturing companies can derive a competitive edge from design cost predictions. Different benefits are possible at each stage of development and production. Early predictions can help to focus research and development for new products on concepts having the greatest potential return on investment. The database collected during subsequent stages of development are likely to enhance an understanding of the cost relationships between maturing processes and details of the design. As a result, continuous cost assessments should improve in accuracy, helping to ensure that each subsequent phase of development funding is justified. In preparation for production, design cost analyses can support product development teams involved in design trades, make/buy decisions, and factory definition (e.g., facility floor space, equipment purchase, and resource allocation). Final product design definition can benefit from cost analyses that ensure structural details are compatable with selected manufacturing processes and the supporting database generated during development.

The accuracy of any detailed design cost analysis is dependent on a good understanding of the manufacturing process as applied to representative structural details. This physical insight can be used to define the critical design variables and their functional relationship to cost. It is important to realize that such insight is not easily derived because it requires data and knowledge from many different sources. This is particularly true for new technologies in which accurate cost analysis may take many years and significant resources to develop. Since the payoff of continuous cost assessments directly relate to a company's success, it should be an integral part of the approach used to advance technology from concept selection through production. The current work has emphasized design cost analyses that support the definition and production of transport aircraft structure, with additional focus on the development of concepts selected by ATCAS for a low-cost composite fuselage.

The cost of aircraft structure is roughly fifty percent of the total acquisition cost of an aircraft. The prediction of aircraft structural cost is extremely challenging due to design complexities, high part count, and numerous fabrication and assembly steps. Figure 1-1, which is intended for discussion purposes only, shows a top level view of typical aircraft structural cost components. Other aircraft costs such as systems, engines, interiors, and avionics also have similar components. Absolute differences between cost components will depend on product details, manufacturing processes, and a company's accounting structure. Only those portions of the cost which are shown as exploded segments of the pie chart in Figure 1-1 will be the subject of detailed discussions in this report.

The underlying thesis for the current work is that a theoretical design cost model must predict process times and the associated labor based on details of the structural concept and manufacturing plan. Although the labor represents only one portion of the costs shown in Figure 1-1, it has strong relationships with many of the others. The quantities of tooling and equipment, and facilities floor space needed to meet production rates depend on process times. Material scrap rates will also depend on the process efficiency,

including rework. In the reverse relationship, process times will depend on material characteristics, automation, tooling aids, and factory layout. The fundamental data needed to predict process times in design cost analyses also serve as a basis for establishing a complete manufacturing plan that is economically feasible.

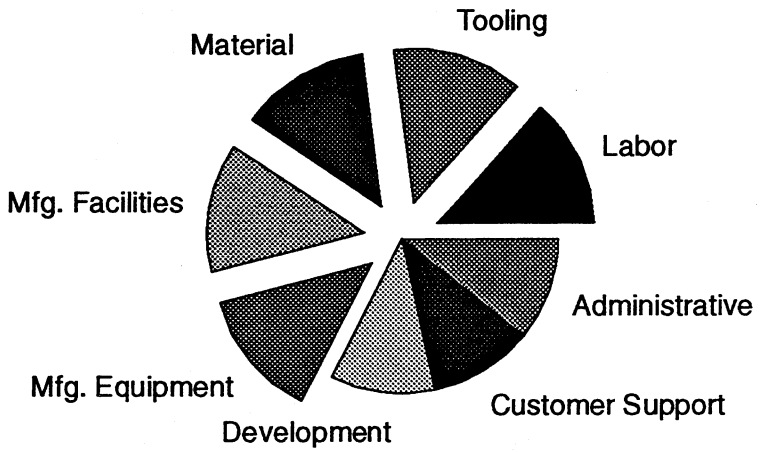

Figure 1-1. Schematic of aircraft structural cost components.

A production commitment to new technology, such as that studied in ATCAS, requires large non-recurring capital (facilities and equipment) and tooling investments. These costs are often justified based on analyses for a return on investment which assumes a market (i.e., total product quantities) and success in developing a design that can be manufactured efficiently with selected processes. Nonrecurring costs must be allocated early in a production program based on available data. As a result, a large fraction of the manufacturing cost for new products are fixed shortly after development, early in the final product definition stage. At this stage, the importance of accurate design cost analyses, as well as the enabling technologies to ensure rapid design cycle times, are paramount to successful product implementation.

As will become evident in the subsequent discussion, integrated product development involving iterative tasks performed by a design build team (DBT) are crucial to total cost analyses. Factory simulations of the manufacturing flow rates within and between each process center in a factory are needed to determine equipment and tooling quantities, and the required facilities floor space. These analyses require process times, crew size, and additional information (e.g., assumptions for learning curves, process improvements, machine performance, factory delay times, and statistical defect data). An iterative DBT process is essential when trading automation, involving high equipment costs, versus processes dominated by touch labor and a multitude of compromises. The cost of each component of tooling and equipment can be determined separately with the help of suppliers; but, an evaluation of the entire factory and business decisions (make versus buy) are needed to complete total cost analyses.

The problem of achieving an accurate cost prediction goes beyond the manipulation of theoretical equations to include a DBT's ability for synthesizing manufacturing and design data into physical relationships with cost. The errors or risks in analysis assuming product implementation are particularly difficult to quantify prior to the end of successful development. As a result, cost analyses for new technology should be continuously updated to represent the most accurate design and manufacturing information available to the DBT. Such efforts will reduce the error in cost analyses approaching major DBT milestones and, ultimately, support decisions for product implementation.

NASA Langley Research Center's initiated development of a "designers' unified cost model" in 1991 under the Advanced Composite Technology (ACT) program (ref. 2). The total effort for this initiative was called Cost Optimization Software for Transport Aircraft Design Evaluation (COSTADE). Primary goals for COSTADE development were to:

1) establish theoretical cost functions that relate geometric design features to summed material cost and labor content in terms of process mechanics and physics, and
2) combine deterministic cost methodology, designers' analytical tools, and supporting databases into software that allows one to trade and synthesize designs with both cost and weight as objective functions for optimization.

This report is focused on the first goal. The second goal was established realizing that the effective use of a design cost model should allow timely, quantitative trade-offs between structural performance and cost. The complete COSTADE development is covered in ref. 1.

Cost groundrules for Phases A and B of the ACT program were established in early cost workshops (ref. 3). A table describing these and other groundrules used in ATCAS design trade studies is included in ref. 5. In summary, the ACT groundrules allowed direct assessment of tooling, material, and labor costs. The assumed production run was 300 shipsets at a rate of five per month. Equipment and facilities costs were accounted for indirectly through ACT wrap (overhead) rates for recurring ($100/hr) and nonrecurring labor ($75/hr). These groundrules helped eliminate company proprietary costs from data shared between ACT Contractors.

The use of constant overhead labor rates for all process cells has several limitations to industry applications. Overhead labor rates are characteristic of production accounting practices in industry; however, some dependencies on the specific processes, facility, and equipment operator skill levels are likely. A more complete assessment of capital equipment and facility costs would also be required in many product implementation decisions. A change in the way in which the capital costs are addressed has been recommended for subsequent phases of the ACT program. Although many of the examples given in COSTADE documentation assume ACT labor rates, the theory and supporting software has been written assuming industry users would apply labor rates that depend on the process.

This document consists of three main sections. Section 3 provides extensive coverage of a theoretical framework for the design cost model, most of which was developed as part of a subcontract with Massachusetts Institute of Technology (MIT). Section 4 describes the recommended steps to follow in creating cost equations and updating them as an understanding of the process and design matures. Data requirements at each stage of development are also highlighted in the second section. Section 5 provides a status of ATCAS applications to composite fuselage structure. This includes a description of cost equations for processes in the ATCAS factory.

3.0 THEORETICAL BASIS FOR PROCESS TIME

Most of the basic theoretical developments established during the course of the ATCAS fuselage study apply to other aircraft structural design concepts and processes, as well as less complex product forms. However, specific equations, cost analyses, and data comparisons documented in this report are directly linked to details of the selected processes and designs. As such, they are examples and not intended to be used in predicting the cost of uniquely different designs, processes, and factories. A company-specific database is needed to formulate meaningful cost equations for parts or assemblies produced using existing process plans and factories.

For the derivation of equations needed to predict the design cost of new technologies, an integrated approach to product development is justified by its importance to both cost modeling and successful productization. A DBT approach similar to that used in ATCAS is recommended (refs. 4 and 5). The DBT members with varying specialties can help define initial cost relationships, coordinate development of the designs and processes, and gather the data needed to update the equations for more accurate analysis approaching new product implementation. New and evolving processes for advanced composite airplane structures require rigorous cost analysis to justify the increased funding needed to mature the technology to "production readiness" in each subsequent stage of development. Continuous cost assessments have been performed in ATCAS, which has pursued automated fiber placement (AFP), braiding, resin transfer molding (RTM), and large bonded panel fabrication (ref. 5).

Much of this section is based on an MIT Ph.D. dissertation by Ein-Teck Neoh (ref. 6). Other ATCAS developments that were added to the "theoretical framework" and some restructuring of the dissertation led to the following outline.

Rationale and requirements for a theoretical basis, including a synopsis of the work's contribution to design cost modeling, is covered in Section 3.1. Scaling equations that link part size to process times are discussed next in Section 3.2. This constitutes a major portion of the analysis which has been applied to date for specific processes and databases. The effect of assumptions for linearity and other equation simplifications (i.e., conversions of length to volume design variables) are discussed. Scaling equations for part complexity, which constitutes another scaling factor, are discussed in Section 3.3. Some examples combining size and complexity scaling are used to show the utility of the theory for common stiffening element geometry. A synopsis of theoretical considerations for material handling tasks, such as transport and positioning, is given in Section 3.4. Other procedures that simplify design cost analyses are discussed in Section 3.5. These include (a) scalar multipliers used to predict summed costs based on the costs of critical process steps and (b) limitations in traditional industrial approaches such as learning curve and power law scaling. Finally, a link between theoretical formulations and those available in COSTADE are summarized in Section 3.6.

3.1 Importance of Theoretical Basis

3.1.1 Overview of Time Estimating Methods

Estimating fabrication time and the associated cost is certainly not a new activity. It can be classified into three broad categories:

(1) predetermined motion time studies (PMTS),

(2) process models, and

(3) parametric models.

These categories are listed in an order that bounds the analysis and supporting database from PMTS dependent on low level detail to predictions based on high level parametrics.

As shown in Figure 3-1, PMTS models require two input sources: i) individual elemental motions to do a task and ii) design variables. The PMTS framework places very heavy emphasis on individual elemental motions and uses design variables as task variables. For example, in the task of picking up a pencil from the floor and putting it on a table, individual elemental motions might be: (a) stoop, (b) reach with right hand, (c) grasp pencil with fingers, (d) raise, (e) position pencil on table, and (f) release. Meanwhile, possible design variables relate to reaching distance, diameter of pencil, distance moved, and placement accuracy. One can easily imagine that the details of the PMTS models are simply overwhelming for the manufacture of aircraft, where the part count is in the order of millions. Examples of PMTS models are MTM, MTM2, MTM3 and work factors. Some useful references include Barnes, Currie, Karger & Bayha, Konz, Mundel, and Niebel (refs. 7-12).

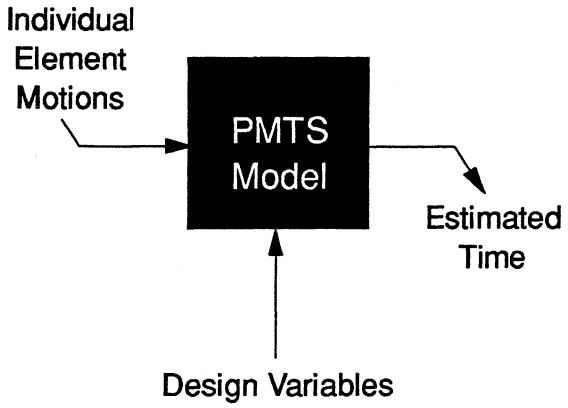

Figure 3-1. Models based on predetermined motion time studies (PMTS)

As illustrated in Figure 3-2, process models also require two input sources. In the case of process models, the manufacturing preplan or script for a specific design may serve as a starting point. For the given design-process pair, each process step is outlined in the manufacturing preplan. Every step will have its own process parameters. Examples of process steps for hand lay-up of prepregs (and the corresponding process parameters in parenthesis) are:

(1) clean lay-up tool surface (cleaning rate),

(2) apply release agent to surface (applying release agent rate),

(3) lay-up prepreg (lay-up rate), and

(4) apply bleeder plies (applying bleeder plies rate).

The design variable of interest in the above example is the lay-up area (i.e., tooled surface area of the part). However, the fourth step (apply bleeder plies) will also likely involve part thickness or the number of plies in the lay-up as an additional design variable. References for process models include: Advanced Composites Cost Estimating Manual (ACCEM) developed by Northrop for the US. Air Force (ref. 13), AM Cost Estimator for machining (ref. 14) and Product Design for Assembly (ref. 15).

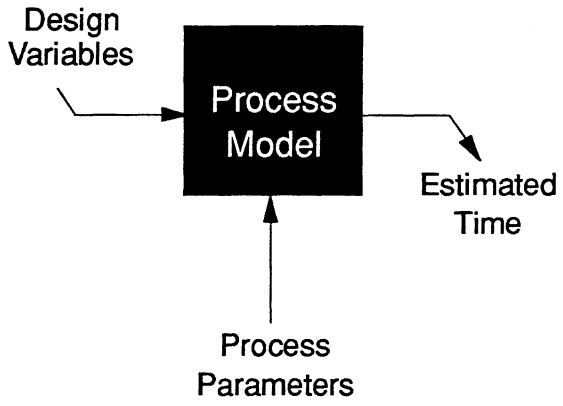

Figure 3-2. Process models.

At the highest level, the parametric models shown in Figure 3-3 require only design inputs, but provide relatively rough estimates. Parametric models often use weight as the generalized design variable in an empirical correlation with fabrication time derived from existing production experience. Thus, weight is used as the fundamental input variable for a model with correlation factors that have little or no physical relationship to the process. Group technology is often used to further refine these models. An example of this is described by Harmon & Arnold (ref. 16), where the first-unit-cost as a function of weight for composites airframe parts is further classified into: i) if the part is a primary or secondary structure, ii) if the part is a fuselage, wing or empennage component, iii) if the part is associated with military or commercial aircraft, and iv) if the part is manufactured by a particular aerospace company.

In industry, fabrication times have often been estimated with some form of detailed process models which estimate each sub process step and then sum them up to get an estimate for the part fabrication time. When sufficient data exists, the time for each of these steps is plotted versus some design parameter (such as length, area and weight) on log-log paper. This procedure has led to a power law relationship between the variables. Such models can be quite complicated, including various processing decisions. In fact, the model often reflects the complexity of the actual manufacturing process.

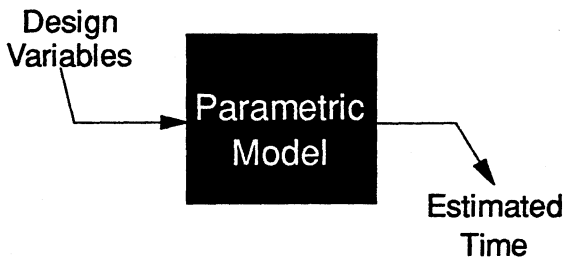

Figure 3-3. Parametric models.

One well known example of composite process models used in industry is ACCEM (ref. 13). The general approach used by ACCEM has been fairly well developed and successful for conventional processes such as machining, mechanical assembly, circuit board assembly and injection molding, where the manufacturing engineer and the cost estimator functions can be simulated by a mathematical algorithm (see Ostwald, Boothroyd & Dewhurst, and Busch, refs. 14, 15, 17, and 18). However, since this method requires empirical data, the accuracy of the estimate will depend heavily on the quality of the data. In addition, this data requirement presents a problem whenever the design space is outside that of the available database. It also makes such models cumbersome to change as processes evolve.

3.1.2 Motivations for Theoretical Model Development

Higher costs associated with past composite structures remain an economic barrier to increased applications. Therefore, further innovations and/or improvements in processing methods and technologies are needed to exploit the performance advantages offered by advanced composite materials. Subsequently, it is not surprising to find that most processes for the manufacture of composite parts are relatively new and constantly being changed and improved upon. Inputs from many different disciplines (e.g., design, manufacturing, industrial engineering, materials & processes, structures, quality control, tooling, facilities, purchases, and finance) are needed to establish credible cost analyses for advanced technologies.

A theoretical framework can be useful in helping to evolve cost analyses from the "order-of-magnitude" projections made for initial concepts into those that accurately predict the cost of designs built in a new or improved manufacturing facility. Such an alternative to the traditional, empirically-based, detailed models would be desirable during early phases of development, when advanced composite process knowledge is vague and absolute accuracy in cost estimates is poor.

A theoretical framework should be rigorously based on physical principles that aid communication between the different disciplines involved in concept development and implementation. The physical principles should provide insights into measurements that

can be made to quantify constants in the theory. Depending on the "production-readiness" of a given technology, such measurements may be extracted from databases for existing processes or derived from fabrication trials during development. In the later case, the cost relationships between emerging processes and representative design details will need to be refined by DBTs throughout development.

The theoretical framework should help provide educational benefits during product implementation as the cost analysis is applied to a constrained design and manufacturing space. Production designers need to know what specific structural details are compatible with efficient use of the selected factory. The producibility guidelines or software used to assess the costs should be simple to use for such designers, who are mostly engineers in the case of aircraft structures. The associated training should assume production designers were not involved in the development; but, seek the necessary physical insight to allow rapid design synthesis in a schedule-driven environment. A physically sound theory relating manufacturing costs to part descriptions and engineering definitions commonly used in industry should help educate designers and other members of the DBT.

Scaling laws which are simple and offer physical interpretation for the effects of part size and complexity appear feasible as the theoretical cost framework for both new and accepted manufacturing technologies. For new technologies, this generalized approach would start by estimating cost relationships based on key design variables and the most costly process steps. Constants in the scaling equations could be initially determined from the best available data. Although having limited accuracy, initial predictions would allow a rank ordering of part costs. Since things are changing rapidly as new processes develop, this scheme would provide a relatively flexible and systematic way to accommodate changes that continuously improve time estimates, including detail (e.g., addition of other process steps) to achieve greater accuracy. In the case of mature processes, databases may be large enough to allow either detailed (e.g., process step) or more general (e.g., process cell) equation formulation using the same theoretical framework. Mature processes can also use parametric models effectively.

3.1.3 Contributions to the Framework

The work at MIT was focused on development of theoretical equations that provided a basis for education in design cost analysis and was general enough to predict the process times for aircraft structural designs, with emphasis on composite manufacturing processes. For reasons discussed in Section 3.1.2, the equations were required to have a strong physical basis, as opposed to purely empirical relationships with data from existing factories. The physical basis for design cost theory should be derived from process modeling and industrial engineering principles. Although useful, an empirical approach would not meet the requirements for a general model that can be used for emerging technologies or provide the same educational benefits. Since the primary focus of the ACT program is composite primary structures for transport aircraft, reliable data for an empirical approach is also not likely to be available for several years.

Theories developed at MIT can be classified as a modified version of the process model discussed in Section 3.1.1. A synopsis of the contribution of research at MIT was in the development of an engineering approach and fundamental equations which not only estimate fabrication time, but also have the following characteristics:

- provides guidance for estimating the cost of new processes
- provide designers with guidelines and insights between design and cost
- capture effects of part size and complexity
- has physical interpretations
- simple and user friendly to facilitate rapid estimation
- easy to modify/update to reflect process changes
- establish cost analysis procedures such that the supporting database, development steps, and assumptions are uniform and clear.

The theoretical framework proposed by ATCAS for estimating fabrication time is shown schematically in Figure 3-4. This framework, which is discussed in Section 4.0, is consistent with the analytical basis developed by MIT for predicting process time. The flow diagram shown in Figure 3-4 illustrates that the theoretical framework includes initial predictions that improve with cycles that account for subsequent data collection and process updates. This differs from most previous process models, which have been empirical, by defining a physical basis that supports manufacturing cost data collection and helps to educate the work force.

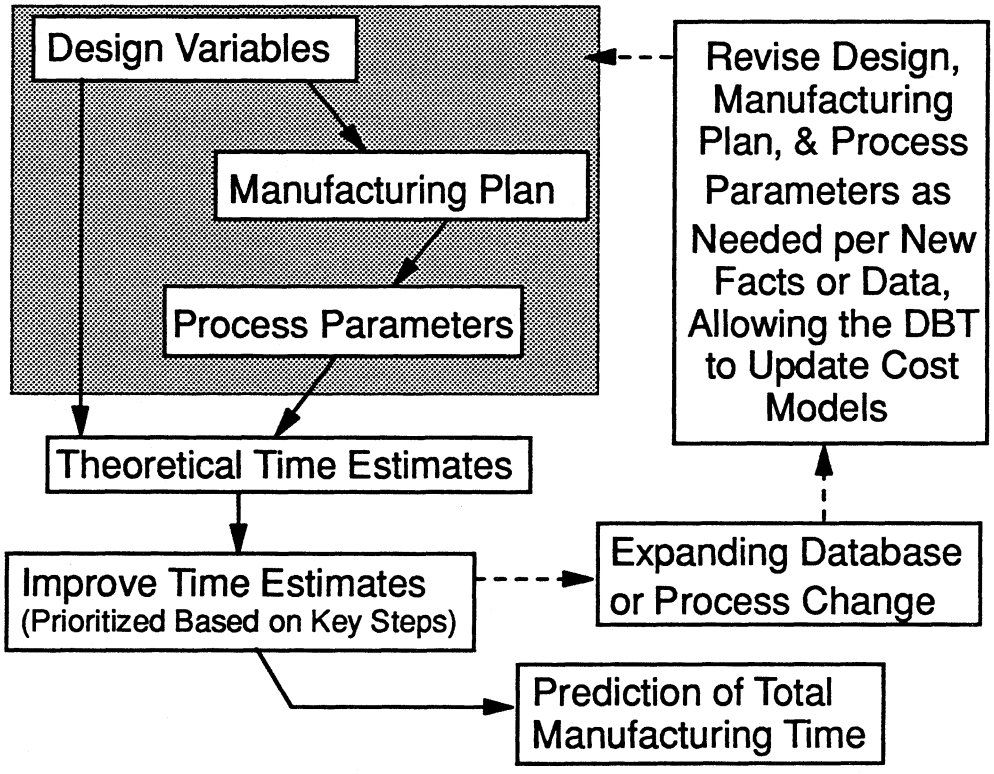

Figure 3-4. Schematic of a proposed theoretical framework.

3.2 Size Scaling

It is well known that large composite parts cost more than small parts. The main reasons for this are that large parts require more materials, larger machines and tools, and more labor. This section explores the scaling between part size and labor time, an issue which can be further subdivided into the major categories:

1) number, and
2) size.

The first category applies to discrete elements in the design which imply discrete operations. Examples are that thicker parts require a larger number of plies to be laid up, or in assembly, larger parts have more fasteners to be installed. Frequently, the corresponding number can be calculated by taking the ratio of some critical size dimension for the part over the size scaling for the basic building unit, e.g. distance along an edge divided by the distance between fasteners or distance between plies.

The second category, size effects, are related to continuous elements and events as opposed to discrete ones. In general, size related costs are due to the fact that manufacturing operations take longer to cover a larger region in space. This section specifically addresses the size scaling for those manufacturing processes that more or less operate continuously through some region in space. These types of operations could also be called "extensive" processes or operations.

3.2.1 Size Effects

The effects of size on fabrication time has typically been estimated based upon data. For automated processes, equipment specifications may also be used to make this time estimate. Extensive processes move over some region in space, and their time of operation will depend upon the extent of that motion. An important group of the extensive processes can be called "curvilinear" processes. These are processes which prescribe their action along a line (curved or straight) in space. There are many processes that have this characteristic. They include removal processes such as drilling, sawing, cutting, milling and turning, and additive processes such as the hand lay-up and automated placement of tapes or tows of fibers. In addition, many of the new "rapid prototyping" technologies such as stereo lithography and 3-D printing work in a similar fashion.

For curvilinear processes such as the ones mentioned above, a generalized relationship between the time required t_L and the length (or extent), L, of the action is

$$t_L = f(L). \tag{3.1}$$

The basic requirements for development of this relationship are, 1) accuracy, that is the estimate must agree reasonably well with the data; and 2) ease of interpretation and modification for new circumstances. A relationship which can provide the basis for a conceptual model for the process, would be highly desirable.

Furthermore, by summing all operations through the number of actions, N_L, for each of the lengths, L_i, one can get an estimate of the total time for this operation.

$$t_\Sigma = \sum_{i=1}^{N_L} f(L_i) \tag{3.2}$$

This sum usually corresponds to some region in space, frequently a perimeter, an area, or a volume. For composites lay-up the region is the part volume, V, and for machining the region is the volume removed V_R.

Since there is always a direct relationship between the length of this action and/or the region in space, and some dimension of the part; these relationships can provide the "extensive" mapping framework between design and fabrication time. Although there are several candidate forms for Equation 3.1, the following observations were made based upon reviewing many processes for both composites and metals. It appears that the function f(L) has the following common features;

1) the range of L is limited to $L_{min} \leq L \leq L_{max}$, where L_{min} is on the order of the process accuracy, and, in some cases, L_{max} is on the order of the machine size. Operations beyond this standard range must be considered a different process.
2) f(L) is monotonically increasing in L, $df(L)/dL > 0$
3) f(L) is convex, $d^2f(L)/dL^2 \leq 0$
4) for large L, $f(L) \sim L$, (a linear length dependence)
5) for small L, $f(L) > 0$, (a finite time is required to make even very small "actions").

One possible form of time estimating relationship which will satisfy the above criteria is

$$t_L = \text{delay} + \frac{L - L_{min}}{v_{avg}}; \quad L_{min} \leq L \leq L_{max}. \tag{3.3}$$

Here v_{avg} is the time average (not length average) velocity along the path (when $v > 0$),

$$v_{avg} = \frac{1}{t}\int_0^t v(t)\,dt. \tag{3.4}$$

Although L_{min} is small and can be ignored, it is shown explicitly here because the time required to get to L_{min} should be accounted for by a length independent time delay. In general, this delay accounts for occasions during processing when $v = 0$; such as initial set-up delay and delay for each "cut" or "course" which may involve positioning as well as other issues. The second term in Equation 3.3, is the "dynamic" contribution to the process time, $f_d(L)$. It involves motion over the length $L - L_{min} \cong L$, at the time average rate v_{avg}.

There are several different ways to approximate the dynamic function, $f_d(L)$. In principle, the relationship for $f_d(L)$ can be derived if the rate or velocity, $v(t)$, is known along the path. Some candidates for $t_d = f_d(L)$ will be discussed in the following sections.

3.2.2 Fundamental Extensive Equation Form

Dynamic Systems with First Order Velocity. Considerable data review at MIT for both composite fabrication and machining operations (e.g., refs. 13 and 14, and industry proprietary data) led to a simple relationship for v(*t*). It was observed that many manufacturing operations (humans and machines) can be represented as dynamic systems with first order velocity response to a step input. This behavior is amenable to physical models that take the recommended form,

$$v = v_o\,(1-e^{-t_d/\tau}), \tag{3.5}$$

which is plotted in Figure 3-5. This approach has the advantage of characterizing the process using the quantities for steady-state velocity, v_o, and the dynamic system time constant, τ. Both are dimensionally correct, and have meaningful physical interpretations. As will be shown in Section 3.2.6, similar equations can be derived using a first order displacement response to a ramp input.

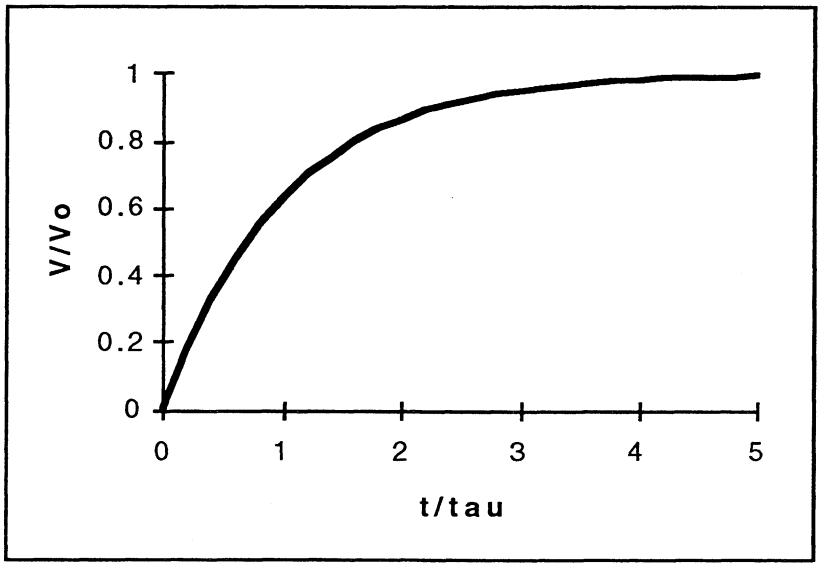

Figure 3-5. Dynamic systems with first order velocity response to a step input.

Integrating Equation 3.5 to get v_{avg} and rearranging the expression for $f_d(L)$ yields the relationship,

$$L = v_o\left[t_d - \tau\left(1-e^{\frac{-t_d}{\tau}}\right)\right], \tag{3.6}$$

which can not be inverted explicitly for time. Figure 3-6 shows a normalized plot of this relationship. Note that the critical length corresponding to $t_d = \tau$, is

$$L^* = \frac{\tau\, v_o}{e}, \tag{3.7}$$

where e is the base of the natural logarithm, i.e. $e \cong 2.72$.

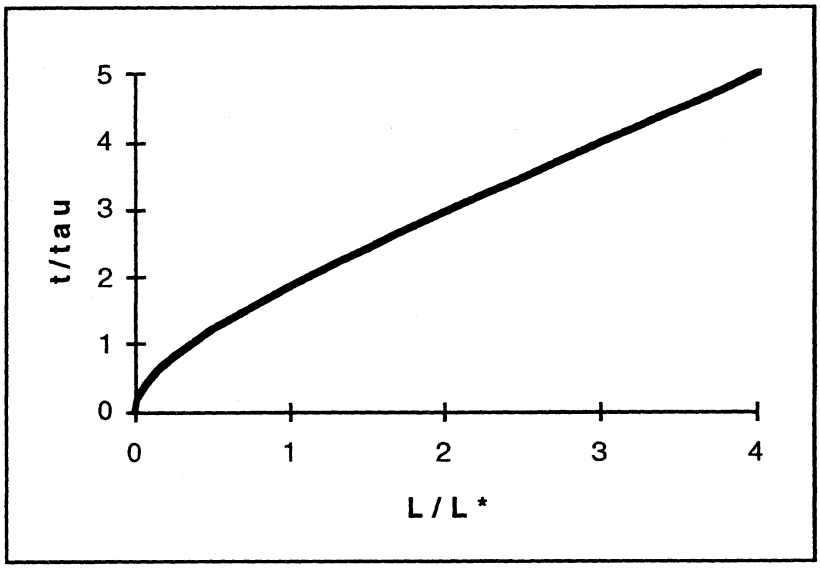

Figure 3-6. Position or distance moved for dynamic systems with first order velocity response to a step input.

The theoretical form given for the dynamic contribution of process time in Equation 3.6 is not unique to the physical basis and assumed first order velocity used in its derivation. The following developments for a control system and mass motion also arrive at the same basic equation form.

Control System. The most general first order linear control system (which is the same as a dynamic system with first order velocity) can be represented in block diagram form as:

$$R(s) \rightarrow \boxed{\frac{a}{bs+c}} \rightarrow C(s) \quad , \tag{3.8}$$

where $R(s)$ and $C(s)$ are Laplace transforms of the input and output respectively, and a, b and c are control system constants.

For the input taken as a unit ramp function and zero initial conditions the output as a function of time $\{C(t)\}$ after taking inverse Laplace transforms is:

$$C(t) = \frac{a}{c}t - \frac{ab}{c^2} + \frac{ab}{c^2}e^{\frac{-c}{b}t}, \quad \text{for } t \geq 0 \tag{3.9}$$

Note that for

$$v_o = \frac{a}{c} \text{ and } \tau = \frac{b}{c} \tag{3.10}$$

then,

$$C(t) = v_o\left[t - \tau\left(1 - e^{\frac{-t}{\tau}}\right)\right], \tag{3.11}$$

which is the same form as Equation 3.6.

Particle Motion with Viscous Drag. The equation of motion of a mass m, subject to force F, viscous damping c, and spring constant k is

$$m\ddot{x} + c\dot{x} + kx = F \ . \tag{3.12}$$

For most manufacturing processes, an argument can be made for setting k equal to zero,

$$m\ddot{x} + c\dot{x} = F \ . \tag{3.13}$$

When the initial displacement and velocity are also equal to zero and F is constant, then the solution to Equation 3.13 is

$$x = -\frac{mF}{c^2} + \frac{mF}{c^2} e^{\frac{-ct}{m}} + \frac{F}{c} t \ , \tag{3.14}$$

or

$$x = \frac{F}{c}\left[t - \frac{m}{c}\left(1 - e^{\frac{-ct}{m}} \right) \right] . \tag{3.15}$$

Note that for

$$v_o = \frac{F}{c}, \text{ and } \tau = \frac{m}{c} \ , \tag{3.16}$$

then,

$$x = v_o \left[t - \tau \left(1 - e^{\frac{-t}{\tau}} \right) \right] . \tag{3.17}$$

Note that Equation 3.17 also has a form and constants dimensionally equivalent to Equations 3.6 and 3.11. Therefore, one equation form can be used for process steps that can be modeled as having any of the two physical bases covered in this section.

3.2.3 Approximations of the Fundamental Extensive Equation Form

For practical use, it is desirable to solve for the time parameter in Equations 3.6, 3.11, or 3.17. However since t cannot be isolated, various approximations can be used. The following details several of these approximations using the mass motion notation from Equation 3.17.

The hyperbolic approximation can be used to obtain

$$t \approx \sqrt{\left(\frac{x}{v_o} \right)^2 + \left(\frac{2\tau}{v_o} \right) x} \ , \tag{3.18}$$

which provides reasonable predictions over the entire domain. This form smoothly transitions from

$$t \propto x^{0.5} \quad \text{for small x to}$$
$$t \propto x \quad \text{for large x.} \tag{3.19}$$

The exponents in the above equations (*0.5* and *1*) bound those normally used when fitting data to power law type forms historically used in cost estimating (see discussion in Section 3.2.5).

The following equation forms can also be used as square root and linear approximations for the time domains indicated,

$$t \approx \sqrt{\frac{2\tau}{v_o} x} \quad , \quad \text{for } t << \tau \quad , \tag{3.20}$$

$$t \approx \tau + \frac{x}{v_o} \quad , \quad \text{for } t >> \tau \quad . \tag{3.21}$$

Figure 3-7 presents a normalized comparison of the approximate and exact equation forms.

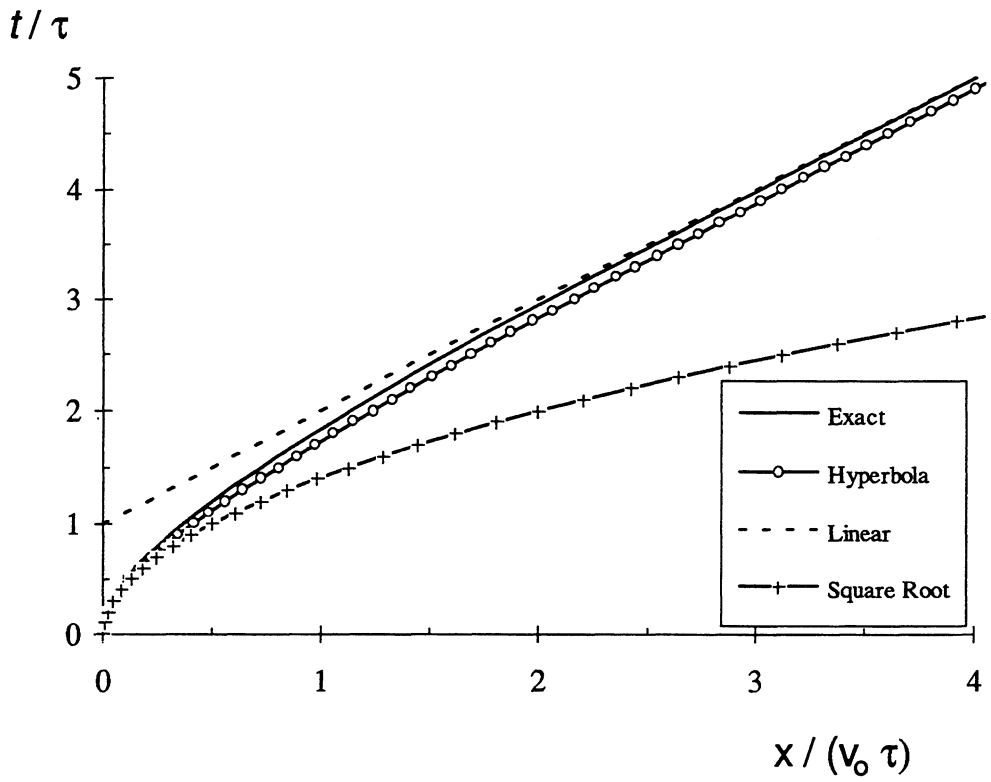

Figure 3-7. Normalized comparison of equation forms for extensive processes.

As shown in Figure 3-7, the hyperbolic approximation in Equation 3.18 is close to the exact equation over the entire range. It also reduces to the other two approximations, Equations 3.20 and 3.21, in the appropriate regimes.

Figure 3.8 shows comparisons of the three approximations (Equations. 3.18, 3.20, and 3.21) to the exact equation (Equation 3.6) for hand lay-up of 12 inch wide prepreg tape plies. This graph also illustrates that the square root approximation is good for short lengths, while the linear approximation is good for long lengths. On the other hand, the hyperbolic approximation is valid for the entire range.

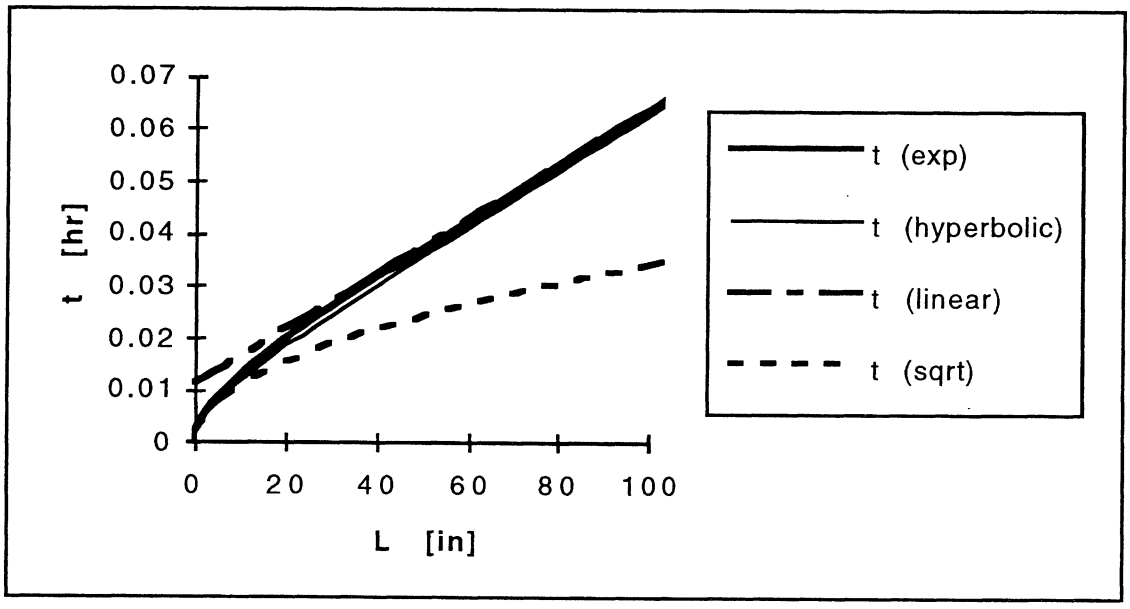

Figure 3-8. Comparison of approximations to the exponential first order equation for hand lay-up of 12 in. tape.

3.2.4 Summation of Size Effects

Algebraic manipulations of cost equations may be used to simplify analyses for a given process cell or group of process cells, resulting in a useful relationship with total costs. For example, equations summing the times for numerous process steps may have terms that collapse because of links to common design variables. Discussions in this section are limited to the summation of repetitive actions for a process whose time relates to a variable with length dimensions, allowing further size scaling to a variable having area or volume dimensions. The current discussion is further bounded by assuming common length variables for the repetitive action (e.g., strips of tape placed to create layers in a laminate) and the linearity of size scaling laws. More general examples of algebraic manipulations for the cost equations used for other processes will be discussed further in subsequent sections of this report.

Once the time estimating equation has a known relationship with length for the entire space of interest, a summation can be performed to get the total time for an operation. As indicated by Equation 3.2, individual times for the complete number of actions comprising a given operation are included in this sum. The corresponding length for each of these times helps define the space of interest. The operation indicated by Equation 3.2 is trivial when performed on a computer, but does not reveal a scaling size

effect other than the individual lengths used in each action. Assuming common linear relationships with length for each action, the resulting sum can be shown to yield a volume. In two special examples that apply this assumption, the summation yields a new critical variable corresponding to the volume of the part for composite lay-up, V_{LU}, and the volume to be removed for machining, V_R.

In order to demonstrate the conversion of a scaling variable having length dimensions to one having volume dimensions, the linear approximation given in Equation 3.21 is used to represent the first order model. As discussed earlier, this approximation is excellent for long times and makes conservative errors for short times. Note that the potential overestimate suggested by Equation 3.21 can be small for many manufacturing processes. Other time delays are added to get the total time as discussed in Section 3.2.1. The dynamic time constant is not physically the same as a delay for set-up. Nevertheless, Equation 3.21 may serve as a type of linearized constitutive equation which is analogous to Hooke's Law. From a mechanics perspective, such an approximation is reasonably correct for many important situations. More work is needed to justify the linear simplification for the manufacturing cost of specific process steps.

Using the approximation in Equation 3.21, individual actions can be summed for the various operations required to laminate a composite part. For example if n strips of width w are required to make a layer of area A then the linear sum in the plane gives:

$$\sum_{1}^{n} t = n\tau + \frac{A}{w\, v_o} \quad . \tag{3.22}$$

Now, summing for N individual layers of thickness h yields:

$$t_d = \sum_{1}^{N}\sum_{1}^{n} t = N_L\, \tau + \frac{V}{w\, h\, v_o} \quad , \tag{3.23}$$

where the total number of strips, N_L, is obtained by summing the number of strips in each layer, n_j, i.e.,

$$N_L = \sum_{j=1}^{N} n_j \tag{3.24}$$

Equation 3.23 can be expressed in the form of Equation 3.3, to include setups and delays,

$$t = \text{Setups} + N_L\,(\text{Delays} + \tau) + \frac{V}{w\, h\, v_o} \quad . \tag{3.25}$$

Note that in addition to the linear approximation for time, the constants (v_o & τ) are assumed to be independent of ply fiber orientation in Equations 3.22, 3.23, and 3.25. Examples can be given to show that this is not the case for some automated processes.

The main difficulty in obtaining a simple size scaling law based on part volume is the possibility of a nonlinear length dependence. However, note that the relative error due to linearization is on the order of:

$$\text{Relative Error} \sim \frac{N_L \tau}{\text{Setups} + N_L \text{ Delays}} . \tag{3.26}$$

If the time constant, τ, is small compared to setups and other delays, then the nonlinearity is not important. This is illustrated for hand lay-up in Section 3.3, where Equation 3.25 is scaled for part complexity and compared to the empirical power law equation found in ACCEM (ref. 13). Of course, it is hard to generalize for every possible situation. Therefore, until nonlinear effects are proven to be negligible for a given process, one might want to use Equation 3.18 instead of Equation 3.21 as the size scaling relationship. As mentioned earlier, such practices should have a minimal effect on the speed of calculations performed with a computer.

3.2.5 Generalized Formulation of Equations for Extensive Processes

The fundamental equation form discussed in Sections 3.2.2 and 3.2.3 represents the theoretical basis currently recommended for modeling the time of extensive processes. Section 3.2.6 provides a better physical interpretation for the machine characteristics of automated processes, resulting in the same basic equation. Section 4.2.3 expands on the machine physics using an example for AFP.

The recommended use of a limited number of equation forms for extensive processes is based on a need to validate the theoretical framework described in Figure 3-4 for a range of applications before expanding numerical degrees of freedom to predict higher order effects. For example, higher order effects may currently be within the errors of database collection. Nevertheless, for purposes of completeness, several other more general equation forms for extensive processes are identified in this section of the text. These forms may prove useful for future applications and, therefore, some provisions in the input options for COSTADE were established to allow their use.

Particle Motion With Aerodynamic Drag. In Section 3.2.2 it was shown that a model for particle motion with viscous drag yields the same fundamental extensive equation form as dynamic systems with first order velocity and a first order linear control system. For the case of particle motion with aerodynamic drag, the equation of motion of a mass m, subject to force F, aerodynamic damping c, and spring constant k can be written as:

$$m\ddot{x} + c\dot{x}^2 + kx = F \tag{3.27}$$

For most manufacturing processes, an argument can be made for setting k equal to zero,

$$m\ddot{x} + c\dot{x}^2 = F \tag{3.28}$$

When the initial displacement and velocity are also equal to zero and F is constant, the solution to Equation 3.28 is

$$\dot{x} = \frac{F\left(e^{\frac{2\sqrt{Fc}}{m}t} - 1\right)}{\sqrt{Fc}\left(1 + e^{\frac{2\sqrt{Fc}}{m}t}\right)} \tag{3.29}$$

or

$$t = \frac{m}{2\sqrt{Fc}} \ln\left(\frac{F + \sqrt{Fc}\,\dot{x}}{F - \sqrt{Fc}\,\dot{x}}\right) . \tag{3.30}$$

Solving for x,

$$x = \frac{m}{c} \ln(1 + e^{\frac{2\sqrt{Fc}}{m}t}) - \sqrt{\frac{F}{c}}\,t - \frac{m}{c} \ln 2 . \tag{3.31}$$

Note that t cannot be isolated in the above equation. The following approximations can be used for small and large t, respectively,

$$t << \frac{m}{2\sqrt{Fc}}, \; t \approx \sqrt{\frac{2mx}{F}} \tag{3.32}$$

$$t >> \frac{m}{2\sqrt{Fc}}, \; t \approx \sqrt{\frac{c}{F}}\,x + m\sqrt{\frac{c}{F}} \ln 2 \tag{3.33}$$

Alternatively, the following approximation may be useful throughout the x domain,

$$t \approx \sqrt{\frac{c}{F}x^2 + \frac{2m}{F}x} . \tag{3.34}$$

Constant Power Input (With Viscous Drag). Section 3.2.2 showed the result for particle motion with viscous drag and constant force. The equation of motion of a mass m, viscous damping c, and spring constant k is:

$$m\ddot{x} + c\dot{x} + kx = F \tag{3.35}$$

For constant power input P, the applied force F can be expressed as

$$F = \frac{P}{\dot{x}} . \tag{3.36}$$

Therefore, for spring constant $k = 0$,

$$m\ddot{x} + c\dot{x} = \frac{P}{\dot{x}} . \tag{3.37}$$

For initial displacement and velocity equal to zero then

$$\dot{x} = \sqrt{\frac{P - P e^{\frac{-2c}{m}t}}{c}} \tag{3.38}$$

or

$$t = \frac{m}{2c} \ln\left(\frac{P}{P - c\dot{x}^2}\right) . \tag{3.39}$$

Solving for x,

$$x = \frac{m\sqrt{Pc}}{c^2}\left[-\sqrt{1-e^{\frac{-2c}{m}t}} + \frac{1}{2}\ln\left(1+\sqrt{1-e^{\frac{-2c}{m}t}}\right) - \frac{1}{2}\ln\left(1-\sqrt{1-e^{\frac{-2c}{m}t}}\right)\right]. \tag{3.40}$$

There are difficulties isolating t in the above equation, however the velocity at large t monotonically approaches

$$\dot{x}\,|_{t\to\infty} = \sqrt{\frac{P}{c}} . \tag{3.41}$$

Constant Power Input (With Aerodynamic Drag). For the assumption of aerodynamic rather than viscous drag, the equation of motion of a mass m, aerodynamic damping c, and spring constant k is:

$$m\ddot{x} + c\dot{x}^2 + kx = F . \tag{3.42}$$

For constant power input P, the applied force F can be expressed as

$$F = \frac{P}{\dot{x}} . \tag{3.43}$$

Therefore, for spring constant $k = 0$,

$$m\ddot{x} + c\dot{x}^2 = \frac{P}{\dot{x}} \tag{3.44}$$

for initial displacement and velocity equal to zero then

$$t = m\left\{\frac{-1}{3cK'}\left[\frac{1}{2}\ln\left(\frac{P-c\dot{x}^3}{(K'+\dot{x})^3}\right)+\sqrt{3}\tan^{-1}\left(\frac{2\dot{x}-K'}{\sqrt{3}K'}\right)\right]\right\} - K'' \tag{3.45}$$

where

$$K' = \sqrt[3]{\frac{-P}{c}} \tag{3.46}$$

$$K'' = m\left\{\frac{-1}{3cK'}\left[\frac{1}{2}\ln\left(\frac{P}{K'^3}\right)+\sqrt{3}\tan^{-1}\left(\frac{-1}{\sqrt{3}}\right)\right]\right\} \tag{3.47}$$

Again, there are difficulties isolating t in the above equation, however the velocity at large t monotonically approaches

$$\dot{x}\,|_{t\to\infty} = \sqrt[3]{\frac{P}{c}} \quad . \tag{3.48}$$

Second Order Linear Control System. In Section 3.2.2, it was shown that a general first order linear control system is identical to dynamic systems with first order velocity and yield the same fundamental extensive equation form as a model for particle motion with viscous drag (and constant force). The general equation for a second order linear control system with unit ramp input is

$$a_3\ddot{x} + a_2\dot{x} + a_1 x = t \quad . \tag{3.49}$$

Solutions for zero initial conditions include i) an overdamped case, ii) critically damped case, and iii) an underdamped case.

For the overdamped case,

$$\left(a_2{}^2 - 4\,a_3\,a_1\right) > 0 \ , \tag{3.50}$$

the solution is

$$x = k_1\,e^{\lambda_1 t} + k_2\,e^{\lambda_2 t} + \frac{t}{a_1} - \frac{a_2}{a_1{}^2} \ , \tag{3.51}$$

where

$$\lambda_{1,2} = \frac{-a_2 \pm \sqrt{a_2{}^2 - 4\,a_3\,a_1}}{2\,a_3} \ , \tag{3.52}$$

and

$$k_1 = \frac{a_2\,\lambda_2 + a_1}{a_1{}^2\,(\lambda_2 - \lambda_1)} \ , \quad k_2 = \frac{a_2\,\lambda_1 + a_1}{a_1{}^2\,(\lambda_1 - \lambda_2)} \quad . \tag{3.53}$$

For the critically damped case,

$$\left(a_2{}^2 - 4\,a_3\,a_1\right) = 0 \ , \tag{3.54}$$

the solution is

$$x = \frac{2\sqrt{a_1\,a_3}}{a_1{}^2}\,e^{-\sqrt{\frac{a_1}{a_3}}\,t} + \frac{t}{a_1}\,e^{-\sqrt{\frac{a_1}{a_3}}\,t} + \frac{t}{a_1} - \frac{2\sqrt{a_1\,a_3}}{a_1{}^2} \quad . \tag{3.55}$$

Note that the underdamped case with

$$\left(a_2{}^2 - 4\,a_3\,a_1\right) < 0 \tag{3.56}$$

results in oscillatory output that is physically unacceptable for cost prediction.

There are difficulties isolating t in Equations 3.51 and 3.55, however the velocity at large t monotonically approach constants.

3.2.6 Approximations Relevant to Automated Processes

Other approximations for the dynamic function $f_d(L)$ can also be obtained for automated processes. Such approximations will likely depend on specific equipment characteristics. For example, machine speeds may ramp with a constant acceleration until a constant steady state velocity is achieved as shown in Figure 3-9. Alternatively, the acceleration rate may increase throughout the startup region.

Constant Acceleration. For the typical machine specification shown in Figure 3-9 (constant acceleration, a, up to the steady state velocity v_{ss}, and then constant deceleration,$-a$), the time to steady-state operation is

$$t_{ss} = \frac{v_{ss}}{a}, \tag{3.57}$$

and the distance to steady-state operation is

$$x_{ss} = \frac{1}{2} a t_{ss}^2 = \frac{v_{ss}^2}{2a}. \tag{3.58}$$

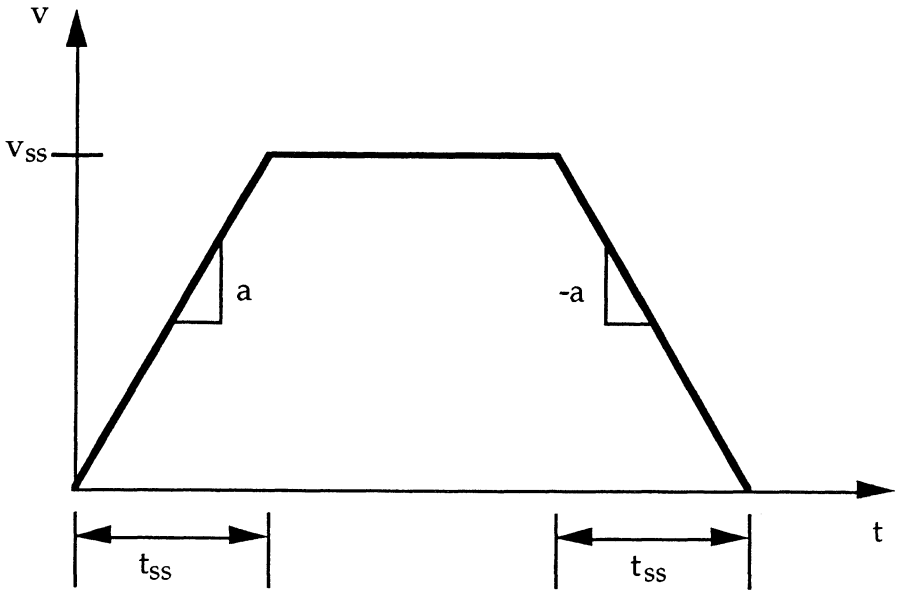

Figure 3-9. Velocity profile over time for machine with constant acceleration and deceleration.

Hence, for short lengths, where $L \leq 2x_{ss}$, the dynamic contribution to time is

$$t_d = f_d(L) = 2\left(\frac{L}{a}\right)^{1/2}, \tag{3.59}$$

and for long lengths, where $L \geq 2x_{ss}$

$$t_d = f_d(L) = \frac{v_{ss}}{a} + \frac{L}{v_{ss}}. \tag{3.60}$$

Length dependencies in Equations 3.59 and 3.60 are similar to approximations used for the first order model. Furthermore, they provide useful information to estimate physical parameters in the first order model. Equation 3.60 was used for AFP in Section 4.2.3.

Increasing Acceleration. Figure 3-9 showed the situation where start-up for the machine or the process is increasing in velocity at a constant acceleration, or

$$v \sim t. \tag{3.61}$$

An alternative assumption, could be that the velocity is proportional to length in the start-up region,

$$v \sim L. \tag{3.62}$$

Integrating yields

$$t = \frac{1}{c} \ln\left(L/L_{min}\right) , \tag{3.63}$$

where c is the constant of proportionality. This result is of interest because it has the same form as one would get from the information theoretic approach. For example, "Fitts Laws" for manual tapping (ref. 21, 22) gives

$$t = a + b \log_2\left(L/L_{min}\right) . \tag{3.64}$$

To date, this equation has not been used to estimate the processing time for composites manufacturing. Furthermore, it must be applied with caution since the denominator in these equations is on the order of the process accuracy and may be interpreted as suggesting the dependence of time on accuracy or tolerance. This worked for Fitts' manual tapping experiments (e.g., see refs. 22, 23). However, Chase and Greenwood (ref. 24) found evidence suggesting that the dependence of machining time on tolerance does not follow this type of law. Specifically, after evaluating different functional forms, they found that the relative machining cost scales linearly with the reciprocal of tolerance (instead of the logarithmic ratio of length and tolerance implied by Equation. 3.64).

3.2.7 Power Law Approximation

The power-law curve, which has been used widely in industry, is another way to approximate the dynamic function $f_d(L)$. This approximation can be obtained by curve fitting data with a linear line on log-log scales yielding

$$t_d = f_d(L) = A L^r . \tag{3.65}$$

Applying the conditions of monotonicity and convex shape gives

$$0 < r \leq 1 \tag{3.66}$$

and, of course, the constant $A > 0$. Typical values for A and r for automated and manual lay-up of composite laminates are given in the ACCEM cost model (ref. 13).

The Equation 3.20 approximation used for the fundamental extensive equation when t is small offers an explanation for the observation that the exponent r in Equation 3.65 is

frequently found to be about 0.50 [e.g., see ACCEM (ref. 13)]. In such cases, the constant A in Equation 3.65 can be related to the physical coefficients in Equation 3.20 as

$$A \approx \sqrt{\frac{2\tau}{v_o}} \quad . \tag{3.67}$$

In general, physical quantities τ and v_o are determined using methods outlined in Section 4. However, if there is a power law relationship for an existing process, the first order model can be fitted to it using the scheme presented in Appendix A. This illustrates the correlation between the first order model and the widely used power law model.

An approximate method to obtain τ and v_o can be based upon the characteristics of a first order system. As $L \rightarrow L_{max}$, $v \rightarrow v_o$, and

$$v = v_o \left(1-\frac{1}{e}\right) \approx 0.63\, v_o \quad \text{at } t = \tau_d \,, \tag{3.68}$$

giving

$$v_o \cong \frac{L_{max}^{1-r}}{rA} \quad \text{and} \tag{3.69}$$

$$\tau \cong (0.63)^{\frac{r}{1-r}} A\, L_{max}^{r} = (0.63)^{\frac{r}{1-r}} t_{max} \quad . \tag{3.70}$$

Hence the critical length,

$$L^* = \frac{\tau v_o}{e} = (0.63)^{\frac{r}{1-r}} \frac{L_{max}}{e\, r} \quad . \tag{3.71}$$

For example, using the method in Appendix A, the power law curve fits given in ACCEM (ref. 13) yielded the following physical constants for the operations listed in Table 3-1 and corresponding graphs in Figures 3-10, 3-11 and 3-12. Similarly, Figure 3-13 illustrates the agreement between the first order model and estimates from the power law model for abrading part surfaces. In general, the differences between the two models for databases used in these examples are too small to differentiate.

Process	τ	v_o	L^*
Hand lay-up 3" tape	0.0191 hrs	10,950 in/hr	76.9 in
Hand lay-up 12" tape	0.0111 hrs	1,896 in/hr	7.74 in
Hand lay-up woven tape	0.0856 hrs	57,500 in^2/hr	1,810 in^2
Disposable bagging	0.0331 hrs	5,137 in^2/hr	62.6 in^2
Reusable bagging	0.00919 hrs	6,219 in^2/hr	21.0 in^2

Table 3-1. Estimates of τ and v_o using the curve fitting approach outlined in Appendix A.

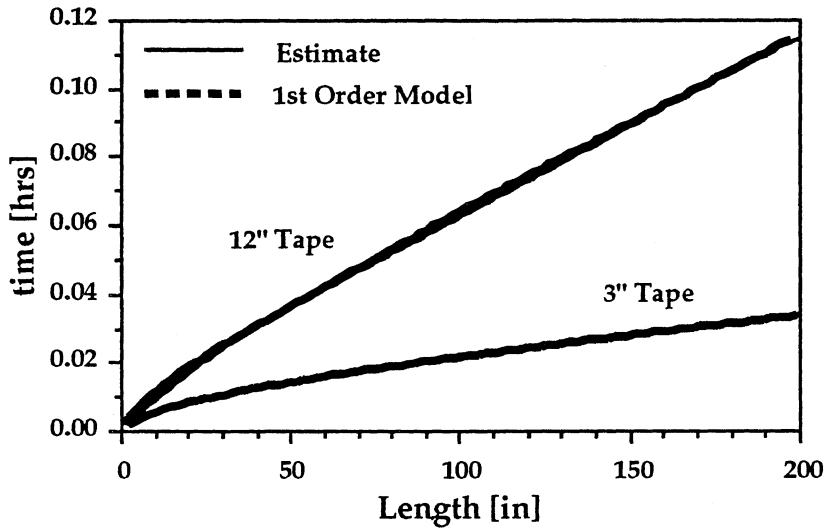

Figure 3-10. Comparison of first order and power law equation forms in fitting data trends for hand lay-up of unidirectional prepreg tape.

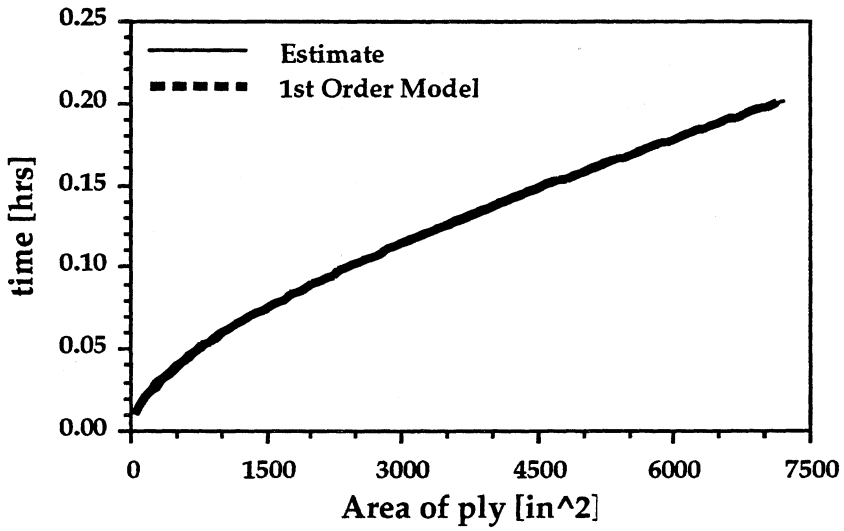

Figure 3-11. Comparison of first order and power law equations in fitting data trends for hand lay-up of woven prepreg tape.

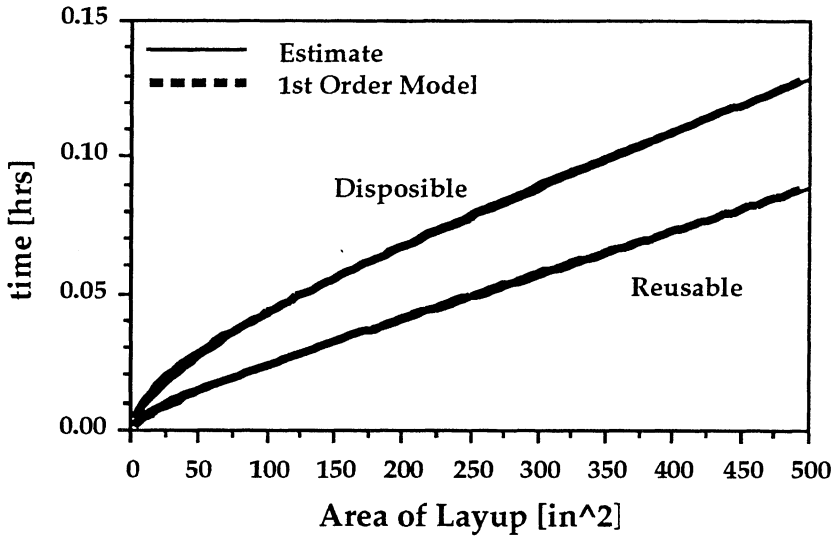

Figure 3-12. Comparison of first order and power law equation forms in fitting data trends for bagging operations.

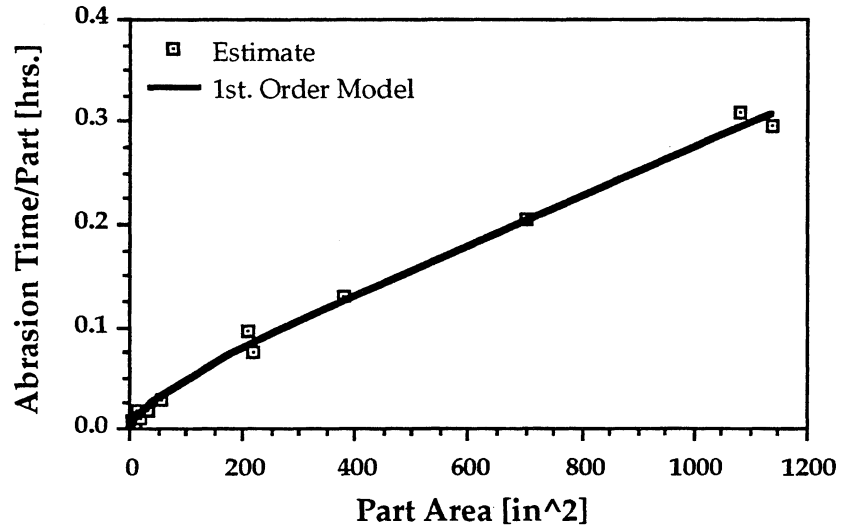

Figure 3-13. Comparison of first order and power law equation forms in fitting data trends for abrading part surfaces.

As will be discussed in Section 3.5, the power law scaling relationship in Equation 3.65 most likely has its early origin dating back to the works of Wright (refs. 19 and 20). Some pitfalls in using the power law approximation for size scaling, especially if there are implied changes in the process, are also discussed in Section 3.5. From a theoretical basis, Equation 3.65 would violate condition 4 for $f_d(L)$ from Section 3.2.1 unless process changes are implied by the power law relationship.

3.3 Scaling for Part Complexity

The previous section showed the importance of part size as a scaling factor for fabrication times. Since complex parts require more time to fabricate than simple parts, additional scaling variables must be considered. Within the concept of a theoretical framework, it is desirable to represent the details of shape variations in a universal and quantitative way which captures the implied complexity of the manufacturing operation. Starting with the extensive mapping framework developed thus far for curvilinear processes, equations can be developed to predict the fabrication times for a part requiring actions that transverse complex fiber paths. Referring to Equations 3.18, 3.20, and 3.21, more complex processing paths will have the effect of either increasing the dynamic time constant τ or decreasing the steady state velocity v_o or both.

This section presents the development of conceptual scaling laws for the effect of part complexity on fabrication time for advanced composite parts. This discussion is limited to three types of part complexities:

i) partial plies (ply drop-offs, build-ups, etc.),

ii) multiple ply orientations, and

iii) geometric part shape complexity, specifically curvatures (see Figure 3-14).

While the examples for partial plies and multiple ply orientations are relatively simple, the treatment for part shape complexity or curvature is not. Hence, the bulk of this section will be directed toward part shape and curvature complexity.

Part complexities generally increase manufacturing time for several reasons. Ply drop-offs, build-ups and multiple ply orientations require more cutting and more pieces per unit volume. Complex curvature parts are often more difficult because they usually imply a change in manufacturing procedures. For example, in the hand lay-up of complex parts (especially those with double or compound curvatures), manufacturing procedures will generally call for cutting darts (triangular pieces), shaping with the hands, and deforming the composite over the complex shape. For automated lay-up, doubly curved regions require complex tool paths and lower deposition rates.

Even relatively simple shapes such as a cone, which can be developed from simple curvature only; may pose difficulties that increase process time. For example, distinct ply orientations, each requiring different process steps, may be needed to fabricate the layers of a conical composite structure. Changes in process steps with both the part geometry and laminate ply orientations increase the challenge for developing universal scaling laws.

3.3.1 Linear Approximation for Laminate Layup Complexity

Since part complexity can be considered a relative measure, it is conceivable that it be accounted for by magnifying the scaling laws used for another appropriate variable (e.g., length or size dimensions). The linear size scaling law developed in Section 3.2.4, with additional assumptions implied through summation (see Equation 3.25), can be used to

demonstrate complexity scaling for a simple problem. In particular, the laws developed in this section will scale relative to the fabrication times for a flat, untapered laminate.

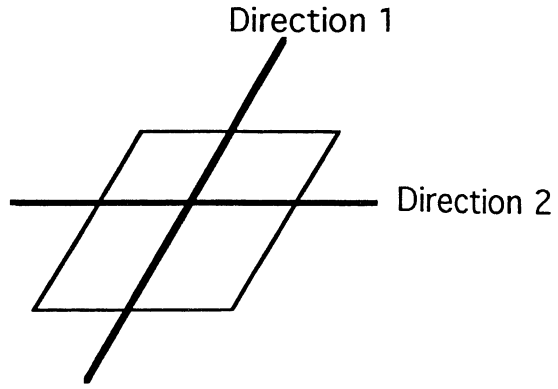

Flat laminate has no curvature.

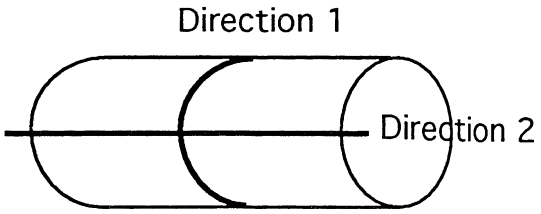

Cylinder has curvature in one direction only.

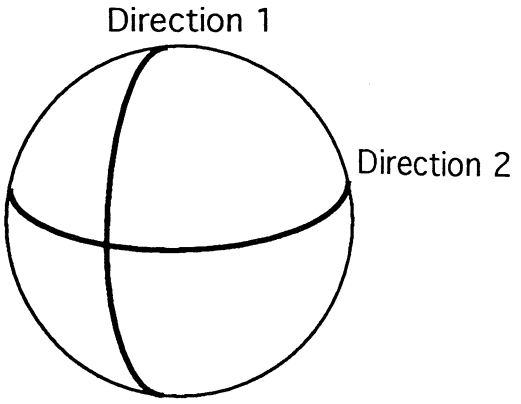

Sphere has curvature in two directions (double or compound curvatures).

Figure 3-14. Different types of part curvatures.

A mathematical approximation for the dynamic contribution to layup of a flat untapered composite laminate was derived in Section 3.2.4 (Equation 3.25). It is rewritten here for convenience as

$$t = N_L \text{ (Delays } + \tau) + \frac{V}{w\, h\, v_o}\,, \tag{3.72}$$

where V is the volume of the part, w is the width and h is the thickness of each of the N_L strips of composite tape. These "design variables" are all directly determined from details of the design. On the other hand, the dynamic system time constant, τ, and steady

state velocity, v_o, are "process parameters". The purpose of proposed complexity scaling laws is to relate the complexity of part geometry and associated manufacturing operations by scaling the process parameters, τ and v_o, with appropriate design detail.

Partial Plies. Ply drop-offs, build-ups, and, in general, making any part consisting of many small and different shaped plies increases the time of the fabrication operation. Assuming the linear approximation and that the task has been properly planned and laid out, these ply drop-offs primarily affect the dynamic process complexity in the number of pieces per volume N_L/V and their size distribution. Example calculations of N_L/V, including the effects of different ply orientations, are given in Appendix B. The results are summarized in Table 3-2.

Ply Orientation. Besides resulting in different ply length distributions, different ply orientations may also lead to different values of τ and v_o. For example, the effect of ply orientation on v_o is well known for automated fiber placement (AFP) machines which have different dynamics for different axes. This example will be covered in Section 4.

Parts	Lay-up	N_L/V
Rect. Beam	(0)	$\frac{1}{wh}\left(\frac{1}{L}\right)$
Rect. Beam	(90)	$\frac{1}{wh}\left(\frac{1}{W}\right)$
Rect. Beam	(±45)	$\frac{1}{wh}\left(\frac{0.707(L+W)}{WL}\right)$
Tapered Beam	(0)	$\frac{1}{wh}\left(\frac{2}{L}\right)$
Tapered Beam	(90)	$\frac{1}{wh}\left(\frac{1}{W}\right)$
Tapered Beam	(±45)	$\frac{1}{wh} \times \frac{1.414\left(\frac{L}{2}+W\right)}{WL}$
Cube	(0/90/±45)	$\frac{1}{wh}\left(\frac{1.207}{L}\right)$
Pyramid	(0/90/±45)	$\frac{1}{wh}\left(\frac{1.811}{L}\right)$

where

w = width of prepreg tape
h = thickness of one layer of prepreg
L = part length
W = part width

Table 3-2. Relative complexity of parts with different lay-up orientation and ply drop-off.

For the special case of quasi-isotropic laminates, assumed to consist of equal numbers and sizes of 0, 90, +45, and -45 plies, the v_o and τ dependence on orientation tends to approach average v_o and τ values for the laminate. Therefore, similar to the effects of partial plies, different ply orientations for this special case primarily affect the dynamic process complexity through N_L/V and the size distribution of layers. Example calculations of N_L/V for special geometry of quasi-isotropic laminates are also given in Appendix B and summarized in Table 3-2.

3.3.2 Geometric Features Affecting Part Complexity

This section discusses two different approaches to investigate the effects of part shape complexity on fabrication time. In both cases, the arguments lead to the conclusion that the appropriate complexity measure is an enclosed angle, θ. Furthermore, to a first approximation, time is assumed to be linearly dependent on this measure.

Part curvature can be subdivided into the categories i) simple and ii) complex. The first category includes all simple bends (single out-of-plane curvature), such as those required in straight untapered stringers. These bends are usually made at sharp discrete points, however, the current treatment will also include gradual bends. The second category is all other types of bends possible. Particularly, the focus is on bends that have double or compound curvatures, which means that the part bends in two different directions. A curved C-channel and a sphere both have double curvature as shown in Figure 3-15.

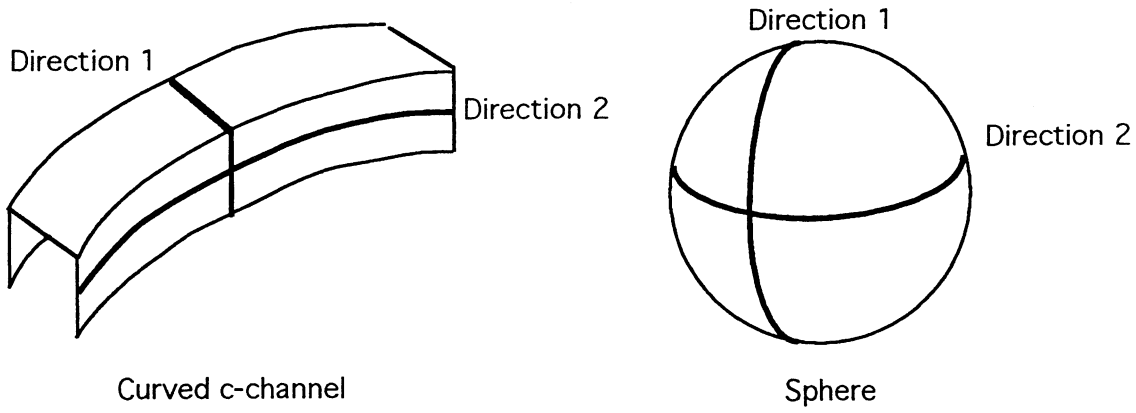

Figure 3-15. Example parts with double or compound curvatures.

Both simple and complex curvatures require that fibers traverse a curved path. The implication is that parts with curved fiber paths are more difficult to manufacture. Two methods were employed in measuring the aggregate curviness of fibers in a composite part: i) discretization of a plane-curved path, and ii) information theoretic model.

3.3.2.1 Discretization of a Plane-Curved Path

The fabrication of complex shaped parts requires that the lay-up step follow curved paths. One approach is to assume that the linearized first order model (Equation 3.21) can be applied to the curved path in a discretized manner. Referring to Figure 3-16, for a curved path of length s, constant radius of curvature ρ, and enclosed angle θ, the largest angular segment $\Delta\theta$ can be written as

$$\Delta\theta \cong \sqrt{\frac{8\varepsilon}{\rho}} \quad , \tag{3.73}$$

for the requirement that the discretization error does not exceed the deviation ε, as shown in Figure 3-17 (i.e., to minimize the error in estimating s). Equation 3.73 is derived using trigonometry and series expansion, and is valid for small $\Delta\theta$. Hence the number of discrete lengths to be laid up is n, where

$$n = \frac{\theta}{\Delta\theta} \quad . \tag{3.74}$$

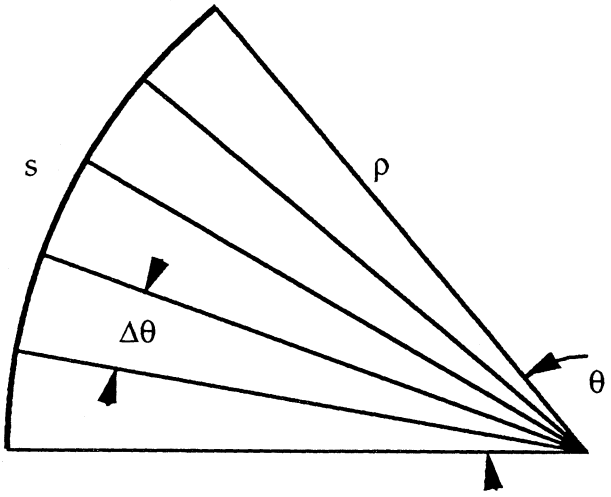

Figure 3-16. Discretizing a curved fiber.

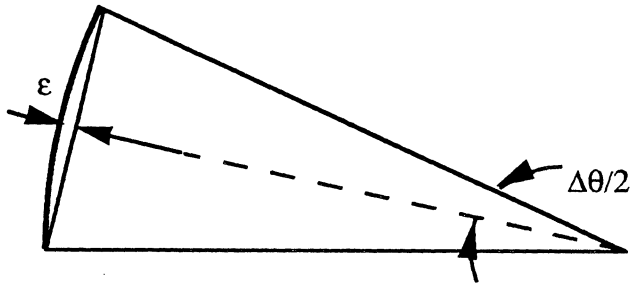

Figure 3-17. ε as the limit of discretizing error.

For lay-up a path of length L = s, and assuming that the lay-up of each small discrete segment is governed by Equation 3.21, then the lay-up time for a curved path can be written as

$$t_d = \tau + (n-1)\,\tau_e + \frac{L}{v_o}, \tag{3.75}$$

where τ is the initial dynamic delay and τ_e is the enclosed angle delay (or extra time required) at each discrete turn. For very large n, this leads to

$$t_d \cong \tau + \tau_e \frac{\theta}{\Delta\theta} + \frac{L}{v_o} \quad . \tag{3.76}$$

This illustrates the linear effect of the enclosed angle θ on the dynamic component of the fabrication time, t_d.

Alternatively, the effect of the enclosed angle θ on velocity can also be investigated by assuming that Equation 3.20 governs for small lengths. In this case, the time increment Δt to lay up the length increment ΔL, is

$$\Delta t_d = \sqrt{\frac{2\tau}{v_o}\Delta L}. \tag{3.77}$$

Summing over the entire length for the time to lay-up length L yields

$$t_d = \sqrt{\frac{2\tau}{v_o} L\,n} = \sqrt{2\,\tau L \frac{\theta}{v_o\,\Delta\theta}} \quad . \tag{3.78}$$

Equation 3.78 can be interpreted as illustrating an effect on the steady state velocity; where the velocity is reduced for laying up curved paths as

$$v_{o_{curved}} \rightarrow v_{o_{straight}} \frac{\Delta\theta}{\theta} \tag{3.79}$$

and

$$\frac{\theta}{\Delta\theta} \geq 1 \quad \text{always.} \tag{3.80}$$

These simple arguments illustrate how both the time constant and/or the steady state velocity might change due to a curved lay-up path with enclosed angle θ.

3.3.2.2 Information Theoretic Approach

An alternative and more abstract approach is to use "information theory" to develop a quantitative information measure that represents the complex features of a part; where the information content, I, is measured in bits. "Information theory" was originally developed in communications engineering, Shannon & Weaver (ref. 25), and recently applied to design, Suh (ref. 26). The hypothesis is that once the part complexity can be uniformly quantified using the information measure, the process parameters τ and v_o can then be correlated to this measure to reflect the effects of part complexities on process parameters. The idea is to represent a part with a fiber map, which essentially is a

collection of equally spaced parallel fibers. These parallel fibers in turn can be viewed as information storage media; in a sense the fibers store all the curvatures needed to replicate the part. Using purely kinematics analysis, Tam, Tam & Gutowski and Gonzalez-Zugasti (refs. 27, 28, and 29) illustrated that there is only one unique fiber map for any given geometry once the initial fiber is placed down. In other words, once the path of the very first fiber is defined, the paths of the rest of the fibers are determined (see Figure 3-18). Therefore, a theoretical calculation of the information encoded in the curved fibers could be used to represent the complexity of the part.

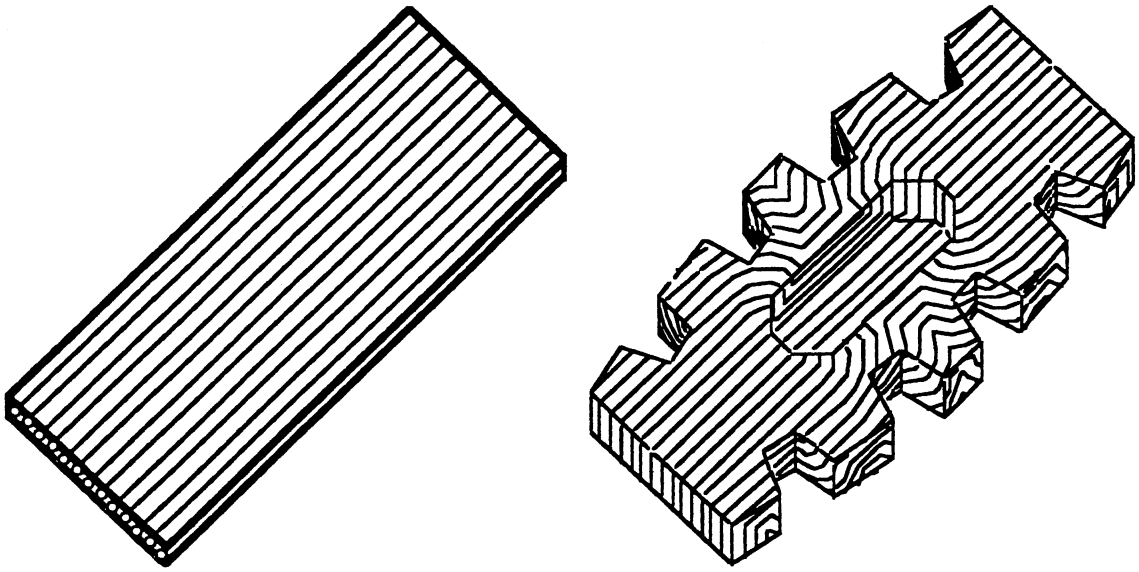

Figure 3-18. Fiber mappings for simple and complex composite parts.

The above idea is then developed by considering a simple plane curve as shown in Figure 3-19, where a detector traveling along the fiber could sense whether the fiber is curving to the right or to the left, as well as the magnitude of that deflection. Hence, the curvature information stored in the fiber can be quantified. For example, as the detector travels along the fiber a distance Δs, there is an angle change of $\Delta\theta$. If the detector has angle accuracy $\bullet\,\delta$, and if the fiber could bend an equal amount of $\Delta\theta$ in the other direction, then the total number of detectable positions in this increment would be $\Delta\theta/\delta$. Furthermore, if each one of these locations is equally likely then the probability, p, that the fiber would be in any one of these locations is

$$p = \frac{\delta}{\Delta\theta} \quad . \tag{3.81}$$

Now for m segments each of length Δs with included angle $\Delta\theta$, the total probability, p_T, that the fiber would be in any particular configuration is:

$$p_T = p^m = \left(\frac{\delta}{\Delta\theta}\right)^m \quad . \tag{3.82}$$

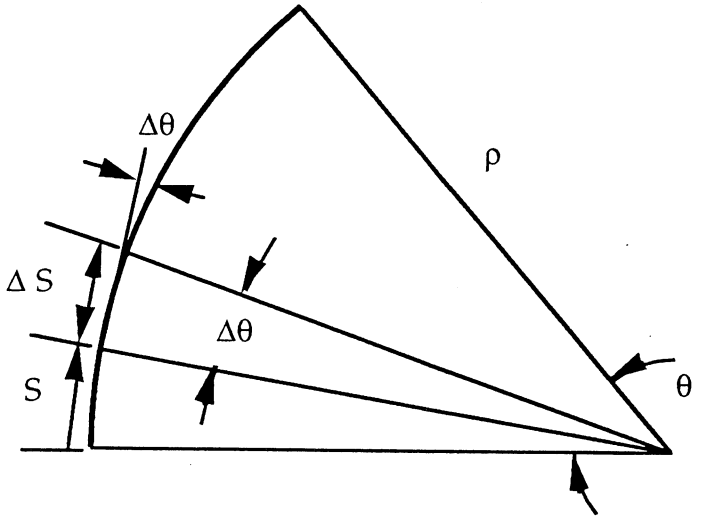

Figure 3-19. Discretizing a curved fiber as an information storage media.

Now since

$$m = \frac{\theta}{\Delta\theta} \tag{3.83}$$

the total probability can be rewritten as

$$p_T = \left(\frac{\delta}{\theta} m\right)^m . \tag{3.84}$$

Hence the probability that the fiber is in any particular state depends on the number of segments into which the fiber is subdivided m. This obtains a minimum value when

$$\frac{dp_T}{dm} = \left(\frac{\delta}{\theta} m\right)^m \left[1 + \ln\left(\frac{\delta}{\theta} m\right)\right] = 0 \tag{3.85}$$

which occurs at

$$m^* = \frac{1}{e}\left(\frac{\theta}{\delta}\right) \tag{3.86}$$

where "e" is the base to the natural logarithm. Hence the maximum information which can be stored in a curved fiber with enclosed angle θ is

$$I = \log_2\left(\frac{1}{p_T}\right) = -\frac{\theta}{\delta}\left[\frac{1}{e}\log_2\left(\frac{1}{e}\right)\right] \tag{3.87}$$

or to a reasonable approximation,

$$I \cong \frac{1}{2}\frac{\theta}{\delta} . \tag{3.88}$$

Hence, information stored in a curved fiber is linearly proportional to θ.

Incidentally, several other publications have illustrated the linear dependence between information content and processing time for information processing tasks (refs. 21, 22, 30, 31, and 32). This is also exactly what was suggested by the development in Section 3.3.2.1 (Equations 3.76 and 3.79); since the reciprocal of the lay-up rate is proportional to the enclosed angle, i.e. for a given large size part

$$t_d \sim \frac{1}{v} \sim \frac{\theta/\Delta\theta}{v_o} \quad . \tag{3.89}$$

To summarize, the appropriate scaling parameter for representing the complexity of a curved path through space is demonstrated to be the enclosed angle θ using two different approaches. Furthermore, in the context of the time estimate given by Equation 3.72, the process parameters τ and v_o should depend upon this enclosed angle as

$$\tau_{curved} = \tau_{straight} + \tau_e \frac{\theta}{\Delta\theta} \tag{3.90}$$

and

$$v_{o_{curved}} = v_{o_{straight}} \frac{\Delta\theta}{\theta} \tag{3.91}$$

Or if we consider $I = \theta$ for scaling purposes

$$\tau_{curved} = \tau_{straight} + b\theta = \tau_{straight} + bI \tag{3.92}$$

and

$$v_{o_{curved}} = \frac{v_{o_{straight}}}{c\,\theta} = \frac{v_{o_{straight}}}{c\,I} \quad , \tag{3.93}$$

where the constants b and c are scaling constants.

3.3.2.3 Calculating Enclosed Angle

Sections 3.3.2.1 and 3.3.2.2 discussed two different approaches to develop a metric which quantifies part shape complexity. However, application of these ideas requires a consistent approach to ensure that the complexity of all parts are evaluated in the same way. This section outlines some of the important issues which need to be addressed such that the complexity metric provides consistent and meaningful measurements. First, the use of differential geometry theory is used to (a) relate the enclosed angle θ with other geometric features of the part and to (b) interpret the physical importance of the enclosed angle θ. Then a systematic set of procedures is outlined to address the issue of multiple ply orientations.

Differential Geometry and Physical Interpretation. As a general hypothesis, the complexity of a composite design can be evaluated by using various measures from differential geometry. Furthermore, these same measures have a physical interpretation as to their effect on fabrication time. The principal measure, representing the complexity

of a shape or a fiber path, has been the enclosed angle θ. Several excellent references on differential geometry theory (refs. 33-35) were used in the following developments.

From differential geometry theory, one can show that any space curve has two important properties, curvature and torsion. Furthermore, if the curvature is known at every point, then torsion is not independent. Hence curvature would be the principal means by which a space curve or fiber could represent information. As will be shown shortly the enclosed angle θ can then be directly related to the curvature.

The curvature at any point can be represented as a vector in a direction normal to the fiber. In relationship to the plane of the part, this vector has two components, one normal to the surface of the part and the other in the plane of the part. This is shown in Figure 3-20. Hence the vector equation for curvature is

$$\hat{k} = \hat{k}_n + \hat{k}_g = \kappa \hat{n} = \kappa_n \hat{N} + \kappa_g \hat{u} \tag{3.94}$$

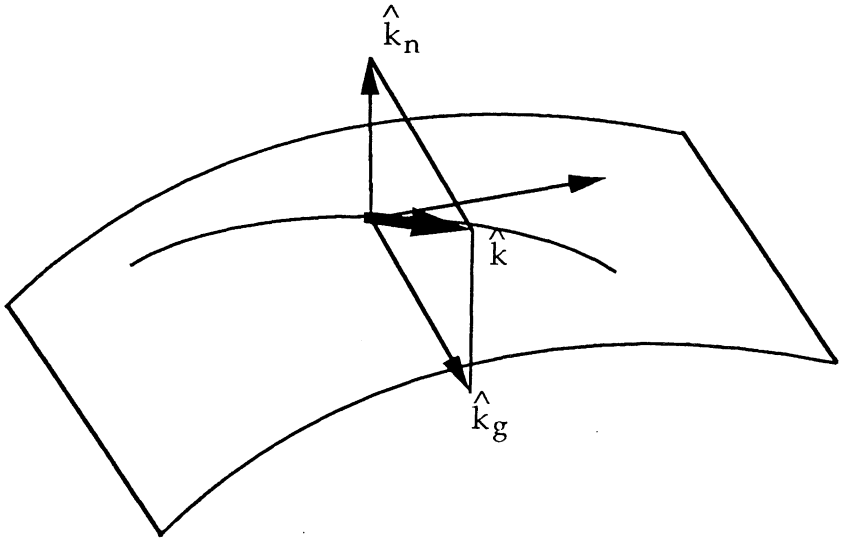

Figure 3-20. Curvature at any point can be represented as a vector in a direction normal to the fiber.

The total curvature vector $\hat{k}$ (written in terms of its magnitude κ and its unit direction $\hat{n}$) can then be written in terms of the in-plane and out-of-plane components. The magnitude of this vector normal to the surface of the part is κ_n. This is the normal or out of plane curvature for the fiber and is the type of curvature required to make singly curved or simply curved parts. The in-plane magnitude of curvature κ_g, sometimes called the geodesic curvature, represents the in-plane curvature required to make double or compound curvature parts. Hence these two curvatures represent vastly different procedures in the manufacturing operation and must be treated separately. The two enclosed angles are related to part curvature by

$$\theta_n = \int \kappa_n \, ds \ , \tag{3.95}$$

$$\theta_g = \int \kappa_g \, ds \ . \tag{3.96}$$

Hence over a section of constant curvature by substitution into Equation 3.94, one gets

$$\theta^2 = \theta_n^2 + \theta_g^2 \ , \tag{3.97}$$

where θ is the total enclosed angle.

The two enclosed angles have clear physical interpretations. They refer to the out-of-plane and in-plane shear slip required to deform an initially flat laminate into their respective enclosed angles. This is illustrated in Figure 3-21. Referring to the figure, the shear slip for the appropriate plane is defined as,

$$\Gamma = \frac{\delta}{H} \ . \tag{3.98}$$

Hence,

$$\theta = \Gamma \ . \tag{3.99}$$

This was shown rigorously by Tam and Gutowski in (ref. 28). Finally, the geodesic curvature κ_g and its attendant enclosed angle θ_g can be related to part curvature through the appropriate use of the Gauss-Bonnet theorem. The Gauss-Bonnet theorem relates the geodesic curvature for the piecewise line segments of an enclosed path C to the Gaussian or double curvature K, in an enclosed region R, and the angles of intersection θ_i. This is given below

$$\int_C \kappa_g \, ds + \iint_R K \, dA = 2\pi - \sum \theta_i \ . \tag{3.100}$$

The Gauss-Bonnet Theorem is illustrated in Figure 3-22, and applications to calculate the enclosed angle θ_g for various complex geometry are given in Appendix C.

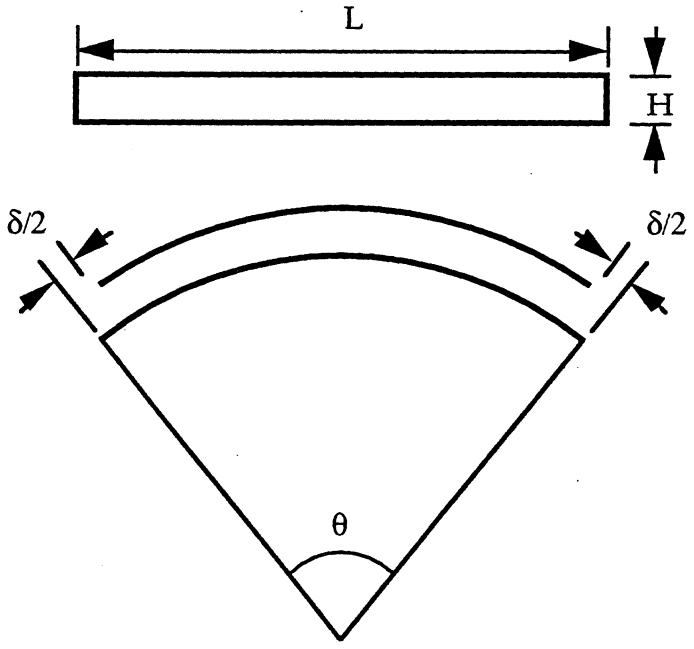

Figure 3-21. Shear slip, $\Gamma = \theta$, required to deform a flat laminate in the appropriate plane.

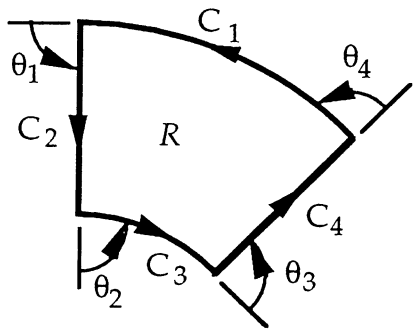

Figure 3-22. The Gauss-Bonnet Theorem. The C_i are smooth curves enclosing a simply connected region R. θ_i are the exterior angles between the curves.

3.3.3 Combined Multiple Ply Orientation and Geometric Shape Complexity

This section discusses the appropriate collection of parallel paths or fibers to represent the complexity of a part. In general, the representation of a part or a shape by a collection of parallel paths leads to a special type of mapping called a "geodesic set". The geodesic set for a given shape is not unique but can be uniquely established based upon some systematic scheme for the location of a single "first fiber". Once an initial fiber is placed, the propagation of the geodesic set is deterministic and routine. Below is a systematic procedure to represent complex part shapes:

i) Locate the part center by finding the geometric center of the projected area,

ii) Now place an initial fiber in the direction corresponding to the zero degree ply for the part ($\Psi = 0°$). This fiber should be placed so that its geodesic curvature is zero. Hence, for this fiber, $\theta_g = 0$ (this procedure is indicative of good design practices for not introducing undue curvature when laying fibers over the required composite shape).

iii) From this initial fiber, propagate the geodesic set to represent the part.

iv) Measure the average enclosed angles, by a procedure which will be described shortly, and

v) Repeat the procedure for $\Psi = 90°$, $\Psi = +45°$, and $\Psi = -45°$ to get a part average.

This procedure is illustrated in Figure 3-23.

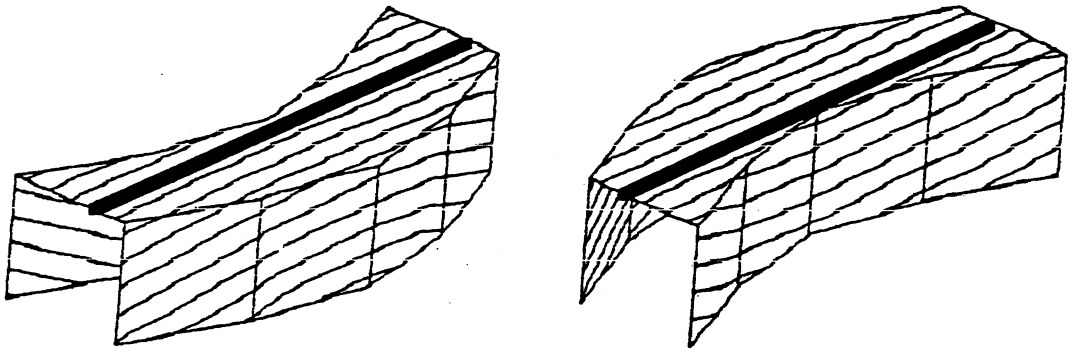

Figure 3-23. Placement of an initial fiber (bold line) to begin determination of the geodesic set.

The procedure described in Steps i) through v) from above could be refined to consider the effect of orientation angle, Ψ, on the path complexity. The suggested calculation can be done routinely using a computer. However, it requires a special algorithm to generate the geodesic set for the particular part shape. Such an algorithm has been presented by Gonzalez-Zugasti (ref. 29) and will not be repeated here. However, a vast simplification of this procedure is often possible when correlating time data with the complexity measure. Only a single angle Ψ is used to scale the shape complexity for certain types of parts. For example, as will be shown later, use of a single fiber angle $\Psi = 90°$ for stringers is adequate to measure the normal angle, θ_n. For curved c-channels, the single fiber direction $\Psi = 0°$ is adequate for measuring the in-plane angle, θ_g.

An example of the Ψ orientation dependence of the enclosed angle θ_n for stringers is illustrated in Figure 3-24. This example included four different orientations on a simple "L" type stringer with a variable tool angle α. Results show perfect correlation between the average measure for enclosed angle, $\bar{\theta}_n$, and the single measure of θ ($\Psi = 90°$) for various values of α. Using the later, total enclosed angles for "L", "Z", "U" and "hat" stringers are given in Figure 3-25. Note that there is a distinct difference in the lay-up of male and female bends. Hence, distinction must be made of the different types of bends when applying this approach to actual manufacturing processes.

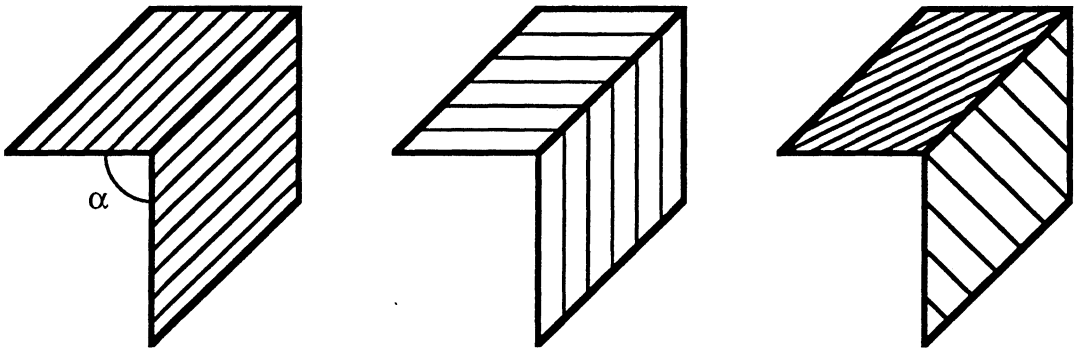

$\Psi = 0°$ $\theta_n = 0$

$\Psi = 90°$ $\theta_n = \alpha$

$\Psi = \pm 45°$ $\theta_n = 2\alpha/3$

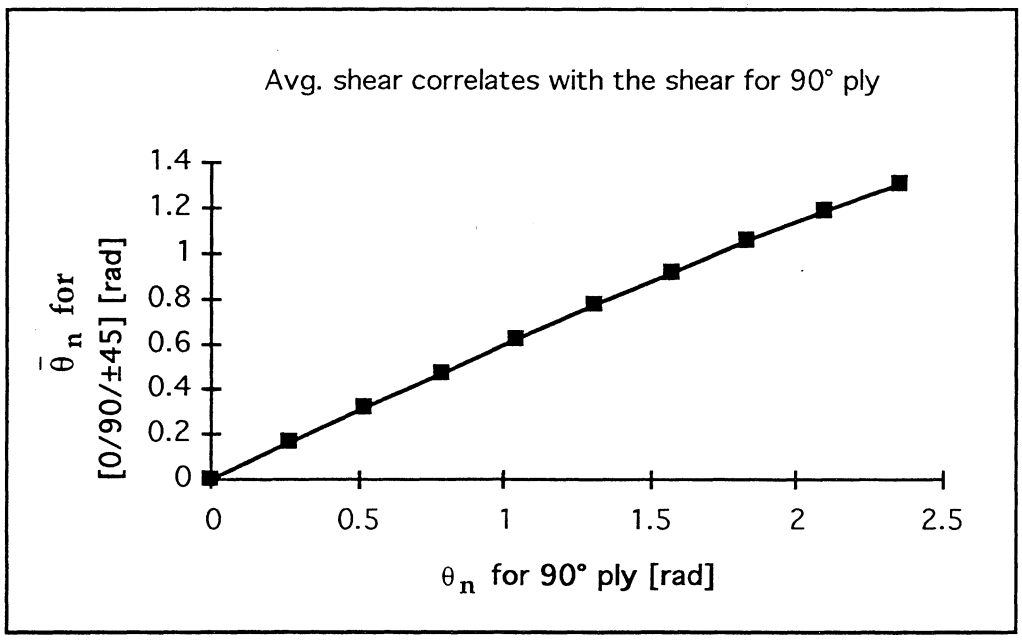

Figure 3-24. Correlation between the average, $\bar{\theta}_n$, for Ψ = 0, 90, +45 and -45 and the single value $\theta_n = \alpha$ for Ψ = 90° . The angle α is varied from 0 to 2.4 radians.

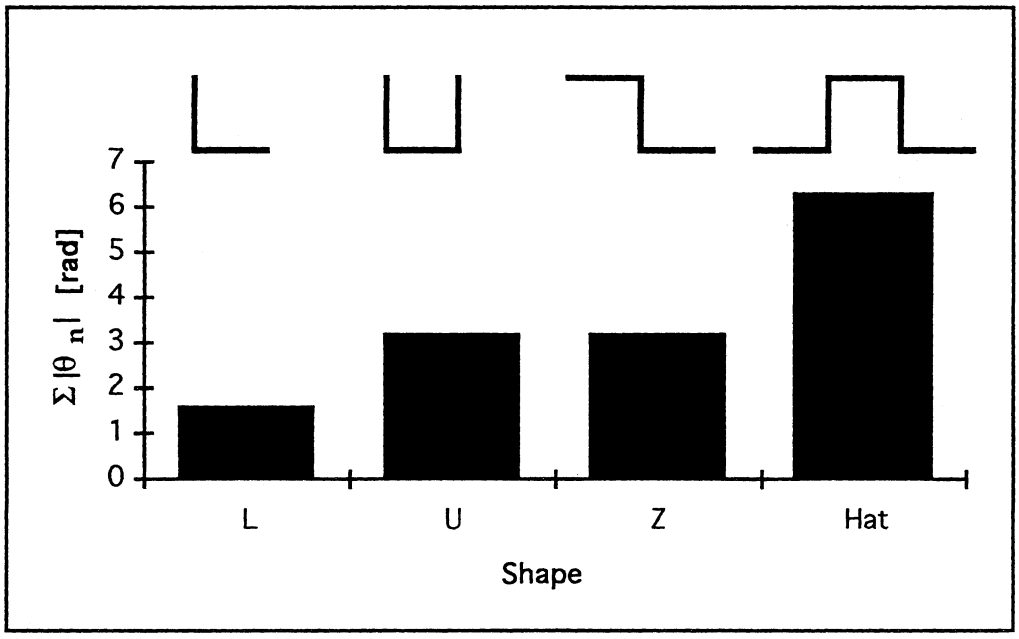

Figure 3-25. Enclosed angle for different shape stringers based on the calculations for orientation $\Psi = 90°$.

3.3.3.1 Weighting Methods for Regions with Different Curvatures

The general idea developed thus far is routine in its application to stringers. However, for other parts, particularly those with complex curvature, some type of averaging method must be developed to weigh regions of the part with different degrees of curvature. For this calculation, an area averaging technique is proposed for the in-plane enclosed angle, $\bar{\theta}_g$,

$$\bar{\theta}_g = \frac{1}{A} \sum \theta_{gi} \Delta A_i \tag{3.101}$$

Here A is the total area of the part, θ_{gi} is the enclosed angle for a given fiber or a region, and ΔA_i is the corresponding area for that fiber or that region. When this calculation is done on a fiber by fiber basis, one can modify this to get

$$\bar{\theta}_g = \frac{1}{A} \sum_{i=1}^{N_f} \theta_{gi} s_i \Delta s_n \tag{3.102}$$

Here s_i is the length of the fiber and Δs_n is the width of the fiber unit. N_f is the number of fibers. This calculation is illustrated for $\Psi = 0°$ for various complex geometric shapes in Figure 3-26. Note that $\bar{\theta}_g$ for the bead stiffener and the box depends on the relative dimensions of the part, whereas $\bar{\theta}_g$ for the hemisphere does not. Examples of calculations for $\bar{\theta}_g$ and $\bar{\theta}_n$ are given in Appendix C.

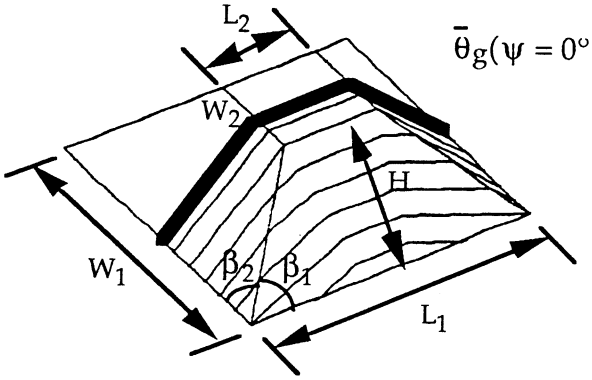

$$\bar{\theta}_g(\psi = 0°) = \frac{(4\beta_1 - \pi)(L_1 + L_2)H}{H(L_1 + L_2 + W_1 + W_2) + L_2 W_2}$$

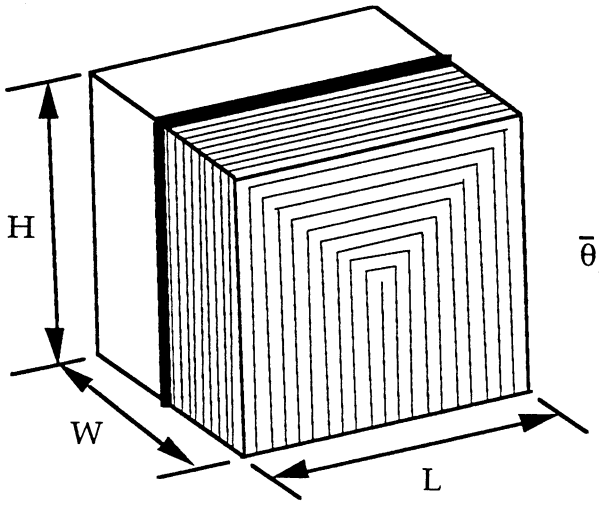

$$\bar{\theta}_g(\psi = 0°) = \frac{2\,\pi\,L\,H}{LW + 2LH + 2HW}$$

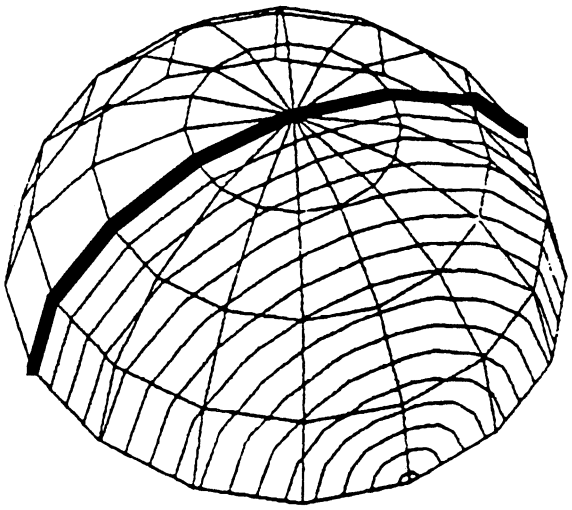

$$\bar{\theta}_g(\psi = 0°) = \frac{\pi}{2}$$

Figure 3-26. Average in-plane angle, $\bar{\theta}_n$, for the different complex shapes for $\Psi = 0°$.

3.3.4 Applications that Include Shape Complexity

The methods described thus far can be used to develop a modified time estimation procedure for complex shaped parts. In general, Equation 3.72 will now be written as

$$t_d = N_L \tau + \frac{V'}{w\, h\, v_o} + \frac{V''}{w\, h\, v_c}\ , \tag{3.103}$$

where V' represents the part volume which is flat or simply curved, and V'' represents the part volume which has double or compound curvatures. These two add to the total part volume,

$$V' + V'' = V \tag{3.104}$$

The velocity v_c corresponds to a reduced deposition rate in the complex curvature region. The time constant t now includes additional effects due to the various enclosed angles.

$$\tau = \tau_o + \sum_{j=1}^{N_e} b_j \bar{\theta}_j, \tag{3.105}$$

The $\bar{\theta}_j$ terms correspond to averaged enclosed angles including, for example, both appropriate normal and geodesic curvatures as well as male and female bends and other types of bends (stretch and shrink flanges) which will be discussed in the next section. The coefficients b_j specify the time per radian for the appropriate enclosed angle. N_e corresponds to the number of types of enclosed angles which need to be summed.

3.3.4.1 Example Correlation for Stringer Geometry

Stringers represent an important class of structural elements characterized by their long aspect ratio and various simple bends which are required to achieve the necessary bending stiffness. For these kinds of elements Equation 3.103 can be simplified by using

$$V = V';\ V'' = 0, \text{ and} \tag{3.106}$$

$$\bar{\theta}_1 = \bar{\theta}_{male,normal};\ \bar{\theta}_2 = \bar{\theta}_{female,normal};\ \theta_g = 0\ . \tag{3.107}$$

To study this problem experimentally, the stringer shapes illustrated in Figure 3-25 were manually laid up at MIT (ref. 6). The approximate dimensions of these parts were about 18 inches long, 5 inches high and 6 inches wide. With these relatively short lengths, the length or volume terms made a small contribution to the total time, hence the primary effect of the bends was in the time constant (i.e., first term in Equation 3.103). Figure 3-27 shows the results for laying up these various shapes plotted versus the total enclosed angle in radians. This data confirms a linear relationship between the time constant and the enclosed angle, as suggested in Equation 3.103.

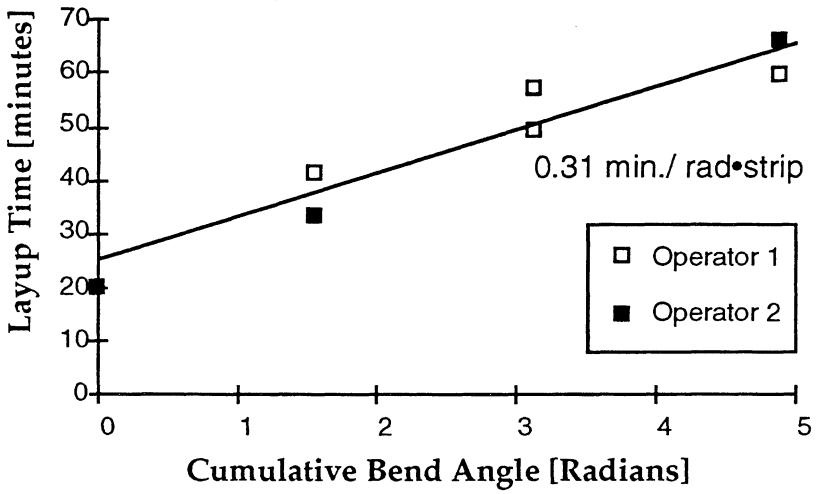

Figure 3-27. Linear cumulative bend angle dependence for laying up 16 plies of 12 in. wide tapes.

In order to evaluate the combined effects of part complexity and size scaling, analysis comparisons were made with the nonlinear ACCEM cost estimating procedure (ref. 13). These analyses used the range of parts shown in Figure 3-28. Note that these parts are up to 30 ft. long, increasing the effect of volume terms in Equation 3.103. The results from analyzing 240 parts are shown in Figure 3-29. As will be discussed further in Section 3.3.5.2, the scatter in predictions near the origin of this figure when compared to the ACCEM power laws is caused by an error due to the linearization assumption from Equation 3.103. The linearization assumption can be traced back to discussions on size effects from Section 3.2.3.

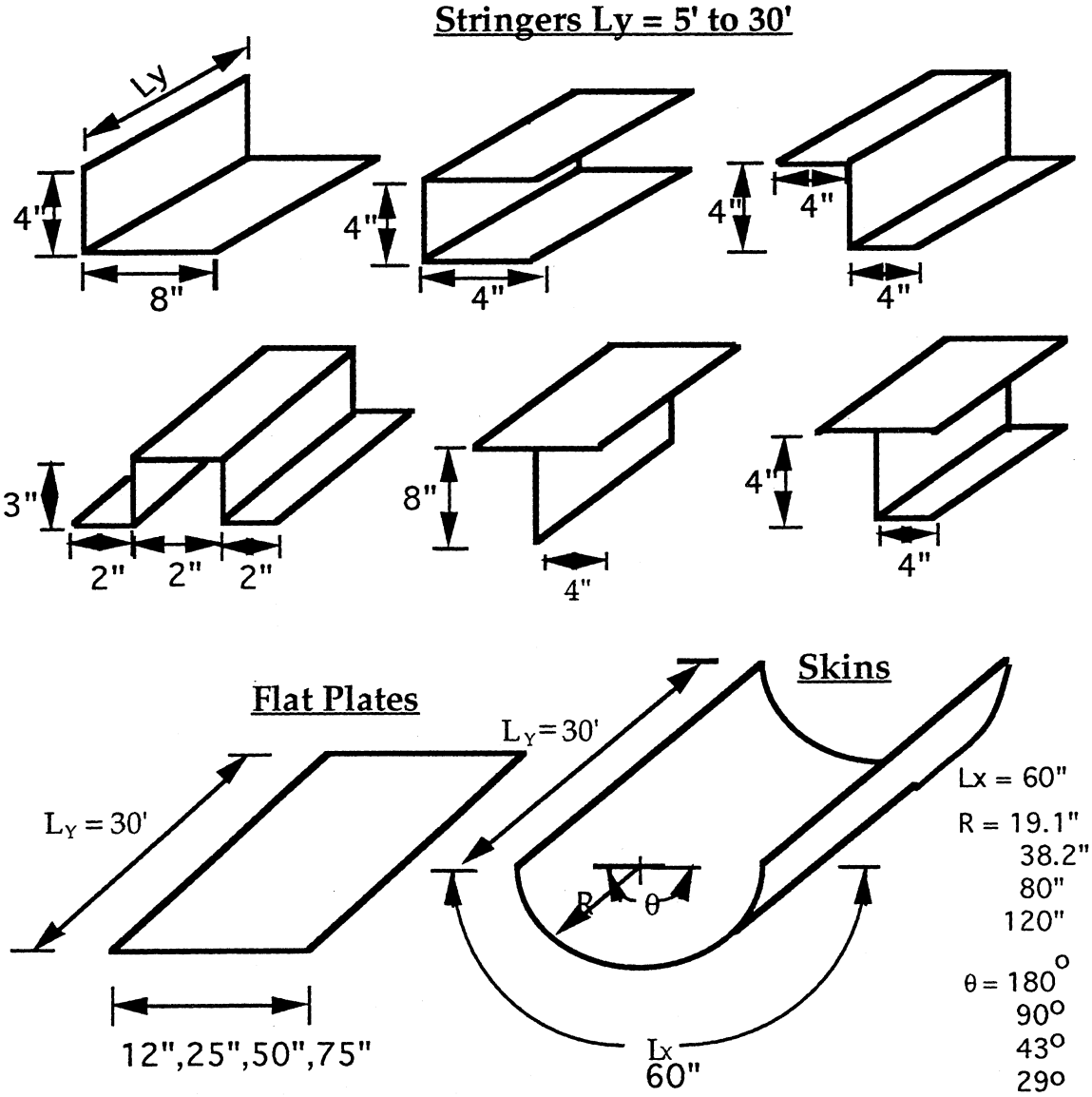

Figure 3-28. Sample composite parts used in comparisons with ACCEM time estimates.

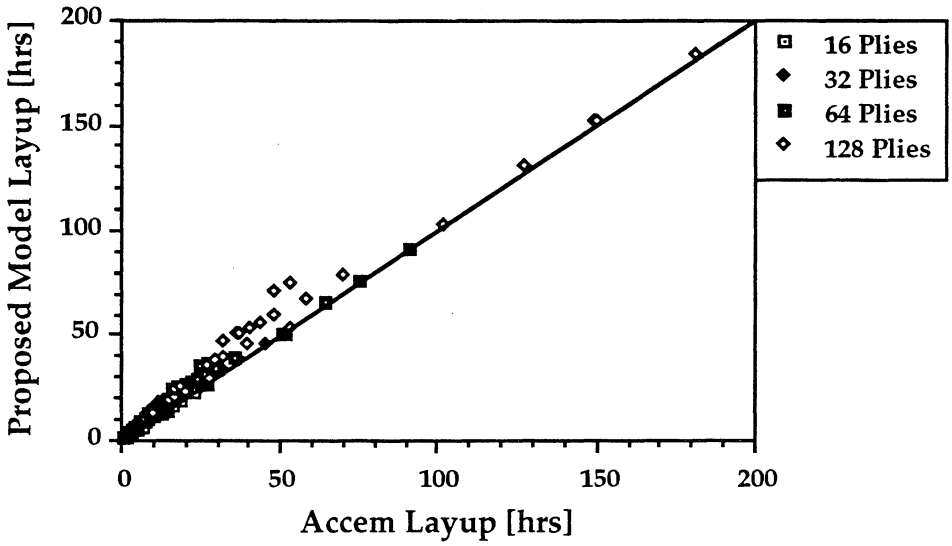

Figure 3-29. Correlation between ACCEM and the linear first order model for the parts shown in Figure 3-28.

3.3.4.2 Example Correlation With Stretch and Shrink Flanges

Another important category of structural composite parts having complex shapes are stretch and shrink flanges. These may be considered as sub-cases of the curved c-channel members shown in Figure 3-23. Elements with these shapes have been studied in detail by Gonzalez-Zugasti and Kim (refs. 29 and 36). Stretch and shrink flanges considered in the current comparisons are illustrated in Figure 3-30. Complexity factors for these types of geometry have been developed in the ACCEM model.

In the case of stretch and shrink flanges, all of the terms in Equation 3.103 are applicable. The coefficients b_j and the velocity in the complex region, v_c, were found by curve fitting to the ACCEM model. In this study, 42 double curvature parts with varying L_b, R, and F were analyzed. Correlation for the layup times between the linear Equation 3.103 and the non linear ACCEM model including the complexity factor is shown in Figure 3-31. This figure combines the results of double curvature parts with the 240 parts from Figure 3-29.

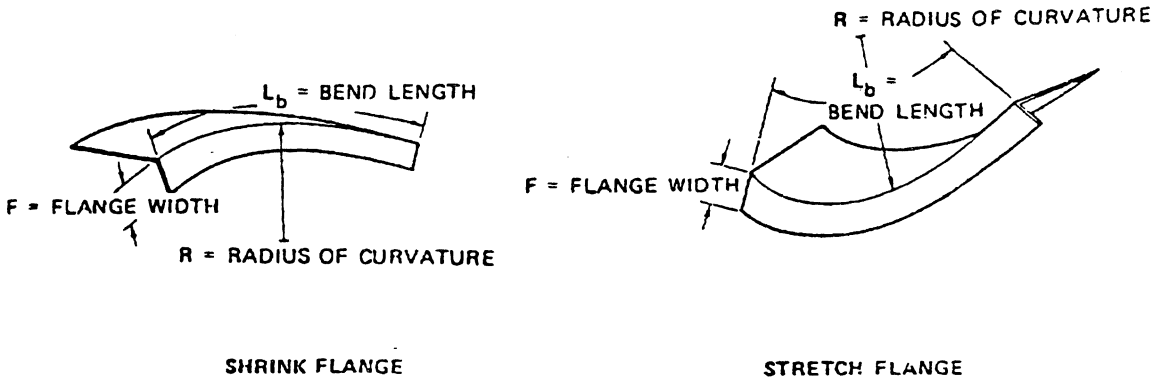

Figure 3-30. Shrink and stretch flanges.

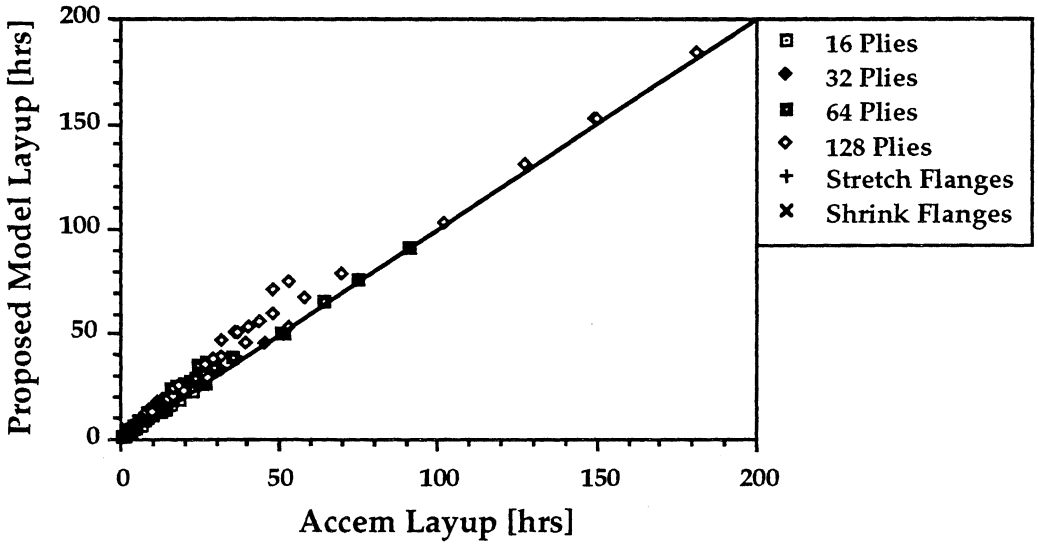

Figure 3-31. Correlation between ACCEM and the linear first order model for the parts shown in Figures 3-28 and 3-30.

Again, the scatter in predictions near the origin of Figure 3-31 is caused by an error due to the linearization assumption from Equation 3.103. The various coefficients and the velocities obtained from the correlation exercises leading to results plotted in Figure 3-31 are given in Table 3-3. For purposes of comparison, the complexity time increments for stretch and shrink flanges for the ACCEM model are also given in Table 3-4.

τ_o	0.0111 hr
v_o	1896 in/hr
Se	12 in
b_m	0.000665 hr/rad•strip
b_f	0.001519 hr/rad•strip
$b_{stretch}$	0.1929 hr/rad•strip
b_{shrink}	0.0726 hr/rad•strip
$v_{c,stretch}$	58.3 in/hr
$v_{c,shrink}$	130 in/hr

Table 3-3. Process parameters for manual hand lay-up of 12 in. wide unidirectional tape (obtained by bench marking with ACCEM).

Note that the "b" coefficients in Table 3-3 for complex bends ($b_{stretch}$ and b_{shrink}) are 48 to 290 times larger than those for simple bends (b_m and b_f), and the velocities in the complex regions are about one to two orders of magnitude smaller than that in the flat and simple curvature regions. These clearly illustrate the huge time penalty for introducing double curvatures into a part, and is consistent with general observation for the hand lay-up processes.

Sharp, Male	$0.00007\ L_b$
Sharp, Female	$0.00016\ L_b$
Radial, Male (R≤2")	$0.00007\ L_b$
Radial, Male (R>2")	No factor applied
Radial, Female (R≤2")	$0.00016\ L_b$
Radial, Female (R>2")	$(0.00047\ R^{-1.3585})\ L_b$
Stretch Flange, Tape	$(0.015\ R^{-0.5532}\ F^{0.7456})\ L_b$
Shrink Flange, Tape	$(0.0064\ R^{-0.5379}\ F^{0.5178})\ L_b$
Flanges, Woven	$(0.00444\ R^{-0.5958} + 0.0007)\ L_b$

Table 3-4. Complexity time increments [hrs] given by ACCEM (ref. 13). L_b = Length of bendline [in], R = Radius of curvature [in] and F = Flange width [in].

3.3.4.3 Improved Correlation Using Generalized Size Effect Equation

Sections 3.2.3 and 3.2.4 discussed limitations of the linear approximation for size effect and assumptions used during summation to simplify equations, respectively. These assumptions have been used in this section for examples that combine size and part complexity. As shown in Figures 3-7 and 3-8, the linear approximation tends to overestimate the time required for short lengths when compared to power law equations, such as those used by ACCEM (ref. 13). For long slender parts, such as the stringers

shown in Figure 3-28, a significant number of short strips are needed to layup angle (e.g., ±45°) and 90° plies.

The accuracy in predicting layup time for many short strips can be improved by eliminating linear approximations. This can be corrected by using the hyperbolic approximation (Equation 3.18) for layup of individual strips,

$$t_{d,strip_i} = \sqrt{\frac{L^2_{strip_i}}{v_o^2} + \frac{2\,\tau\,L_{strip_i}}{v_o}} \tag{3.108}$$

When using this generalized formulation for layup time, it is also important to avoid simplifying assumptions when summing all of the individual strips in a volume (i.e., Equation 3.103). The time to layup a part becomes the sum of all the times to lay-up the number of individual strips, N_L, as expressed by

$$t = \text{Setup} + \sum_{i=1}^{N_L} t_{d,strip_i} \tag{3.109}$$

Note that in this formulation, values of v_o and τ can be allowed to vary for different fiber orientations.

Combining Equations 3.108 and 3.109 with formulations for the enclosed angle presented in this section, allows a more generalized prediction of the combined effects of part size and complexity. Figure 3-32 shows results from using the hyperbolic approximation and the summation of times for each individual strip to estimate lay-up time for stringer geometry, stretch flanges and shrink flanges from previous examples.

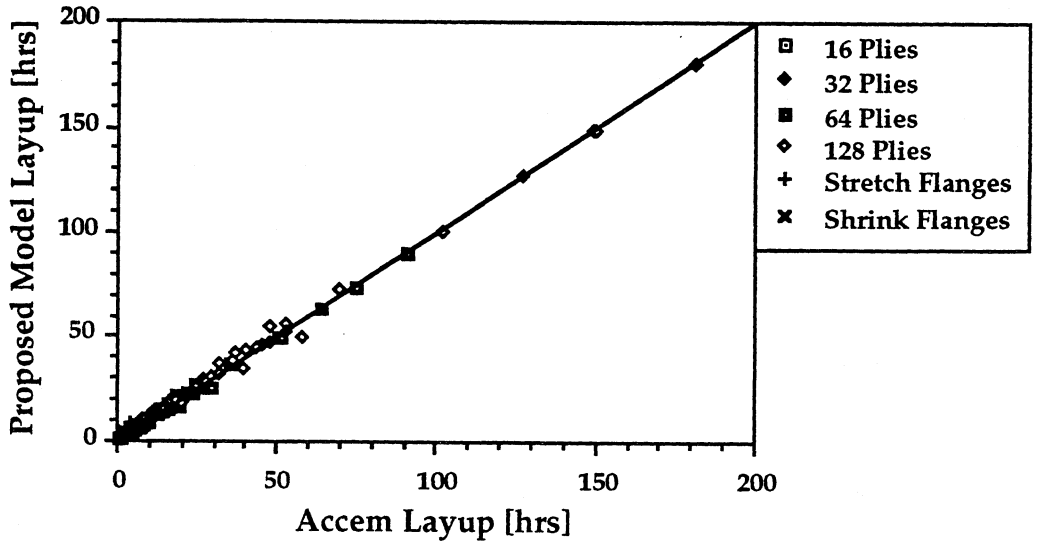

Figure 3-32. Correlation between ACCEM power law estimates and the hyperbolic first order model for the parts shown in Figures 3-28 and 3-30.

3.3.5 Concluding Remarks On Part Size and Complexity Scaling

Sections 3.2 and 3.3 present cost model theories to predict fabrication time as a function of part size and part complexity, respectively. Some assumptions used during equation development helped to simplify equation forms for the purpose of discussion and illustration. When studying processes that have characteristics which do not satisfy the assumptions, the more general formulations should be applied. Such practices will have minimal impact on the time required to perform calculations, since even the most difficult cost analysis procedures presented in Sections 3.2 and 3.3 become trivial when performed on a computer.

As judged by comparisons with existing databases, the first order model appears to be a good candidate for the size scaling relationship. The first order model is based on two physical quantities (time constant τ, and steady state velocity v_o) that are objective, have simple interpretations and are dimensionally consistent. In addition, these physical quantities also make the model easy to modify or update for new or evolving processes. These traits are characteristic of the requirements placed on equations to predict time from the theoretical framework.

Power law curves will probably continue to be used in industry for estimating fabrication times. However, the results given in Section 3.2.7 will allow for a physical interpretation of these relationships. The subject of learning curve, its implication on process changes, and its potential for misapplication as power law size scaling are further discussed in Section 3.5.

The hypothesis of Section 3.3 is that the information theory, originally developed in the field of communication engineering, can be adapted as a complexity metric to reflect the impact of part geometry on the manufacturing complexity. For composite manufacturing processes, the fiber network is thought of as an information storage media. Using two different approaches, the fiber curvature (enclosed angle) necessary to replicate a part is found to be a good metric to quantify part shape complexity. In order to predict fabrication times, the complexity metric is incorporated with the first order model from Section 3.2 to get the combined effects of size and complexity scaling. This is accomplished simply by scaling the two physical constants, τ (time constant) and v_o (steady state velocity), in the appropriate directions. Specifically, as the part geometric complexity increases, making it more difficult to manufacture, τ increases and v_o decreases.

As described in Section 3.3.4, the use of "information" as a complexity metric was found to be suitable in estimating the time for hand lay-up. Its use, however, has not been verified in automated processes such as drape-forming, AFP, braiding, and NC machining. Future work will be needed to investigate the sensitivity of the fabrication times for different processes to the proposed complexity metric. In addition, complexity scaling may replace lower level process definition (such as cutting and darting in hand lay-up and pleating a vacuum bag over complex geometry for part cure). In which case, the use of size effect equations for lower level process definition may be traded against the determination the higher level complexity coefficients. In either case, future work

will need to define efficient experimental procedures to gather the relevant coefficients for a given design-process space.

3.4 Material Handling Tasks

This section addresses some of the major issues in estimating the time required to perform various material handling tasks in the manufacturing environment; such as lifting, lowering, pulling, pushing, and carrying. The approach used is to dissect material handling tasks into two distinct components, namely, transport (or gross travel), and positioning (secondary or corrective type motion) to bring the object within desired orientation and location. These two components are further subdivided into whether the task is to be accomplished manually or mechanically. The criteria/guidelines for whether a handling task can be carried out manually is briefly summarized in Section 3.4.1. More detailed discussions on this subject can be found in ref. 6. The rest of this section covers the different models to predict the time required for each of the different components and subcomponents as described above.

3.4.1 Synopsis of Limits for Manual Material Handling

Recommended limits to be used in judging whether a material handling task can be performed manually have been set by the US National Institute of Occupational Safety and Health (NIOSH). Judgments are made based on weight and awkwardness. For example, Figure 3-33 shows a manual limit on lifting under ideal conditions to be 51 lbs (ref. 38). As shown schematically in the figure, when the lifting task becomes more awkward, the recommended weight limit decreases.

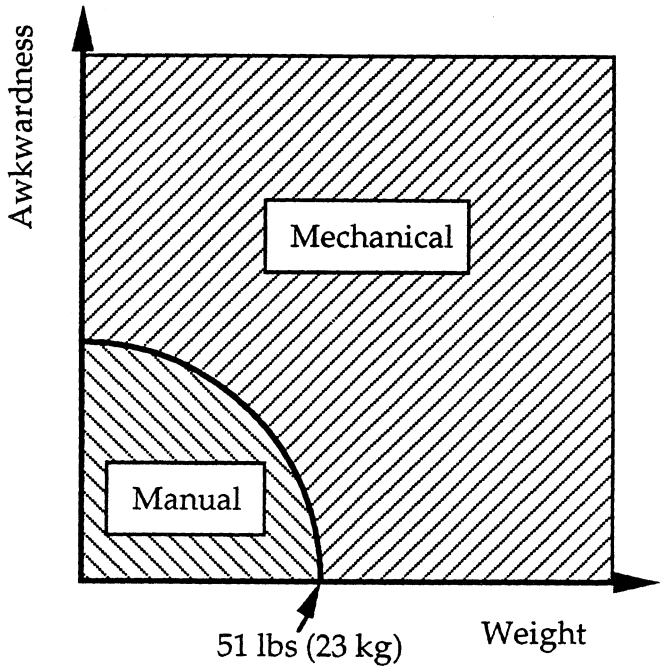

Figure 3-33. Schematic of the two main variables used to establish the limit for manual material handling.

Recommended limits (refs. 38 and 39) for manual material handling have been determined based on constraints from three criteria; i) biomechanical, ii) physiological, and iii) psychophysical. Biomechanical constraints, which are most often applied to infrequent handling tasks, are determined from calculations of mechanical stresses in the body. Physiological constraints, which are often applied to repetitive and longer duration tasks, are based on the total energy expenditure throughout the day. Psychophysical constraints, which apply to either infrequent, repetitive, or long duration tasks, are generally determined by experiments in which participants are asked to "work as hard as you can without straining yourself".

As presented in greater detail in ref. 6, equations, tables, and ergonomic rules have been established for manual material handling tasks. A lifting equation based on the three criteria described above has been established by NIOSH (ref. 38). In most cases, the ideal lifting conditions are not satisfied, resulting in maximum lifting weights below the 51 lbs shown in Figure 3-33. For the more general problem of manual material handling tasks such as pulling, pushing, carrying, lifting, and lowering, ref. 39 published extensive tables of loads and forces found acceptable by male and female workers for continuous tasks. Guidance to avoid industry-related injuries from manual handling tasks have been documented as ergonomic rules (ref. 40). Results from studies indicate that help from other persons to stabilize and balance a load was not found to be fully additive (i.e., the load carrying capability of multiple people involved in lifting is not the sum total of their individual strengths due to timing of efforts).

3.4.2 Transport (Gross Material Movement)

The transport component of material handling involves moving the object from point A to the vicinity of the desired point B. Take for example the task of locating a subassembly onto an assembly jig. The transport component will be the gross movement of the subassembly from point A to a rough location and orientation of the final desired position without any effort to position the subassembly within the desired tolerances. For the sake of estimating the required time, the transport component is further subdivided into manual and mechanical operation. The equations, tables, and guidelines summarized in ref. 6 can be used to help establish if a given transport task is suitable for manual labor.

3.4.2.1 Mechanical Transport

Mechanical transport equipment such as hoists, winches, cranes, forklifts, trucks, and conveyor systems, are widely used for tasks exceeding the recommended limits for humans. They also help to achieve economy of scale for highly repetitive tasks. Obviously, times required to accomplished a transport task will depend on the distance moved and the transport velocity of the mechanical devices. Therefore, the equation to estimate the dynamic component of time for mechanical transport, $t_{transport}$ is simply

$$t_{transport} = \frac{\text{distance moved}}{v_{transport}} \quad . \tag{3.110}$$

For mechanical transport, the transport velocity, $v_{transport}$, can typically be obtained from the machine specification, actual setpoint in the factory or the speed limit imposed in the factory; whichever is the slowest. Furthermore, assuming that the weight of the object moved does not exceed the capacity of the equipment, one can expect the transport velocity to be constant (independent of weight) for mechanical transport in general.

3.4.2.2 Manual Transport

The time required for transporting an object manually (such as lifting, lowering, pushing, pulling and carrying) can be estimated with the same equation as that for mechanical transport (Equation 3.110). However, the issue here is whether the transport velocity, $v_{transport}$, is weight dependent. From Barnes ref. 7, the walking speed for humans generally ranges from 2.5 miles per hour to 4.5 miles per hour when walking empty handed. In addition, Karger and Bayha (ref. 9) tabulated walking speed as a function of weight from the official methods-time-measurement (MTM) system data card. These speeds are shown in Table 3-5 and plotted in Figure 3-34.

In order to get a sense of the weight dependence of walking speed, the information in Table 3-5 can be used to determine times to walk a distance of 100 feet. For example, the walking speed is 3.57 mph for the case of 0 to 5 lbs load, resulting in 19 seconds to cover the 100 ft distance. Similarly, the walking speed is 2.53 mph for the case of a 50 lb load (i.e., ≈ recommended weight limit set by NIOSH and ref. 39 for stationary tasks), resulting in 27 seconds to cover the same 100 ft distance.

Load [lbs]	TMU per foot
0 < loads ≤ 5	5.3
5 < loads ≤ 35	6.0
35 < loads ≤ 50	7.5
50 < loads	8.5

Table 3-5. Walking data for average operators assuming unobstructed condition (1 TMU=0.00001 hr or 0.036 sec).

In accordance with the NIOSH recommendation, the maximum allowable weight for manual material handling tasks should be well within the strength and capability of the majority of the workforce. Subsequently, a load heavy (or awkward) enough to significantly affect the walking pace of an individual is, per NIOSH, not permissible for manual handling. Therefore, assuming that these recommendations are adhered to, the manual transport velocity, $v_{transport}$, can be assumed to be constant at $v_{transport}$ = 3 mph (i.e., average of the empty handed walking speed from ref. 7) for simplicity. The time difference between these assumptions and the weight dependent examples given in the previous paragraph is only ±4 seconds.

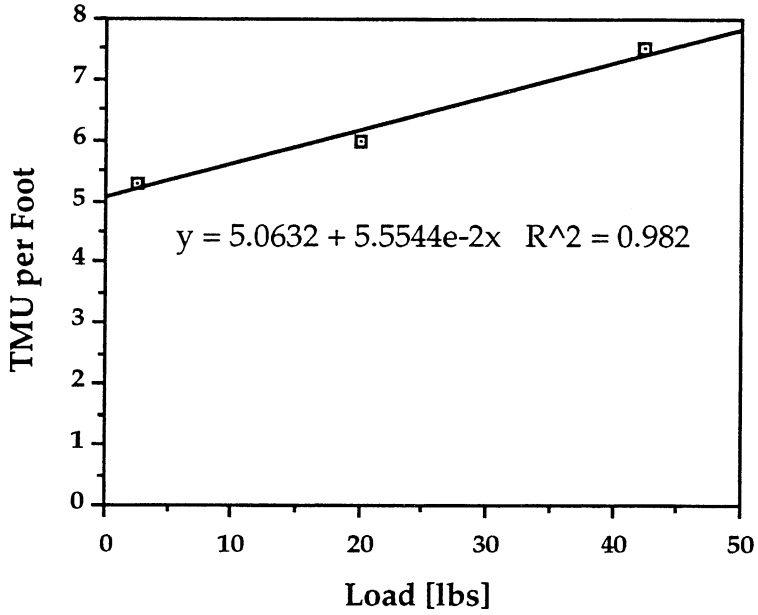

Figure 3-34. Data from the official MTM data card shows weak dependence of walking speed with weight carried.

3.4.3 Positioning (Small Corrective Movement)

The positioning component involves small corrective type motion to locate an object to within the desired orientation and tolerances; following the transport component which merely brings the object to the rough final location. Again, take for example the task of locating a subassembly onto an assembly jig. The positioning component will be the fine corrective type action to move the subassembly to the final desired position and orientation. Again, as in the case of the transport component, the positioning component is further subdivided into manual and mechanical operation when estimating the time required. Accordingly, the equations, table, and guidelines summarized in ref. 6 can be used to help establish if a given positioning task is suitable for manual labor.

3.4.3.1 Mechanical Positioning

When machines are used in a positioning task, the time required can be estimated from equipment specifications such as rise time, settling time, machine stiffness, and damping ratio. The dynamics of such machines can be modeled as a second order system. Figure 3-35 shows a schematic of such a system where the task is to position an object of mass, m, from the initial position, x_o, to within $\pm x_\delta$ of the targeted location.

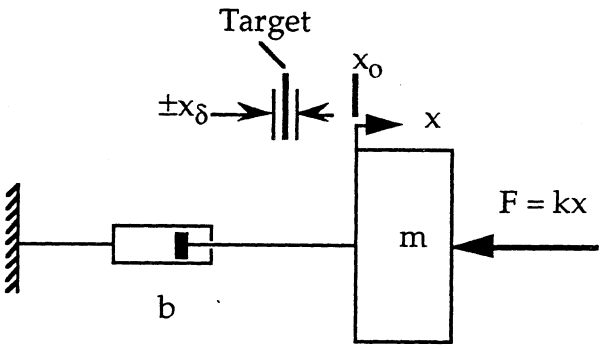

Figure 3-35. Schematic diagram of a second order system.

For the classic case of a mass-spring-damper system, the second order equation becomes

$$m\ddot{x} + b\dot{x} + kx = 0 , \tag{3.111}$$

where m is the effective mass on the manipulator and b is the damping coefficient. Note that this is the same as Equation 3.13, except the applied force term, F, has moved to the left side of the equation. The applied force in Equation 3.111 is further assumed to be proportional to the distance away from the target, and thus is the same as the force that would be applied by a linear spring, i.e., F = -kx. Various system/control textbooks such as Karnopp and Rosenberg (ref. 41) and Ogata (ref. 42) can be consulted for more rigorous treatment on this subject.

For the second order system in Equation 3.111 and Figure 3-35 above, the system parameters are natural frequency, ω_n, and damping ratio, ζ, which are defined as

$$\omega_n = \sqrt{\frac{k}{m}} \tag{3.112}$$

and

$$\zeta = \frac{b}{2\sqrt{m\,k}} \tag{3.113}$$

yielding the system time constant as

$$T = \frac{1}{\zeta\,\omega_n} . \tag{3.114}$$

Therefore, the time required to position within tolerance x_δ is

$$t = T \ln\left(\frac{x_o}{x_\delta}\right) \tag{3.115}$$

where x_o is the initial position and x_δ is the tolerance of the positioning task. For most positioning tasks, the ratio x_o/x_δ is relatively large such that the natural log term in Equation 3.115 is essentially constant as a first approximation. Subsequently, the time

required for a translational positioning task can be derived to be proportional to the weight of the object,

$$t \sim \frac{2\,m}{b} \quad . \tag{3.116}$$

Similarly Equation 3.111 can be rewritten in rotational form for the case of rotational positioning. Doing so will lead to an analogous result as linear positioning; where the time required for a rotational positioning task can be derived to be proportional to the mass moment of inertia of the object, J, about the rotational axis,

$$t \sim \frac{2J}{b} \quad . \tag{3.117}$$

In summary, the time for mechanical positioning tasks is proportional to either the weight of the object for translational positioning; or the mass moment of inertia about the rotating axis for angular positioning.

3.4.3.2 Manual Positioning

The time required to accomplish a manual positioning task can also be estimated with a mathematical model. As discussed by Sanders and McCormick (ref. 23), a person performing a positioning task usually overshoots and then hunts for the exact adjustment by overshooting in both directions, the magnitude diminishing until arriving at the correct adjustment.

Given the fact that linear systems are much more tractable to analysis, as compared to non-linear systems, it would be very convenient if the human operator acted as if he/she were an approximately linear element. As with physical systems, one could proceed to predict approximate human response by knowing the input and the dynamics of the controlled process; without having to build up a catalog of responses for every possible set of input-process combinations. Along the same principle, Sheridan and Ferrell (ref. 22) showed that a linear differential equation with constant coefficients is the simplest model that gives realistic results for humans in a manual control situation. Furthermore, it was also suggested that the human operator does on the average what a well designed servo controller would do. Therefore, as in the case of mechanical positioning tasks, manual positioning tasks may be modeled as a linear second order system as shown in Equation 3.111 (Section 3.4.3.1) for the classic case of a mass-damper system. Subsequently, the time required to perform a manual translational positioning task is

$$t = \frac{2\,m}{b} \ln\left(\frac{x_o}{x_\delta}\right) \tag{3.118}$$

and that for manual rotational task is

$$t = \frac{2\,J}{b} \ln\left(\frac{\theta_o}{\theta_\delta}\right) \tag{3.119}$$

where m and J are the mass and mass moment of inertia respectively, and b is the damping coefficient. Similarly, x_o (θ_o) is the initial linear (angular) position and x_δ (θ_δ) is the linear (angular) tolerance of the manual positioning task.

A series of translational and rotational manual positioning experiments were performed at MIT to evaluate Equations 3.118 and 3.119. Participants in the experiments positioned different lengths of 2" x 4" wood beams. Details on the results of these experiments are covered in ref. 6. All experiments indicated that positioning time was linearly proportional to beam length. This is predicted for translational positioning, but rotational positioning tasks should be proportional to L^3. Possible explanations for a lack of correlation with L^3 for the rotational tasks were that a dominant translational motion was also present in the experiment and the wood beams used were relatively light. Other findings from these experiments indicate that locating guides or jigs help increase the speed of manual locating tasks and walking speeds prior to locating tasks did not seem to depend on beam weight.

3.4.3.3 Relationships Between Manual Positioning and Fitt's Law

Notice the similarity of Equations 3.118 and 3.119 with Fitts' Law, which is stated as:

$$t = a + b \log_2\left(\frac{2D}{W}\right) \tag{3.120}$$

where

t = movement time

a and b = empirical constants depending on the nature of the movement involved

D = distance of movement from start to target center

W = width of the target.

Fitts' law has been widely tested, such as in manual tapping experiments (ref. 22) and manual circuit board assembly (ref. 31). It is found to hold for movement with sufficient time for visual feedback. However, the effect of the weight of the object moved on the time predicted by Fitts' law has not been investigated. Two plausible modifications to Fitts' law that will be consistent with Equation 3.118 are

$$t = \left(a + b \log_2\left(\frac{x_o}{x_\delta}\right)\right) \text{weight} \tag{3.121}$$

and

$$t = a + b \bullet \text{weight} \bullet \log_2\left(\frac{x_o}{x_\delta}\right). \tag{3.122}$$

However, the nature of the experiment does not facilitate the differentiation of Equations 3.121 from 3.122. Furthermore, in most positioning tasks, the ratio x_o/x_δ is relatively large such that, as a first approximation, the logarithm term in these equations is essentially constant. Subsequently, for simplicity, the time required for a manual translational positioning task can be treated as

$$t \sim \text{weight}, \tag{3.123}$$

and that for manual rotational positioning as

$$t \sim \text{mass moment of inertia.} \tag{3.124}$$

3.4.4 Concluding Remarks On Material Handling Tasks

The time required for material handling tasks can be estimated by combining both the transport and positioning component. As discussed in Section 3.4.1, the NIOSH guidelines and recommended weight limits should be consulted when deciding if a handling task is suited for manual labor (38, 39, 43). As it turns out, both manual and mechanical operations can be estimated with the same equation form for both transport and positioning component; but the coefficients will depend on whether the task is manual or mechanical.

The time required for handling tasks can be estimated as

$$t_{\text{handling}} = a + \frac{\text{distance moved}}{v_{\text{transport}}} + b + c \bullet \text{weight} \tag{3.125}$$

where a and b are the delays associated with the transport and positioning component, respectively, and $v_{\text{transport}}$ is the transport velocity (which could be assumed to be 3 mph for manual operations). For mechanical operation, $v_{\text{transport}}$ will depend on the machine specification or factory practices; whichever is slowest. The coefficient, c, represents the sensitivity of the positioning task to weight. Again for mechanical positioning, c can be derived from machine dynamics or specification. However, as shown by the manual positioning experiments in ref. 6, c is task (translational or rotational positioning) and equipment (use of jigs and fixtures) dependent.

3.5 Other Simplifying Analyses

A number of simplifying analyses have been pursued in industry to estimate the cost of emerging technologies. In each case, the analysis is simplified based on observations from past data trends, rather than rigorous theoretical developments. This section will present each simplifying analysis with a discussion of the associated benefits and limitations. The three analyses covered in this section will be referred to as: i) cost drivers, ii) learning curve effects, and iii) power laws.

3.5.1 Cost Drivers

The theory presented in Sections 3.2 through 3.4 pertains to time predictions for a given individual process step. The total time for a series of steps needed to fabricate a part is equal to the summation of predicted times for each step. For example, hand lay-up of a part includes steps to clean tool, apply mold release, lay-up prepreg plies, debulk, apply bleeder plies, etc. Based upon composites manufacturing data and industry estimates, there appears to be a reoccurring structure in the fabrication time data for hand lay-up, AFP, and composite assembly. Figures 3-36, 3-37, and 3-38 shows the data that supports the following observed trends:

1) the fiber structure fabrication step for hand lay-up and AFP appears to be the longest step,
2) the other "extensive" steps (excluding cure) appear to correlate with the fiber structure fabrication step, and
3) a Pareto chart of the times for all process steps appears to yield a distribution where a very small number of operation steps dominate the fabrication time.

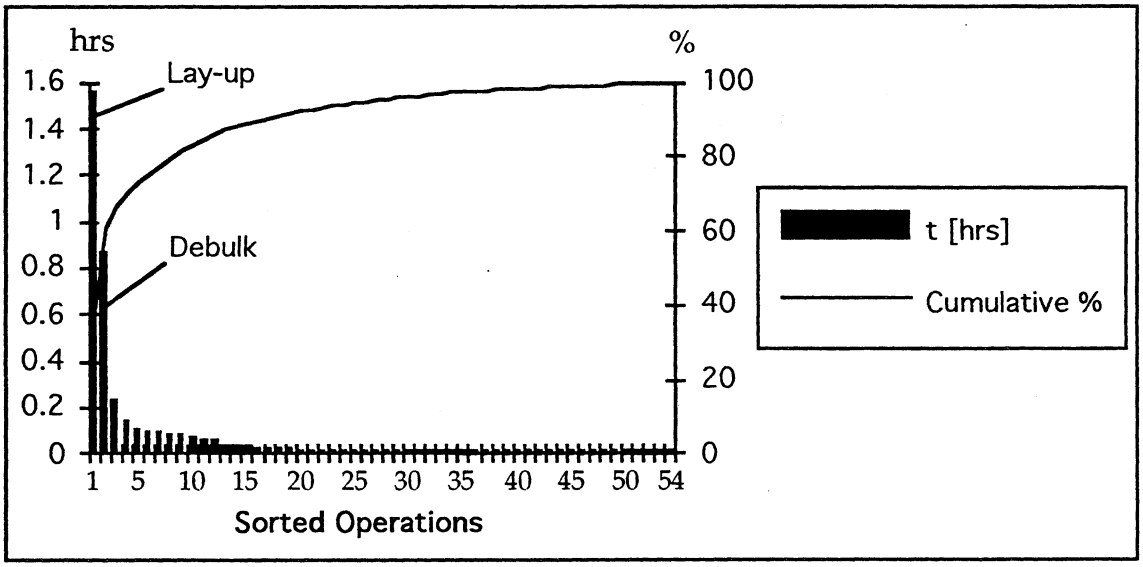

Figure 3-36. Pareto chart of process times for the hand lay-up of a 10' J stringer using ACCEM (ref. 13).

The third observation from above has also been made by Barkan and Hinckley for over 200 mechanical assembly operations (ref. 44). The observation that estimates are dominated by cost centers (also known as the "vital few and trivial many" or 80/20 rule) has some major implications in pursuing cost predictions for composite processes. For example, cost data and understanding for the most important process steps should be pursued first, hence improving accuracy for a significant portion of the estimate.

The observed trends shown in Figure 3-36 through 3-38 also suggest, that once the structure of the time steps is identified, it may be possible to scale the sum of the times for the trivial many steps to that of the vital few steps. Within a given design-process window, a simple multiplier "m" may be sufficient to scale an estimated time for the dominating step to the total fabrication time[1].

---

[1]Note that in this report, total fabrication time refers to touch time or value added time only. Non-value added time such as down time and waiting time are beyond the scope of this report.

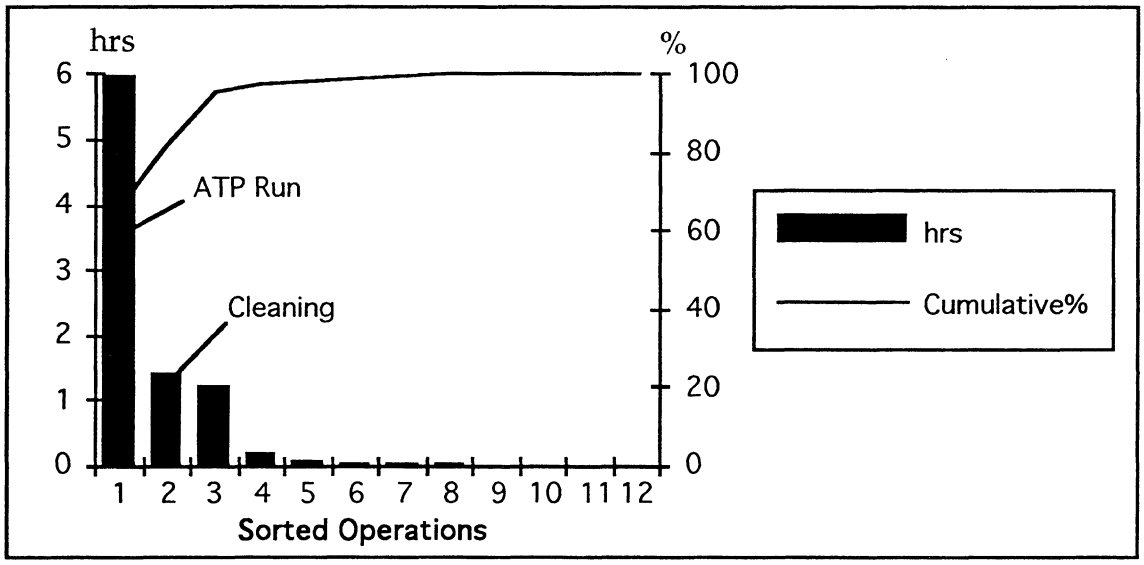

Figure 3-37. Pareto chart of process times for Automated Fiber Placement (AFP).

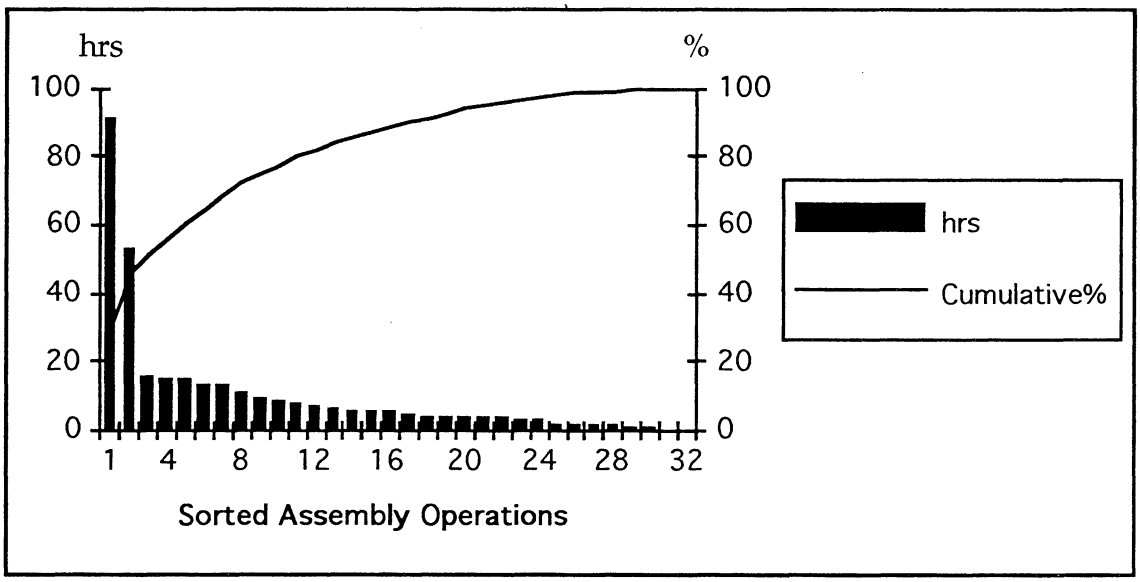

Figure 3-38. Pareto chart of process times for composite assembly.

For example, Figure 3-39 shows a correlation of the sum of all other hand lay-up process step times (apart from lay-up time) with the lay-up time step for the 240 parts of different shapes and sizes shown in Figure 3-28. In this example, the time contribution from the other process steps correlate closely with the lay-up time step. Therefore, for the purpose of rapid estimation, the total time can be estimated by scaling from the lay-up step alone using the multiplier, m, i.e.,

$$t_{\text{total}} = \text{m} \bullet t_{\text{lay-up}} \ . \tag{3.126}$$

In general, the total fabrication time can be classified into

$$t_{total} = t_{most\ dominating} + t_{2nd\ most\ dominating} + \Sigma t_{for\ other\ steps} \quad . \tag{3.127}$$

And if the total fabrication time is scaled from the time for the most dominating step

$$t_{total} = m \bullet t_{most\ dominating}, \tag{3.128}$$

the multiplier m is thus equivalent to

$$m = 1 + \frac{t_{2nd\ most\ dominating}}{t_{most\ dominating}} + \frac{\Sigma t_{for\ other\ steps}}{t_{most\ dominating}} \quad . \tag{3.129}$$

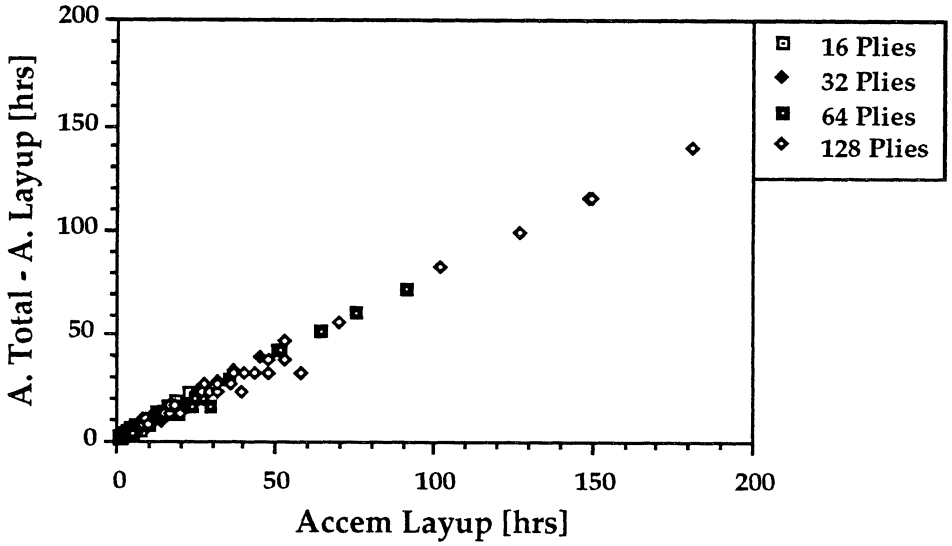

Figure 3-39. Correlation between time for the most dominating process step and the total times for hand layup.

As indicated in Equation 3.129, this multiplier requires a-priori knowledge of the times for other process steps. The most important finding attributed to the "vital few and trivial many" may, therefore, be in the observation that the process step related to $t_{most\ dominating}$ warrants the greatest attention in developing design cost relationships and seeking cost credibility for new processes.

3.5.2 Learning Curve Effects

This and the following section discuss the origin of the learning curve, its implication on process changes, and its potential for misapplication as power law size scaling. In this section, the basic idea of a learning curve will be presented together with the underlying assumptions. This will be followed by two examples illustrating the utility and limitations of the learning curve. Next, some of the problems and pitfalls of blindly applying the learning curve will be discussed.

3.5.2.1 The Principles Behind Learning Curve

The "Learning Curve" or "Progress Function" has its origin dating back to 1936 in the paper "Factors Affecting the Cost of Airplanes" (ref. 19) authored by T.P. Wright, who started studying the variation of airplane production cost with quantity in 1922. The premise of the learning curve is that the cost required to fabricate a part decreases as its production volume increases. The main explanations for this phenomenon are that humans learn and get better at doing repetitive tasks, and that there are economies of scales for large production quantities. To quote from Wright's original paper (ref. 19):

> "The improvement in proficiency of a workman with practice and particularly if time studies for economy of motion are made, is well known. This applies particularly in assembly operations but also holds for other types of work. It may also be anticipated that there will be less changes to disconcert the workman as the quantity increases. Another factor is the greater spread of machine and fixture set up time in large quantity production. As previously mentioned, one of the principal factors is the economy of labor which greater tooling can give as the quantity increases. A final factor allied to the one last mentioned, is the ability to use less skilled labor as more and more tooling and standardization of procedure is introduced."

Figure 3-40 shows two examples of learning curves where the labor time (cost) is plotted versus quantity on a log-log grid. The slopes of these curves are the learning rates (75% and 85% as shown). Mathematically, the average labor time per unit can be expressed as

$$t_N = t_1 N^{-\alpha} , \tag{3.130}$$

where t_N = average labor time per unit
t_1 = labor time for the first unit produced
N = number of units produced
α = constant (as defined in Equation 3.133 below).

Accordingly, Equation 3.130 can be rewritten as

$$\log t_N = \log t_1 - \alpha \log N . \tag{3.131}$$

The self similarity of the learning curve is such that the parameter "percent learning", L, is the factor by which the average labor time in any quantity (N) shall be multiplied to determine the average labor time for twice that quantity (2N), or mathematically,

$$L = \frac{t_{2N}}{t_N} = \frac{t_1 (2N)^{-\alpha}}{t_1 N^{-\alpha}} = 2^{-\alpha} , \tag{3.132}$$

which yields

$$\alpha = \frac{- \ln L}{\ln 2} . \tag{3.133}$$

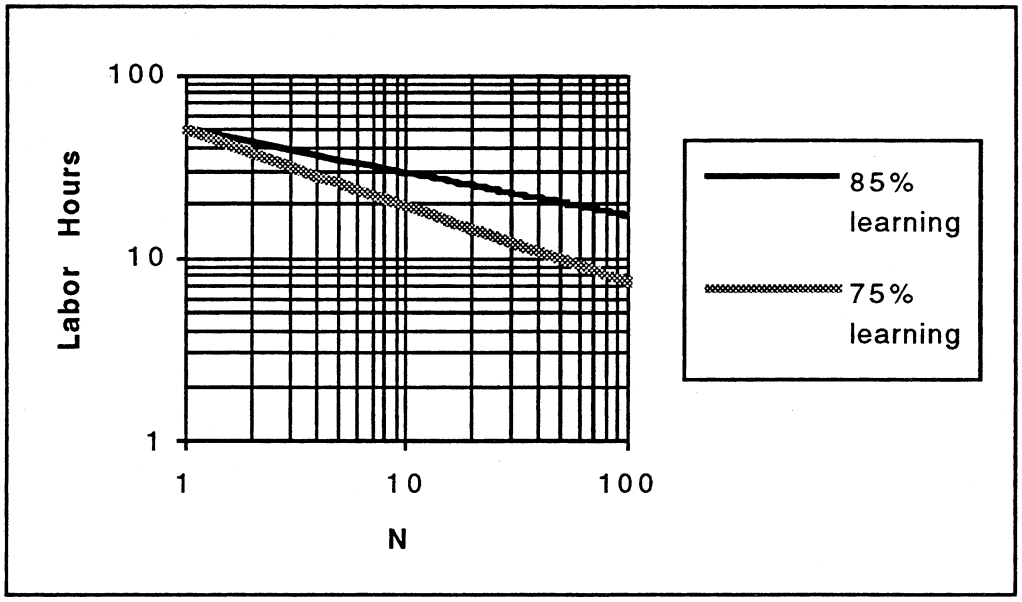

Figure 3-40. Examples of 85% and 75% learning curves.

The most common misconception when applying the learning curve is that direct labor alone accounts for the learning effects (i.e., humans will get progressively better and better at a repetitive task without any changes in the environment or equipment). Furthermore, such improvements are often assumed to be inherent or automatic. However, as pointed out by Tanner (ref. 45), such learning curve effects are not automatic and they often require capital investment. Furthermore, the curve results mostly from management action and management learning, not worker learning. Wright has this to say in his original paper in 1936 (ref. 19):

> "As originally developed, the abscissa of the curve expressed by the above formula was total quantity to be built. It was on this total contract basis that the amount of tooling, on which to a considerable extent the justification of the slope of the curve depends, was determined. It was not contemplated that the curve might be applied indefinitely beyond the original quantity."

Kivenko (ref. 46) went as far as quantifying that direct labor alone is only responsible for about 25% of the learning effects. Another 35% derives from writing and issuing logistics paperwork (e.g., orders, blueprints, etc.) which are indirectly related to management. The remaining 40% is directly attributable to management and engineering functions like supervision, planning, and tooling specification. Therefore, about 75% of the learning effect in manufacturing may not be related to direct labor learning.

The following factors should be kept in mind when using the learning curve to predict a decline in unit cost as cumulative output increases:

(1) job familiarization by workmen, which results from the repetition of manufacturing operations,

(2) general improvement in tool coordination, shop organization, and engineering liaison,

(3) development of more efficiently produced subassemblies,
(4) development of more efficient parts supply systems,
(5) development of more efficient tools and fixtures, and
(6) improvements in the manufacturing process itself.

Keeping in mind it was written in 1936, the quote below from Wright (ref. 19) clearly illustrates the discussion above :

> "The operation of welding, however, was one which in large quantities could not progress in time saving beyond a certain point. The chief gain, therefore, in reducing production costs was in the use of better tools and fixtures rather than anything inherent in the construction which lent itself to progressively cheaper fabrication in large quantities. Riveting is also extremely expensive at the present time but is sufficiently better adapted to tooling and further developments in automatic riveting machines so that for large quantities in the future it holds good prospects of being accomplished economically."

In summary, one needs to be constantly aware of the various assumptions of changes and process improvements implicit in the learning curve. As aptly pointed out by Dutton, Thomas, and Butler (ref. 47), the use of learning curves requires a-priori prediction of anticipated improvements. Data showing that such predictions have been prone to high (and costly) error rates is not surprising given the extreme and often unexplained variation in progress patterns. Furthermore, analysis of airframe production during World War II revealed significant disparity in the rates of improvement for different model-facility combinations. In addition it was also found that fitting progress curves to the past performance of a facility in order to predict its future performance resulted in high margins of error in labor costs.

3.5.3 Power Laws

Application of the learning curve to power law size scaling will be discussed in this section. In particular, the similarity and differences in size scaling between the first order model described in Section 3.2 and the power law will be described. Subsequently, trends in the power law model will be explained and incorporation of learning curve effects into the model will be illustrated.

As discussed in Section 3.2.7, the widely used standard to approximate the dynamic function $f_d(L)$ is the power-law curve, obtained from curve fitting data with a straight line on log-log scales yielding

$$t_d = f_d(L) = AL^r;\ 0 < r \leq 1 \quad . \tag{3.134}$$

This section presents the two most plausible sources for power law size scaling: i) results using weight as the fundamental unit to measure labor output of "surface" manufacture, and ii) a direct translation from learning curve by treating the size or extent of an operation as a surrogate measure for quantity. Arguments can be made for which the former should be based on linear dimension squared. In any case, it will be shown that

the power law size scaling can be explained with the proposed first order model, and that the learning curve effects can be easily incorporated into the process parameters τ and v_o.

3.5.3.1 Derived Using Weight as the Fundamental Unit

Weight is often used as the fundamental unit of measure for power law size scaling. This is often done out of convenience, when measuring labor output of some surface type operations, which should have been scaled with area. This argument can be traced back to Wright's report written in 1943 (ref. 20):

> "Previous studies have indicated that variation in size is a positive factor in reducing costs per pound, arriving at almost identical conclusions. It can perhaps be reasoned that labor engaged in production is working on "surface" manufacture, whether wings, tail units or fuselage, and that, therefore, the unit in making estimates of labor output should be based on a linear dimension squared. So many variables would enter into a computation basically using any linear dimensions however, that it appears sounder to use weight as the fundamental unit, modifying the resultant index (which measures output as lbs per employee) so obtained by the inverse ratio of the cube roots of the weights of airplanes being compared. Put in another way, the cost of the airplane, or the total hours per airplane will vary as the weight to the 2/3 power."

For example, if one were to model the time required to clean and wax cars, one would probably correlate the time for each car to the surface area of the car. However, this would require that one has information of all the linear dimensions of all the cars in order to calculate their surface areas. Alternatively, one could also simplify the data requirement enormously by correlating the weight of each car to the time required. Assuming that the cars have roughly the same densities, this latter approach would lead to the results where the time required to clean and wax a car vary as weight to the 2/3 power. Thus, it is not surprising to find that the indices in most power law size scaling relationships are close to 2/3. This is especially true for parametric cost models (as described in Section 3.1.1), where weight is used as the generalized design variable to correlate fabrication time data.

3.5.3.2 Direct Translation from Learning Curve

An alternative source for the power law size scaling can be attributed to the convenience and simplicity of the learning curve which often lends itself to widespread use/misuse. For example, besides using it to project the cost-quantity relationship, the learning curve is often translated into power law size scaling; where the cost or time is plotted against size (such as weight, area, length, etc.) and not quantity. This is based on reasoning that size, or the extent of the operation can be used as a surrogate measure for quantity. However, this is often done without any consideration of the underlying process and equipment changes embedded within the learning curve. As discussed in Section 3.5.2.1 (ref. 47), many studies overlooked adaptation efforts made by indirect labor and technical personnel to improve process design, increase tooling, improve shop organization, and in other ways to reduce direct-labor input. The derivation below illustrates the fact that implicit in a power law model is that the process constantly changes/improves, as reflected by the constantly changing process parameters τ and v_o.

Equation 3.130 gives the average labor time per unit for N number of units produced. Therefore, the cumulative labor time for the total on N units is

$$t_{total} = \sum_{i=1}^{N} t_i = t_1 N^{1-\alpha} . \tag{3.135}$$

Subsequently, substituting λ (e.g., length or area) as the surrogate for N yields the dynamic function $f_d(L)$ of the labor time required as

$$t_d = t_1 \lambda^{1-\alpha} . \tag{3.136}$$

Here, t_1 is the time required for the first unit of measure (such as the first inch or the first inch^2, etc.). On the other hand, the linearized first order model gives the time for the first unit of measure (λ=1) as

$$t_1 = \tau_1 + \frac{1}{v_{o_1}} . \tag{3.137}$$

Substituting Equation 3.137 into Equation 3.136 yields

$$t_d = \tau_1 \lambda^{1-\alpha} + \frac{\lambda}{v_{o_1} \lambda^{\alpha}} . \tag{3.138}$$

Therefore, comparing terms leads to

$$\boxed{\tau_\lambda = \tau_1 \lambda^{1-\alpha}} \tag{3.139}$$

and

$$\boxed{v_{o_\lambda} = v_{o_1} \lambda^{\alpha}} . \tag{3.140}$$

For simplicity, by letting A = t_1 and r = 1-α, Equation 3.136 reduces to

$$t_d = A \lambda^r \tag{3.141}$$

which is essentially Equation 3.134. Differentiating Equation 3.141 yields

$$\frac{dt_d}{d\lambda} = A r \lambda^{r-1} \tag{3.142}$$

Similarly, the linearized first order model and its differential are

$$t_d = \tau + \frac{\lambda}{v_o} \tag{3.143}$$

and

$$\frac{dt_d}{d\lambda} = \frac{1}{v_o} . \tag{3.144}$$

Subsequently, letting λ=1 and equating Equations 3.141 to 3.143 and 3.142 to 3.144 yield

$$\boxed{\tau_1 = A(1-r) = t_1 \alpha} \tag{3.145}$$

and

$$\boxed{v_{o_1} = \frac{1}{Ar} = \frac{1}{t_1 (1-\alpha)}} \quad . \tag{3.146}$$

Equations 3.145 and 3.146 show that the process parameters in the proposed first order model can be derived from the constants in the power law model. However, the more important fact is that, as shown by Equations 3.139 and 3.140, the process parameters clearly scale with size in the power law model. Based on the physical meanings of v_o and τ, the implication is that the process or method changes as size increases. A simple explanation for this effect is that typically a more primitive process, one with lower rate and often smaller setup, is selected for small sizes. However, as the size increases, one is forced to change the method and/or process to achieve economy of scale. Typically, one would change to a more sophisticated process with higher rates but often with a larger setup. An analogy for this is cleaning a table by hand (low rate and small setup) and setting up a vacuum cleaner to clean the floor of a big room (high rate but larger setup).

For example, take the lay-up of 3 inch wide prepreg. The dynamic component of the time required to lay down a strip of length L is given by ACCEM (ref. 13) as

$$t_d = 0.0014\, L^{0.6018}, \tag{3.147}$$

where t_d is in hours and L is in inches. The graph of Equation 3.147 is shown in Figure 3-41. This graph also shows the linear first order model (Equation 3.143) with different process parameters τ and v_o in different regimes (see Table 3-6). The set of parameters listed in Table 3-6 were determined using Equations 3.139, 3.140, 3.145 and 3.146.

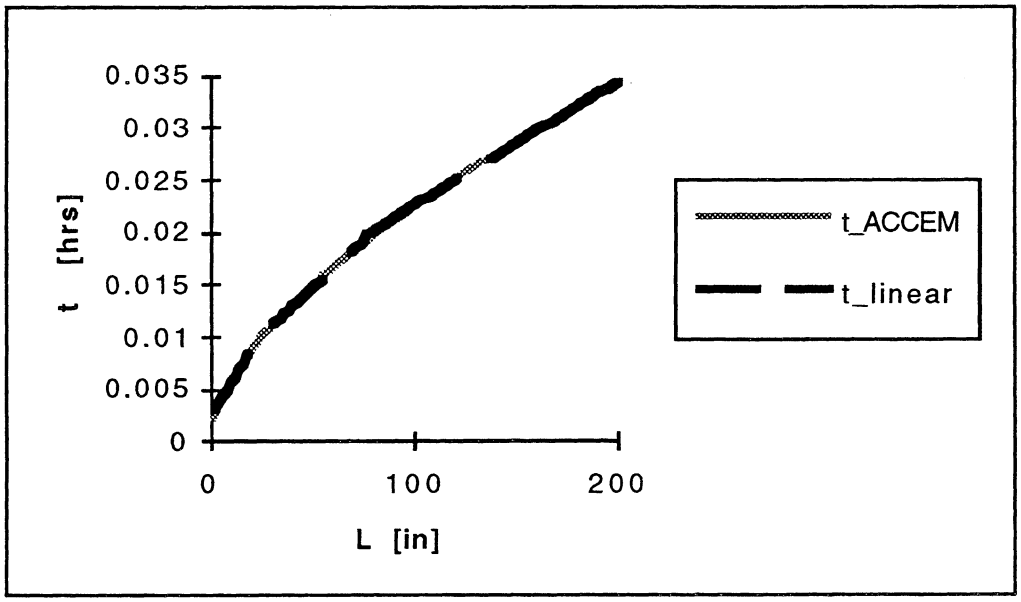

Figure 3-41. Comparison of size scaling based on power law learning curves and the linear first order model using different τ and v_o (Table 3-6) for process changes.

The changes in process and/or equipment which may be implied by the power law size scaling can be explained with the linear first order model and changing process parameters. As listed in Table 3-6, both τ and v_o increases as size (in this case, length) increases, though at different rates. One can imagine the following scenarios; for $L \leq 25$ in. the prepreg is relatively short and is probably laid down by one person. However, longer plies would probably involve two persons (longer time constant for coordination) to aid in positioning the prepreg and allow for higher lay-up rate. For plies in excess of 75 inches, one would probably use a ply transfer tool (increasing the time constant) to allow for further improved lay-up rate and quality.

Length [in]	τ [hr]	v_o [in/hr]
$L \leq 25$	0.00255	3245
$25 < L \leq 75$	0.00587	5636
$75 < L \leq 200$	0.0108	8431

Table 3-6. List of different τ and v_o to reflect changes in process and/or equipment to lay-up 3 inch wide prepreg.

Therefore, unlike the proposed first order model, one can argue that power law scaling dictates that the process is constantly being changed and optimized to minimize the time required. However, this is only possible within physical limits and resource constraints. Hence, care should be taken to ensure that the implied process changes and improvements are indeed realistic and achievable. This is especially true given the popularity of the power law size scaling relationships in process based models (see Section 3.1.1). Using the theoretical framework proposed in Figure 3-4, it may be more desirable to maintain and update design cost relationships as the process improves.

3.5.3.3 Adding Learning Effects to the First Order Size Scaling Model

A major benefit of the first order scaling model comes from the physical and objective interpretation of the dynamic time constant, τ, and steady state velocity, v_o. Most values presented for these coefficients assume that the processes have matured and learning effects have diminished to a second order influence. This section will illustrate how learning effects can be easily incorporated into the proposed model for new and evolving processes; assuming that the rate of improvements/changes follow that of the learning curve given in Equation 3.130. Such analysis is very useful as it quantifies the required improvement in the process (in terms of the process parameters) to realize a given learning curve benefit. As such, unrealistic improvements are less likely to be assumed.

Accordingly, the proposed model gives the average time to produce a unit of size λ to be

$$t_N = \tau_N + \frac{\lambda}{v_{o_N}} \tag{3.148}$$

where τ_N and v_{o_N} are the average dynamic time constant and average steady state

velocity for producing N units, respectively. Using Equation 3.148, the time required for the first unit is given as

$$t_1 = \tau_1 + \frac{\lambda}{v_{o_1}} \quad . \tag{3.149}$$

Next, substitute Equation 3.149 into Equation 3.130 yields

$$t_N = \tau_1 N^{-\alpha} + \frac{\lambda}{v_{o_1} N^{\alpha}} \quad . \tag{3.150}$$

Thus, comparing the terms in Equation 3.148 and 3.150 leads to

$$\boxed{\tau_N = \frac{\tau_1}{N^{\alpha}}} \tag{3.151}$$

and

$$\boxed{v_{o_N} = v_{o_1} N^{\alpha}} \quad . \tag{3.152}$$

This shows that the learning curve effects can be readily incorporated into the linear size scaling model. Implicit in Equations 3.151 and 3.152 are the learning curve effects which assume that the process is constantly being changed and optimized to minimize the time required. As mentioned in the previous section, this is only possible within physical limits and resource constraints. Therefore, care should be taken to ensure that the implied process changes and improvements are indeed realistic and achievable.

3.6 Options Available in COSTADE

The COSTADE cost algorithm is based on a general framework which allows numerous model types to be used. Cost model equation forms and cost coefficients are contained in an input data file, allowing for model changes without recompiling COSTADE. The cost algorithm input file is analogous to a bulk data file for a structural finite element analysis program, where the model geometry, material properties and loading conditions are contained in the input file and not in the finite element analysis program.

Detailed estimating procedures, parametric models, scientifically-derived equations, and other models can be used in COSTADE. This allows the user to select the equations that are most appropriate for their situation, and does not tie COSTADE to one type of cost estimating procedure. All of the equation forms developed in Section 3 can be accomodated. Many modified equation forms, representing future cost model enhancements, can be also used in COSTADE.

Details of the cost algorithm are presented in the COSTADE User's Manual (ref. 48). Automated methods of creating cost input files for COSTADE have been developed as part of the Process Cost Analysis Database, PCAD (ref. 55). PCAD manages cost model data, provides cost input files for COSTADE, performs stand alone cost estimates for a given design, and can have its design variables updated by files generated by COSTADE.

4.0 STEPS TO COST-EFFECTIVE ADVANCED TECHNOLOGIES

Continuous cost assessment of the value of technology has been a crucial part of the ATCAS program. Meaningful cost predictions for new composite technologies considered in ATCAS required inputs from many disciplines that supported the DBT. Figure 4-1 shows how the theoretical framework presented earlier in Figure 3-4 relates to the approach used by the program for technology development. This section will describe the steps taken by ATCAS in pursuit of cost-effective composite fuselage technology.

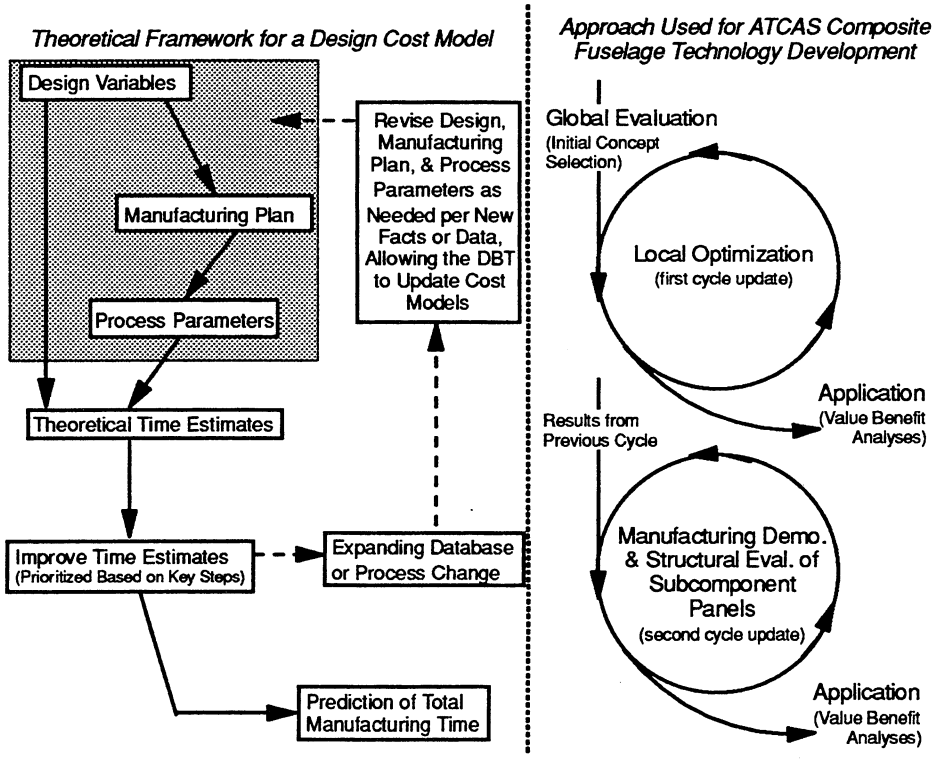

Figure 4-1. ATCAS has pursued the proposed framework as part of DBT cost and weight trade studies.

Section 4 is broken into three parts. In Section 4.1, early ATCAS cost and weight trade studies are summarized as background leading to the initiative to establish a theoretical design cost model. Section 4.2 starts with a detailed description of the ATCAS DBT for concept selection. It also outlines the procedures to formulate cost equations for advanced technologies, including examples for composite fuselage designs and processes. Section 4.2 ends with an overview of the recommended stages for cost method and database development. Section 4.3 describes applications for a design cost model from technology development through final design definition for production.

4.1 Background for Design Cost Model Initiative

The shaded box in the upper left corner of Figure 4-1 shows the data needed to make time estimates within the proposed theoretical framework. This information is updated by a "cycle" that expands the database as schematically shown by boxes which are linked by dashed lines. One may imagine the need for numerous cycles to continuously update the cost estimate and supporting database during technology development, approaching production. As illustrated, at the bottom of the theoretical framework in Figure 4-1, total manufacturing time predictions may occur to support applications during any cycle. Section 4.3 will help illustrate this further with specific examples of applications.

4.1.1 ATCAS Approach in Pursuit of Composite Cost Savings

The ATCAS approach described on the right side of Figure 4-1 includes two cycles that have been active in the program since 1989. The first cycle started with cost and weight trades (global evaluation) for differing design and manufacturing concepts. The purpose of these initial trades was to select a single concept for more rigorous studies (local optimization). The second cycle continued to expand the database with manufacturing trials and structural evaluation of subcomponent panels having representative process and design details. Figure 4-2 shows relative timelines for global evaluation and the two cycles used to update the database. Note that the database and design cost model were established by the middle of the first cycle, and then continuously updated at the end of each subsequent cycle.

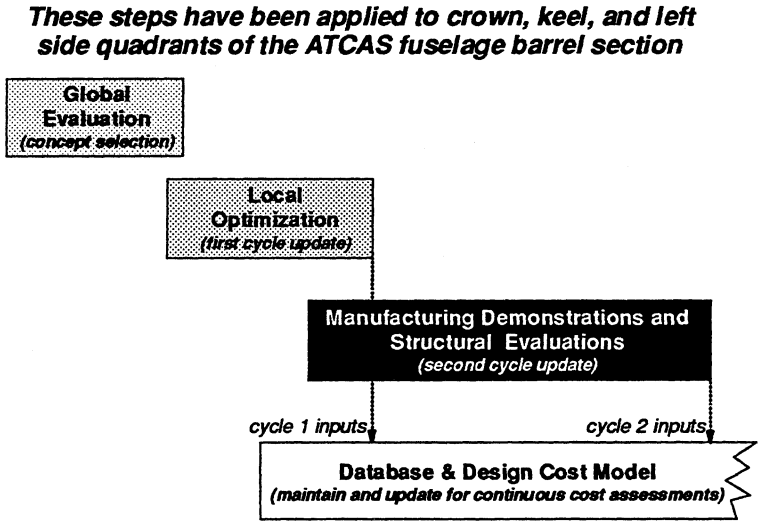

Figure 4-2. ATCAS timelines applied during Phase A and B technology development.

The DBT approach used by ATCAS for global evaluation and local optimization was established at the start of the program. It was first documented in work performed for

the crown quadrant (ref. 4). This approach has evolved since the start of the program. Figure 4-3 shows the steps currently recommended to be used in global evaluation.

During the step described in the first box shown in Figure 4-3, several DBT meetings were held to select a limited number of concepts for rigorous cost and weight assessment. Activities shown in the second and third boxes were used to compile the design and manufacturing information needed to make credible cost estimates. Much of the work in these two steps occurred simultaneously, rather than sequentially as implied by Figure 4-3. Finally, cost and weight analyses were performed for each concept, providing results used by the DBT to select a single family for more detailed study. Over the course of ATCAS, the last step evolved to include potential and risk analyses that gave better definition of the cost and weight space for a given design family.

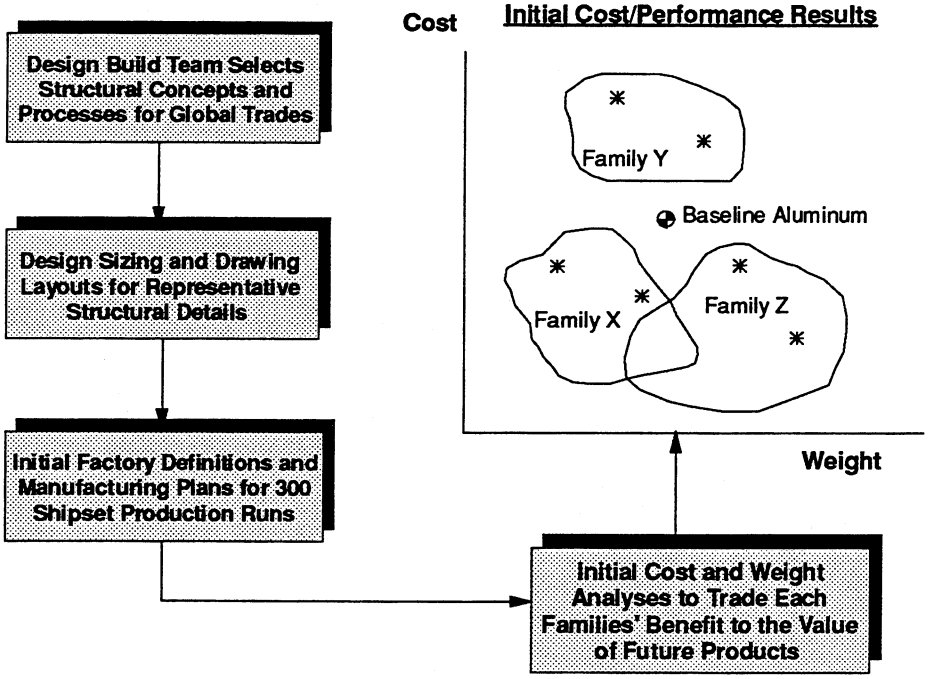

Figure 4-3. ATCAS global evaluation studies.

Figure 4-4 shows how the concept of "design families" was derived by a 1989 ATCAS DBT. It originated in the pursuit of composite design and manufacturing concepts that have the potential cost savings for transport fuselage applications (ref. 4). Appendix D shows the design families which were defined by the DBT to support global evaluation.

As shown schematically in Figure 4-3, each design family is thought to span a unique optimum range in the cost and weight space. This rationale relates to specific design criteria and manufacturing processes suitable for a given family, as well as the load and configuration constraints imposed by specific applications. Each design family was considered during initial DBT meetings for crown, keel, and side quadrants. However, the only families selected for global evaluation studies were B, C, and D (refs. 4, 49, 50). Although global evaluation has focused on quadrants, a full barrel sandwich design concept (Family G) remains an option for ATCAS due to the high cost savings potential.

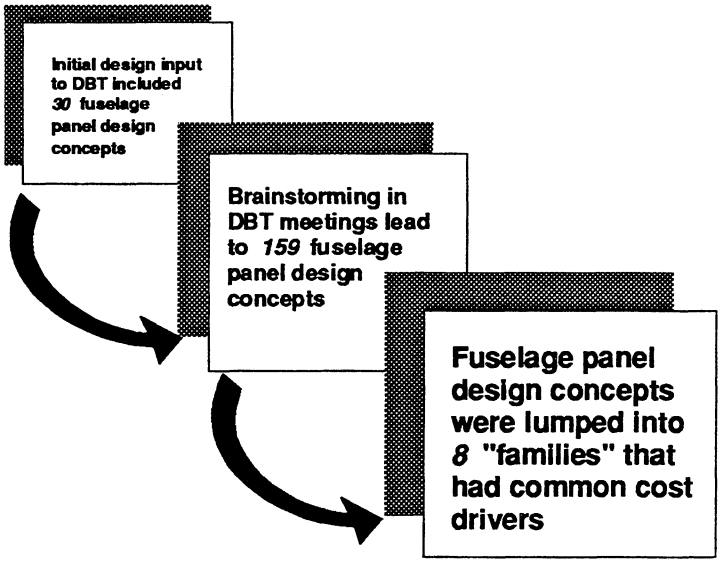

Figure 4-4. Design concepts identified in initial ATCAS DBT efforts were classified into 8 families.

Figure 4-5 shows that the time for global evaluation increased for each subsequent ATCAS quadrant. Despite longer timelines, the number of concepts considered for each quadrant decreased from crown to keel to side. This was directly related to the increased structural design complexity and additional manufacturing steps inherent with keel and side panels. For example, keel and side quadrants are affected by cutouts, increased part counts, and numerous attachment details (floor, bulkhead, and systems) that make them more difficult to design and analyze than the crown. Note that the side quadrant took longer than the keel primarily due to the passenger door cutout and a large area size difference (i.e., the keel quadrant is a 34° segment and the left side quadrant is an 113.5° segment, as will be discussed in Section 5.1.1).

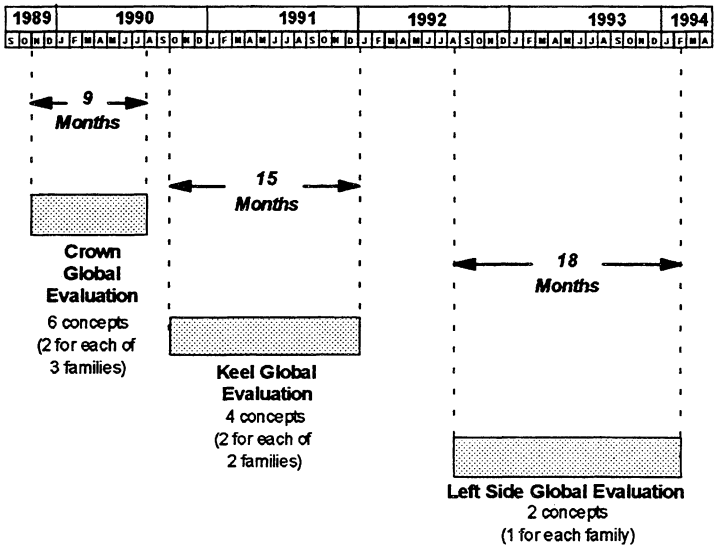

Figure 4-5. Global evaluation timelines for ATCAS quadrants.

Global evaluation has proven to be a very labor intensive DBT effort, involving team members from most technical disciplines that support ATCAS. These included design, structural analysis, materials & processes, industrial engineering, manufacturing, quality control, and finance. Figures 4-6 and 4-7 show milestones from the schedules used to complete global evaluation studies for the crown and side quadrants, respectively. These figures also show statistics for the manhours spent, helping to quantify efforts applied to the global trade studies. In comparison to the crown, about twice the manhours and time were spent in side studies that evaluated two-thirds less concepts (i.e., two versus six).

Much of the DBT efforts shown in Figures 4-6 and 4-7 were spent generating design and manufacturing data that was essential to make credible cost and weight assessments for each concept considered in the trade. The necessary design and manufacturing data was not readily available for many of the new composite technologies pursued for their cost savings potential (i.e., those labeled on pictorial inserts in Figures 4-6 and 4-7). For example, the factory layout and manufacturing sequence had to be defined for composite fuselage parts that used processes not currently in production for any aircraft structure. In many cases, structural sizing efforts also required the development of suitable stress analyses for fuselage loading conditions and innovative design concepts (e.g., pressure pillowing assessments of bonded frame elements). Cost analyses also took considerable time because the lack of data for newly defined processes required estimates based on a physical understanding of the process rather than accounting practices. Section 4.2.1 will give a complete description of rigorous efforts leading to concept selection.

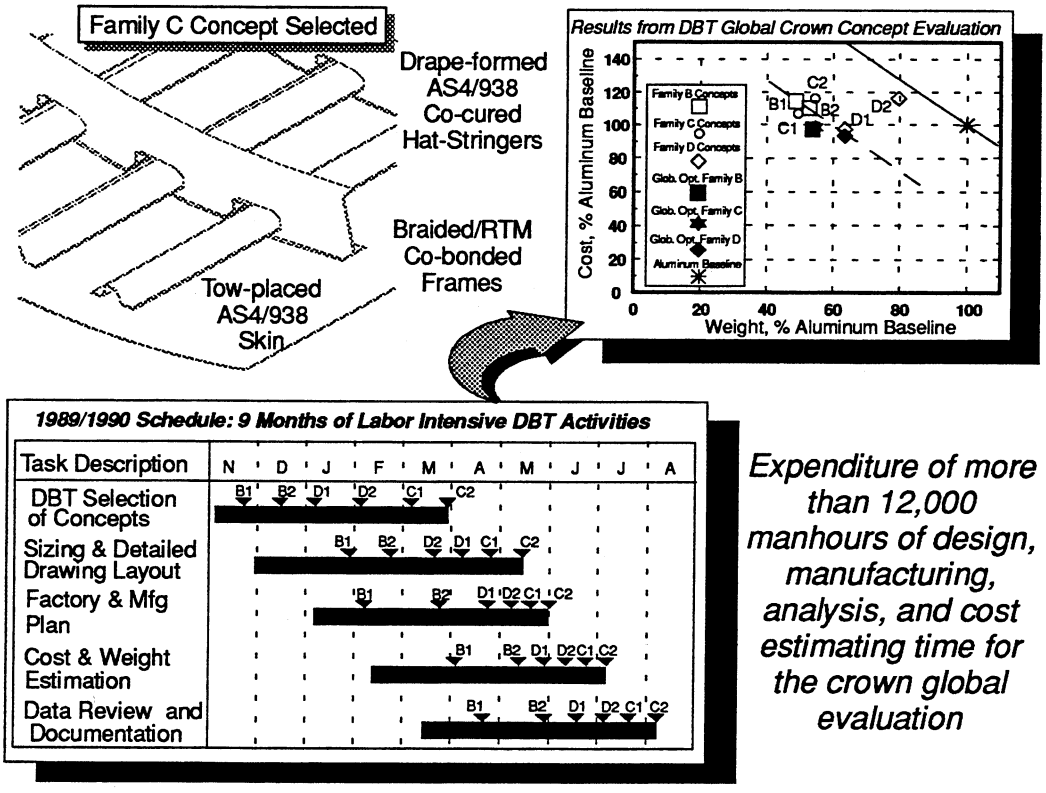

Figure 4-6. Timelines and results from crown global evaluation.

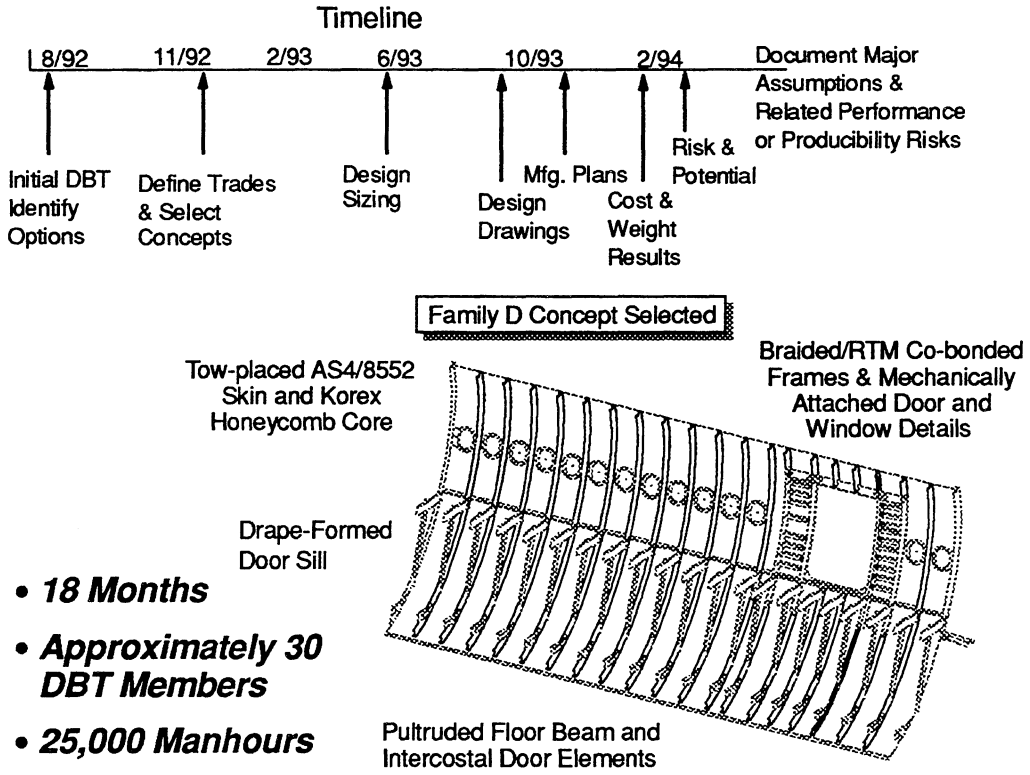

Figure 4-7. Timelines and results from side global evaluation.

The combined technical and cost insights derived in global studies have generally lead the ATCAS DBT to accept greater risk in development only when it is justified by an increased potential value to a product. Perhaps more important than the rigorous cost and weight results that came from global evaluation, was the improved communication between design and manufacturing disciplines that came while generating data for candidate concepts. This interaction was crucial to the team integration needed in subsequent development tasks. Other benefits from global trade studies included the identification of technical issues, cost centers, and design drivers for the selected concept. These insights helped plan for the next stage of development - local optimization - which yielded further design and manufacturing integration.

A team approach that followed the theoretical framework identified in Figure 4-1 for each quadrant helped ensure the expanding database benefited subsequent cost and weight trades. In some cases, the team's confidence in resolving structural or manufacturing issues for one quadrant helped them select concepts in other quadrants. This was the case in selecting a sandwich design over a stiffened-skin concept for the side quadrant. Confidence arising from the first cycle of sandwich keel development, combined with concerns for the added cost of a skin/stringer design with bolted frames, helped the side DBT make its choice.

Figure 4-8 shows the steps currently recommended for use in local optimization. Manufacturing trials are used to assess key process steps, provide structural test articles,

and update the cost database. The combined cost, manufacturing, structures, and maintenance databases are used to update local design details and manufacturing plans. Design cost equations for selected process steps have also been established to support this refinement. In fact, the phrase "local optimization" relates to the design cost analyses used to seek an optimum area in the cost and weight space. The first example of this, which came during ATCAS crown studies, is given in Section 4.1.2.

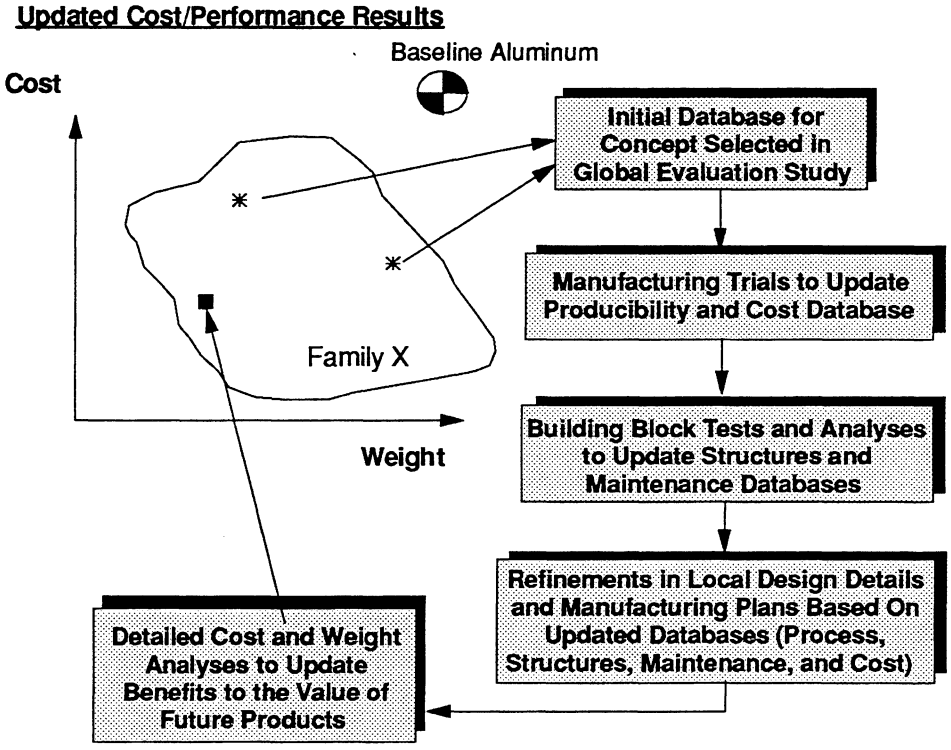

Figure 4-8. ATCAS local optimization studies.

The data collected during local optimization ultimately helped to define subcomponent panels which were fabricated and tested in a second development cycle (referred to as "manufacturing demonstration and structural evaluation" in Figure 4-2). This second development cycle also followed steps similar to those identified in Figure 4-8. Each successive level of development used to expand the database would likely repeat these steps, but at larger scales of hardware demonstration. Development cycles will blend into specific product definition as the hardware demonstrations used to support the effort are produced at sizes and with design detail (e.g., systems attachments) representative of the functional structure.

4.1.2 Initial ATCAS Cost Equations

The effort required to develop the first design cost equations used in ATCAS represented a breakthrough in communication barriers between different disciplines that supported the DBT. In 1990, a team member from the crown quadrant DBT was given the task of deriving cost equations for the design family and processes selected during global evaluation. This task required synthesis of the data gathered by designers, industrial

engineers, manufacturing specialists, and detailed cost estimators for global cost and weight trades. Many of the design features and process steps were innovative and, hence lacked supporting databases. As a result, the crown design cost equations were derived with minimal data. The multi-functional nature of this task required coordination with each discipline and final approval by the entire DBT. Lack of a theoretical framework or even common vocabulary for a design cost model initially caused communication barriers between team members. It took approximately four months to create and gain DBT approval to use the initial design cost equations in crown local optimization.

Focusing on the Family C design concept chosen for local optimization, individual process step cost equations were determined from a breakdown of the detailed cost estimate. Each process step was evaluated in terms of how it would change as a function of the design details. A design function (i.e., an equation relating several design variables to a single parameter) was selected for each process step equation. The process step equations simply consisted of either 1) the design function multiplied by a proportionality constant (similar to the term including velocity in the linear approximation to the extensive equation form, Section 3.2.3) or 2) a constant (analogous to process delay or setup parameters discussed in Section 3.2.4).

Figure 4-9 shows an example of how design/manufacturing cost relationships were derived from detailed estimating data. The figure includes 1) a list of the processes considered in the crown panel development, 2) a list of the design functions used in the cost breakdown, and 3) an example of how the functions were assigned to each detailed process step. As shown in Figure 4-9, each detailed process step was coupled with the design function that directly affects the cost. If none of the design functions were perceived to have a direct effect, that individual step was assumed to be constant.

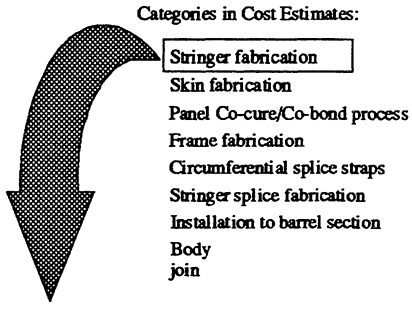

Design Functions:

- f1 = Constant
- f2 = Total stringer weight
- f3 = Number of stringers
- f4 = Total stringer material cost
- f5 = Total skin weight
- f6 = Total skin material cost
- f7 = Number of frames
- f8 = Number of stringer * frames
- f9 = Stringer Trim Parameters
- f10 = Skin Trim Parameters

Example of Stringer Fab Breakdown:

Stringer fabrication	recurring		non-recurring			Related Design Function
	rec hrs	mat'l $	tooling		planning	
			hrs	mat'l $	hrs	
- prepare ATLM	0.05	0.00	--	--	--	Constant (f1)
- layup material	1.55	1000	--	--	--	Total stringer wt (f2)
- identify part number	0.03	0.00	--	--	--	No. of stringers (f3)
- prepare for trim	--	--	--	--	--	Constant (f1)
- trim	--	--	--	--	--	Str. Trim Param. (f9)
- etc ...	--	--	--	--	--	etc ...

Figure 4-9. Design variables and their relationship to the baseline crown manufacturing cost.

The approach described in Figure 4-9 effectively converted design and manufacturing insights of the global DBT into simple functional relationships at the process step level. An added benefit of the functional forms used for each process step, was that terms with common design functions could be easily combined through algebra. For example, the summation of process step cost equations collapsed to a simplified form which predicted crown panel cost as a function of eleven design variables. A representation of this cost equation for the skin/stiffener/frame cobonded crown panel assembly is shown in Figure 4-10. The result was an estimate of how local design variation (e.g., number of laminate plies, stringer spacing) would affect the combined manufacturing cost of processes selected to produce a crown panel.

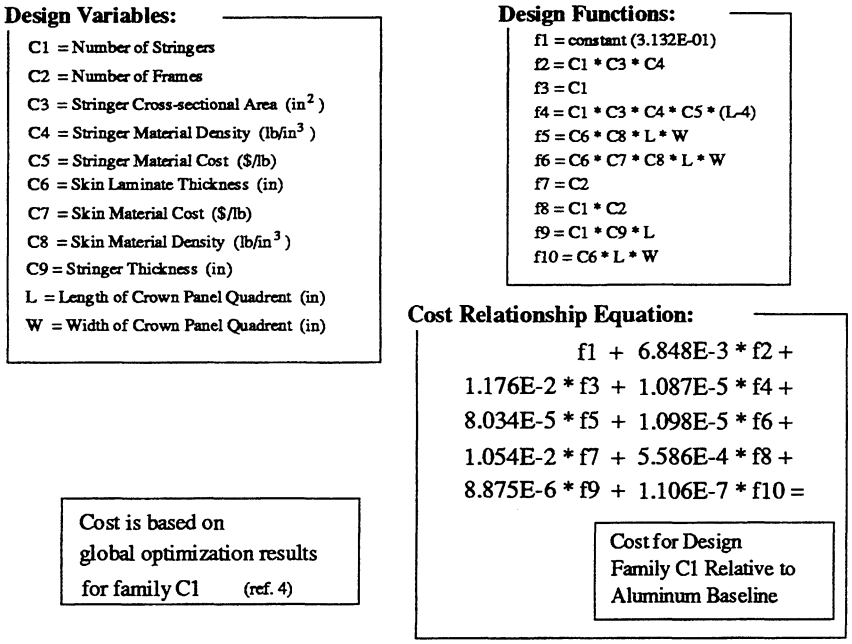

Figure 4-10. Cost relationship used for initial crown local optimization.

Note that Figure 4-10 also has several characteristics which have not been discussed in the text presented thus far. First, the equation has terms based on cost rather than time. As discussed in Section 4.3, process times can be converted to labor costs through simple relationships. Cost estimating groundrules used in the ACT program applied a solitary "wrap rate" which was independent of the process to calculate a cost for recurring labor. Although cost estimates for global evaluation were based on the time to complete a process step, some equation terms in Figure 4-10 embed the combined effect of time and assumed wrap rate in the coefficients. Material costs are also calculated in several equation terms. Finally, costs shown in Figure 4-10 were normalized to the baseline aluminum design cost, further disguising physical meaning in this predictive tool.

The collapsed equation form shown in Figure 4-10 had several advantages and disadvantages. The primary advantage was in its simplicity and ease of use. Since the equation represented the summation of numerous process steps, the total effect of

variations in a given design detail could be quickly accounted for in the crown panel cost. Optimization analyses that combined the cost equation with structural analyses yielded cost and weight data showing the effect of critical design details (ref. 51). For example, Figure 4-11 indicates that stringer spacing was found to have a significant effect on cost.

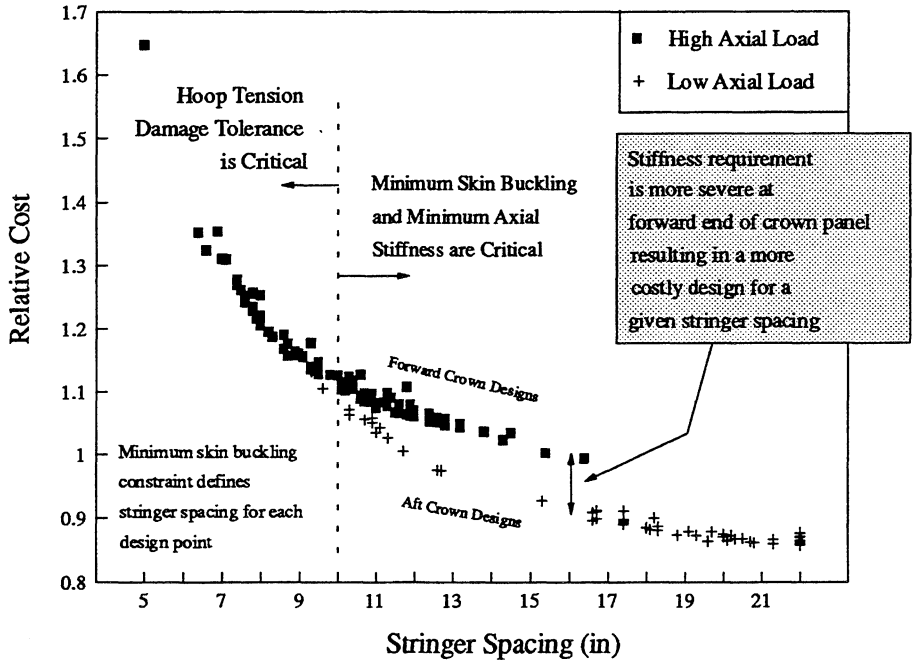

Figure 4-11. Predicted relationship between stringer spacing and crown panel cost from ref. 51.

The percentage breakdown of total crown panel cost shown in Figure 4-12 helps to explain the strong relationships with stringer design variables. Categories shown to be affected by the number of stringers (or stringer spacing) account for 66% of the total cost. In the case of stringer fabrication, labor and material costs are close to directly proportional to the number of stringers. The effect of the number of stringers on other categories may not be directly proportional, but is still significant. For example, in the case of the crown panel assembly, both longitudinal and circumferential splices are included in the cost breakdown. The number of stringers affects the cost of process steps for the circumferential splice only. A significant part of the assembly cost is therefore directly proportional to the number of stringers, yet the remaining part is unaffected.

The increased crown panel cost with number of stringers goes beyond the effects of part size and complexity discussed in Section 3. Numerous process steps are affected by the number of stringers; and hence the summed costs yield a more significant effect than considering the stringer fabrication costs separately. As an example, a study considering a range of stringer fabrication costs was conducted, with the results shown in Figure 4-13. It is evident that the original trend to eliminate as many stringers as possible to minimize total crown panel cost is true for stringer element costs varying from 50% to 400% of the original assumptions. For this range, geometrical details of hat stiffeners for

each optimum design point were nearly identical and cost differences directly related to the assumed change in stringer costs. From a geometric standpoint, the most significant variable is stringer spacing, helping to indicate the importance of summed effects.

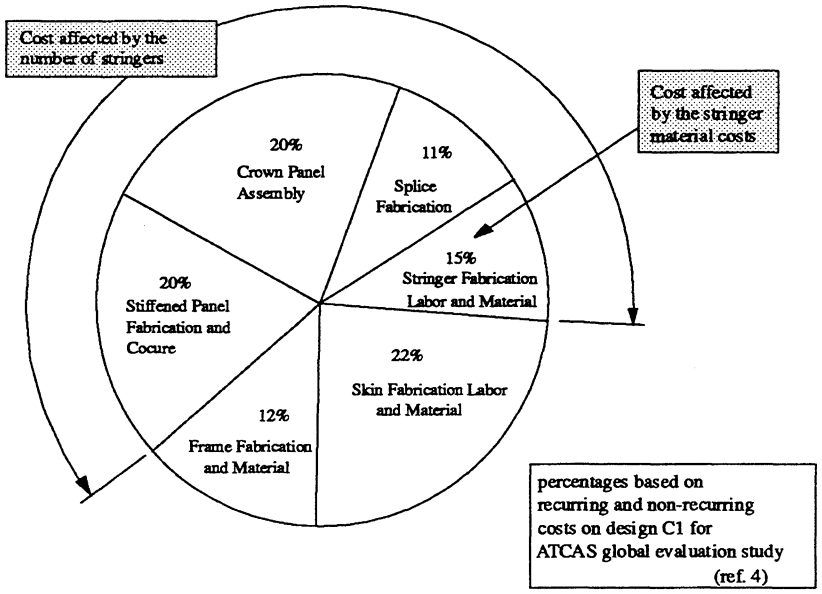

Figure 4-12. Cost breakdown for the composite crown panel design concept selected in global evaluation.

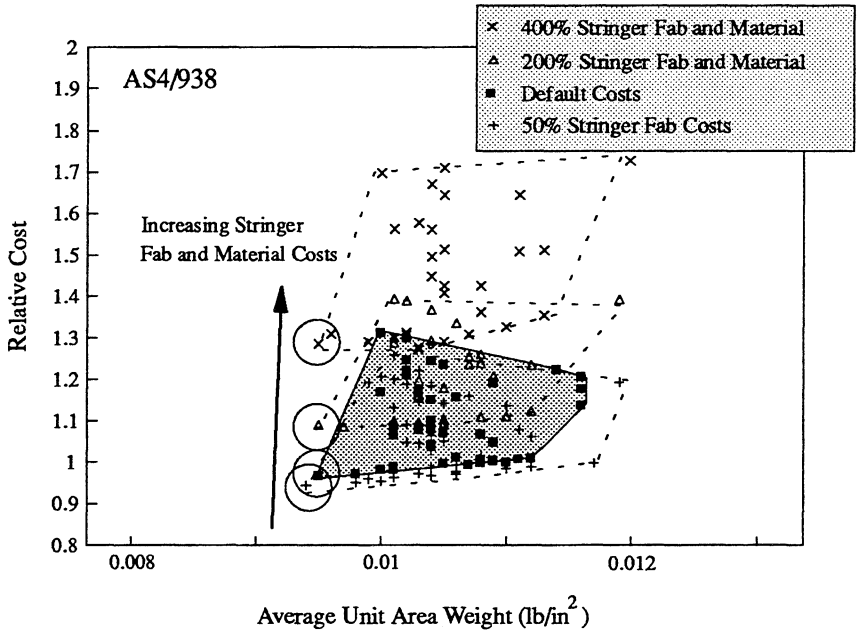

Figure 4-13. Effects of increased stringer element costs on the optimum crown design from ref. 51.

Although the simplified equation form shown in Figure 4-10 provided advantages in synthesizing the effects of a constrained design and process space, it does not provide the visibility desired for making significant updates. The coefficients in the equation shown in Figure 4-10 were valid only for a particular design family, panel size, and associated manufacturing processes. Using this equation, small variations in the structural details from the baseline design were evaluated from a cost standpoint and the major cost drivers exploited. Any major design differences from the global design or any process changes are likely to result in changes to the equation coefficients. At the time, a more generalized cost evaluation analysis was envisioned for future work. This ultimately lead to the additional design cost model developments proposed to NASA in 1991 (ref. 2), including the theoretical basis and results documented in other sections of this report.

4.2 Data to Create and Update Cost Equations

In Section 4.1, early program cost studies were discussed as leading to a modification to the ATCAS contract for additional design cost model development from 1991 through 1995. The additional contracted effort was to generalize the approach pursued by ATCAS in establishing a rigorous design cost framework. Section 3 provided a mathematical basis for the framework established between 1991 and 1995. This section provides a detailed description of other steps in the framework developed by ATCAS, including physical examples of how design cost model equations are first derived and then updated. Throughout the discussion, it is implied that the technology under study is evolving from an initial concept to become production ready. This does not discount the use of the framework for existing technologies, in which a supporting database allows the derivation of equations without large development costs.

4.2.1 Stage 1: Concept Selection

Concept selection provides a starting point for technology development. In this context, the word concept refers to an integrated design and manufacturing idea for a product form. In order to make a good selection, detailed cost and weight trade studies are recommended for a number of alternative concepts. In ATCAS, this stage of development was referred to as global evaluation. As discussed in Section 4.1 (see Figure 4-3), global evaluation not only lead to concept selection but also helped identify technical issues, development risks, and associated payoffs. All are generally needed to justify the additional costs of subsequent stages of development. References 4, 49, and 50 document the global evaluation of ATCAS crown, keel, and side fuselage quadrants, respectively.

4.2.1.1 Importance of Design/Manufacturing Integration

Representative design detail must be identified to select appropriate manufacturing processes and describe the process steps. Iterative DBT interactions become crucial to agreement on the process plan and structural feature which are best-suited for minimizing cost, weight, and technical risk for a given concept. In ATCAS, whenever the solution to this compromise was not immediately obvious, it became desirable to mix/match various combinations of process and design detail between the different concepts analyzed during

global evaluation. For example, braided/RTM frames were traded against compression molded frames for the crown quadrant. After more data is gathered to complete rigorous cost and weight analyses, optimum combinations were applied to all pertinent concepts such that none got penalized for original design or process assignments.

Figure 4-14 shows an example of typical design details considered in ATCAS global evaluation. In this particular case, views taken from the skin stringer side panel installation show details of circumferential and longitudinal splices. These include panel, frame, and splice part numbers; fastener types, grip lengths, and head locations. This level of design detail is typical of production part drawings, and as such provides validity to cost estimates that are based on the drawings.

Figure 4-15 shows an example of typical process steps considered in ATCAS global evaluation. In this particular case, which comes from the side quadrant, selected stages of barrel assembly are shown. This data, showing sequences of floor structure, keel quadrant, and side quadrant installation, supports cost estimates by spelling out the steps used to create assembly features such as those in Figure 4-14.

A combination of the process steps that comprise detail part fabrication and assembly cells will allow definition of a factory layout. For the purpose of initial cost trades, this layout should show the flow of parts between the cells and a preliminary estimate of the number of tools, equipment, and factory floor space needed to produce the product form. The ATCAS studies defining manufacturing cells for a composite fuselage barrel section uncovered a need to apply several unique processes for cost-effective fabrication of different elements of the design. References 52 and 53 describe the processes considered and selected for development in ATCAS.

A good understanding of each process as related to part design details is essential for total cost assessments. Although an accurate cost may not be expected at the time a concept is selected, some understanding of the payoffs and issues is crucial to selecting the right process. Automated processes are typically traded against steps involving touch labor. Depending on structural detail and, in many cases, the quantities of a specific part, automation or manual labor could prove to be optimum for various process steps.

Figure 4-16 shows two optimized processes, having the same unit costs for approximately eighteen units. The solid and dashed lines represent efficient production of small and large quantities, respectively. The objective of each scenario is the same: to minimize the total fabrication costs. However, efficient low rate production may differ greatly in terms of processes and designs from efficient high rate production. An efficient low rate production scenario (and suitable designs) may minimize the amount of non recurring costs (capital, facilities, setup etc.) at the expense of higher recurring costs (recurring labor and materials). This type of tradeoff may be appropriate due to the lower number of production items available to distribute the non-recurring costs over. Efficient high rate productions may have sufficient production items to justify much higher non recurring costs provided the overall result is reduced total costs.

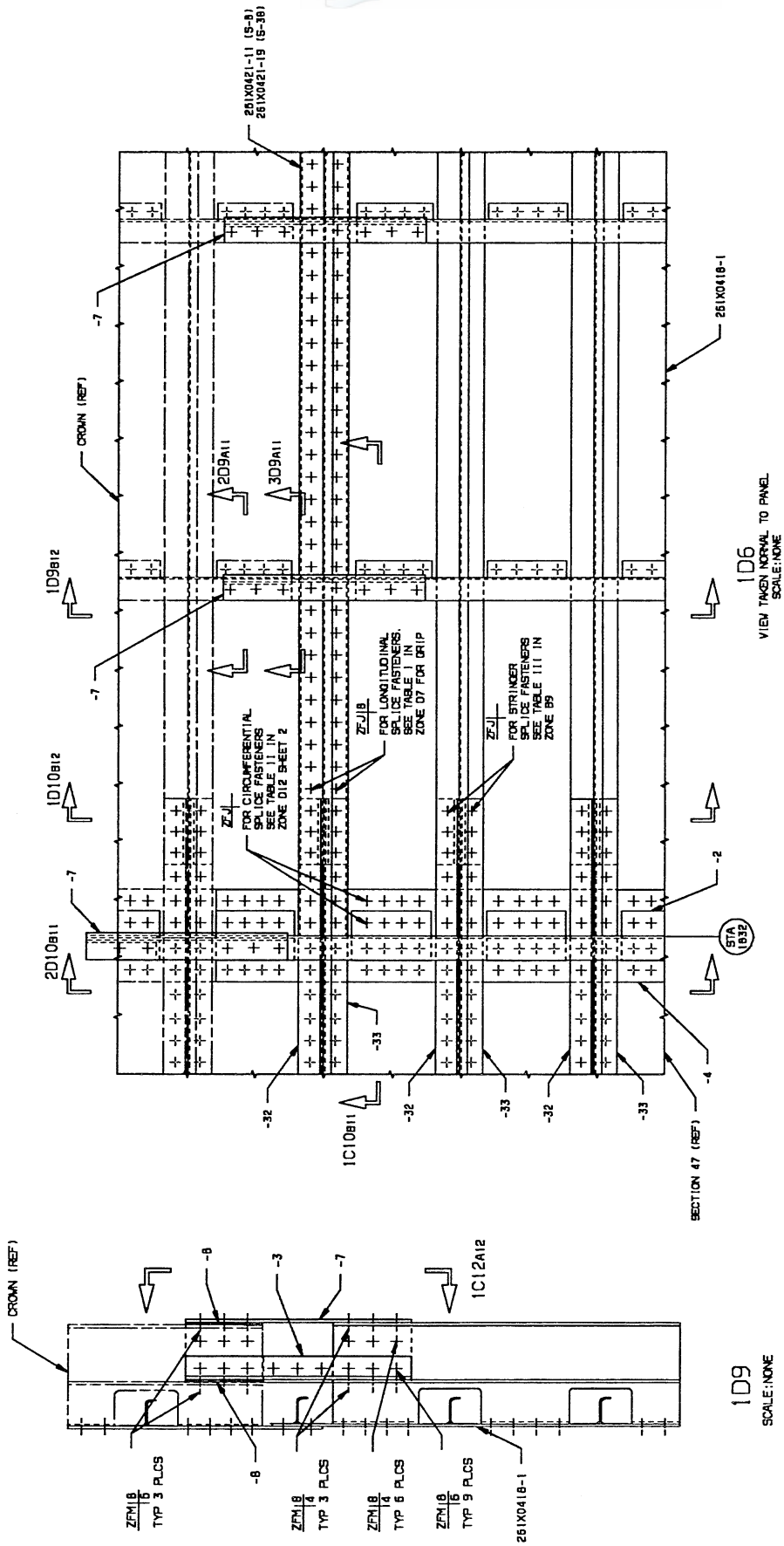

Figure 4-14. Representative design detail from a side/crown quadrant splice.

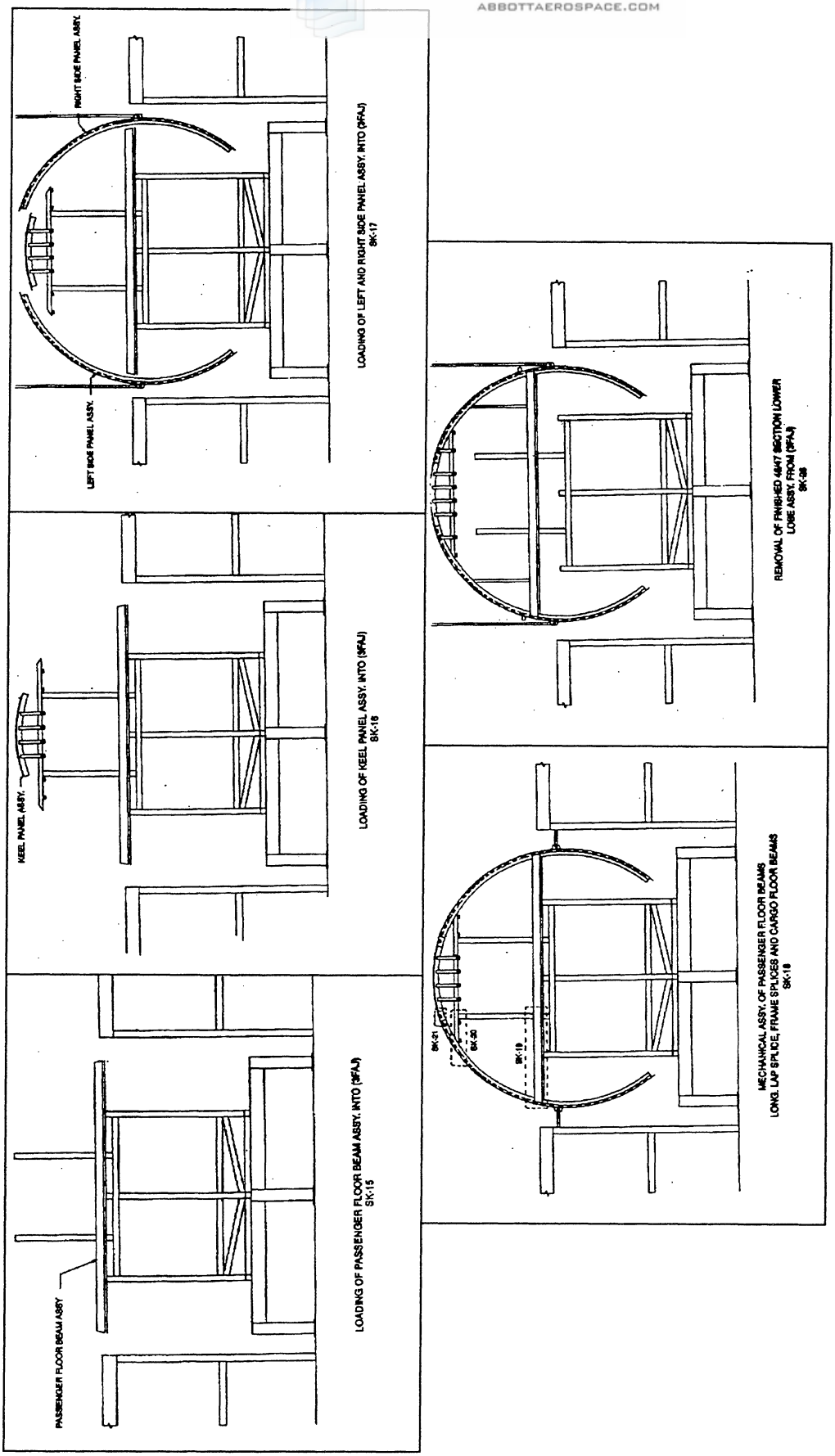

Figure 4-15. Selected Barrel Assembly Process Steps.

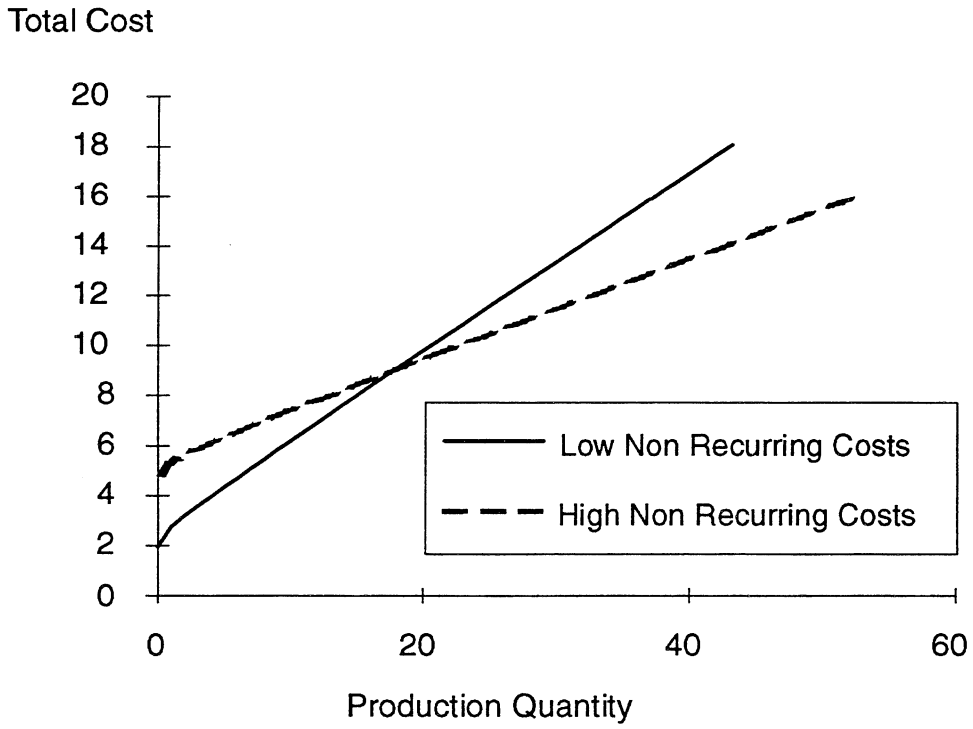

Figure 4-16. The optimum process is often dependent on the production quantity

4.2.1.2 Review of the Works of T.P. Wright (Refs. 19 and 20)

Pioneering work in concept (design and manufacturing process) selection was performed by T.P. Wright to support the need for increased aircraft production for World War II. Wright had identified some of the efficiency trades that occur when selecting processes for differing production quantities. These included:

(1) new facilities (machine tools, plants and buildings),

(2) managements (know how to operate new plants and expand existing organizations without spreading them too thin),

(3) materials (priority schemes and conservation programs to satisfy the competitive needs of many other war industries), and

(4) manpower (increasing the efficiency of available labor and tapping new labor sources).

Since available manpower was limited at the time, Wright identified parameters and compared production facilities in order to optimize the efficiency of the labor force.

Wright related the above arguments to aircraft production and designs for World War 2. Stick, wire, and fabric construction was well suited for quick and cheap construction of prototype or low quantity production machines. In spite of the inherent low costs which this type of construction permits in small quantities, Wright thought that other designs and production methods would be more efficient for increased rates of production.

Semi-monocoque construction, requires to a greater extent, the use of proper tools and fixtures for efficient quantity production and therefore can be relatively expensive for prototypes and small quantities. In very large quantities the costs greatly decrease and indicate a reduction in unit costs. Monocoque construction may be expected to show good results from a cost standpoint when very large quantities are considered. For example, welded steel tubing allows the use of jigs and fixtures (non-recurring costs) which, when any reasonable quantity is involved, permits more efficient production.

From Wright's perspective, maintaining efficient low rate production and design scenarios may not be the best approach even during peace when production rates would be slow. Rather using the most efficient production and design scenario for large quantities, but at low rates may be the better approach from the standpoint of military preparedness. Of course, this insight is tempered by the fact it was derived in the 1930s and 1940s.

4.2.1.3 Initial Cost and Weight Estimates

The credibility of initial cost and weight estimates is strongly dependent on the care taken in integrating representative design and manufacturing details. Conceptual designs that have not been subjected to sizing and configurational constraints can mislead the definition of suitable processes. For example, some composite processes are incapable of tailoring part thickness cost-effectively (e.g., most types of pultrusion); and therefore, lack of sufficient design detail may lead to a poor selection of processes. Similarly, process definitions (e.g., a step-by-step manufacturing plan) must trace the fabrication and assembly of each design detail. Without such resolution, it becomes difficult to make accurate cost estimates (including process times and tooling & equipment quantities) for new concepts.

When a particular design detail or series of process steps represent concepts common to a company's database, then step-by-step information may not be as crucial. For example, analytical or empirical relationships, tables, and data sheets may exist to (1) quickly estimate the size of structural parts, and (2) link critical design metrics to the most expensive process steps. Such databases generally also have specific design constraints and an associated process window over which structural analyses have been validated and the process has been proven to be "production-ready". Credible cost and weight estimates for parts with extensive production history may be made without gathering data for every design and process detail (e.g., see discussions on "cost drivers" from Section 3.5.1).

For the purpose of trade studies, unbiased comparisons are essential. Meetings held by the DBT to discuss details of design and process definition were crucial to eliminating any bias in ATCAS global evaluations. Technical experts will have the best insights on a given manufacturing process or structural concept, but also some prejudice related to their time invested in gaining the specialty. An assessment of overall design producibility requires insights to be blended during DBT discussions. In the end, concept selections are made based on a) cost and weight information, b) supporting data gathered by the DBT, c) team discussions, and d) perceptions on the technical issues that must be resolved in concept development. In cases where there is no clear winner, team leaders and management may have to help force a selection.

Figure 4-17 shows detailed cost and weight results from the ATCAS side global evaluation. This effort, which was performed by an ATCAS DBT over a period of eighteen months, was the last and most labor intensive of the three studies. Factors that made the side quadrant difficult to analyze include: the size of the panel in combination with a variety of loading conditions, integration of the overwing longeron, attachment of cargo floor beams, attachment of the lower foward side panel to the wheel well bulkhead, and the design and analysis of window belt, door cutout surround, and passenger floor structure.

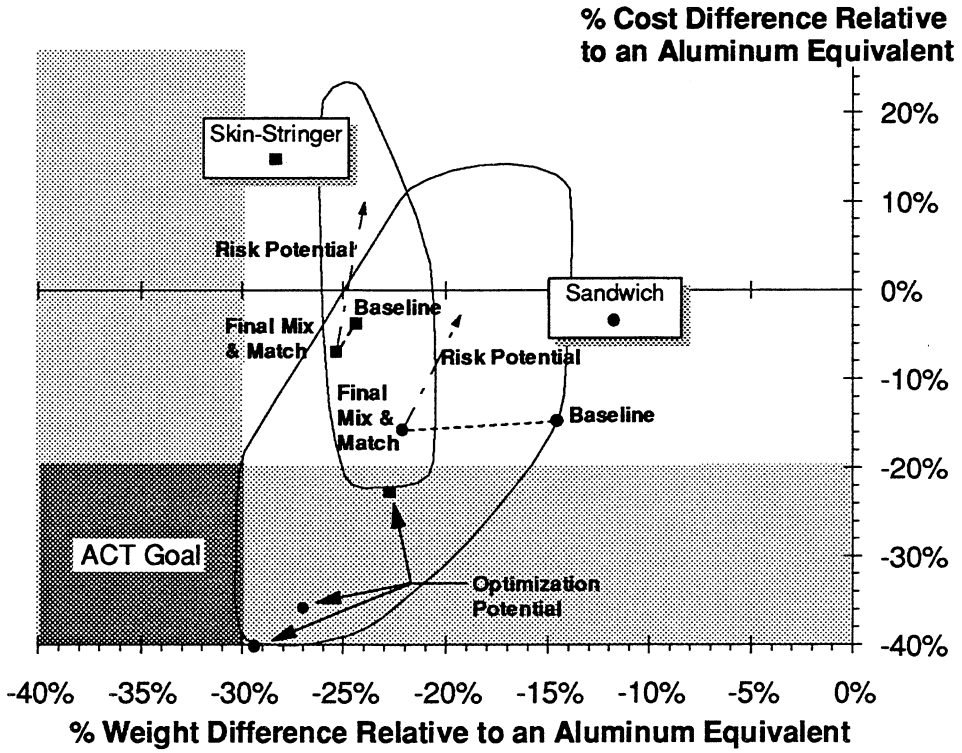

Figure 4-17. The potential and risk of skin-stringer and sandwich concepts for side global evaluation.

The side quadrant panel (33 ft. long by 20 ft. arclength) has an area 3.33 and 1.2 times as large as that of the keel and crown quadrants, respectively. In addition, several different load cases are critical to the design of the side panel, whereas the crown and keel were primarily driven by a single load case. The overwing longeron is a discrete point of load introduction along the forward edge of the side panel and as such is a variable in load path considerations. The cargo floor beam attachments add complexity to the fuselage frame splice. The lower forward side panel is attached to the wheel well pressure bulkhead, also adding complexity. Finally, cutouts in the side panel (windows and doors) add more design complexity and associated effects on processes.

4.2.2 Definition of Functional Forms for Critical Process Steps

Section 4.1.2 describes the approach used by ATCAS to derive initial design cost equations for the advanced processes considered in crown local optimization. At the time of ATCAS crown panel studies, the theoretical framework described in this report had not been established to guide the development and update of cost model equations for new processes. As discussed in Section 4.2.1, the rigorous DBT activities that support concept selection provide an initial step in the theoretical framework for monitoring the costs of new technologies. This section will extend the framework further with discussions on the formulation of initial cost equations.

Early workshops held by NASA, Boeing, and subcontractors for the COSTADE initiative established the goals and requirements for a design cost model. Of foremost interest to the ACT Program, was a theoretical framework for assessing emerging composite technologies with potential manufacturing cost benefits. Such a framework would initially not require an extensive database to perform cost analyses, and hence, has a non-empirical basis. Once the process cost centers and critical design details were identified, then the framework would have procedures to help enhance the database and increase the credibility of cost predictions before implementing new technologies into production. Another key requirement imposed on the framework was that it should not embed logic which violates the proprietary rights of industry involved in developing the cost analyses. This was achieved by treating all company-sensitive data as user input to the model.

4.2.2.1 Key Process and Design Considerations

The first stage of the theoretical framework described in Section 4.2.1 stressed the need for integrating design and manufacturing insight during concept selection. The accuracy of initial cost and weight assessments supporting this stage are dependent on the definition of representative design and process details. For example, material costs and structural weights directly relate to the: (1) material type, (2) part configuration, (3) gages needed to meet loads, and (4) utilization rates for selected processes. Step-by-step description of the manufacture of each design element also provides some indication of the associated process times and factory needs (i.e., floor space, equipment, and tooling). These are related to labor and non-recurring costs, respectively. Data generated during concept selection provides the necessary information to begin design cost equation development.

The designer's cost model, as set forth in ref. 2, consists of cost functions that relate design variables (size, shape, tolerances, geometric complexity, and material properties) to summed recurring material cost and computed labor content. These relationships should be based on independent variables, posed in terms familiar to a designer, and parameters that are mathematically linked to process physics. Experiences gained on derivation, utilization, and update of selected ATCAS design cost equations have been documented in the remainder of this report. A more complete treatise of all the ATCAS process-step cost equations and an associated database software tool can be found in ref. 55. Note that the applicability of the cost equations developed to other problems is tempered by the specific composite fuselage design and process space pursued by ATCAS.

Factory Definition. Development of process-step cost equations requires a factory definition to identify major process centers and resource requirements, and a detailed description of the process steps occurring at each location. In many cases, the number of process steps can provide a qualitative measure of the design complexity and associated fabrication costs. Each process-step cost equation models a relationship between touch labor activities, machine physics, and critical design variables. Equation forms and processing parameters are established by combining an understanding of the process with existing manufacturing and time study databases (see Sections 4.2.2.3 and 4.2.2.4).

Development of the factory begins by identifying the major process cells to be used for a particular design. A process cell typically represents a location within a factory where a sequence of related process steps is performed. A proposed sequence of major process cells selected for the baseline ATCAS fuselage produces the factory flow outline shown in Figure 4-18, and assignment of facilities and equipment to particular areas produces the factory layout defined in Figure 4-19. The next level of factory definition outlines the process steps occurring at each process cell. For example, breakout of steps in the AFP process cell is shown in Figure 4-20.

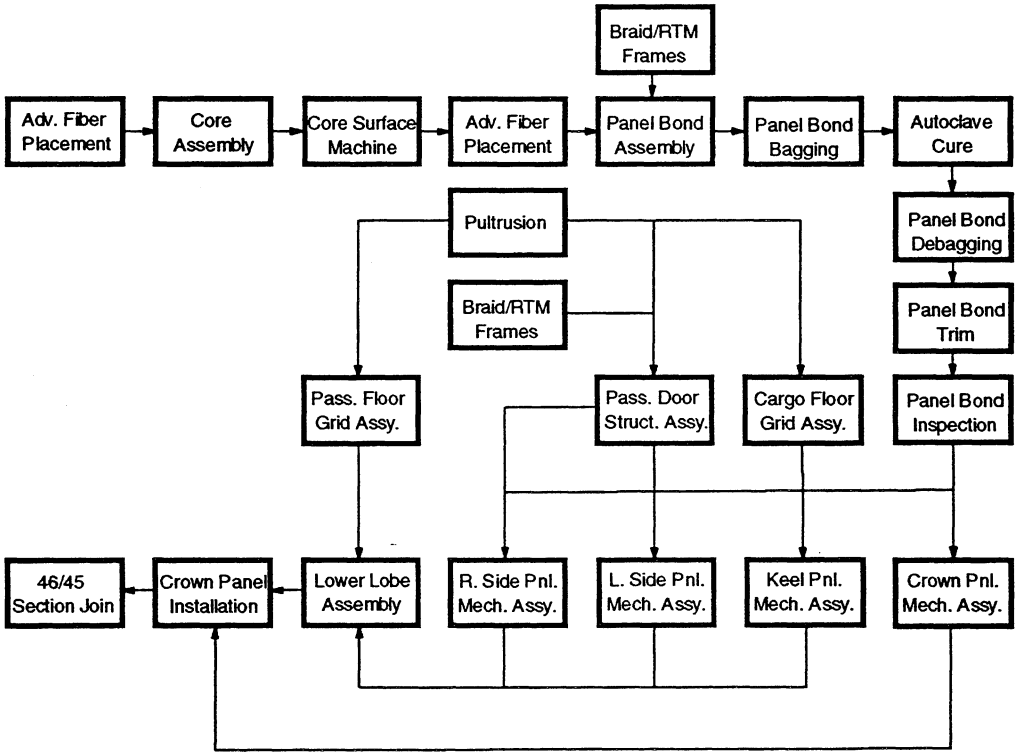

Figure 4-18. ATCAS factory flow outline.

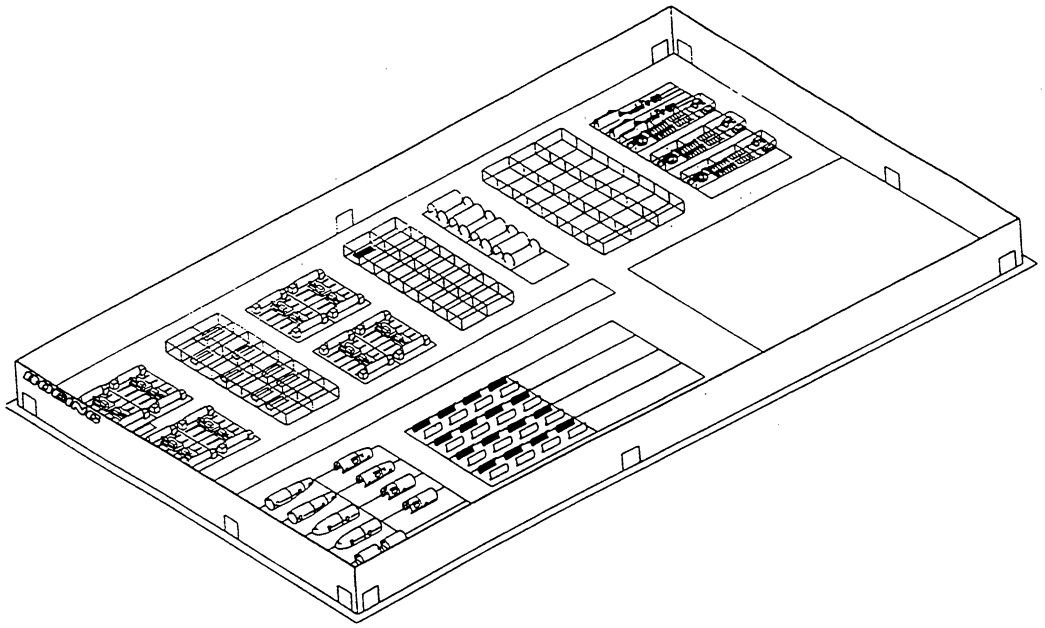

Figure 4-19. ATCAS factory layout.

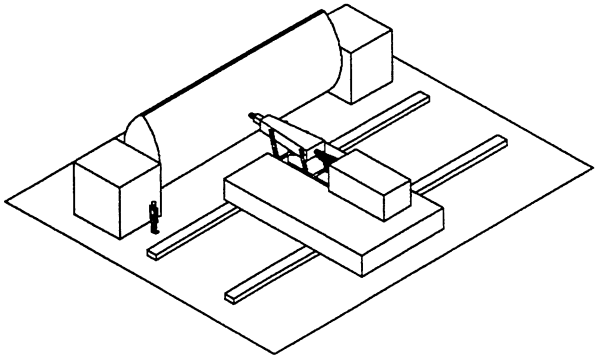

RESOURCE		PROCESS		PART
FACTORY	AREA	STEP	PROCESS STEP DESCRIPTION	PART NUMBER
1	2	10	Identify require items	261X0401-1
1	2	20	Clean OML cure tool surface	261X0401-1
1	2	30	Apply Parting agent to OML cure tool surface	261X0401-1
1	2	40	Hand layup fabric ply over OML cure tool	261X0401-1
1	2	50	Position skin debulk bag	261X0401-1
1	2	60	Debulk hand layed up fabric ply	261X0401-1
1	2	70	Remove debulk bag from skin	261X0401-1
1	3	80	Setup AFP equipment for skin layup	261X0401-1
1	3	90	Layup skin using AFP equipment	261X0401-1
1	3	100	Reload prepreg tow onto AFP equipment as required	261X0401-1
1	3	110	Position OML cure tool into AFP cell	261X0401-1
1	3	120	Transfer skin from winding mandrel to OML cure tool	261X0401-1
1	3	130	Remove OML cure tool with skin layup form AFP cell	261X0401-1
1	1	140	Protect skin on OML cure tool	261X0401-1
1	1	150	Identify skin on OML cure tool	261X0401-1

Figure 4-20. Advanced fiber placement process steps for the ATCAS composite fuselage factory.

Complex interactions between factory flow and design traits continuously change, justifying a need to establish and maintain relational databases that support cost equations. During development, cost equations change rapidly based on design and process refinements and/or an improved database generated from manufacturing trials. As the factory matures over time, cost equations must be updated to guide design development towards efficient use of the available factory. For these reasons, the process-step cost equations were entered into the ATCAS database, herein referred to as the Process Cost Analysis Database or PCAD, in terms of the part definition, manufacturing process, and resource requirements (see ref. 55).

A complete manufacturing plan is needed to generate process-step equations for the entire factory and predict the summed costs. This plan is generally presented as a series of process steps, outlining flow within and between all process cells. The factory area code (e.g. see Figure 4-20) corresponds to a physical location in a company's production system. Resource requirements such as personnel, capital equipment, inventory, facilities, energy, etc., will depend on the combined efficiency of process cells addressing specific design details. Delays or inefficiencies within any cell can have a synergistic effect which may be overcome in time through design change, technology advancement or reallocation of resources.

Critical Design Space. The design space of interest for selected fabrication methods must be established to help bound efforts in developing (a) production-ready processes and (b) design cost equations. Without sufficient design constraint, it is difficult to imagine generic process or cost equation developments achieved in a timely and cost-effective manner. For example, the AFP process would require significant developments to laminate stringer and frame elements in a geometry of interest for fuselage structures. Since AFP was not thought to be suitable for achieving such geometry without additional process steps (e.g., laminate drape forming), ATCAS did not attempt to develop a viable process window. Similarly, the braided/RTM process used to make ATCAS frames was not selected for quadrant skins, and therefore, process developments were limited to curved stiffening element geometry.

As is the case for manufacturing plans and cost equations, design details will also evolve with the supporting database. Efforts to refine the critical design space should, therefore, be performed as part of a technical approach that has been integrated with manufacturing developments and cost assessments. The ATCAS program has pursued such an approach (ref. 5). The PCAD software described above becomes an important tool for DBT communication and technology updates occurring in such an environment.

Examples of design cost equations for the process steps highlighted in Figure 4-20 will be presented in Sections 4.2.3 and 4.2.4. One was developed by modeling the physics of an AFP machine (Section 4.2.3). The other was created by correlating design parameters and time study data to clean an outer mold line (OML) cure tool (Section 4.2.4). Section 4.2.4 also includes a discussion of process trial data correlation with cost analyses for braided/RTM frame fabrication and crown panel bond processes. In order to facilitate a

discussion of the former, the following sub-section will provide an example of the likely design space for fuselage frames which are candidates for the braided/RTM process.

4.2.2.2 Example: Braided Fuselage Frames

To construct a good cost model it is important to first understand the key design variables and process cost drivers for a particular design/process space of interest. Mathematical relationships to quantify the interactions of design variables and process parameters can then be established. These relationships can be updated throughout development and during production based on manufacturing trials and actual production cost data.

The method by which a DBT derives an understanding of the key design variables and process parameters is best inferred through a specific example. Appendix E discusses design and process considerations for the braided/RTM frames pursued in ATCAS. A total of nineteen composite frame design groups were categorized by curvature, length, and gage for wide-body transport fuselage applications. Figure 4-21 shows these and other important braided/RTM frame design variables. Fuselage locations of the nineteen design groups are shown in Appendix E. Descriptions of a candidate process cell for fabricating braided/RTM frame groups, including concepts for tooling and equipment, are also given in Appendix E. As discussed in Section 4.2.4, tooling becomes a very important component of the costs of frames fabricated using the braided/RTM process.

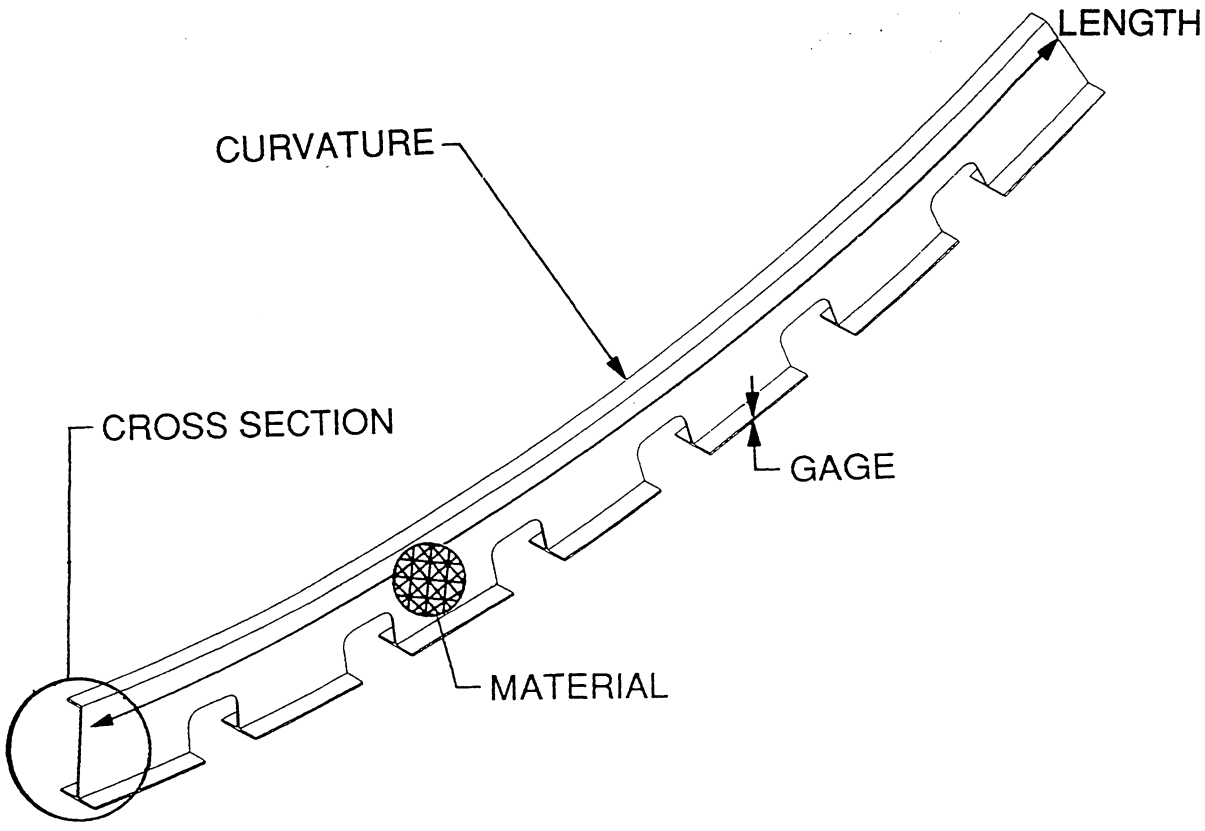

Figure 4-21. Fuselage frame design variables.

Design variables shown in Figure 4-21 are set during different stages of concept development and product definition. Frame length is dictated by manufacturing breaks and cutout locations. Frame curvature variation is largely a function of the optimum balance between aerodynamic design, required passenger capacity, and location within the fuselage. Frame gage is a function of loads, which also depend on location within the fuselage, and manufacturing capability. Frame cross section is influenced by the loads and skin panel design. Frame material selection is driven by design performance goals and manufacturing capabilities.

The effect of skin panel design on the frame cross-section has been found to affect frame fabrication cost in the ATCAS program. Figure 4-22 helps to illustrate this for two design families considered in ATCAS global evaluation studies. In the case of sandwich skin panels, bonded J-frames were selected for development. As shown in Figure 4-22, the frame cross-sectional geometry becomes more complicated for skin/stringer designs. Unlike the sandwich design, the outer frame flange of the skin/stringer design must also be trimmed to "mousehole" the stringer. If damage were to occur or progress into the skin area under the mousehole, a J-frame would fail due to an applied moment. Therefore, an additional frame flange (called an "F" frame in Figure 4-22) is required above the mousehole in a skin/stringer design for the structural redundancy needed to achieve damage tolerance. This added complexity increases the fabrication cost (i.e., braiding, RTM tooling, and mousehole machining) of frames for skin/stringer concepts relative to those for sandwich designs.

Another factor leading to lower costs for the frames used in a sandwich design versus those applied to a skin/stringer is the difference in size (cross-sectional area) needed to meet frame loads in the two concepts. As discussed in ref. 4, sandwich frames are expected to be significantly lighter and have associated less material and labor costs for a braided/RTM process. This relates to the added bending stiffness of sandwich skin panels.

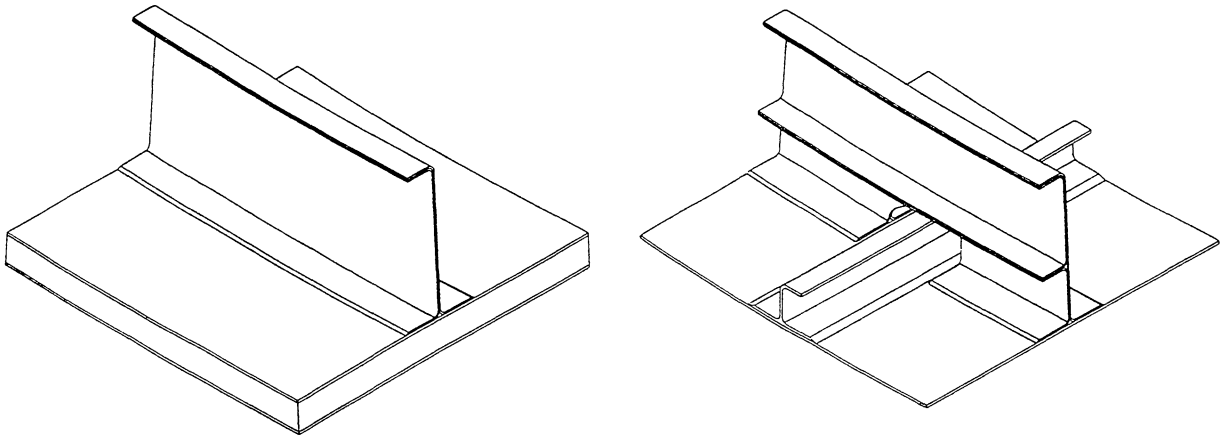

Figure 4-22. Frame cross-sections for different skin panel designs.

Other design details (that are not shown in Figure 4-22) at the stringer and frame intersections for a skin/stringer panel design concept have been found to be prime cost drivers in the ATCAS program. This was true for both bonded frame and fastened frame concepts considered in the crown and side global evaluations, respectively (refs. 5, 50, and 52). As discussed in Section 4.1.2, numerous manufacturing steps are affected by stringer spacing. Many of these relate to the number of frame and stringer intersections. For example, the complexity of inner mold line (IML) tooling aids and bags used to cure the skin/stringer crown panel concept become more complicated with co-bonded frame details. In areas of the fuselage where compression and shear loads become critical (e.g., ATCAS side and keel quadrants), stringer clips may also be required at frame and stringer intersections. These clips help to minimize concentrated peeling stresses due to pressure, compression, and shear load paths in the frame and skin panel attachment near the mousehole. Clips also help to stabilize the frame from rolling due to compression loads.

For purpose of the current discussion, we will focus on the effects of curvature, length, and gage for braided/RTM J-frames used in wide-body transport fuselage applications. In order to consider an F-flange frame concept, either changes to the braided/RTM fabrication process or additional steps to attach (mechanically fastened or bonded) a frame flange would be required. In ATCAS, F-flanges were mechanically attached to crown skin/stringer manufacturing trials.

The number of frames per airplane and associated frame lengths for each of the nineteen design groups defined in Appendix E are shown in Figure 4-23. In addition to the design variables that segregated J-frames into groups, the relative cost of a given frame is strongly dependent on the production quantity, production rate, and part commonality.

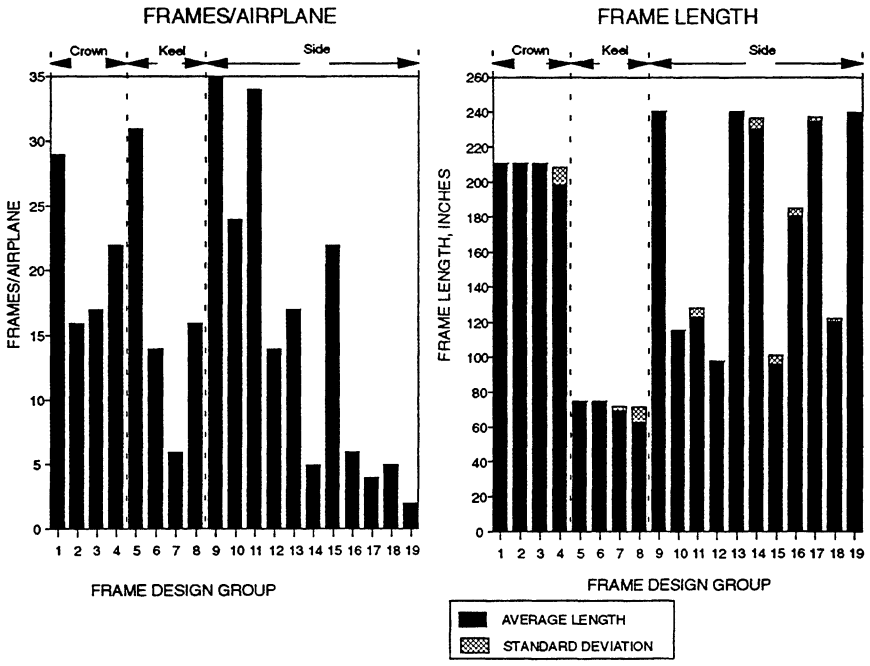

Figure 4-23. Quantity and length of frames for each design group

Figure 4-24 shows predictions of the relative times to complete process steps for crown frames considered in the ATCAS program. Note that the process step to remove parts from the RTM tool (i.e., "part off"), which involves routing to separate the two frames that were braided and cured on the same mandrel, was the most time consuming. Section 4.2.4 will discuss the use of crown manufacturing trials to update the cost model time predictions shown in Figure 4-24. The enhanced analysis will then be applied to predict the cost of all 19 frame groups, including nonrecurring (braiding and cure tools) and material costs. Costs for braided/RTM fabrication will also be plotted as a function of frame length, frame commonality, and the production scenario.

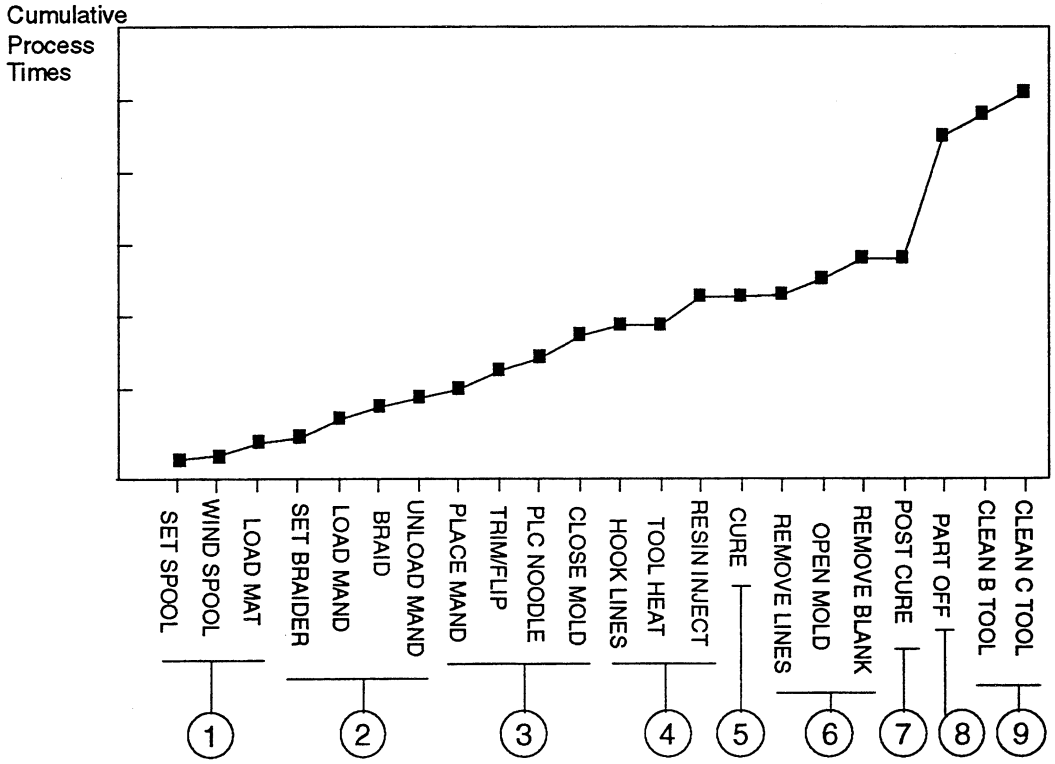

Figure 4-24. Predictions of the average relative process times of steps for a 300 shipset production run of 8 ft. crown frames.

4.2.2.3 Selecting Equation Form

As part of the desire to follow a theoretical framework, design cost equation forms should be selected based on physical rationale. A number of different mathematical equation forms for the proposed theoretical basis were discussed in Section 3. Size scaling laws should be used for extensive processes or tasks thought to scale according to the dimension or size of key design variables. As a quick overview, the size scaling law proposed in Section 3.2 for curvilinear processes is based on two physical parameters; time constant, τ, and steady state velocity, v_o. A number of different approximations for the size scaling law were presented, with accuracy depending on the particular size range of interest. Section 3.3 discusses how the processes related to size can be further scaled

to reflect the effects of design complexities on manufacturing time. This scaling is dependent on the definition of a design variable that provides a quantitative measure of part complexity. Finally, Section 3.4 proposes dynamic models for material handling tasks which involve physical parameters such as transport velocity, effective mass, damping, and stiffness. Some difference in the models for material handling is expected depending on whether the task is performed manually, mechanically, or by some combination of the two.

Different equation forms to predict time may be selected for each process step or some combination of steps. Parameters in each equation will have different physical meanings depending on characteristics of the process and whether the time for individual steps or groups of steps are being estimated. In either case, total times are determined through summation. The approach used by the ATCAS team has focused on the summation of multiple cost equations, each based on individual process steps. However, the mathematical basis presented in Section 3.0 and the COSTADE software algorithm (refs. 1 and 48) was developed in such a way that generalized equations, representing the effects of multiple process steps, can be incorporated in the theoretical framework. For example, part complexity scaling (Section 3.3) and other simplifying analyses (Section 3.5) can take the place of multiple terms in a sum by representing process effects at a higher level.

The Boeing ATCAS DBT experience in predicting times for new fabrication methods is based on process-step equations. These equations give the DBT visibility of critical design cost drivers, and allow for increasing levels of sophistication, as manufacturing data becomes available, and understanding of processes improve. The open architecture style of the process-step equations document assumptions and accommodates easy updates as technologies advance. This is particularly useful in the rapidly advancing field of composite manufacturing, allowing for vital changes which can update an otherwise obsolete model. A synopsis of the cost equations and a relational database that represent the current understanding of processes selected by ATCAS to produce a composite fuselage barrel are provided in Section 5 and ref. 55, respectively.

Most of the ATCAS process-step equations represent some variation of the most accurate approximation of a size scaling law, i.e.,

$$t \approx \left[\left(\frac{\text{Setup}}{\text{Run}}\right)+\left\{\left(\frac{\text{Delay}}{\text{Operation}}\right)+\sqrt{\left(\frac{x}{v_o}\right)^2+\left(\frac{2\tau}{v_o}\right)x}\right\}\left(\frac{\text{Operations}}{\text{Run}}\right)\right]\frac{\left(\text{Parts}/\text{Shipset}\right)}{\left(\text{Lots}/\text{Run}\right)\left(\text{Parts}/\text{Lot}\right)}. \quad (4.1)$$

The main exception is for automated laminate layup processes (AFP or contoured tape lamination) which use some variation of

$$t \approx \left[\left(\frac{\text{Setup}}{\text{Run}}\right)+\left\{\left(\frac{\text{Setup}}{\text{Ply}}\right)x_4+\frac{x_1}{v_{o_1}}+\frac{x_2}{v_{o_2}}+\frac{x_3}{v_{o_3}}\right\}\right]\left(\text{Runs}/\text{Shipset}\right). \quad (4.2)$$

where x_j are different design variables (e.g., x_4 represents the number of plies/run).

4.2.2.4 Estimating Model Parameters for New Processes

In general, physical parameters in the equations used to predict time can be quantified using four different approaches: (i) dynamic models, (ii) physical limits, (iii) comparison to similar processes, and (iv) experimental/measurement methods. Initially, new processes may be estimated based on some combination of the first three. As will be discussed in Section 4.2.4, experiments and measurements taken with process trials help to update equations. Recommended stages of cost model development which follow the theoretical framework (Section 4.2.5) continue to promote updates to cost equations based on the "best available data".

Dynamic models. Characterization of the parameters used to predict time in dynamic models require an accurate physical description of the system. For example, models of the time needed to complete tasks that are linearly dependent on a design variable with length dimensions have proportionality constants which physically relate to the inverse of velocity. Initial estimates of the velocity are simply achieved by studying the physics of machine or manual motions that occur in the process.

Obviously, the usefulness of a given dynamic model depends on the validity of its assumptions. Unfortunately, the assumptions of a model become more difficult to evaluate as increased degrees of freedom are added. For example, linear theories are more easily proven inaccurate than are nonlinear theories. Therefore, it may be prudent to select the simplest equation forms as a starting point. Such theories can be generalized to account for nonlinear response as the database and physical understanding improves.

A simple equation to model a system's dynamic behavior is the first-order linear control system equation. The size scaling relationship for curvilinear processes discussed in Section 3.2.2 and 3.2.3 is based on the response of such a model. Examples of higher order dynamic models were discussed in Section 3.2.5. Two examples of dynamic models for machines were discussed in Section 3.2.6 (i.e., machines with constant acceleration and machines with initial velocity proportional to length). Section 4.2.3 provides an example derivation of a dynamic model and associated parameters adopted for use with the composite AFP process. General textbooks on dynamic modeling and control such as Karnopp & Rosenberg and Ogata (refs. 41 and 42) are excellent reference sources.

Selection of a particular dynamic model to represent a process step can also benefit from past experiences. As described in Section 3.4, a second order linear differential equation has proved useful in estimating the time required for positioning tasks. Even though real positioning systems often exhibit higher order behavior, one can argue that for the purpose of time estimating, they can often be reasonably approximated by a second order model. According to a second order model, the time required for positioning is proportional to the weight of an object for translational positioning tasks, and is proportional to the mass moment of inertia about the rotating axis for angular positioning.

Physical Limits. Another analytical method that supports the derivation of process parameters is an understanding of the principle rate governing phenomenon in the process. Since different mechanisms may affect a process under various operating regimes, one

needs to be aware of all the rate limiting phenomena when using dynamic modeling to estimate the process parameters. This can be as simple as looking up machine/material specifications (such as power available and material conformance) or as detailed as understanding the interaction phenomena and failure modes of the process (such as surface finish, tool wear, etc.).

The use of physical limits to bound the magnitude of process parameters is illustrated in Appendix F with the help of two examples for metal processes. The first example, machining, illustrates how different interaction phenomena can govern the rate of a process in different regimes such as power limitation and tool wear considerations. The second example, welding, illustrates how the governing mechanism changes from heat flow to that of positioning. Future efforts should identify physical limits for composite processes to bound the values of model parameters used to predict time.

Comparison to Similar Processes. One of the key features of the proposed equations to estimate fabrication time is that they are based on physical parameters which are simple and objective. Accordingly, these constants have physical interpretation and can be rank ordered in a fashion that is consistent with general observation. Therefore, one would expect that the parameters can be derived by comparing processes from different fields, such as hand lay-up of composites (ref. 13), building construction (ref. 60), machining (ref. 14), time motion studies (refs. 7, 9, 11), and other industrial data. These parameters can be (a) compiled in a common database, (b) ranked by relative value, and (c) plotted in a form referred to as "Master Charts" in this report.

Given that processes involving touch labor are usually more prone to the many sources of variations, the use of Master Charts is particularly suitable in predicting the average trends in manual operations. Comparisons with similar processes allows one to utilize data that is available for processes that involve similar motions from different fields. This is particularly useful in estimating the time for new processes; where no data exist within one's organization. The master charts for linear velocities "v_o", areal velocities "v_a", and volumetric rate "v_v", for different processes from various fields, are shown in Appendix G. Some of the velocities in these figures represent those currently assumed for ATCAS composite fuselage processes. Appendix H tabulates (i) individual ATCAS process steps, (ii) critical variables for process-step equations, and (iii) units for equation constants. Further details on the equation form for each ATCAS process-step is included in ref. 55. A synopsis of ATCAS cost analysis for some key process-steps is given in Section 5.

The master charts are also very valuable as a tool to check the process parameters obtained for new processes. This is because any mistakes leading to vastly different numbers will be very apparent when compared to the values for similar processes in the master chart. As discussed in Section 4.2.2.5, reasonable approximations of the times to hand lay-up parts having various shapes and sizes are possible using parameters derived from some laboratory fabrication data (ref. 61) and comparisons with similar processes. Results suggest that model parameters estimated in this manner lead to the same rank ordering as more rigorous analysis with comprehensive databases and, therefore, provide a starting point in the evaluation of new technologies.

4.2.2.5 Example: Predicting Hand Layup from Limited Data Sources

The following discussion illustrates how the proposed framework can be used to provide initial estimates when little or no data for the specific process is available. Predictions from the empirical analyses compiled in ref. 13 (also presented in Section 3.3.4.1) were used for purposes of comparison with the preliminary estimates in this sub-section. The 240 single curvature parts of different sizes and shapes used in this exercise are depicted in Figure 3-28. Both size and complexity scaling laws were used to make predictions that utilize the proposed framework. The required parameters, v_o and θ, were both set based on data from laboratory experiments. The former value was compared with areal velocities obtained for similar processes to gain confidence in its use.

Figure 4-25 shows the lay-up rate as a function of tape width obtained from some experiments at MIT (ref. 6). For the current example, the tape width is chosen as 12 inch and thus the lay-up rate is v_o=3,000 in/hr (36,000 in^2/hr). As discussed in Appendix G, analogies can be drawn between laying up prepreg, laying down carpet, and putting up wallpaper. Therefore, it is no surprise that the value v_o=36,000 in^2/hr is very similar to that of laying down carpet (18,000 to 24,000 in^2/hr)[1] and putting up wallpaper (20,000 to 40,000 in^2/hr) as published for building construction (ref. 60).

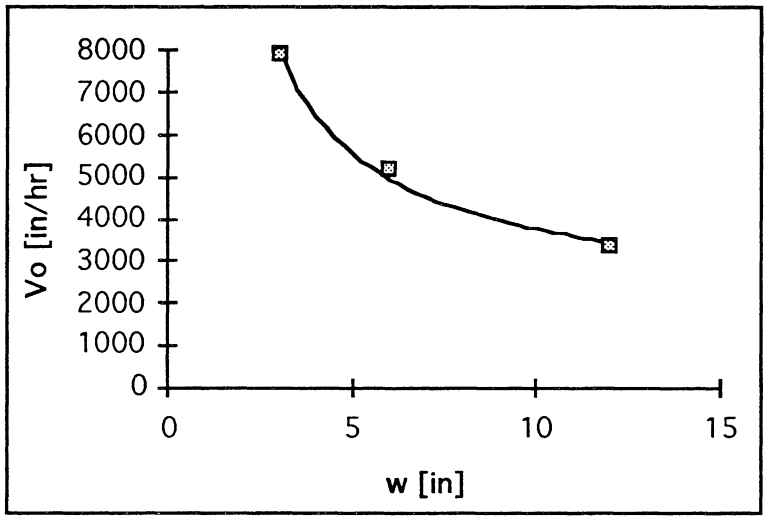

Figure 4-25. Lay-up rate as a function of tape width based on MIT experiments.

Figure 4-26 (copy of Figure 3-27 shown for convenience) shows the linear cumulative bend angle dependence for laying up 12 inch wide tape based on MIT laboratory experiments. Referring back to Equation 3.103 and assuming the linear approximation for size effect, the time to lay-up a part with single curvature is

---

1 After scaling up the published rates to account for the additional cleaning and applying adhesive steps required in hanging wallpaper and laying down carpet.

$$t_d = N_L (\tau_o + b\,\theta) + \frac{V}{w\,h\,v_o}. \qquad (4.3)$$

Since the parts in Figure 4-26 are of the same size (but of different geometry), the graph's slope = N_L b = 8.55 min/rad, assuming that $b_{male} = b_{female}$ = b for simplicity. With N_L = 28, b = 0.31 min/rad•strip. Similarly, the intercept of Figure 4-26 is

$$\text{intercept} = N_L \left(\tau_o + \frac{\bar{L}}{v_o} \right) \qquad (4.4)$$

where the average strip length, $\bar{L}$ = 10 in. With intercept = 23.3 min, N_L = 28, and v_o= 3000 in/hr, τ_o is thus derived as τ_o = 0.0105 hr.

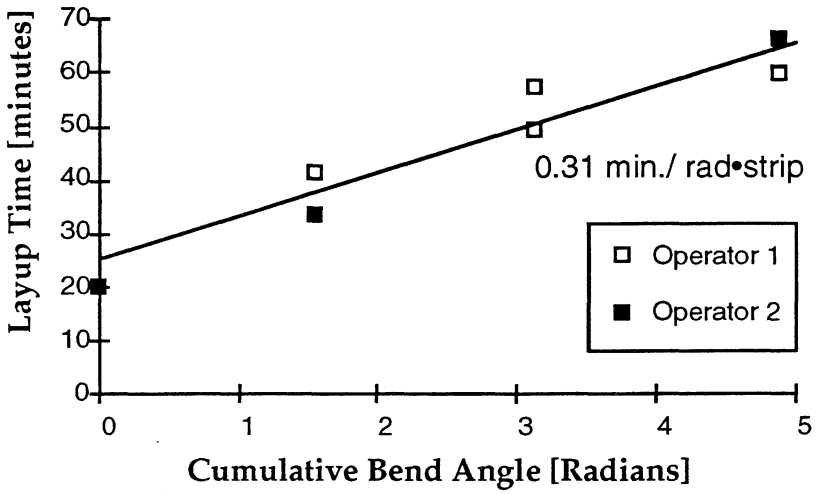

Figure 4-26. Linear cumulative bend angle dependence for laying up 12 inch wide tapes, 16 plies, N_L=28 (MIT lab data).

Thus, with τ_o = 0.0105 hr, v_o = 3000 in/hr and b = 0.31 min/rad•strip, the lay-up time is estimated using Equation 4.3, and the results are compared to that using the empirical models from ACCEM (ref. 13) in Figure 4-27. As discussed in Section 3.3.4.1 through 3.3.4.3, the scatter near the origin of Figure 4-27 is due to the linearization error of Equation 4.3 when compared to the ACCEM power laws. Note that while the results are not as accurate as the original comparison in Figure 3-29, which uses best fit parameters derived from ACCEM, the results using the in-house parameters do manage to preserve the rank ordering and general trends predicted by ACCEM.

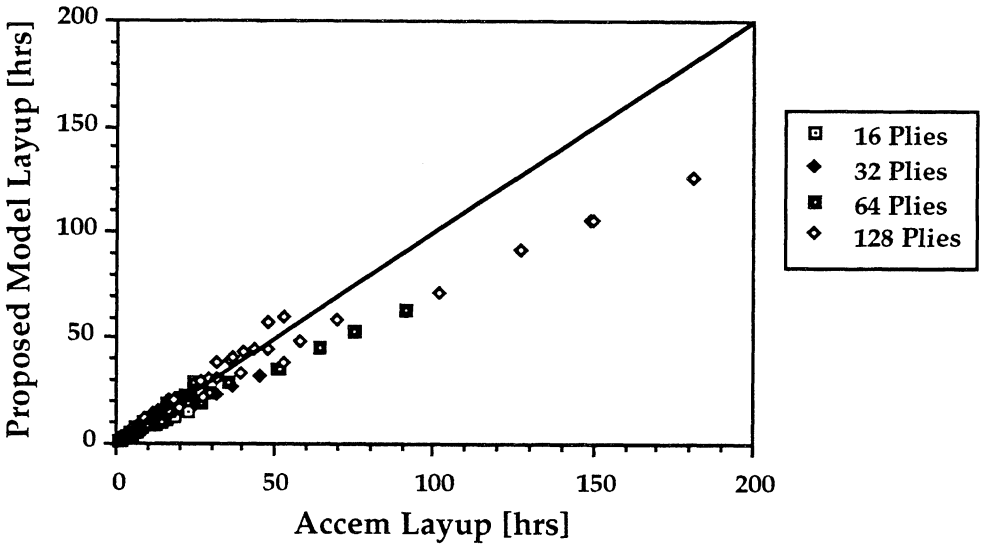

Figure 4-27. Comparing lay-up time with parameters derived using MIT lab data to that using ACCEM.

The example in this section helps illustrate the benefits of a design cost model framework that has (1) equations with a theoretical basis, (2) parameters with physical meaning, and (3) procedures for defining the parameters when little data exists (e.g., new technologies under development). This framework was shown to yield initial estimates for prepreg tape layup time that were close to the predictions possible with an empirical model based on years of experience and a large database. Additional correlations that used velocities from similar manufacturing operations to make initial predictions of other hand layup process steps for stringer geometry are given in ref. 6. For example, the aerial velocity for debulking was assumed to equal that for laying down carpet. The end result was reasonable correlations to results based on a larger database; therefore, again illustrating the benefit of a theoretical basis for establishing a starting point.

4.2.3 Example for Automated Fiber Placement

Dynamic motions for automated processes can be modeled to predict the associated fabrication times. The automated fiber placement (AFP) process has been selected by ATCAS to lay-up composite fuselage skins (ref. 5). This process uses prepreg tow material forms. Dynamic motion of an AFP machine has the necessary degrees of freedom to achieve the cost and weight efficiency required to be competitive with state-of-the-art metal processes (e.g., high-speed machining). This section will derive the AFP cost equations based on machine physics and then apply the model in an example of sensitivity studies which have been used to guide ATCAS developments.

4.2.3.1 AFP Machine Physics

The fundamental activity performed by an AFP machine is to lay-up individual strips of composite material. Strip lay-up is performed a number of times (in different locations

with generally different strip lengths) to complete an individual ply. Several plies, of often differing shapes and fiber angles, are deposited to form a designed part.

The tow lay-up step from the ATCAS AFP process cell, "step 90" in Figure 4-20, has been modeled using machine physics (ref. 62). The machine time to lay-up a single ply is a combination of the following items:

(a) Ply initialization time
(b) Strip initialization time
(c) Head up and down time
(d) Head accelerate and decelerate time during lay-up
(e) Max speed time during lay-up
(f) Head accelerate and decelerate time during dead head return
(g) Max speed time during dead head return

4.2.3.2 AFP Cost Equations

Each of the above step times can be defined in terms of the AFP machine speeds and accelerations. This sub-section provides equations to predict AFP as a function of each ply fiber angle and geometry used in a part. The derivation uses equations that have the theoretical basis for dynamic motion presented in Section 3.2.6 (i.e., constant acceleration case). As ply starts and stops are taken into account, the total AFP time for realistic laminates can be credibly estimated as the sum of times to layup individual plies. The AFP equations have successfully been used with COSTADE design element discretization to blend layups and properly locate padups for composite fuselage skin concepts (ref. 1, 62, and 63).

The fundamental activity performed by an AFP machine is laying down strips of material on a tool. A ply is made up of a number of strips. The ply initialization time, strip initialization time, head down-time and head up-time are treated as machine constants for each activity. Tow lay-up times are estimated by writing equations of motion for the AFP head. Three motions for the machine head are assumed: (i) stopped, (ii) under constant acceleration or deceleration, or (iii) at constant non-zero speed. The head accelerate and decelerate times are defined in terms of the maximum machine speed and the acceleration and deceleration rate.

$$\text{head accelerate time} = \frac{v_{max}}{a_{accel}}, \tag{4.5}$$

$$\text{head decelerate time} = \frac{v_{max}}{a_{decel}}, \tag{4.6}$$

where

v_{max} = maximum machine speed
a_{accel} = acceleration constant
a_{decel} = deceleration constant

The time at maximum speed during lay-up is a function of the strip length, acceleration and deceleration rates, and maximum machine speed. Depending on the specific capabilities of a given AFP machine, different characteristics can be used during lay-up from dead head. If a bidirectional lay-up procedure is used, dead head activities may be replaced by additional strip initialization time associated with head turn around.

$$\text{max speed time} = \frac{l_{strip}}{v_{max}} - \frac{v_{max}}{2a_{accel}} - \frac{v_{max}}{2a_{decel}}, \text{ for } l_{strip} > l_{crit} \tag{4.7}$$

or

$$\text{max speed time} = \sqrt{2l_{strip}\left(\frac{1}{a_{accel}} + \frac{1}{a_{decel}}\right)}, \text{ for } l_{strip} < l_{crit} \tag{4.8}$$

where

$$l_{crit} = \begin{pmatrix}\text{distance to accelerate to max speed} + \\ \text{distance to decelerate from max speed}\end{pmatrix} = \frac{v_{max}^2}{2a_{accel}} + \frac{v_{max}^2}{2a_{decel}} \tag{4.9}$$

Note that if Equation 4.7 is used to estimate a strip shorter than the critical length, an overestimate of the max speed time will result.

Figure 4-28 illustrates the process to lay-up an individual strip for a ply with rectangular geometry. The number of strips required to lay-up a rectangular ply of width W, length L, and angle θ, is calculated as follows, assuming all strips are greater than l_{crit}:

$$\text{Number of strips starting on the vertical edge} = \frac{W\cos\theta}{w_{strip}} \tag{4.10}$$

$$\text{Number of strips starting on the horizontal edge} = \frac{L\sin\theta}{w_{strip}} \tag{4.11}$$

$$\text{Total number of strips for this ply} = \frac{L\sin\theta}{w_{strip}} + \frac{W\cos\theta}{w_{strip}} \tag{4.12}$$

where w_{strip} is the strip width used during lay-up.

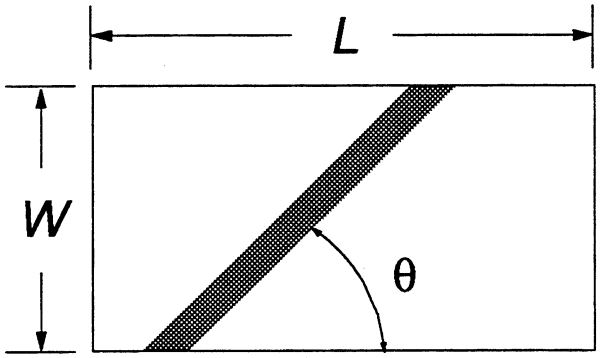

Figure 4-28. Strip lay-up geometry.

After some manipulation, the time required to lay-up the rectangular ply can be written as:

$$\text{Ply lay-up time} = \text{ply initialization time} + \frac{L\sin\theta + W\cos\theta}{w_{strip}}\left[\begin{array}{l}\text{strip initialization time} + \\ \text{head down time} + \\ \text{head up time} + \frac{v_{max}}{2}\left(\frac{1}{a_{accel}} + \frac{1}{a_{decel}}\right) + \\ \frac{v_{dh\max}}{2}\left(\frac{1}{a_{dhaccel}} + \frac{1}{a_{dhdecel}}\right)\end{array}\right] + \frac{LW}{w_{strip}}\left(\frac{1}{v_{max}} + \frac{1}{v_{dh\max}}\right) \tag{4.13}$$

where

$v_{dh\max}$ = maximum dead head machine speed

$a_{dhaccel}$ = dead head acceleration constant

$a_{dhdecel}$ = dead head deceleration constant

The equation above is strictly valid for plies that contain only strips of lengths greater than l_{crit}. However overestimates, resulting from a short strip length in corner areas, occur when the linear equation is used for general plies. Equation 4.13 allows plies to consist of a non-integer numbers of strips. Strictly speaking, this may be considered a restriction on the equation's accuracy; however, such a case is physically possible within limits for individual tow cutting capabilities found in some AFP machines. Additional equation manipulations were performed in ref. 62 to accommodate multiple design elements used in COSTADE for variable load conditions over large panel areas.

In order to convert a fabrication time to a cost, the resource cost multiplier K is used. For recurring labor only, K is defined as:

$$K = (\text{variance})\ (\text{recurring labor rate})\ (\text{crew size}) \tag{4.14}$$

The lay-up time in Equation 4.13 can be multiplied by K to get the ply lay-up cost. Note that the effects of different labor skills, capital costs, inventory costs, overhead costs, learning curves and unplanned events can be simulated by modifying the multiplier K. In general, different values of K will be needed for each process step.

4.2.3.3 AFP Sensitivity Study

The AFP equations contain the required detail to evaluate complex layup patterns. The sensitivity study performed in this sub-section compares the cost to lay-up a complete ply with the cost to lay-up several individual strips (e.g., narrow padups beneath stringers or frames). The cost components considered include machine lay-up and dead head times,

material cost, material reload, and cutter clean. The ATCAS baseline manufacturing parameters for the AFP process are listed in Table 4-1. The added costs associated with multiple starts and stops, and material cuts for a strip configuration, are traded with the extra material cost in the full sheet model. A transition point exists, where the cost of the strip design is the same as the cost of the full sheet design. Note that the vehicle operation cost, associated with an increase in structural weight can be evaluated separately. For example, COSTADE has an optimization procedure to consider the acceptable cost increases for weight saved (ref. 48).

AFP Machine Characteristics	
Acceleration/Deceleration during laydown	30 in/sec/sec
Max speed during laydown	740 in/min
Acceleration/Deceleration during deadhead	30 in/sec/sec
Max speed during deadhead	1500 in/min
Strip laydown width	5.74 in
Head up time	1 sec
Head down time	1 sec
AFP Material Characteristics	
Material cost	33 $/lb
Material spool size (32 spools)	5 lbs per spool
Material reload time (32 spools)	2.5 min per spool
Cutter clean time	15 min
Cuts per clean	1000

Table 4-1. ATCAS baseline AFP manufacturing parameters

A frame padup trade, for ATCAS baseline material cost and machine speed, is presented in Figure 4-29. This figure shows the sum total of fabrication and material costs to lay-up a tow-placed strip (i.e., 5.74 in. wide) for the full ply length versus multiple padups. The full ply and padups in this example both have fibers oriented in the panel axial direction. Also note that strip width is measured perpendicular to fibers and strip length is measured parallel to fibers. The panel length is 398 inches, over which a total of 21 padups are assumed (i.e., as the padup strip length increases, the gap between padups decrease). Both lines in Figure 4-29 intersect at a "strip length threshold" of approximately 17 inches. Multiple padups which are each shorter than this strip length threshold are less expensive to fabricate than the full sheet designs (for strip lengths greater than the minimum allowed by the AFP machine). This occurs due to the dominance of material cost. However, if

padups longer than the strip length threshold are required (for structural or manufacturing reasons), it is more economical to layup a full sheet. This occurs due to efficient AFP utilization, allowing it to complete a full ply much faster than the multiple padups, overcoming the material cost difference.

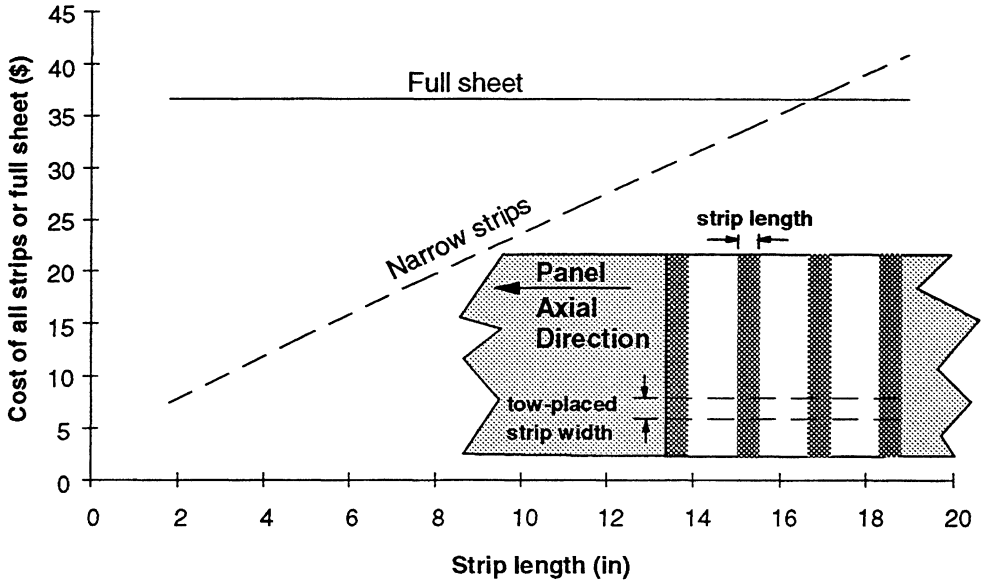

Figure 4-29. Ply cost trade: full sheet versus narrow strips.

Variations in manufacturing parameters, such as material cost, machine speed, labor rate, lay-up strip width, spool tow length, and head up time, will change the strip length threshold. Figure 4-30 shows curves for the strip length threshold versus a manufacturing parameter multiplier which was applied separately to each variable in the legend (i.e., all other parameters were held at baseline values to create a curve). A multiplier value of 1 corresponds to the ATCAS baseline manufacturing parameters. Panel and ply definitions applied in the previous trade (i.e., Figure 4-29) were also used to create Figure 4-30.

Two distinct trends are indicated in Figure 4-30. The first shows that as material cost, lay down strip width, and machine speed decreases, the strip length threshold becomes very small. Conversely, as these parameters increase, the strip length threshold asymptotes near the full strip length. Note that material cost and strip width curves superpose. Smaller strip widths and decreased machine speed both increase the percent contribution of AFP time to total cost (i.e., more strips have to be fiber placed to achieve the same width of material); hence, affecting the strip length threshold in a manner similar to lower material costs. The key difference is in the fact that decreased machine speed or strip width increase total ply lay-up costs, while decreased material costs do the opposite.

The second trends shown in Figure 4-30 is associated with spool tow length, head up time, and labor rate. As the values for these parameters decrease relative to the baseline, the critical strip length increases. As the values for these parameters increase, the strip length threshold decreases.

The trends in Figure 4-30 will be magnified or compressed if multiple parameters are varied simultaneously. Note that other potential factors affecting the trade are possible if a greater number of AFP machines or higher maintenance costs occur with more starts and stops required to place multiple padups.

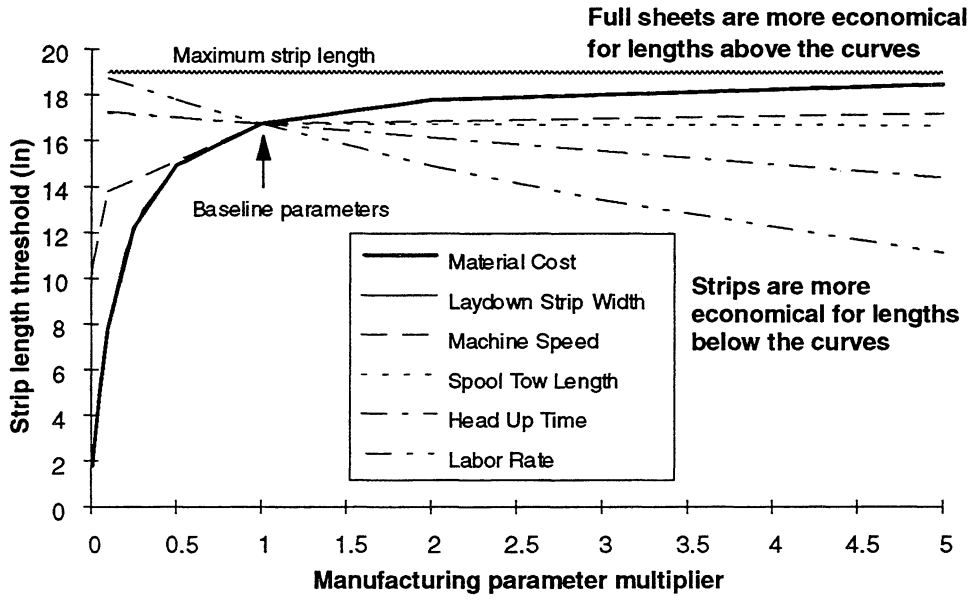

Figure 4-30. Strip length threshold as a function of variation in the manufacturing parameters.

The sensitivity study performed in this subsection helps to confirm the selection of AFP as an efficient process to manufacture laminated fuselage skins. For the majority of manufacturing parameters investigated, the strip length thresholds were found to be larger than "typical" ATCAS fuselage padups. This fact indicates that most strip-style configurations are less expensive than full plies. Further, when vehicle operating costs are included (i.e., the designer is willing to accept additional cost to save a pound of weight), the strip length threshold for nearly all parameter variations was found to approach the maximum possible strip length. Yet, it is important to understand the location of the transition zone, and those factors which most affect it. The steep gradients (e.g., those associated with slow machine speeds or decreased lay down strip width), identify areas which must be understood in order to avoid potential cost risers and achieve anticipated cost savings. The interaction between AFP process times and total equipment needs for a given application must also be understood to avoid incremental increases in capital costs for additional machines.

4.2.4 Manufacturing Trials for Data to Achieve Desired Accuracy

Sections 4.2.1 through 4.2.3 have addressed the design and manufacturing process definitions needed to develop initial design cost equations for new technologies. The current section supplements these discussions with interpretations on the value of

manufacturing data collected during development and production. Two examples of the utility of manufacturing data collected in ATCAS are also presented.

4.2.4.1 Value of Design and Manufacturing Demonstrations During Development

Achieving cost credibility for new technologies with a high degree of confidence prior to production commitment is difficult. Manufacturing trials for structure with representative design detail have proven invaluable to ATCAS cost studies during early stages of development. The goal of such trials have been to demonstrate producibility and supplement the existing cost database. The former goal helps reveal process constraints and ensure the step-by-step accuracy of manufacturing plans and tooling approaches for new technologies. Time studies for process trials involving automated equipment and touch labor are also crucial to calibrating the design cost model. In addition, manufacturing demonstrations often serve a dual purpose in evaluating critical design details and the effects of manufacturing-induced performance traits.

Size and product related scaling issues need to be considered in the interpretation of data from manufacturing development efforts. Size scaling issues go beyond those described in Section 3.2, to include factors inherently related to complexity. For example, mid-panel design details for a sub-scale panel may be easier to deal with than the same features found in the middle of a full-scale panel. Product scaling issues consider changes to the process as applied during development versus that used in production. Without insights on product scaling, the relevancy of data captured in a test or laboratory environment as it applies to production experience is questionable. This is due to the numerous differences in tooling concepts, drawing specifications, quality control techniques, and the experience of the people performing the processes. Accurate size and product scaling require a significant process database, supporting cost analyses, and special DBT attention to differences between process steps used in production and development.

Narrowing the scope of time studies in ATCAS to particular process steps has helped to collect a manufacturing database that supports cost analysis. The resulting data represents the ideal production scenario and worker for some of the critical process steps. As discussed in previous sections, a cost equation is developed through selection of critical design parameters, (surface area, length, width, quantity, etc.), and a functional form, which best represent the physics of the problem for a range of likely structural details. A comparison of predictions versus actuals has lead to a measure of the historical variance to ideal conditions. As the database expands in moving new technology from development into production, the constants and, conceivably, the equation form should be continually changed based on the best available data. This building block approach is analogous to that used for structural sizing tools, where analysis methods are verified and calibrated as test data becomes available.

Manufacturing information gathered during development has a high potential leverage on the ability to optimize the production cost by exposing process sensitivities to the DBT as critical decisions are being made. Time studies conducted during fabrication of full-scale test parts is particularly valuable when existing manufacturing data is at a scale that is significantly different than the parts currently being designed (ref. 64). For example, if the

cost estimate to clean a quadrant panel OML cure tool (i.e., process step 20 from Figure 4-20), is based purely on the extrapolation from previous production experience, the prediction may underestimate test panel data by a significant amount (see Figure 4-31). However, time studies performed during large-scale manufacturing trials can help predict the process time with greater accuracy due to the similarity in size and complexity to the production tool. At least physical limitations (e.g., access) will be better understood, helping to isolate other differences between full-scale test panel data and production processes. In the case of many advanced processes, production data doesn't exist at any scale, making the extrapolation to production more dependent on the right combination of sub- and large-scale manufacturing trials.

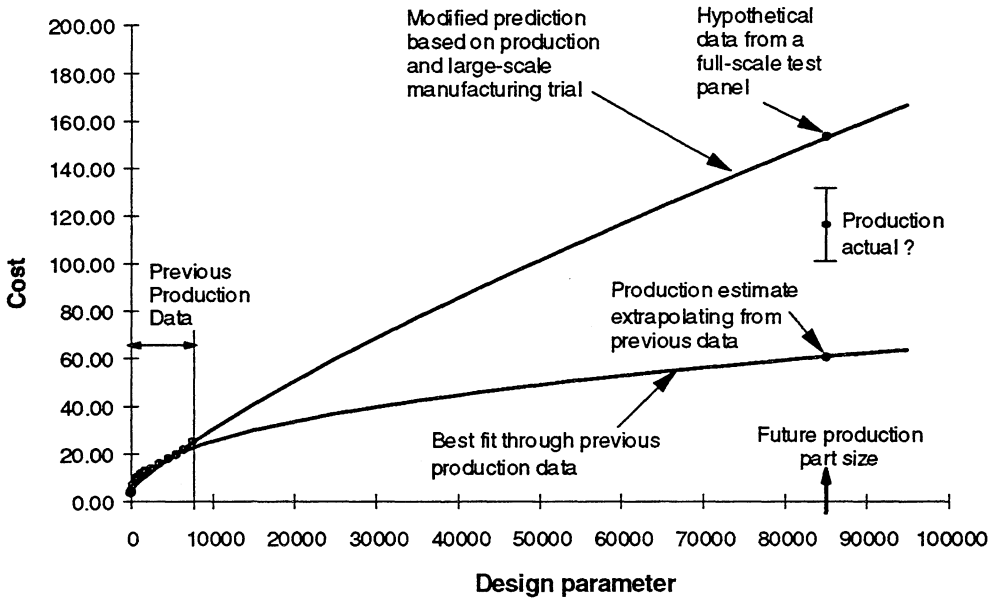

Figure 4-31. Schematic illustrating potential manufacturing data extrapolation error.

4.2.4.2 Manufacturing Data for Braided/RTM Fuselage Frames

Section 4.2.2.2 and Appendix E described the key design variables and process parameters for a braided/RTM process selected by ATCAS for most of the circumferential frames in a wide-body transport aircraft. A total of nineteen design groups were identified based on differences in curvature, length, and gage. A model was developed at the process-step level which was suitable for predicting fabrication times for each design group. In addition, material and tooling costs were estimated. A number of eight foot crown frames, representing one of the design groups, were fabricated to evaluate producibility issues and collect process step data suitable for updating the cost models. The updated model was then used to predict costs for the other design groups.

Two types of data were available to calibrate the model for braided/RTM frame fabrication. The first consisted of detailed estimates performed for the ATCAS keel and crown design studies. Roughly thirty percent of this cost estimate is based on labor

standards which apply directly to current fabrication methods used in production. Additional cost data was developed from Manufacturing Research and Development inputs and extrapolation of existing data for processes and equipment. The second source of cost information was actual time studies performed on braided/RTM fabrication of eight foot "J" frames used on the ATCAS test panels (refs. 52 and 54). The comparisons of actual fabrication touch labor and Boeing estimated standard labor, averaged over 300 shipsets, is shown in Figure 4-32. While only the Boeing estimate had learning and variance factors applied, the data from manufacturing trials gave a good reference point for comparison.

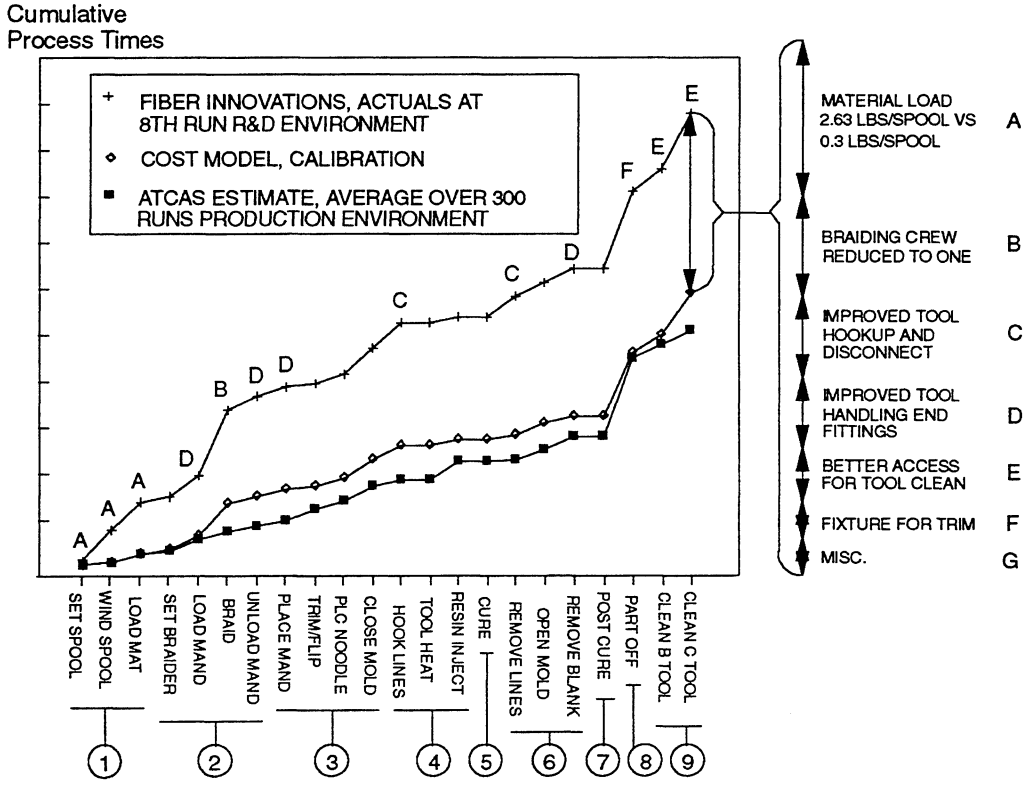

Figure 4-32. Updates to the relative times needed for braided/RTM frame process steps.

The calibration curve in Figure 4-32 is broken into the nine basic processing steps. Areas of improvements between the process used successfully in an R&D environment and that assumed for a full-scale production environment are noted as A through G. Figure 4-32 lists these areas, which are related to product scaling for production, next to scales that highlight their relative effect on process times.

The first major area of improvement possible in production involves loading more material onto the braiding equipment. Braiding equipment used for ATCAS had 216 spools of fiber. Only one third pounds of fiber were loaded per spool. Due to the number of different parts being fabricated and fiber types being used at the braided/RTM frame manufacturer (Fiber Innovations), it was impractical to load more material per spool. In a

production environment, where production rate would require dedicated braiding equipment and consistent fiber types, these limitations could be removed by simply loading more material onto each spool. This allows for amortization of material load times over more parts, thus lowering the final cost. For example, loading 2.63 pounds of fiber per spool in a production environment would allow the braider to produce frames at a normal operating speed for 70 hours between cleaning and reloading of the braiding equipment.

The second area of improvement is the number of operators required for the braiding equipment. Two operators were used at Fiber Innovations with the second person preforming quality control. The ACT cost estimating ground rules require quality control to be accounted as an overhead function. In addition, projected future improvements in braiding equipment could self monitor the braiding process. Therefore it was judged that one operator would be sufficient for the production scenario.

Capital and equipment improvements not justifiable for ATCAS R&D efforts were considered as realistic improvements for future braided/RTM frame production. These include improved connectors to hook-up and disconnect the heater, thermocouple, and injection lines. Other advancements include tool handling using overhead equipment, optimized factory layout, and improved fixtures. Tool clean in resin transfer molding can be time consuming but improvements in tool design and cleaning methods, such as resin knock outs, can improve labor costs.

Using the calibration for braided/RTM process steps based on ATCAS manufacturing trials and projections to a production environment, fabrication costs for the various fuselage frame design groups described in Appendix E were predicted. As shown in Figure 4-33, there are large cost differences between the various design groups considered for a wide-body transport fuselage. These differences are largely due to tooling costs.

Although the cost breakdown for each design group is evident in Figure 4-33, reasons for the differences can be elusive. One of the fundamental reasons for the cost difference between frame design groups is tooling. Most of the constant curvature frames did not require any more tooling than was needed to support production rate. The non-constant curvature frames required a different closed mold tool for every frame. In addition, the quantity of frames in any one design family was not always sufficient to fully utilize the tooling. Frame length can also be seen to have a slight effect on labor costs due to the amortization of setup costs over smaller frames.

While the information plotted in Figure 4-33 is important to identifying cost centers, it does not allow the designer to find the optimum point between design details and cost. The primary advantage of a cost model is to allow the designer to incrementally vary design details and gain an understanding of how this affects cost. As shown in Figure 4-34, one strong relationship between cost and frame design details predicted by the model was frame length. This figure assumes an average of 17 frames per design group. Significant improvements in frame cost were seen for increasing lengths up to about 100 inches. These cost improvements were largely due to the effects of operations in the process (e.g., setup times) which are required regardless of how short the frame is.

Superimposed is processing improvements which interact with frame length to allow for batching of additional frames per tool, amortizing the setup cost over more frames.

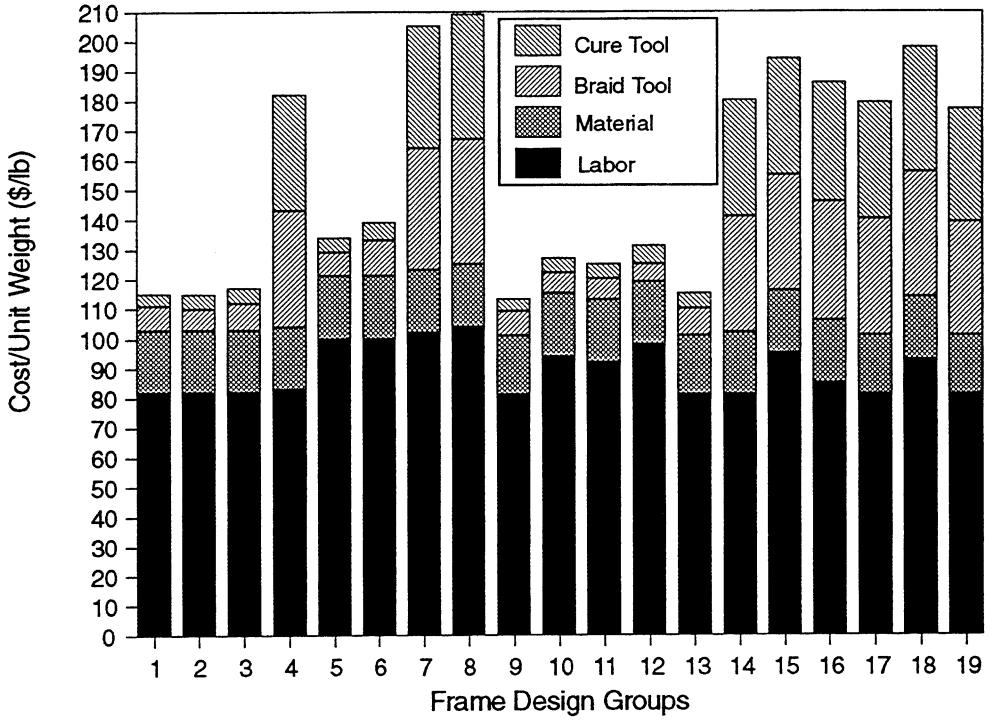

Figure 4-33. Fuselage frame family fabrication cost

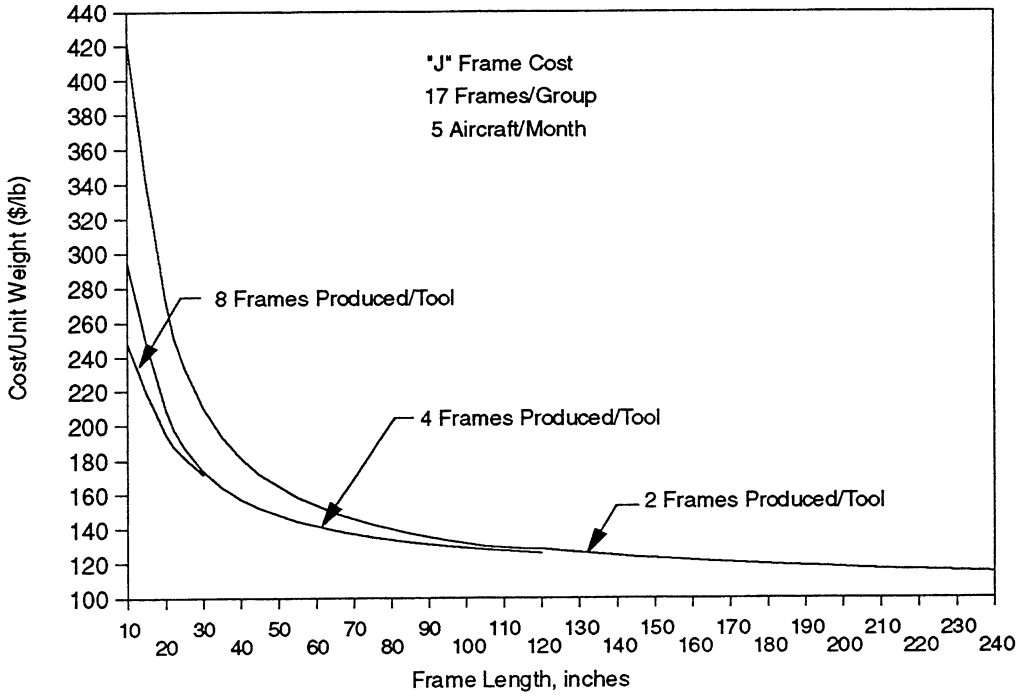

Figure 4-34. Predictions of the effects of frame length.

Another strong relationship predicted by the cost model was that of frame commonality. For example, commonality of four represents an average of four common frames in every design group. Figure 4-35 plots the cost verses frame commonality. As frame commonality increases frame costs decrease, leveling out at about six frames per group. This asymptote is a result of the rate tooling requirement which drives the frame cost. Frame commonalities greater than six will not result in any significant advantage in the projected production environment (5 shipsets/month).

One design detail which can strongly effect frame commonality is tailoring to save weight. The cost model would give the designer non-ambiguous thresholds for the impact of weight savings on cost through its impact on commonality. In addition, suppose the optimum cost/weight commonality for fuselage frames is three frames per group. In this case, improvements in unattended cure cycle time would have little impact on frame cost due to the under-utilization of tooling at this frame production rate. If the frame commonality of the design is nine, then improvements in the cure cycle time could improve the frame cost by lowering rate tooling requirements.

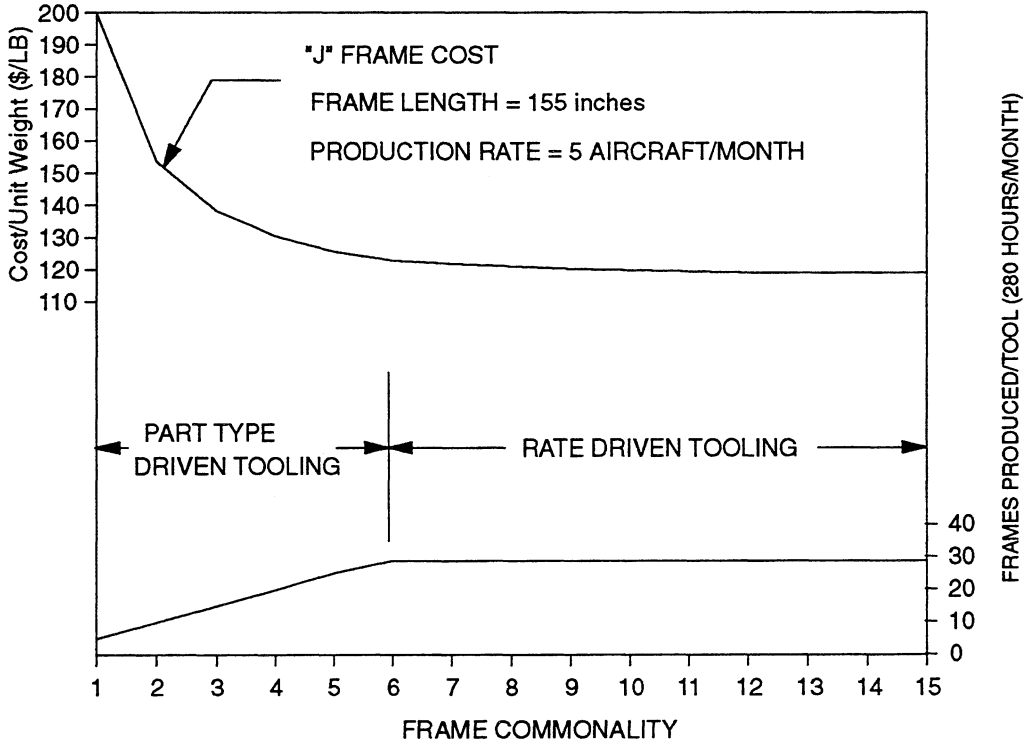

Figure 4-35. Predictions of the effects of frame commonality.

Since frame commonality was seen as such a strong driver it follows that aircraft production rate should also be important. The current ground rules used in the ACT program calls for a production rate of 5 aircraft/month over 5 years. Actual commercial transport production rates have varied between 1 and 21 aircraft/month depending on the aircraft model and the existing market. Figure 4-36 shows frame costs verses aircraft production rate. This was also predicted by the model to be a strong cost driver.

Although such a variable is not at the discretion of a fuselage frame DBT, they should be aware of potential markets since there is a synergistic effect on the selection of other design variables.

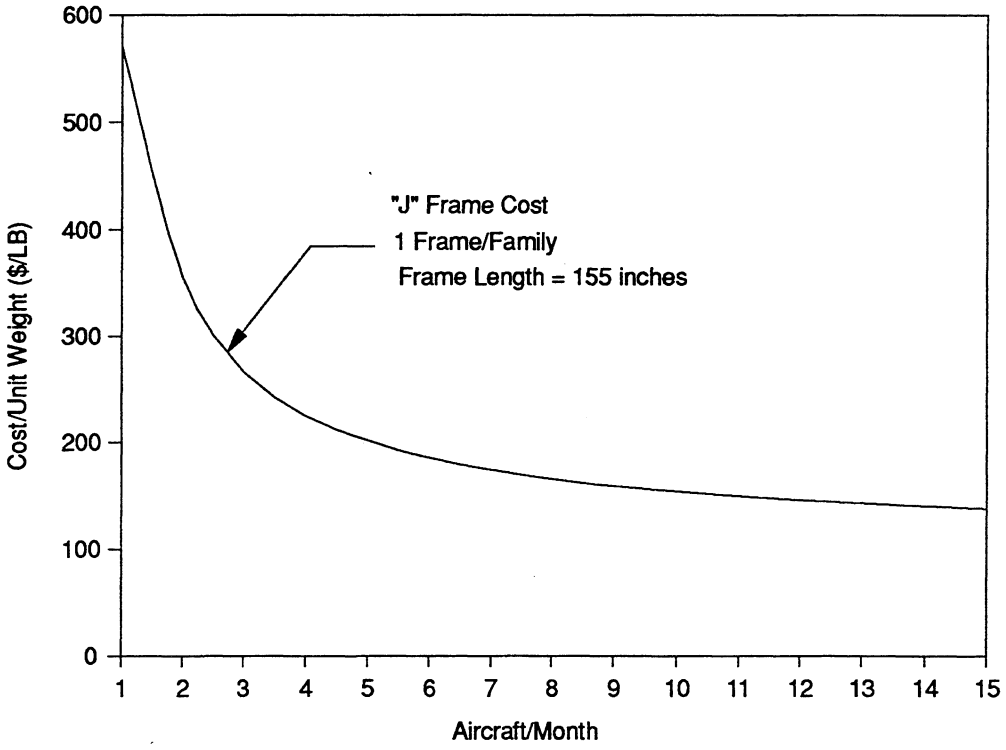

Figure 4-36. Predictions of the effect of production rate.

The aircraft production rate becomes important to the DBT through its interaction with the design detail of frame commonality. Figure 4-37 plots constant frame cost lines as a function of frame commonality and aircraft production rate. Low values for frame commonality would not impact the frame cost for a high production rate aircraft as much as it would for a lower production rate. The cost model would help a DBT understand the compromise between frame commonality and cost and weight savings for application in the baseline production environment. If tied to design cost models for alternative processes, the optimum process may be found to depend on the production scenario.

The braided/RTM fabrication process, when applied to fuselage frames, is most cost effective in high production quantities. Whether the higher frame fabrication rate is due to higher aircraft production rate or increased frame commonality does not matter. This is due to the requirements for tooling being driven by rate rather than part number variations. Conveying this information to the DBT early, could head off production problems which are difficult and expensive to solve after tooling or part design release.

In summary, strong cost drivers predicted by the cost analysis of braided/RTM fuselage frames were frame length, frame commonality, and production rate. When a design and production environment are correctly matched, significant cost savings are possible. The ATCAS cost studies indicate that braided/RTM fuselage frames are not only cost effective

verses other advanced composite fabrication methods, but on par with the detail fabrication cost of metal fuselage frames.

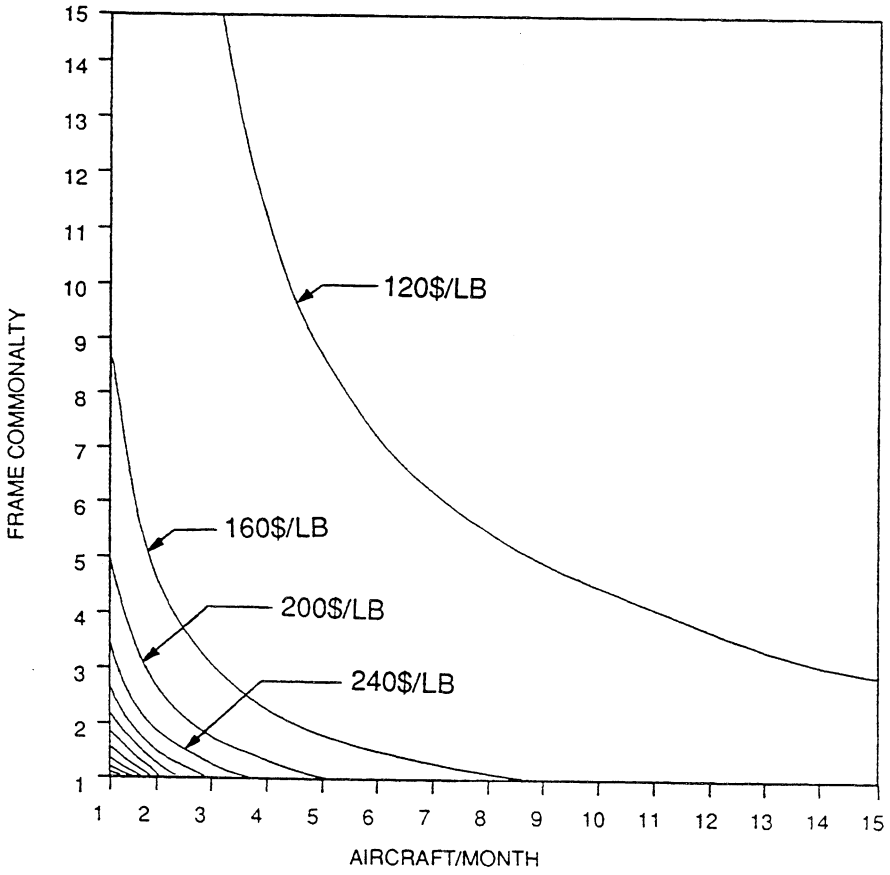

Figure 4-37. Cost model predictions of the combined effects of frame commonality and aircraft production rate.

4.2.4.3 Manufacturing Data for Crown Skin/Stringer Panels

This sub-section focuses on the integration of manufacturing trials for subcomponent panels into a design/cost database for the composite fuselage crown quadrant. First, results are presented for test panel fabrication time studies performed during concept development. Next, a description is given on how these fabrication trails can be used to improve the preliminary cost analyses developed for crown panel bond process steps.

Subcomponent panels fabricated for manufacturing and structural evaluation of the ATCAS crown design were also used to evaluate cost methodologies (ref. 64). The panel configuration and processes used in these fabrication trials are shown in Figure 4-38. Reference 52 gives a complete description of the fabrication efforts. Since manufacturing and structural properties can be closely linked, test panels were fabricated incorporating the processes, equipment, and tooling that were chosen for the full-size crown quadrant concept. These choices were made based on cost savings that included both recurring and nonrecurring labor and material (excluding capital equipment costs), with the nonrecurring costs amortized over 300 shipsets.

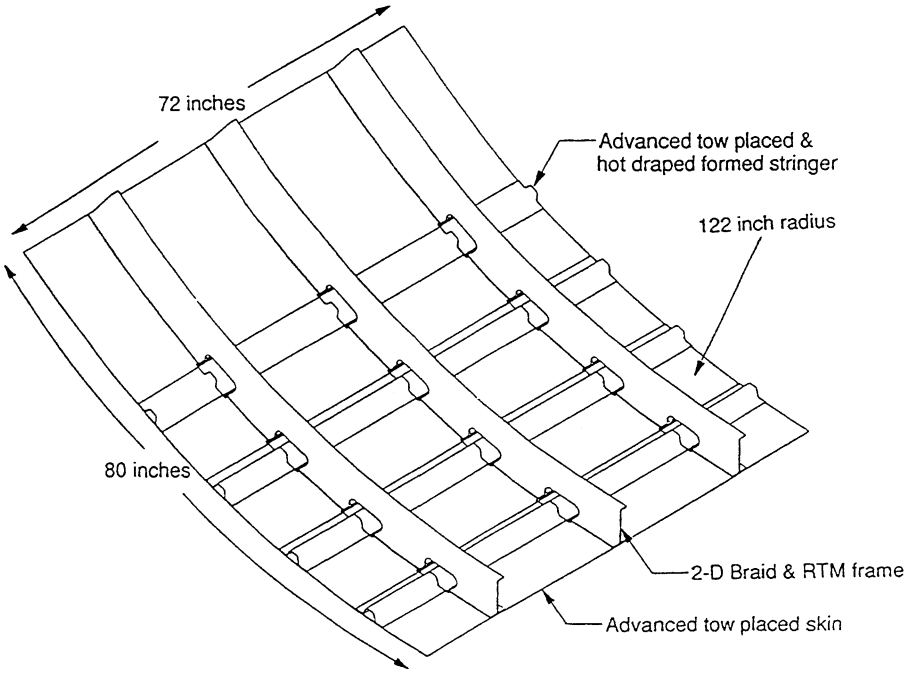

Figure 4-38. Crown test panel design configuration and fabrication processes

Time trials were performed during fabrication of the crown fuselage test panels[1]. Cost was established from the actual touch labor required to build the test panels, material purchase orders, and tooling fabrication costs. Material wastage was estimated at approximately 25 percent. Results of the cost collection are shown in Figure 4-39. The cost collection data was segregated into five areas; tooling, material, detail fabrication, panel bond assembly, and frame/fail safe chord installation using mechanical fasteners.

For comparison with test panel time trials, a cost prediction was prepared using the same detailed estimating procedures applied to get the initial full-size crown quadrant costs described in Reference 4 (also see Figure 4-6 in Section 4.1.1). As discussed in Section 4.2.1, detailed estimates ("bottoms-up" assessments) can be used as a starting point in cost equation development for new technology. Test panel cost estimates were based on the same ACT groundrules as the crown quadrant estimate. As shown in Figure 4-39, the actual and estimated costs for crown test panels compared surprisingly well.

The cumulative touch labor, consisting of 163 process steps, is shown in Figure 4-40. The configuration of Panel #5 differed from Panels #3 and #1 in that the frames were mechanically attached. While the panel bond portion of the touch labor was reduced in Panel #5, this reduction was offset by the fastening of the frames to the skin. This is a

[1]Task order contract (NAS1-19349)

typical trade study result, in that advantages in one area of the process can be offset by disadvantages in another.

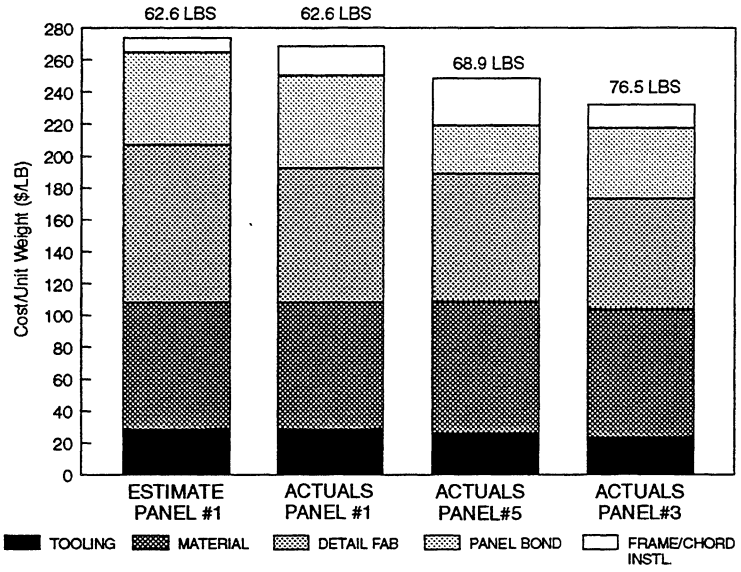

Figure 4-39. Results of crown test panel fabrication.

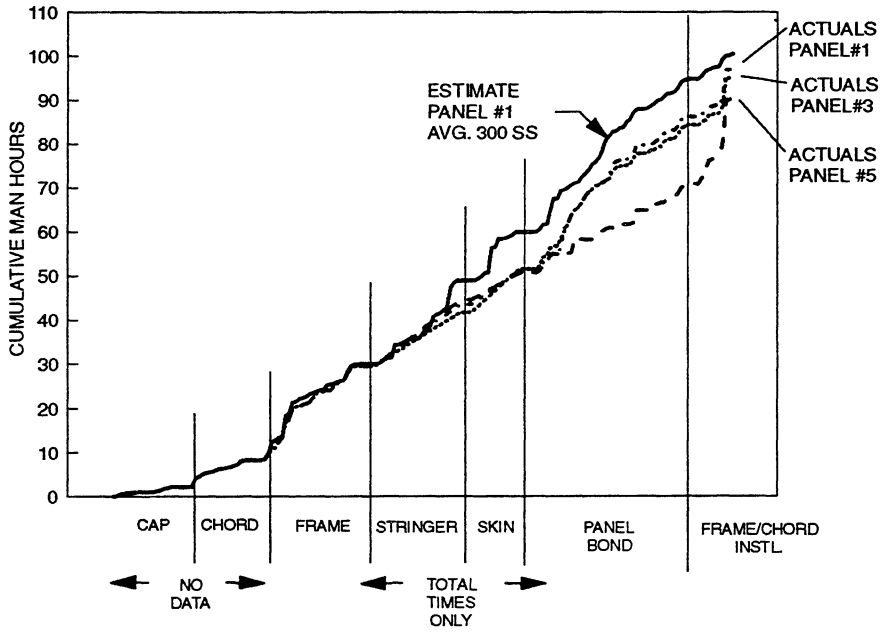

Figure 4-40. Cumulative touch labor for crown test panel fabrication.

The panel bond assembly labor, both cumulative and for individual process steps, is shown in Figure 4-41. While the cumulative actuals and estimate track well, the results for individual process steps have a much lower correlation. Much of the lack of correlation in step-by-step information may relate to measurement errors (e.g., mis-communication between the cost estimator and an individual taking time data for when one step ends and

the next begins). Considering the potential for such errors when first exposing a fabrication shop to test procedures that support cost analyses, the cumulative time information provides a very encouraging trend. The predicted and actual cumulative times at intermediate stages of panel bond (e.g., every 10 steps) compare very well, indicating that higher-level measures of the progress in completing panel bond improve as the total task is completed. Additional panel results would also quantify statistical variations in the step-by-step data, helping to isolate the source of errors occurring at the detailed level.

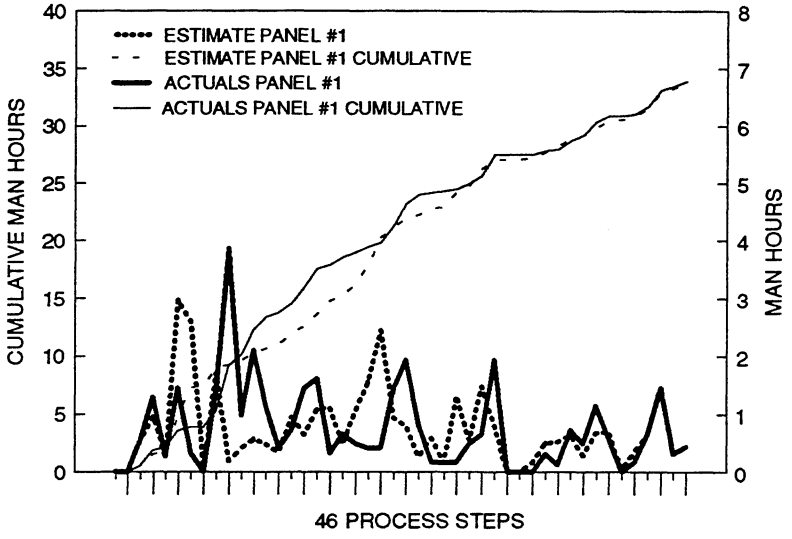

Figure 4-41. Step by step comparisons for panel bond assembly labor.

The production environment differs in many ways from concept research and development. As shown in Figure 4-42, a production environment applied to the subcomponent crown panel size may be expected to lag repetitious fabrication trials performed during research and development. In the early phase of a production program, there are a number of factors that can cause high initial cost. Some of these factors include the learning of new processes and designs, over-manning for cross training prior to rate increases, bottlenecks in factory flow, and, generally, a higher number of problems meeting specifications (some of which require tooling, process, or design changes). As the production program evolves, the crew becomes experienced with the processes and designs, there are fewer design changes, manning levels stabilize, and the factory-related problems (bottlenecks, tooling, and tolerances) become resolved. By contrast, concept development often includes the involvement of manufacturing experts in process trials, adequate manning levels, less bottlenecks between detailed fabrication and assembly tasks (i.e., because a dedicated shop workforce has not been assigned to a single project and idle time cannot be charged to it), and less design or process constraints.

Panel #1 in Figure 4-42 was actually the fifth in a series of crown test panels fabricated and the development team had solved most of the manufacturing problems for the subcomponent scale. The times recorded did approximate the lower level of the production estimate. This implies that the research and development phase of a program can potentially yield insights into how a particular design would fare in a mature

production environment, provided special attention is paid to details crucial to factory flow. Examples of concept development activities that have meaning to production include (i) maturation of robust design features (i.e., structural, producible, and maintainable), (ii) identification of required process labor skill levels, (iii) measurement and control of manufacturing tolerances, and (iv) mathematical simulation of factory flow (requiring process time predictions). Design cost theories described in this report supplement most of these activities.

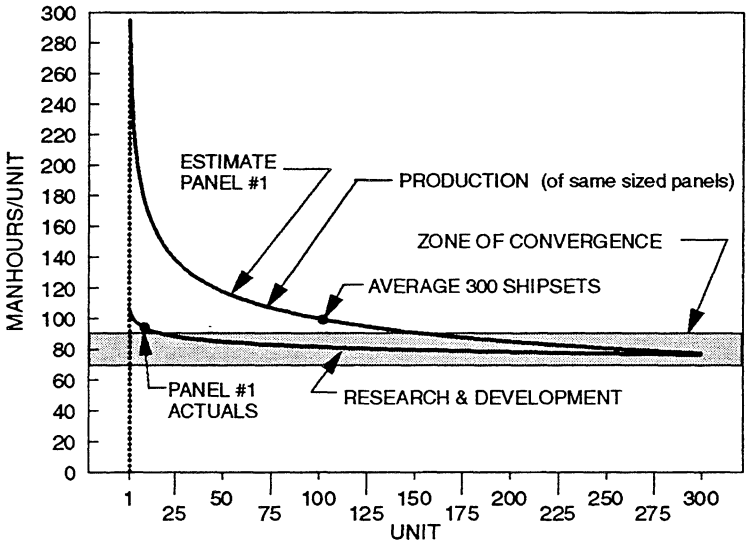

Figure 4-42: Crown subcomponent-sized test panels: production estimates of manual labor versus ATCAS actuals.

Repetitious labor trials using new process technologies can provide insight on the cost effectiveness of particular designs and processes. Without a significant process database and supporting cost analysis, cost effectiveness cannot be proven prior to production commitment. Past experience combined with the processing trials required to fabricate structural test panels can add credibility to the cost analysis supplementing both design and process decisions.

Time studies conducted during the crown test panel fabrication were also compared to the full-size crown panel estimate as cost percentages in Figure 4-43. This simple method for normalizing differences between the sizes of subcomponent panels and full-scale quadrants allows a relative check of cost centers. Percent actuals collected for the test panels compare very well to those from the crown panel estimate in each of the cost centers. Again this illustrates that time trials can yield valuable insight into the relative difficulty of various processes and design details. Assuming similar tooling and equipment are utilized, design details that are difficult to fabricate in research and development may also be difficult to fabricate in production. Note that the nonrecurring estimate for tooling is one area in which the results from subscale trials may have less meaning to production (e.g., more structural reinforcement may be needed for durable production tools). An increase in the nonrecurring production estimate for ATCAS fuselage crown tooling versus that shown in Figure 4-43 is discussed in ref. 5.

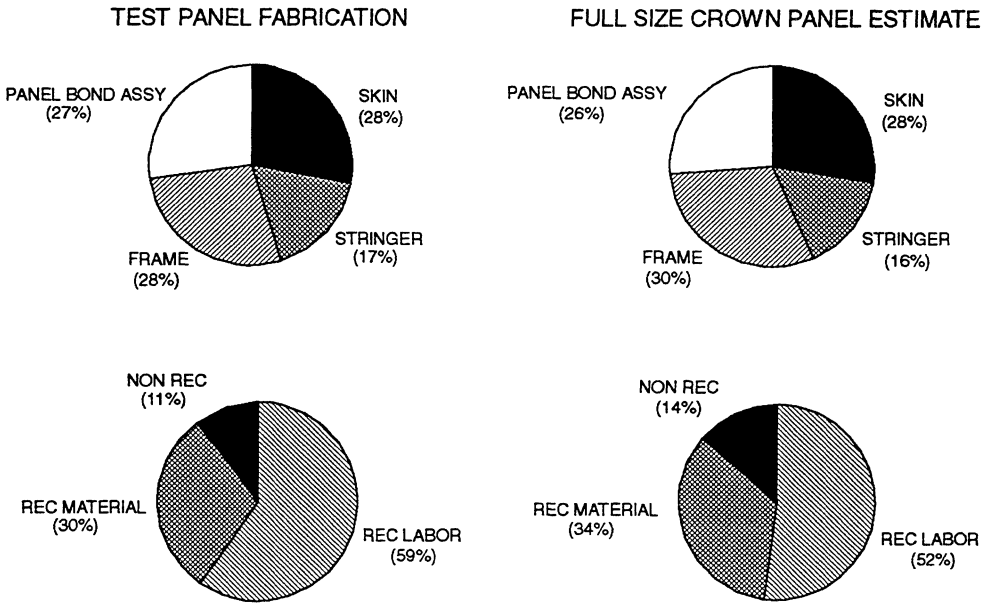

Figure 4-43. Comparison of cost centers derived from subcomponent test panel actuals and full-size crown panel cost estimate.

4.2.5 Recommended Stages of Development

Sections 4.2.1 through 4.2.4 have shown recommendations for the initial derivation of design cost equations and subsequent updates to improve the model's accuracy with expanding databases. The focus has been on procedures that follow the proposed theoretical cost framework for new technology, including specific examples from ATCAS. This section will summarize these procedures as applied during idealized stages of development.

One of the most important benefits that came from design cost evaluation in ATCAS has been the interface between team members with diverse backgrounds. Helpful insights for criteria to status the technology readiness of an integrated database have been derived from these interactions. Continuous cost assessment by the DBT, which required inputs from design, manufacturing, and other functional technology areas, has been the primary discriminator for judging the success of each development phase performed to date (i.e., Stages 1 and 2 in Figure 4-44). Findings from ATCAS have been extended to other technology development and product implementation stages shown in Figure 4-44. The following discussions give the recommended status for continuous cost evaluations and specific cost technology deliverables (i.e., analyses and databases) at each stage shown in the figure. Deliverables to measure the readiness of manufacturing, structures, and maintenance technologies pursued in ATCAS are covered in another report (ref. 5).

Four classes of deliverables have been established for cost-related developments. A brief definition of each is given in Table 4-2. These deliverables are expected to mature at each stage of technology development.

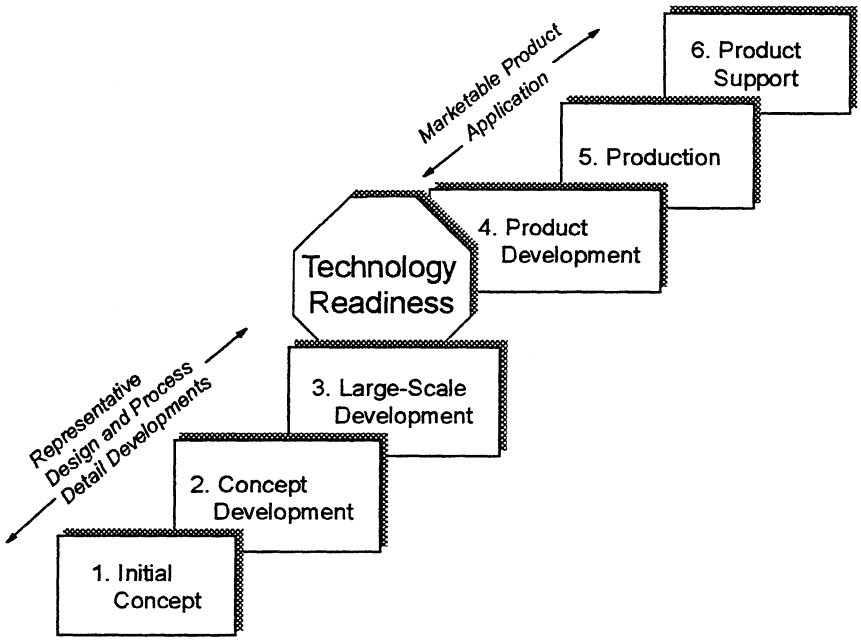

Figure 4-44. Stages of development with a purpose to ensure successful product implementation.

1.	**Total manufacturing cost evaluation.** Studies to quantify labor, material, tooling, equipment, and facilities costs for candidate concepts. Initially determined in DBT efforts used to select a cost-effective concept. These costs are then continuously re-assessed throughout technology development and product implementation for updates occuring with an expanding database.
2.	**Cost methods and manuals.** Documentation and software used to capture critical aspects of cost databases and total manufacturing cost evaluation in a form suitable for DBT support during various stages of development and implementation. For example, specific methods and manuals for selected concepts taken to production should help guide detailed design definition within producibility constraints.
3.	**Cost databases for selected concepts.** Information collected to support total manufacturing cost evaluations from development through implementation. Priorities set for expanding databases should seek to resolve issues and assumptions for cost centers first, followed by the detailed information to achieve the accuracy desired for production commitments. Maintainable links between cost methods, manuals, and databases are essential.
4.	**Value-added assessments of Total Direct Operating Costs (DOC).** A combined measure of total manufacturing costs, fuel and other weight-related costs, and maintenance costs. The Total DOC is of interest to potential airline customers and, therefore, serves as a measure to resolve development trades and eventually market the product (see Ref. 5 for examples and further discussion).

Table 4-2. Key cost deliverables used to status advanced technology development and implementation.

4.2.5.1 Initial Concept

During this stage, manufacturing cost evaluations and a preliminary assessment of Total DOC should lead to the selection of a concept with potential to meet development program goals. In order to make such evaluations, applicable design, manufacturing, and maintenance information and the associated cost database will need to be collected (see Section 4.2.1). In order to justify movement from this stage to the next, the advanced technology selected for further study should have predicted benefits to the value of future products that exceed the associated development costs.

It is also recommended that general cost relationships between selected design features and manufacturing processes be established prior to completing this stage. This may simply be identification of the design variables affecting the cost of specific process steps. In addition, plans should be established to enhance the design cost relationships and develop methods, manuals, and databases needed for the selected concept.

4.2.5.2 Concept Development

Manufacturing cost evaluations and the assessment of Total DOC should be continuously updated based on the database generated during concept development. Manufacturing, design, and maintenance database deliverables in this stage of development are focused on the subcomponent panel level. Information collected during the course of these activities should update the producibility and cost databases for selected design and manufacturing details. As discussed earlier, the processing assumptions most critical to cost should be evaluated first. In addition, the potential to meet development program goals should be updated based on any new technical issues uncovered during subcomponent panel fabrication or structural test. In order to justify further movement from this stage to the next, the advanced technology should continue to have a predicted product value benefit that exceeds the development costs. The development costs used for this comparison should also be updated per additional technical insights gained during stage 2.

General cost relationships from the initial concept stage should be enhanced (e.g., process step equations that predict time) during concept development. For reasons discussed earlier, these equations should have a theoretical basis with constants that have physical meaning. Members of the DBT should be conversant with the specific cost equations related to their area of specialty, facilitating their participation in data collection. Nonrecurring cost analyses for tooling, equipment, and facilities should also be updated based on predicted flow rates for each process cell.

4.2.5.3 Large-Scale Development

Additional updates to manufacturing cost evaluations and the assessment of Total DOC continue during large-scale development. Manufacturing, design, and maintenance database deliverables in this stage of development are focused on panel sizes as close as feasible to full scale. As will become evident in discussions from Section 4.3, large-scale development is normally linked to the fourth stage, product development. Confidence gained from the results of large-scale development is important to airline customer

acceptance of new technologies and, ultimately, helps justify production. This would likely lead to the use of configurations and processes representative of a near-term application for large-scale development. As a result, information collected during the course of large-scale demonstrations is invaluable to updating producibility and cost databases for most design and manufacturing details.

Design cost tools (manuals and software) and associated cost equations should be rigorously evaluated during large-scale development. This should include both an evaluation of the utility of the design tools and the accuracy of process time predictions during design and manufacturing efforts, respectively. Several large-scale design and manufacturing demonstrations may be justified to verify that a concept is both reproducible and has the required flexibility (e.g., tooling) to span the design space for a particular product. Large-scale manufacturing efforts are particularly crucial to assessing many of the assembly steps, which are difficult to evaluate with the subcomponent panels fabricated during concept development.

It is crucial to achieve accurate factory definitions and the associated cost analyses prior to production commitments. Therefore, non-recurring cost analyses for tooling, equipment, and facilities should improve through the course of large-scale and product development cycles. Updated predictions of flow rates for each process cell and an assumed production schedule support such analyses. It is also crucial to update the data supplied from equipment and tooling manufacturers in order to improve the accuracy of factory cost assessments.

4.2.5.4 Product Development

Manufacturing cost and Total DOC predictions are a very important part of product development. By this stage, cost studies go beyond technology assessment to support the definition of a product that is both marketable and profitable. In the case of new technologies, cost and weight results from large-scale development are an important part of achieving the credibility required for airline acceptance and production commitments. Therefore, it is desirable to establish a strong link between aircraft structures considered in product development and the facts and data collected during large-scale demonstrations (i.e., Stage 4). This requires a certain amount of foresight on marketable aircraft configurations, ranges, and payloads.

Design cost equations and supporting databases should be updated as needed to trade design configuration and factory layout differences. Any missing database elements for desirable configurations will have to be pursued through additional development efforts. Design cost tools, such as manuals and software, become increasingly important approaching production, as design cycle time becomes a critical cost element of the product. These tools will be exercised for different configurations and process sequences during product development, but then constrained to support the detailed design of specific concepts selected for production.

As discussed, product development efforts to continuously improve non-recurring cost assessments will ultimately lead to factory definitions that are set by the start of

production. Manufacturing characteristics that need to be understood include processing rates, delays, scrap, quality rejections (e.g., fabrication defects and unacceptable assembly tolerances), rework, and maintenance for tooling and equipment. The combined effect of these database elements, which will likely depend on specific design traits, may benefit from factory computer simulations. Note that such simulations are part of the deliverables that have been recommended for stages of manufacturing development (ref. 5).

4.2.5.5 Production

Final definition of design and manufacturing plans occur after a commitment to production. Much of the *potential cost savings* of a concept have been set by the path taken in previous developments (e.g., favored processes, materials, and factory definitions). However, the ability to *achieve minimum manufacturing cost* relates to the design cost insights, database, and tools available to help production DBT make timely decisions. The goal is to select design details for optimum overall product value (i.e., minimizing weight, while ensuring producibility and maintainability).

As a recommendation, all cost deliverables applied to production should be constrained for decisions made previously and at a level of readiness that allows their reliable use in a schedule-driven environment. An appropriate analogy for changes in design cost tools from the versions used in development to those required for production can be seen in the difference in machine specifications for prototype and production equipment. As is the case with prototype equipment, cost tools used in development have more degrees of freedom. Approaching production, both design cost tools and equipment are best constrained to a design/manufacturing space and associated databases that can reliably support production.

The collection and synthesis of production data can prove invaluable in support of derivative aircraft definition and future technology developments. During the course of a production program, the expanding database should be used to update design cost equations, databases, and tools. Again, it is recommended to maintain a theoretical basis during such assessments. Empirical determination of traditional production parameters such as learning curves and variances may not be as helpful as the data synthesis that allows a more rigorous understanding. Two examples of this include (1) updates for design cost equations based on process changes that led to improvements, and (2) the identification of undesirable design characteristics that slow processes and result in an inordinate number of defects.

4.2.5.6 Product Support

It is desirable to update cost databases with insights from service experience. Therefore, some efforts in design cost evaluation should also be linked to product support. The primary issue is to better understand how the technology applied to a product affects its service reliability and life. For example, in the case of aircraft structure, the Total DOC has components related to maintenance. Actual data from service may help identify unreliable or difficult to repair design and process details.

During development phases it is very difficult to quantify maintenance costs for new technology. One recommendation is to include airline maintenance participation in developmental DBT activities. In ATCAS, airlines support to concept selection and repair technology development at the subcomponent panel level proved invaluable in acquiring insight on maintainable structure (ref. 5). Future design cost efforts should focus on a quantitative approach to predicting the maintenance costs for new technology.

4.3 Design Cost Model Applications

A company that is in business to design and manufacture an advanced product form wants to quickly complete development, win customers, minimize production startup costs, and achieve income. In the case of commercial aircraft, technology for structural design, manufacturing processes, and maintenance procedures are needed to win customers and produce a profitable product. The ability to recoup development and capital investments depends on timely product definition and efficient use of manufacturing facilities, including equipment and tooling. Figure 4-45 shows that a design cost model and supporting tools (manuals & software) can help meet development and production goals. The proposed theoretical framework for design cost model development is also set up to support multiple applications. Initially, it can help focus development on marketable technology and definition of an efficient factory. Once the technology is established, it can help train an engineering workforce to identify design features compatible with the chosen factory.

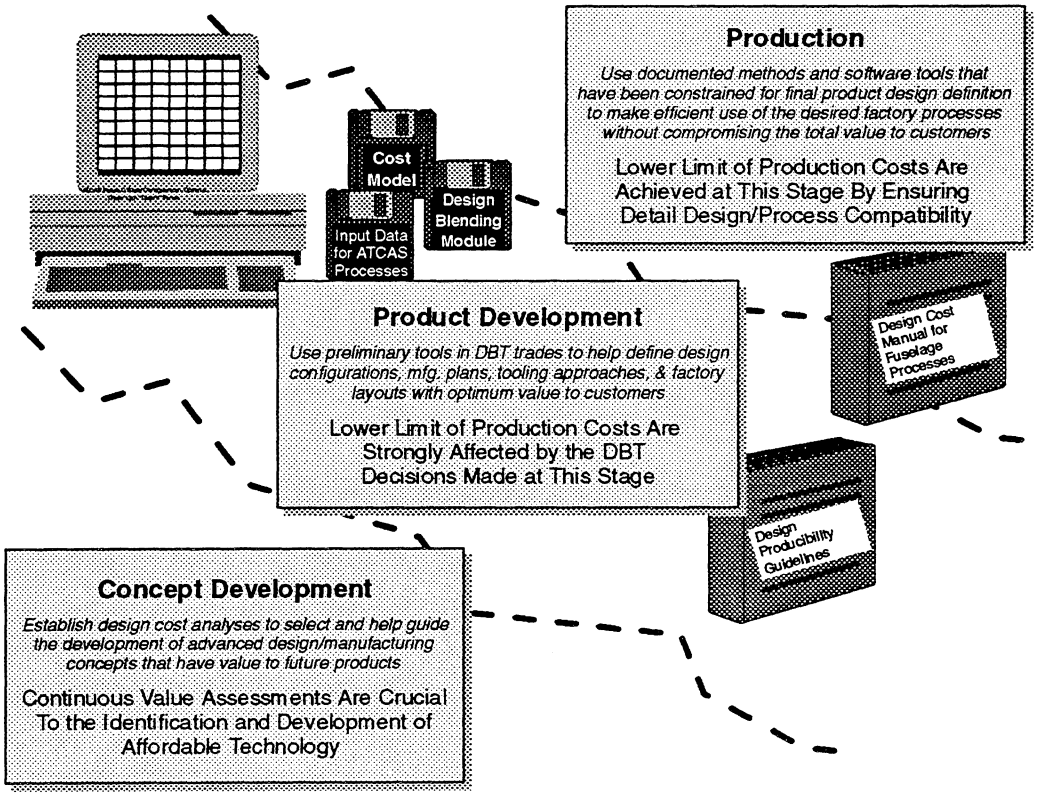

Figure 4-45. Three Applications of a Design Cost Model.

Applications for a design cost model change with the stages of development and product implementation discussed in Section 4.2.5. The theoretical framework proposed for such a model has a flow diagram which shows both applications and cycles for updating cost analyses (see Figure 4-1). Three types of applications are envisioned, each crucial to guiding the DBT at different stages. These include:

(1) Early applications for a design cost model focus on quantifying benefits of the technology and guiding developments.

(2) Approaching the implementation of a particular product, the model will help optimize the design configuration and define the manufacturing facility.

(3) Finally, a design cost model can help complete product definition with an assessment of how specific design details affect process flow and the resulting manufacturing cost.

This section will briefly cover some considerations for the three applications of a design cost model. These applications are covered in Sections 4.3.2, 4.3.3, and 4.3.4. To date, ATCAS efforts have mostly been limited to the first application, with a focus on the analysis of process times during initial stages of development. The early focus on process times will be justified by discussions in Section 4.3.1.

4.3.1 Importance of Process Time and Manufacturing Efficiency

Much of the cost for manufactured products have some relationship with the times to complete process steps (including setups and delays) and manufacturing efficiency (including material utilization, quality control, defect rejections, and rework). Process times and efficiency are obviously important to recurring labor costs. In addition, nonrecurring costs for the quantities of equipment and tooling needed to make production rate and the associated facilities floor space also depend on process times and efficiency. This realization has led ATCAS efforts with new technologies to focus on a theoretical framework for predicting process time and material utilization rates.

The conversion of manufacturing times to labor costs is relatively simple, yet company and process specific. Labor costs for a given process are generally a function of:

(a) the required crew size,

(b) labor rates (cost/unit time) for a given skill level,

(c) burden rates (e.g., employee medical and retirement benefits) for a given job description, and

(d) overhead rates that depend on a company's accounting practices.

Overhead rates can confound the calculation of costs associated with labor by including the effects of other costs. For example, overhead rates may include amortized equipment and facilities costs and management or other administration costs.

The NASA ACT Program established cost estimating groundrules for Phases A and B that did not directly assess capital equipment or facilities costs. Instead, a constant

recurring labor "wrap rate" of $100/hr was applied to allow cost assessments during the first two stages of composite technology development (initial concept and concept development). Tooling was more directly assessed; however, a non-recurring "wrap rate" of $75/hr was also used to determine the labor (and hidden equipment and facilities) portion of tooling costs. The cost understanding for new technologies considered in ATCAS has evolved to allow more accurate assessments of equipment, tooling and facilities in subsequent phases of the program. As will become evident in discussion of the following applications, such analysis is crucial during large-scale and product development stages to define a factory for production.

In order to elaborate on how process times can affect tooling, equipment, and facilities costs, consider the following scenarios. By definition, an "efficient factory" has processes that require a minimal combination of labor, equipment and tooling costs, whereas an "inefficient factory" may require more workers, equipment, and tooling for the same production rate. Considering the mathematical theories presented in Section 3, part quantities, sizes, and/or design complexity that are inappropriate for a given process can lead to high dynamic time constants or low velocities. This not only increases processing times, but forces a larger workforce or the purchase of more equipment, tooling and facilities floor space to meet demands for the product. The combined effect of all these factors determine production costs. Alternately, design concepts that decrease process times (i.e., smaller complexity scaling factors, low dynamic time constants or higher velocities) or improve efficiencies (i.e., minimum setup or down times for maintenance) may reduce equipment or tooling needs.

Interactions between process cells in a factory are also crucial to overall factory efficiency. One or two inefficient process cells will have to expand to maintain the rate of other cells. Alternatively, the entire factory could be slowed to the pace of inefficient process cells. This could be achieved by effectively slowing the rate or increasing the dwell (inactive) times of efficient process cells. Part inventories could also be created by operating the efficient processes at full rate, with the added expense of storage costs. All of these scenarios are undesirable because either (a) total production costs increase, (b) the return on investment is delayed, or (c) potential customers are lost.

In general, the cost for raw materials bought from outside suppliers depend on the purchase price, internal receiving inspection costs, and the efficiency of specific processes that use the material. When raw materials are bought from an outside company, the associated purchase price is generally driven by the supplier's production costs (which depend on their labor times, facilities, etc.), required quantities, and the market or demand for the material. Receiving inspection costs may depend on specific engineering requirements applied to control the raw material quality. The material utilization rates for specific processes may depend on features of the design.

4.3.2 Benefits Analyses to Guide Development

Figure 4-46 shows the development cycles leading to the first applications of a design cost model (i.e., benefit analyses performed to quantify the value of new technologies in

future products). These analyses help to justify the selection of a concept for development. During the first two cycles shown in the figure, analyses are continuously updated based on the data collected to address cost centers, producibility, design drivers, and technical assumptions that are most critical to the benefits. The two cycles in Figure 4-46, which link to initial selection and concept development, are the only stages performed to date for ATCAS fuselage technology.

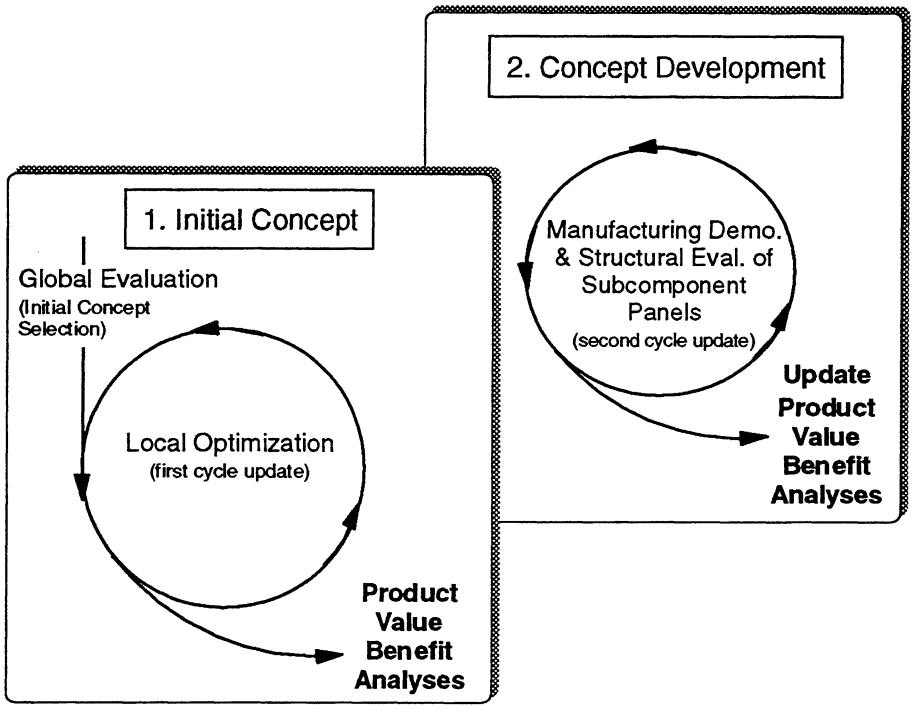

Figure 4-46. Application and update to a design cost model during initial concept selection and development.

As compared to large scale and product development, the combined cost of the first two stages shown in Figure 4-46 are likely to be smaller. Nevertheless, the length of time to complete initial concept selection and development will be comparable to subsequent stages. This investment in development time should be justified by pursuit of advanced concepts with potential benefits to new products. Continuous cost assessments, with increased accuracy as the database expands, is essential to make commitments to the third stage, large-scale development, which has significantly higher costs.

Benefit analyses require predictions of the production costs that have been discussed throughout this report and an assessment of the required development costs. The production costs for existing (state-of-the-art) technology and those for advanced concepts under development are both needed. In the case of ATCAS, the former is currently represented by 1995 aluminum fuselage technology (ref. 5). Simple calculations can be performed to predict the return on investment (ROI) in development costs for advanced technologies. These calculations should show that the added product value for advanced technologies under development yields an acceptable ROI. The time

value of money should be considered in such assessments. Note that transport fuselage and wing technology that meet the ACT goals for cost and weight savings versus state-of-the-art aluminum have been found to more than justify the investment costs projected to complete all development stages.

4.3.3 Analyses Supporting Design Configuration and Factory Definition

Figure 4-47 shows development cycles leading to the second type of applications for a design cost model, which are focused on specific company product strategies. These include analyses to (1) quantify the value of different producible design configurations, and (2) define the associated manufacturing facility (i.e., factory, equipment, and tooling). These analyses complete technology development stages and prepare for a specific production program. During the first of two cycles shown in Figure 4-47, analyses are continuously updated based on the large-scale producibility and manufacturing cost data collected. The product development cycle shown in the figure, uses the existing database from a space that has been deemed "technology ready" to define the design and manufacturing plans for marketable products. Complementary to these efforts, are detailed analyses of the cost to facilitize a factory capable of producing the expected production quantity and rate.

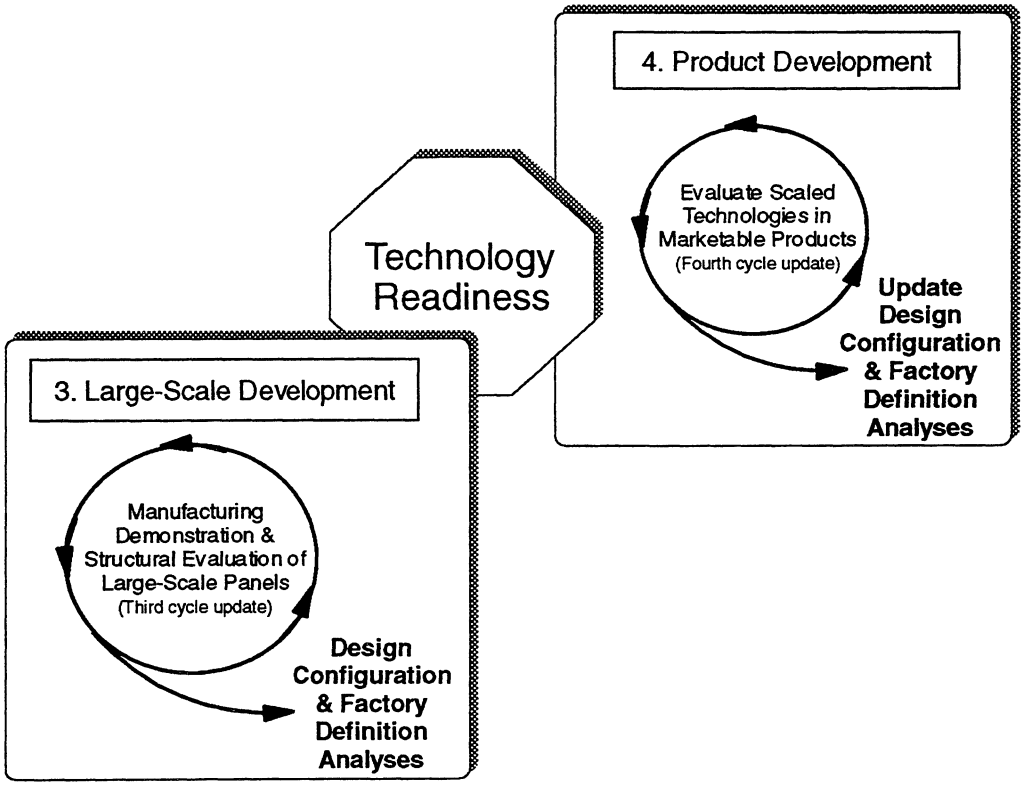

Figure 4-47. Application and update to a design cost model during large-scale and product development.

Large-scale development efforts are very important to defining equipment and tooling requirements. Production equipment and tooling cost assessment may require some

special attention. Since prototype equipment may be used to develop many different products, it could have significantly more degrees of freedom and an associated higher cost than production equipment. As such, the actual cost of prototype equipment used for large-scale development may not provide a good basis to estimate production equipment. The tooling used for large-scale development may also not be representative of production tooling. In this case the actual cost of the tooling used in development may be less than that for production. Alternatively, special efforts may be required to predict the durability of production tools and avoid the high cost of conservative design approaches used to extend tool life. Tooling and equipment maintenance costs, which may relate to design complexity, should also be considered in support of credible non-recurring cost estimates.

The production rates (number of products required per month), total production run, and process step times will each have a strong effect on non-recurring cost assessments. The first two factors depend on the demand for a product and, therefore, will be linked to market assessments. Process step time predictions should improve to become very accurate through the last two development cycles which are shown in Figure 4-47. As discussed in Section 4.3.1, this is important to determining some of the tooling & equipment quantities and associated floor space. These and other factors crucial to tooling, equipment, and facilities assessments are described below.

4.3.4.1 Tooling Assessments

The number of tools needed for production will depend on production tooling utilization rates. These rates depend on a number of factors starting with the fabrication or assembly time of the process that uses the tool. Other factory efficiencies that determine tooling needs include the flow of adjoining processes that either (1) input detailed parts which are assembled on the tool or (2) remove a finished assembly from the tool. Any input or removal delays may force the part to remain on the tool, which in many cases is also a handling fixture, for a longer time. Other factors affecting tool utilization rates include the cleaning time and maintenance required before the tool can be used again.

The cost of a particular tool will relate to most of the same factors that affect product manufacturing costs. This includes design development, labor, raw materials, and non-recurring burdens for the facility and equipment used to manufacture the tool. The durability of tools used to fabricate composite parts should be considered in design. A non-durable design may trade lower unit costs for shorter life and higher maintenance costs. This is particularly crucial in the case of autoclave or RTM cure tools which are cycled to extreme temperatures and pressures. For example, graphite/epoxy cure tools may appear to be cheaper than those fabricated from a dimensionally stable metal (e.g., invar) but durability could become an issue for high production rate programs.

As discussed in Section 3.4, additional tools may be required when manual operations become overly strenuous (e.g., handling or locational jigs). The design size and complexity scaling issues discussed in Sections 3.2 and 3.3 may also affect the number of tools by slowing the process. Structural details that would likely lead to decreased tool utilization and, therefore, higher non-recurring costs should be identified. A compatible

design space and appropriate constraints could then be documented as part of producibility guidelines for production design. It may even be possible to use design cost software tools to simulate the effect of incompatible design details on step changes in the non-recurring costs for additional tools.

4.3.4.2 Equipment and Facilities Assessments

Equipment resources are allocated based on the minimum quantity of products expected, the required production rate, and equipment utilization rates. In ATCAS, the first two were assumed to be 300 shipsets and a rate of 5 shipsets/month, respectively. Often a company's equipment costs will be amortized over an assumed number of shipsets. This can be achieved through labor burden rates as discussed in Section 4.3.1. In practice, the production rate will not likely remain a constant through the life of a program. When production goes beyond the assumed number of shipsets, some changes to the program's cost structure are likely. Additional costs related to increased equipment utilization, maintenance, and replacement will need to be evaluated.

Equipment assessments are affected by some of the same factors that were discussed for tooling in Section 4.3.4.1. The cost of a particular piece of equipment will relate to most of the same factors that affect product manufacturing costs. These include design development, labor, raw materials, and non-recurring burdens for the facility used to manufacture the equipment. For a given production scenario, the amount of equipment needed will depend on the equipment utilization rates and process flow between cells. Unlike tooling, which may hold a finished part until the next process cell is available, equipment that has completed one part should be ready for immediate use in fabricating the next part. However, equipment utilization could be delayed by the availability of required tools. The added complexity of moving parts, electrical controls, and other systems that comprise automated equipment may lead to more maintenance for equipment than for tools.

A trade between automation and labor for some strenuous manual tasks should consider both production costs and factory safety. Such a trade may change depending on design size and complexity scaling factors for a specific product. As discussed in previous sections, such factors are likely different for automated and manual processes. Once committed to an automated process, structural details that would likely lead to decreased utilization and a need for more equipment should be identified. As was the case for tooling, a compatible design space and appropriate constraints could then be documented as part of producibility guidelines for production design. It may even be possible to use design cost software tools to simulate the effect of incompatible design details on step changes in the non-recurring costs for additional equipment.

The required facilities floor space will relate to the factory layout and the space needed for all equipment and tooling. Again, a significant dependence on the production rate is expected. For example, a facility may be designed to include more space than that required at the start of production because of plans to expand for increased rates based on market analysis. Generally, equipment and tools will not be purchased until they are needed for production. Special facility considerations may include structural foundations

that depend on the weight of tools and vibration requirements for equipment. Energy resources and the associated systems needed to run the factory must also be considered.

4.3.4 Analyses Supporting Production

Figure 4-48 shows the third type of application for a design cost model, which is focused on a specific production program. These analyses help finalize design and manufacturing process details to meet product cost and weight goals. At this stage, accurate process time predictions are needed for allowed changes in design details and flow through the factory that has been committed for production. As a result, cost analyses are constrained to a finite space and it is desired to help guide the design towards options that permit efficient factory utilization. In order to accomplish this in a timely manner, the developments of previous cycles should mature the design cost model to be ready for production problems. Pressure to achieve reduced cycle times and lower costs in future applications will continue to force all design cost tools used in production to be quicker and more accurate.

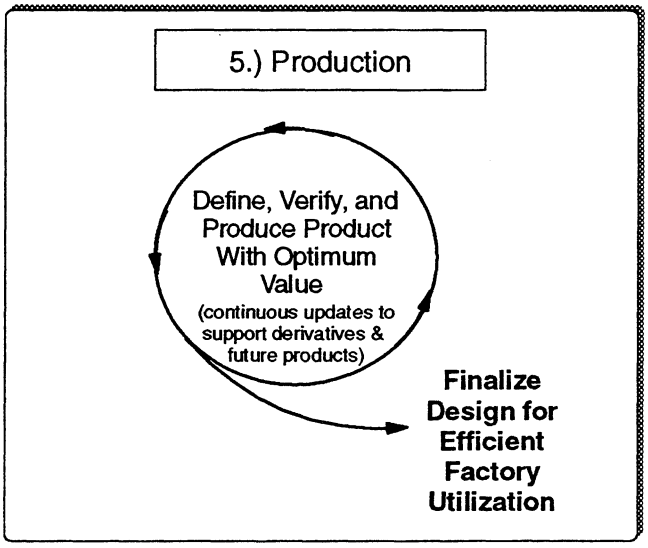

Figure 4-48. Application and update to a design cost model during final product design and production.

During the production cycle shown in Figure 4-48, analyses should be continuously updated based on the manufacturing data collected. These analyses will benefit any derivative product definitions expected to use the same manufacturing facilities. The data collected during production runs will also help guide future development efforts to best suit a company's product line and achieve the technologies needed for cost improvements.

5.0 COMPOSITE TRANSPORT FUSELAGE STRUCTURE APPLICATIONS: STAGE 2 STATUS

The ATCAS program has developed and demonstrated an application of the theoretical design cost framework discussed in Sections 3 and 4 of this report. Section 4.2.5 provided recommended stages of cost model development with the goal for supporting successful (i.e., cost-effective) implementation of an advanced product form. Section 4.3 highlighted the type of design cost model applications likely to occur during each stage of development. To date, ATCAS has progressed well into Stage 2 development with composite fuselage design concepts. This section will highlight status of the Process Cost Analysis Database (PCAD), including examples of the key design variables and process parameters found to have the greatest effect on current cost projections. As a prelude to this discussion, a synopsis of the designs and processes selected for development in ATCAS will be given.

5.1 Synopsis of the ATCAS Concepts

The ATCAS program started in 1989. The primary objective of ATCAS is *to develop an integrated technology and demonstrate a confidence level that permits the cost- and weight-effective use of advanced composite materials in primary structures of future aircraft with the emphasis on pressurized fuselages*. Phases A and B of the ATCAS program ended in early 1996. Work performed in these first two phases relate to all of the first stage (concept select) and part of the second stage (concept development) described in Section 4.2.5.

The ATCAS program cost and weight goals, including aircraft resizing, are:

1.) 20 to 25% reduction in acquisition costs, and

2.) 30 to 50% reduction in structural weight.

These goals are expressed relative to state-of-the-art aluminum technology. Note that aircraft resizing for the weight saved yields both cost and weight benefits.

Rigorous trade studies performed during Phases A and B of ATCAS have focused the program on the development of potentially cost-effective designs, materials, and processes (refs. 4, 5, 48-53). Related cost model developments focused on characterizing the cost of designs by summing the effects manifested at the individual process step level. Such characterization allows greater potential utilization of the current production experience contained within any new process. For example, most advanced processes include steps that are the same or similar to other activities currently performed in a production environment. Those ATCAS process steps that do not have production equivalents have generally been governed by equipment parameters and related operations. As discussed in Section 4.2.4, manufacturing time trials performed during development can (1) demonstrate the applicability of production experience to the new designs/processes and (2) support creation of a database to predict missing cost components.

5.1.1 Baseline Quadrant Design Definition

Figure 5-1 shows the baseline fuselage section used for ATCAS studies. It has a constant diameter of just over 20 feet, and a length of 33 feet. This section is immediately aft of the main landing gear wheel-well bulkhead and is representative of the constant diameter portion of Section 46 on Boeing airplanes. The baseline section was selected because it contains most of the structural details and critical manufacturing issues found throughout the fuselage while avoiding higher program tooling costs associated with non-constant cross-sections. In addition, this section has significant variations in design detail due to high axial loads in the forward end which diminish, allowing transition to minimum gage structure, in the aft end. Structural scale-up of this study section requires consideration of a wide range of critical design criteria and load cases, such that the resulting technology is directly applicable to other areas of the fuselage.

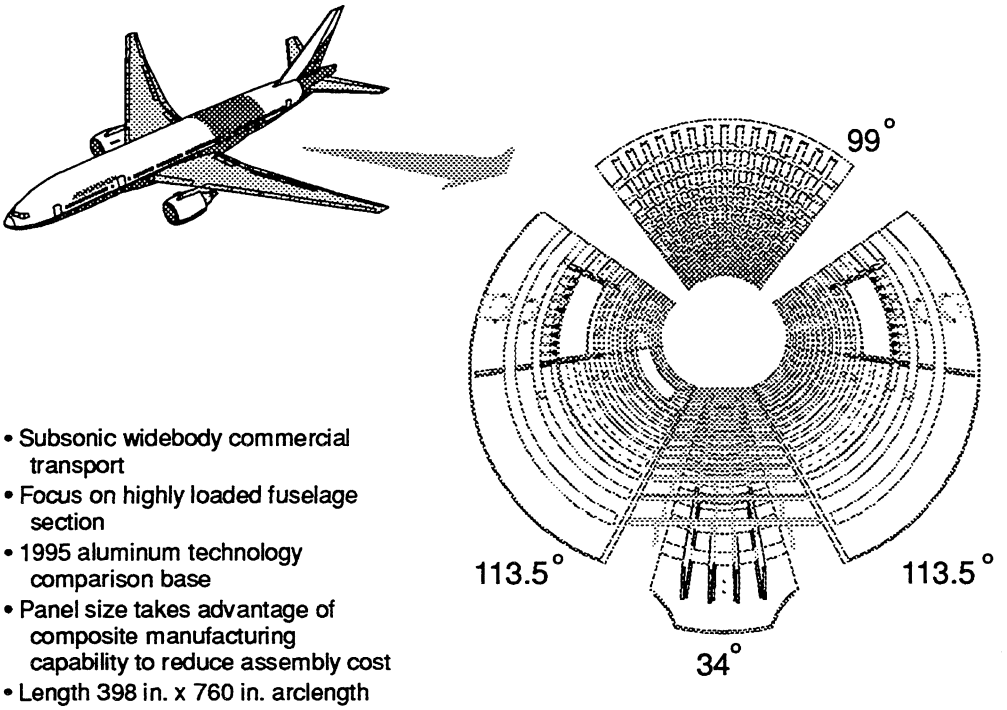

Figure 5-1. ATCAS fuselage barrel and quadrant definitions.

Also shown in Figure 5-1 are the four panel assemblies, called quadrants, that comprise the ATCAS barrel segment. The equivalent metal aircraft section is made up of ten individual panels due to limitations of rolling highly polished aluminum skins. Top, side, and bottom ATCAS quadrants have been referred to as crown, side, and keel panels, respectively. The current ATCAS crown is a stringer-stiffened skin concept, while both keel and side quadrants are sandwich panels. The ATCAS studies performed to date have assumed similar left and right side quadrants, ignoring the right side cargo door. The only ATCAS quadrant comparable in size to a typical metal fuselage panel is the 34° keel. Additional details on the quadrant designs pursued in ATCAS can be found in ref. 5.

Large skin panels were selected for ATCAS to reduce panel assembly costs and leverage the size-related efficiencies of the automated fiber placement (AFP) process for laminated skins. The ATCAS section has the advantage of six less longitudinal splices which, for carbon composite structure, require the use of expensive titanium bolts rather than the low-cost aluminum rivets used in metal fuselage. However the fewer but larger composite crown and side panels present significant technical issues, such as handling and assembly of large stiff structures. Typically during assembly of current metal fuselage sections the skins and stringers are left unfastened for approximately 30 inches at each circumferential splice so that the individual stringers can be "wiggled" for splice alignment.

5.1.2 Processes Leading to Potential Cost Savings

The ACT goals to achieve cost savings versus state-of-the-art aluminum require significant advances in technology beyond that currently realized in composite production. Designs and processes selected for ATCAS have the potential to meet these program goals (ref. 5). The approach used to achieve this potential has included aggressive pursuit of low cost materials, producible designs, large lot sizes, and advanced processes. Although the promise of potential cost savings exist in the concepts pursued by ATCAS, significant technology hurdles remain to be addressed. At the forefront of evaluating the readiness of new technology, are continuous value assessments that utilize design cost models and databases.

As discussed in Section 4.1.1, the ATCAS DBT approach began work in each quadrant with a global cost and weight evaluation of full-scale panels. Further insights on the steps used for global evaluation of ATCAS quadrants are given in Sections 4.2.1 and refs. 4, 49, and 50. Global studies resulted in the selection of design concepts and manufacturing pre-plans with the potential to achieve ACT goals. The latter included a factory layout of process and assembly cells. For purposes of illustration, Figures 5-2 and 5-3 show the factory layout used for sandwich side quadrant fabrication and barrel assembly manufacturing plans, respectively.

The side quadrant processing cells in Figure 5-2 include (1) AFP for skin lamination, (2) core blanket fabrication (forming, splicing, and machining), (3) braided/RTM frames, (4) panel subassembly on OML cure tools, (5) autoclave cure, (6) panel trim, and (7) ultrasonic inspection. The keel quadrant is envisioned to be fabricated using a similar process flow. Sandwich core processing cells are replaced by tape lamination and drape-forming cells used to process hat-stringers for the baseline crown quadrant.

Cost and weight assessments performed in ATCAS included window, door, and floor installation. Only floor installation is evident in Figure 5-3. Also included in cost and weight analyses were barrel assembly steps to achieve longitudinal quadrant splices, and circumferential splices to join adjacent body sections. Note that half the cost and weight of each circumferential splice was added to get totals for the barrel section. Assembly cells in Figure 5-3 include (1) pultrusion/continuous RTM for floor beams and stanchions, (2) cargo floor installation to the keel quadrant, (3) passenger floor subassembly and installation, (4) side to keel longitudinal splices, and (5) crown to side longitudinal splices.

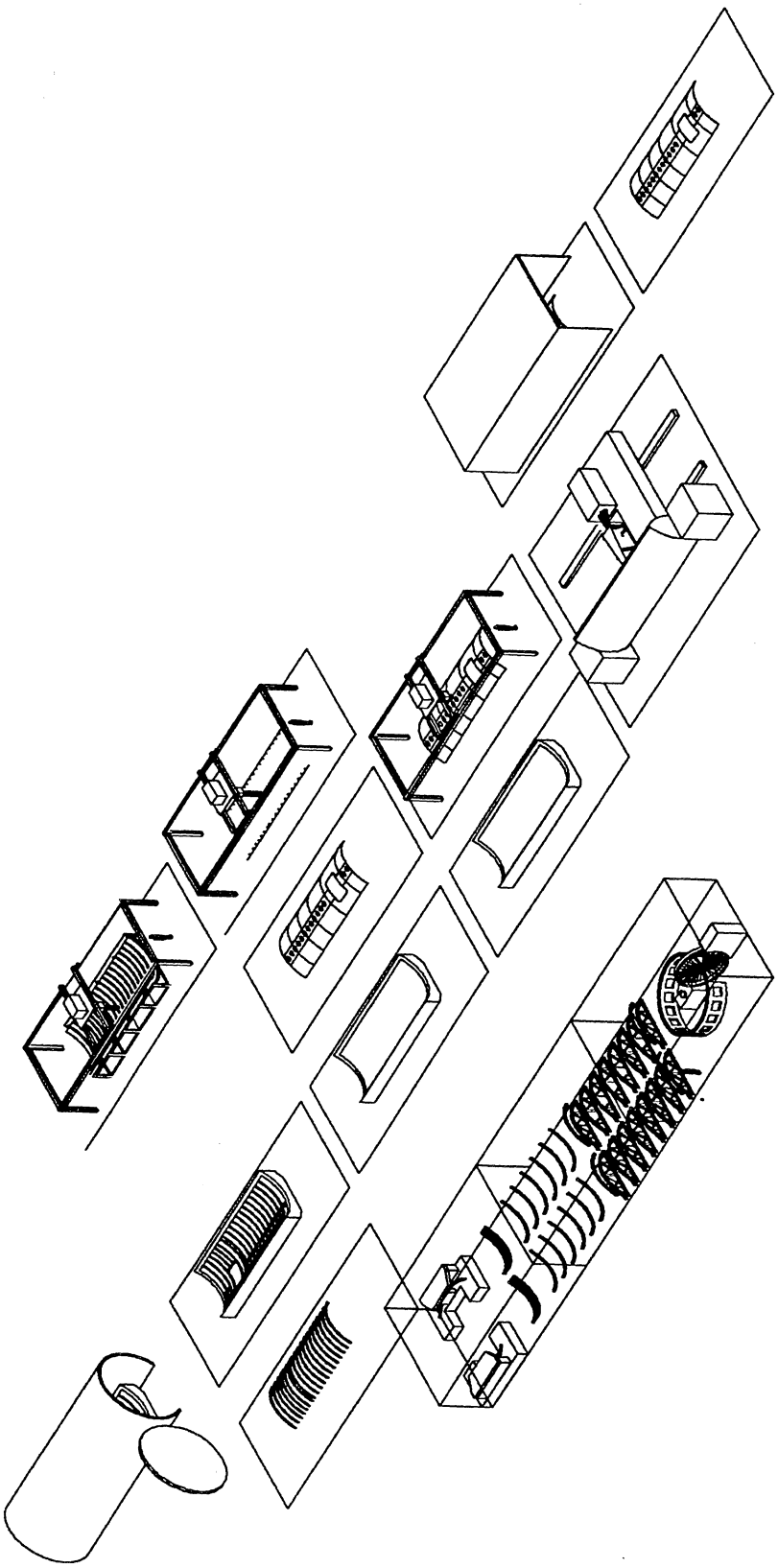

Figure 5-2. ATCAS baseline side panel fabrication cells.

Figure 5-3. ATCAS baseline barrel section assembly cells.

All ATCAS processes were selected based on analysis indicating potentially lower total manufacturing costs for transport fuselage structure. Throughout Phases A and B of the program, process development of selected concepts have included a thorough evaluation of fabrication steps crucial to projected cost savings. Manufacturing demonstrations were performed in the crown, keel, and side quadrants. As discussed earlier, these demonstrations helped supplement cost databases with insights on producibility and time trials for key process steps. Process development for splices was limited to small elements and sandwich panel close-outs due to budget and schedule constraints. However, each large panel was subjected to tolerance (panel thickness and element location) and warpage measurements to quantify the success of fabrication in reducing variation and, hence, minimizing assembly costs (i.e., gap/gauging & shimming). Additional details on the ATCAS manufacturing plans and process developments can be found in ref. 52.

5.2 ATCAS Cost Equations and Database

This section will highlight predictions from the cost equations and database used for ATCAS baseline processes and designs. Since ATCAS technology is under development, accuracy of the equations and database is also evolving. The PCAD software has been created to support this evolution in three main ways (ref. 55). These include: (1) help the DBT manage cost equations and coefficients over time through a relational database architecture, (2) predict the cost of a *given* design entered as input, and (3) provide preprocessing of cost data decks for COSTADE. Cost analyses performed with COSTADE differ from those performed with PCAD via added links to practical optimization, blending, and other design utilities which can automatically synthesize and *change* a design while evaluating cost (ref. 1, 48).

Cost equations that represent ATCAS baseline processes/designs (at the end of Phase B) and a limited number of other configurations can be found in ref. 55. This reference also includes user instructions for the PCAD software, including tutorial descriptions of basic data elements (i.e., parts, configurations, manufacturing plans, and cost methods).

The following three subsections cover predictions using the ATCAS cost equations to differing levels of detail. Section 5.2.1 presents a breakdown of the components of total baseline concept costs, including labor, tooling, and material. Note that most of these costs are currently predicted using equations in the PCAD software (ref. 55). In Section 5.2.2, the physical significance of typical equation parameters and the effect on labor cost predictions will be discussed. Section 5.2.3 discusses cost predictions for the four most critical process cells, three of which relate to quadrant panel fabrication.

5.2.1 Synthesis of Design Cost Predictions

Cost predictions using ACT groundrules for the ATCAS design and process concepts considered baseline at the end of Phase B yielded a total cost of approximately $369 million for 300 shipsets (ref. 5). As shown in the upper right corner of Figure 5-4, this prediction includes recurring labor and material costs and non-recurring tooling (labor and material) costs. Recurring labor appears to be the largest portion of the total cost.

However, the recurring labor wrap rates used in the cost estimating groundrules have values (i.e., $100/hour) that imply some burdening (e.g., accounting for facilities, capital equipment, and administrative costs). As was the case for technologies pursued by NASA ACT, constant wrap rates may be suitable for early stages of concept development. However, the values implied by a constant wrap rate can be misleading. A more rigorous cost analysis, using labor rates that depend on the specific process or business situation, is recommended to support decisions on product design and factory implementation (i.e., see the second application for a design cost model described in Section 4.3).

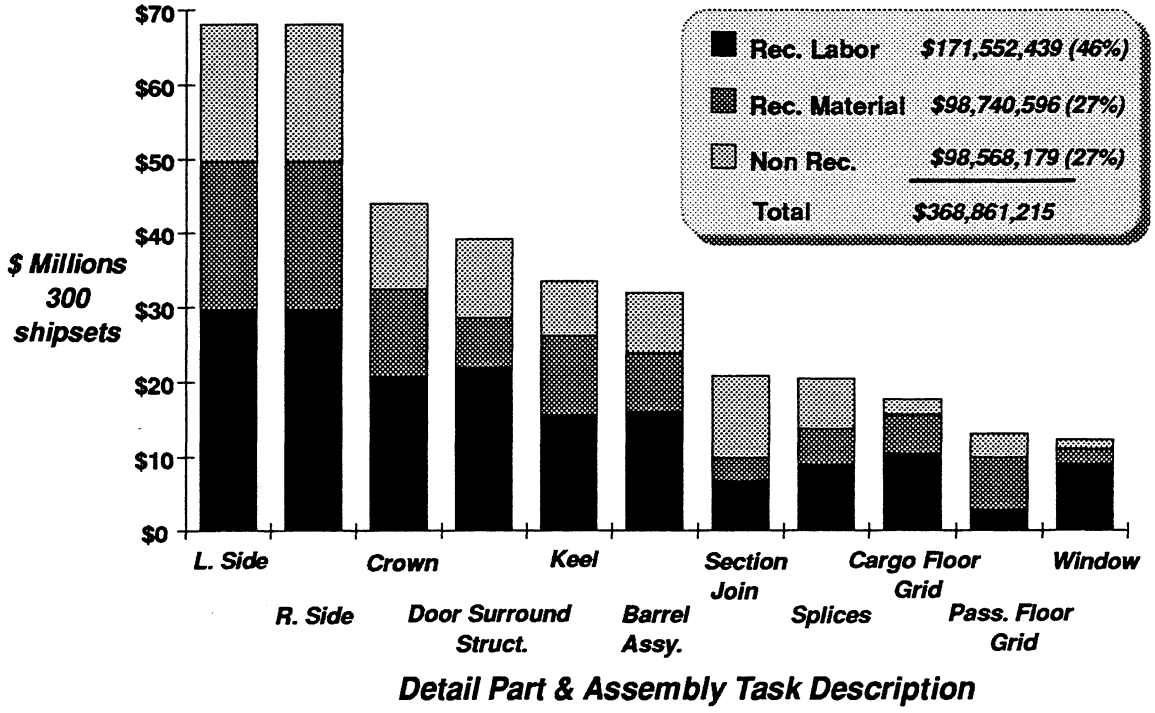

Figure 5-4. Part costs for the ATCAS baseline fuselage section.

Figure 5-4 also shows the breakout of costs per detailed part fabrication and assembly tasks. Most of the task descriptions in this figure are self-explanatory. Note that "Barrel Assy." includes mechanical attachment of floor grids to the quadrants and longitudinal splice assembly.

Figure 5-5 shows an additional breakdown on the costs for a side quadrant. It is interesting to note differences in the cost components for each part comprising a side quadrant panel. Materials dominate the cost of tow-placed skins, while labor is crucial to frame fabrication. Panel bond assembly is dominated by labor and tooling, while core costs are affected by all three components of cost.

Types of design variables crucial to the cost analysis are shown in Figure 5-6 in diminishing order of their total effect. This figure helps illustrate effects due to the type of design variable (e.g., part area) but does not distinguish specific design features (e.g.,

quadrant panel area). Note that the word "constant" applies to terms in the equation that are invariant to changes in the design. Cost components are found to change as a function of the design variables in Figure 5-6. For example, material costs are strongly related to composite prepreg weight and the number of fasteners. Fabrication and assembly tooling costs are a strong function of part and mechanical interface areas, respectively.

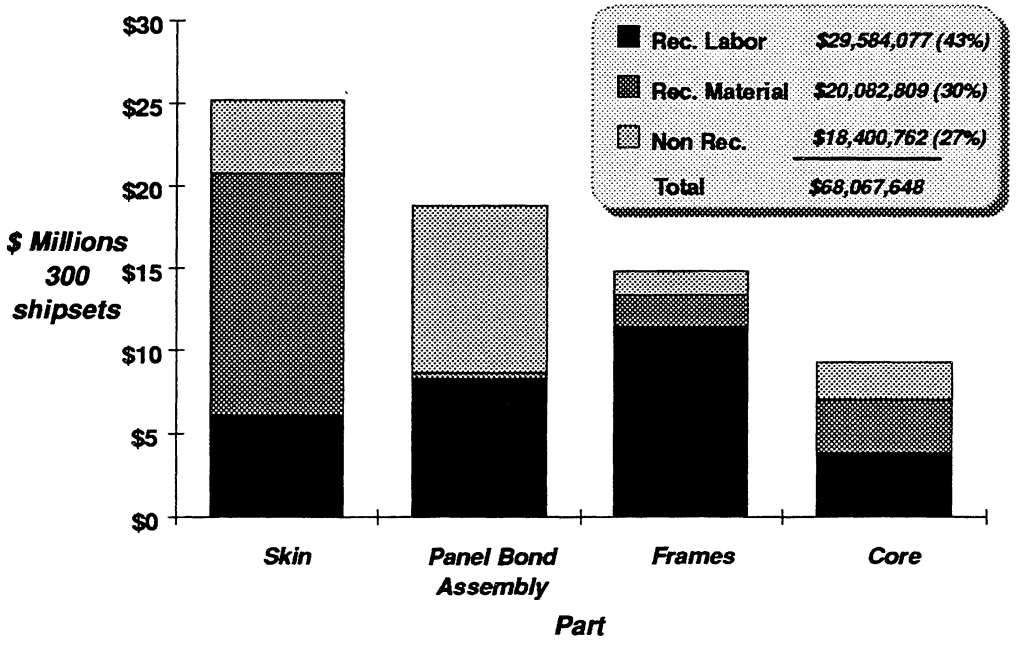

Figure 5-5. Part costs for the left side quadrant

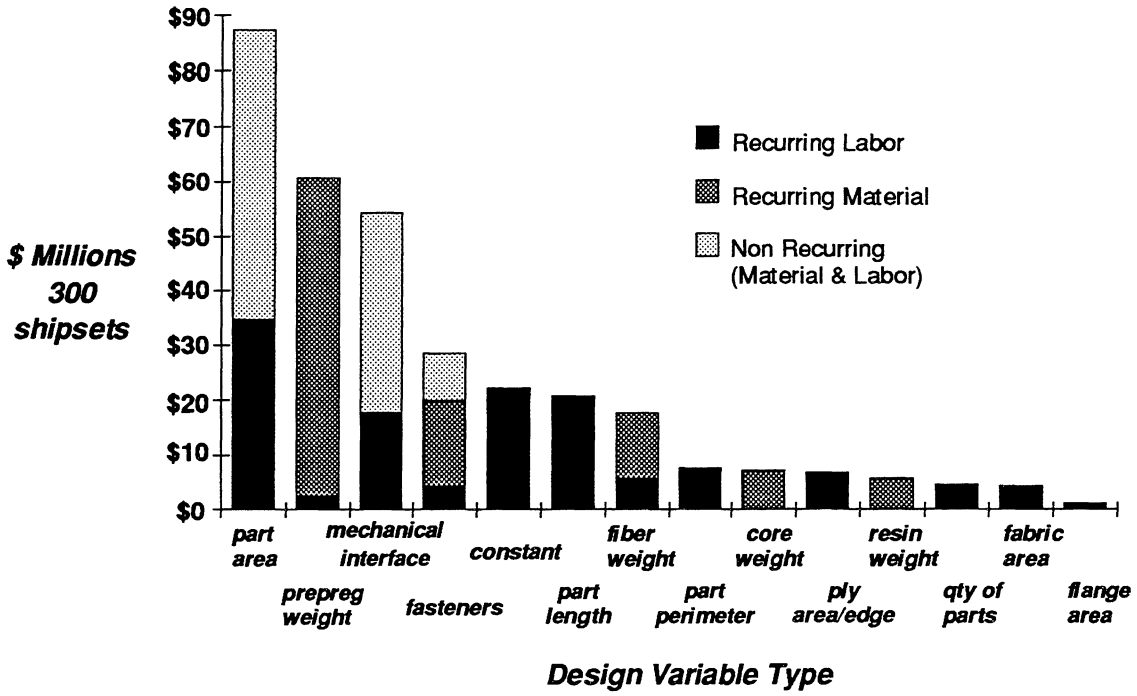

Figure 5-6. Costs plotted per design variable type.

Processes contributing to the cost of a composite full barrel are shown in Figure 5-7 in diminishing order of their total effect. Similar trends in cost centers to those shown in Figure 5-5 for parts of the left side quadrant are evident for the corresponding processes used to manufacture the full barrel. Braided/RTM processes used for circumferential frames and other detail parts have the highest recurring labor content. Tow placement of quadrant skins utilizes the highest percentage of recurring material costs. Panel bond assembly is dominated by both the highest tooling costs and significant labor content.

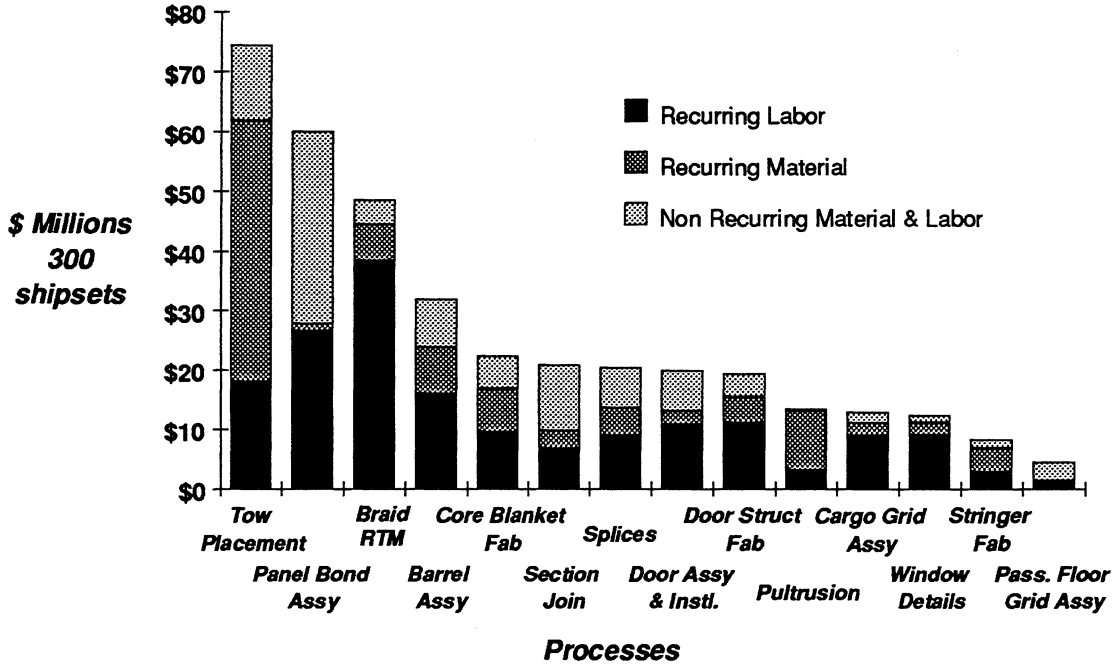

Figure 5-7. Costs plotted for major processes

The top three cost centers shown in Figure 5-7 all relate to part fabrication. These processes have received the most attention in manufacturing development since the start of ATCAS (See Sections 4.2.2 through 4.2.4 for discussions on equation developments and manufacturing trials for tow placement, panel bond assembly, and braided/RTM). Section 5.2.3 will elaborate further on critical process steps for each of these. The fourth bar in Figure 5-7, barrel assembly, will also be covered in Section 5.2.3.

Cost predictions for the ATCAS fuselage barrel combine results from detailed estimates and process-step based equations. At the start of ATCAS, nearly all of the costs were determined using the former. Since the start of the design cost model initiative, process-step based equations have slowly replaced portions of the estimate, providing insights into the effects of changes in the design on costs. The development and application of process-step equations has also required the involvement of more DBT members in cost analyses. This has helped improve communication between DBT members on cost-related issues, even when they did not involve use of the design cost model. Figure 5-8 shows a breakdown of the final Phase B prediction derived from

detailed estimates and process-step equations. Approximately 80% has come from the later.

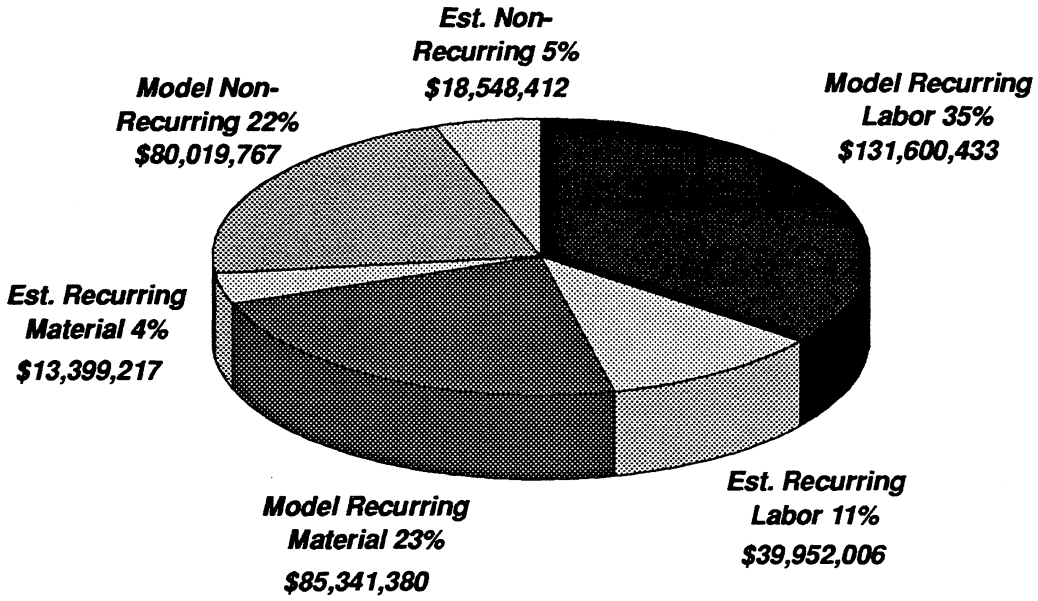

Figure 5-8. Parts of the ATCAS Phase B fuselage determined from the process-step cost analyses and detailed estimates.

Tooling comprises about 27% of the total projected fuselage barrel costs. Most of this is predicted using equations that have been entered into PCAD (ref. 55). Most tooling costs are predicted at a higher level than the process-step equations used to analyze labor times. Note that the total non-recurring costs have increased based on DBT insights gained since the start of ATCAS. PCAD is invaluable to the DBT for managing changes in cost equations.

Figure 5-9 shows classes of tools that sum to nearly 75% of the non-recurring costs. Some attempts have been made in ATCAS to evaluate the number of tools needed to make the presumed production rate of 5 shipsets/month. Future efforts should utilize process-step time predictions and a factory flow simulation to improve the accuracy of rate tooling estimates.

Material comprises about 27% of the total projected fuselage barrel costs. Most of this is also predicted using equations that have been entered into PCAD (ref. 55). The fabrication processes selected for the ATCAS design make efficient use of relatively low-cost composite materials. More expensive fiber and matrix combinations considered during the course of study have generally not provided enough weight savings to justify their additional costs (refs. 4 and 53). Figure 5-10 shows material types that sum close to 90% of the material costs. Prepreg tow used in the skin represents the highest material cost component. This combined with the mechanical fasteners, which in this case are generally titanium bolts, comprise almost half of the total material costs.

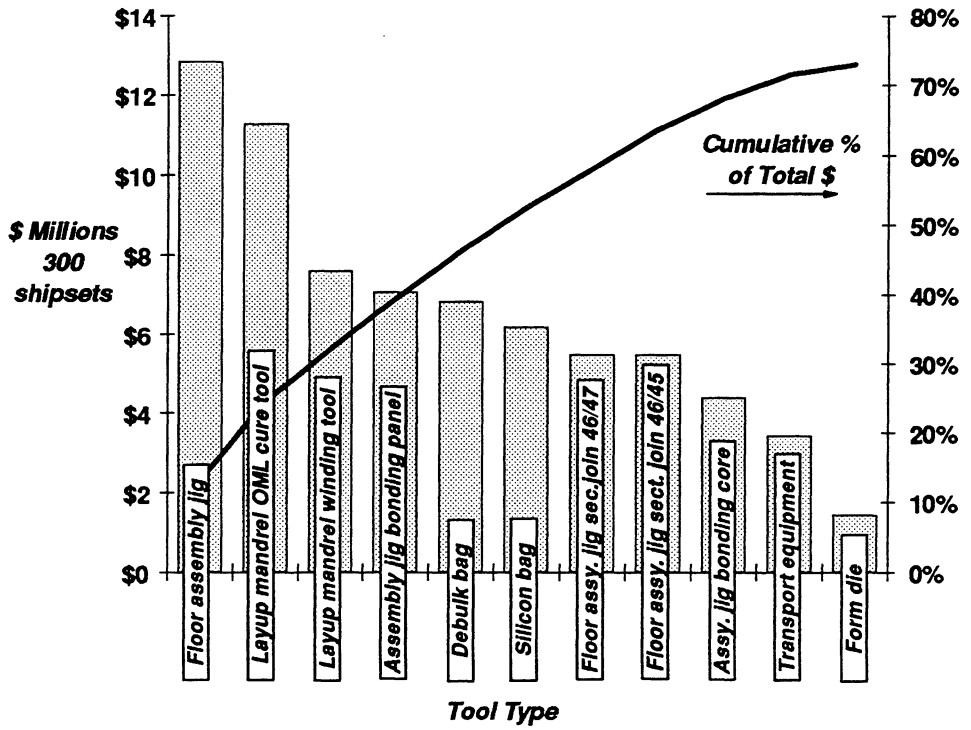

Figure 5-9. Key tooling cost components.

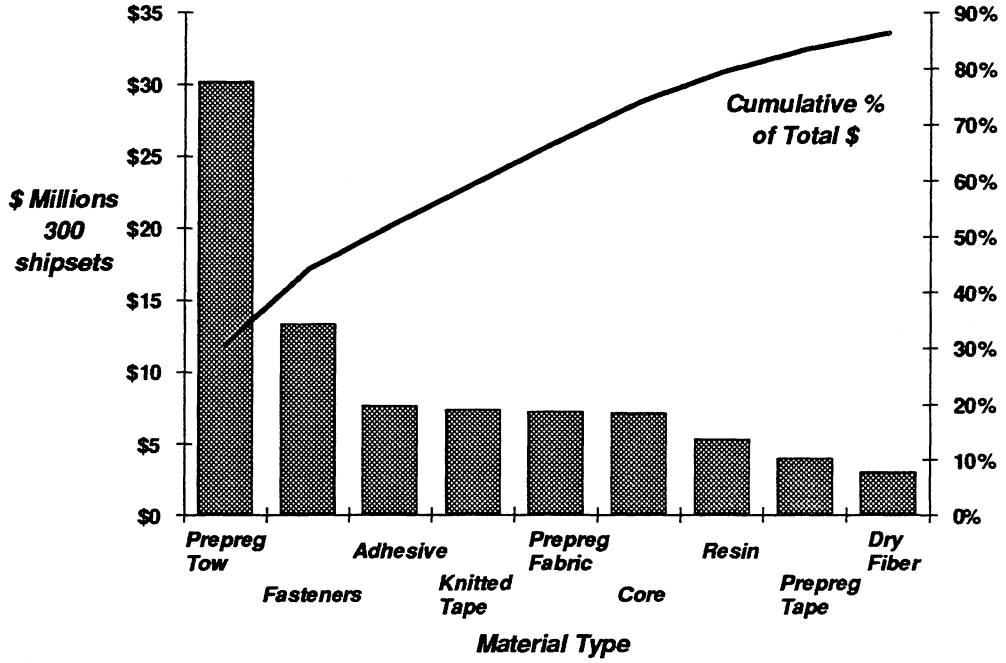

Figure 5-10. Key recurring material cost components.

Labor comprises the remaining 46% of the total projected fuselage barrel costs. Referring back to Figure 5-8, most of the recurring labor costs are predicted using equations that

predict process-step time. Again these equations have been entered into PCAD (ref. 55). Figure 5-11 shows process types that sum close to 75% of the total labor costs to manufacture a full barrel. The process for braided/RTM frames represents the highest labor cost component. The top four processes in terms of labor content combine to yield more than half of the total labor costs.

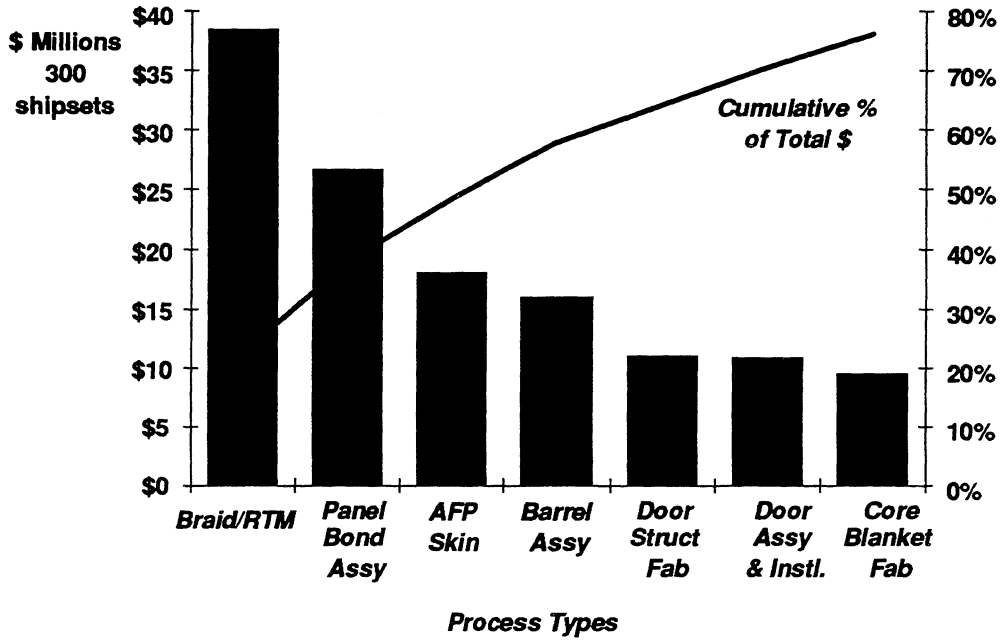

Figure 5-11. Key recurring labor cost components.

5.2.2 Physical Significance of Typical Cost Equation Parameters

There are more than 1,900 factory process steps which are performed to fabricate and assemble the ATCAS baseline fuselage barrel section. Figure 5-12 shows the relative contribution of these steps (each represented by one of 214 equations) to the total labor cost predicted for 300 shipsets. Since some of these steps involve repetitious activities (e.g., tow-placed skin lamination, hole drilling, mechanical fastening), the corresponding 214 cost methods are called approximately 65,000 times to calculate total cost.

Evaluation of the combined effect of all equations show that both time-consuming steps that rarely appear and those that occur frequently contributed significantly to the total labor content. Figure 5-13 shows the cumulative effects of labor cost predictions for all 214 cost equations listed in order of occurrence (i.e., number of times needed to make a calculation of process time to manufacture the complete fuselage barrel). Approximately 50 cost equations account for about 95% of the occurrences. As shown by the other curve in the figure, the equations used numerous times account for about 40% of the labor costs. The remaining 60% of labor costs come from equations that are rarely used. This suggests that most of the equations used to predict labor costs for the ATCAS baseline fuselage are important.

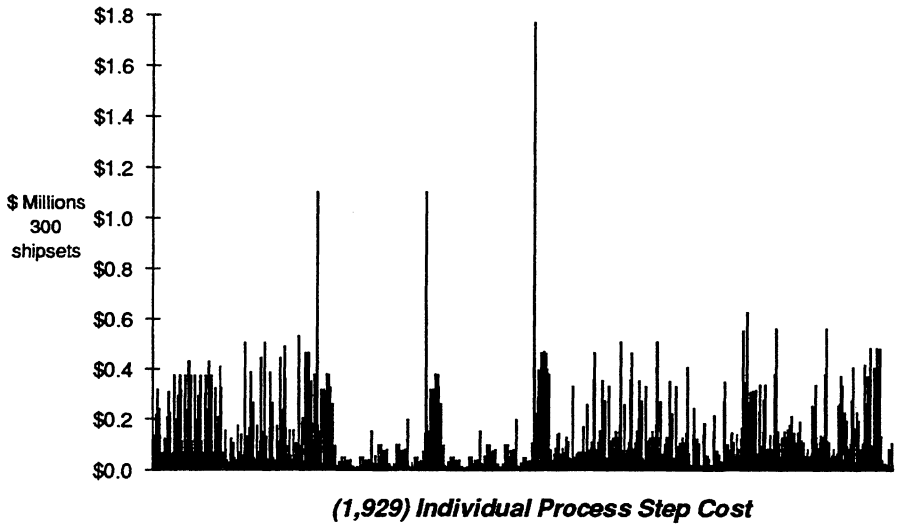

Figure 5-12. Process step labor cost distribution.

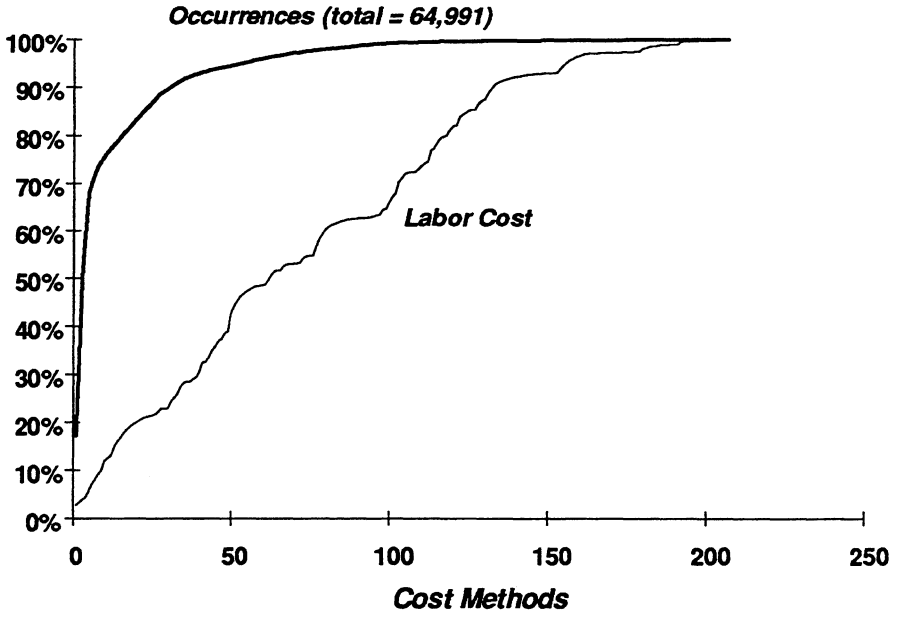

Figure 5-13. A total of 214 equations contribute to recurring labor cost predictions.

Figure 5-14 provides another way of illustrating the importance of individual cost equations. Note that those equations with more than 100 occurrences are associated with relatively small average labor content. Although step-by-step contributions from these equations are small, the summed effect is generally significant (see Figure 5-15). Equations that do not occur as often (i.e., less than 100), have a wide range of average labor contents. As shown in Figure 5-15, there appears to be no discernible trend between occurrences from 1 to 100 and importance to the total labor costs. Figures 5-14 and 5-15

show that only those equations that do not occur often and have relatively small average labor minutes are unimportant to the total labor costs.

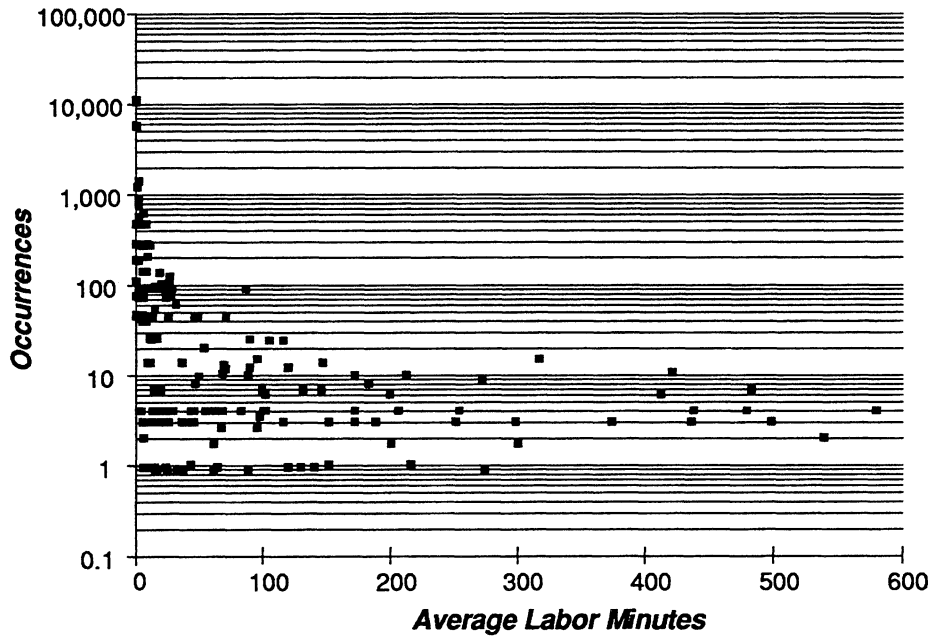

Figure 5-14. Two ways by which time equations affect total labor costs.

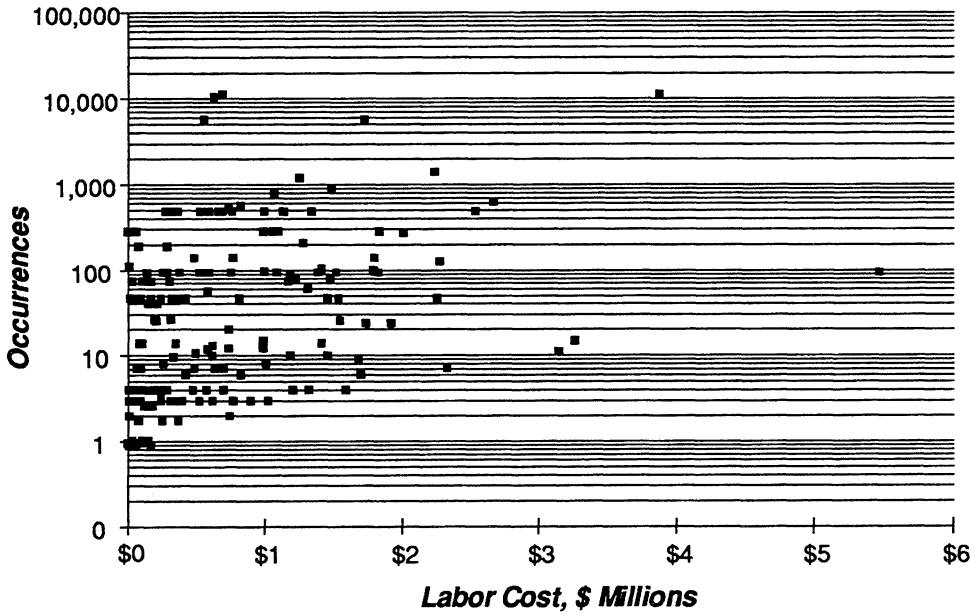

Figure 5-15. Combined effect of equation occurances and average times on total labor costs.

As mentioned earlier, most of the ATCAS equations for predicting process times for the baseline concepts use the most accurate approximation of the fundamental form for extensive processes. Rewriting the equation here for purposes of discussion,

$$t \approx \left[\left(\frac{\text{Setup}}{\text{Run}}\right)+\left\{\left(\frac{\text{Delay}}{\text{Operation}}\right)+\sqrt{\left(\frac{x}{v_o}\right)^2+\left(\frac{2\tau}{v_o}\right)x}\right\}\left(\frac{\text{Operations}}{\text{Run}}\right)\right]\frac{\left(\text{Parts}/\text{Shipset}\right)}{\left(\text{Lots}/\text{Run}\right)\left(\text{Parts}/\text{Lot}\right)} \quad .(5.1)$$

Figure 5-16 helps to illustrate the physical significance of terms in this equation for a typical ATCAS process step, machine edge trim of graphite/epoxy parts.

The setup time per run is equal to 2.0 minutes which physically relates to time lags occuring at the start of a machine operation, prior to a series of trims (comprising a "run", i.e., the process step being predicted). This activity only occurs at the start of a series of trims and, therefore, adds once to the total time per run. The note in Figure 5-16 suggests that this parameter does not include machine setup time because, for this process, the machine is setup to perform several runs.

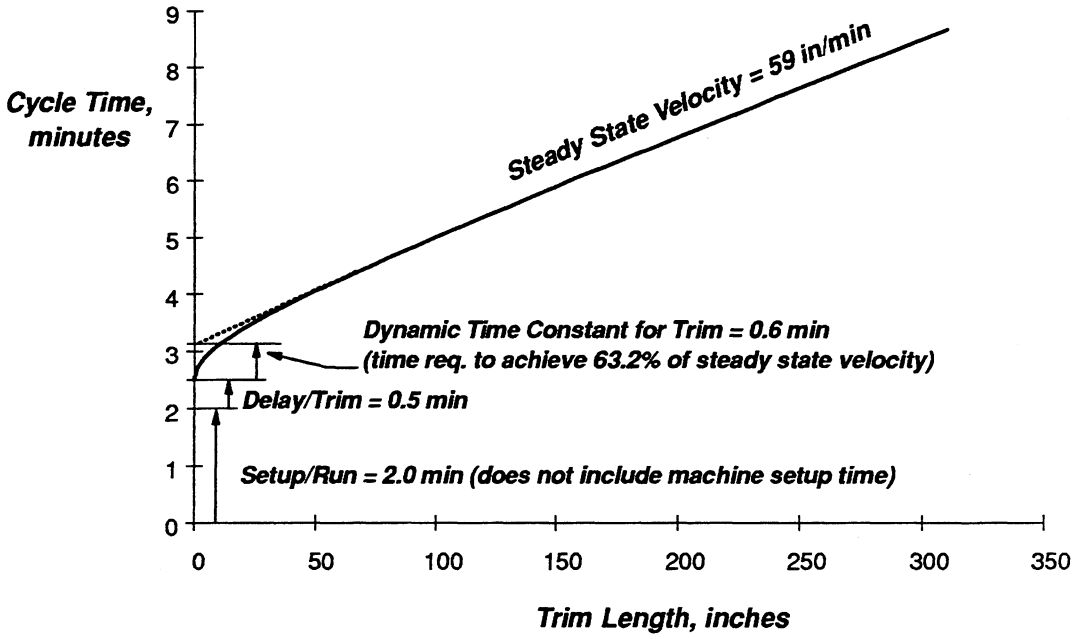

Figure 5-16. Example of an ATCAS cost equation, #2200 (machine graphite/epoxy edge trim).

The delay per trim in Figure 5-16 is 30 seconds. This physically relates to the time lag between trims occuring in the same run. The dynamic time constant for this example is 0.6 minute. As shown in the figure, this parameter, which relates to τ in Equation 5.1, physically relates to an acceleration in the edge trim operation prior to reaching the steady state velocity, v_o. A dotted line is shown to illustrate the latter. In the current example, the panel cost variable (x) is described as a trim length, which directly relates to a design length parameter on the part drawing.

The remaining parameters in Equation 5.1 relate to the manufacturing plan, production rate, and other design variables not shown in Figure 5-16. For example, the number of trims per run (operations/run) will depend on the manufacturing plan. The combined effects of terms outside the major parentheses in Equation 5.1 yield the runs/shipset, which relate to part design commonality, manufacturing plans, and production rates.

As discussed in Section 4.2.2.4 and Appendix G, relative comparisons of the velocities used to make time predictions can be beneficial. For example, Figure 5-17 show lineal velocities for the ATCAS process step equations which are dependent on a design length variable. Some of the individual points are highlighted to illustrate a trend from those steps which have high velocities to those that are relatively slow. Many of the velocities shown in Figure 5-17 are for processes which have a significant production experience, whereas others are for emerging technologies. In the case of process steps which have a limited database, such comparisons can help evaluate if the initial estimates of a velocity are realistic.

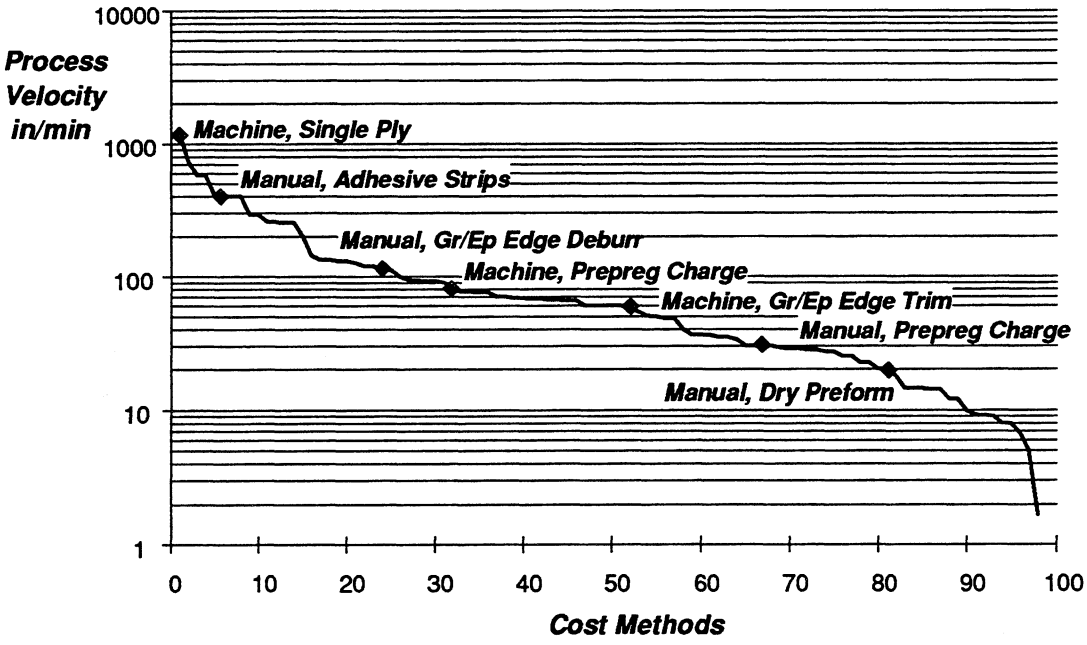

Figure 5-17. Lineal process velocities linked to part length.

Figure 5-18 shows areal velocities for ATCAS processes dependent on a design part area variable. As was the case for lineal velocities in Figure 5-17, dramatic differences are seen for areal velocities used to predict the time of different processes. While most lineal velocities were between 10 and 100 in/min., most areal velocities range in speeds between 100 and 1100 in^2/min. The fastest processes in Figure 5-18 are automated, while the slowest tend to be manual. This does not suggest that automation would make the slower process steps less costly.

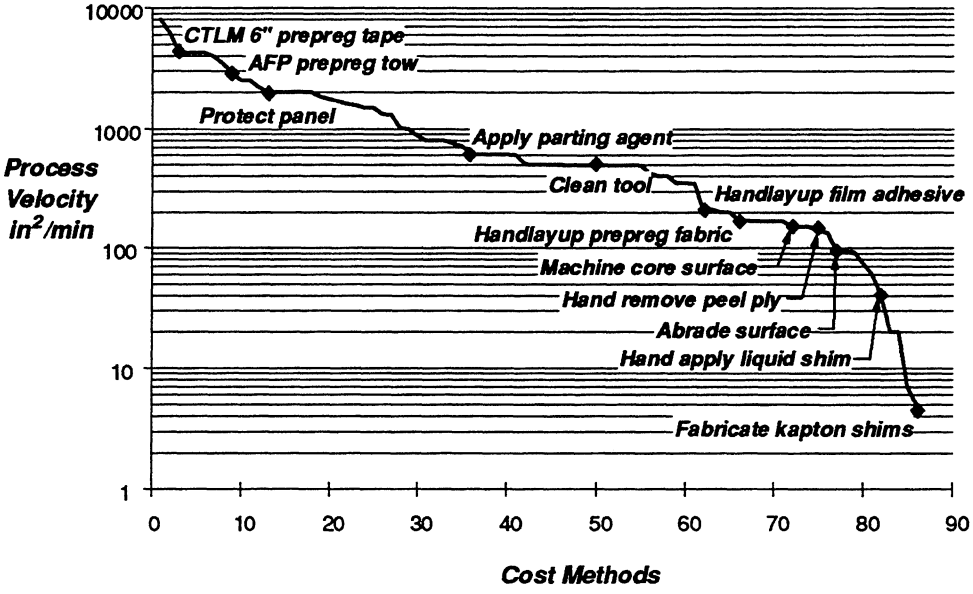

Figure 5-18. Areal process velocities linked to part area.

Several points highlighted in Figure 5-18 are worthy of special note. Ply layup using a contoured tape lamination machine (CTLM) reaches slightly higher areal velocities than an AFP machine, primarily due to differences in the width of prepreg material being laminated. On the other hand, the AFP process has other time efficiencies and capabilities (add/drop) that make it more suitable for fuselage skin applications. Some of the slowest velocities highlighted in Figure 5-18 relate to assembly steps used in shimming, illustrating the importance of controlling detailed part tolerances to avoid costly assembly steps.

Plans for future improvements in accuracy. Now that most process steps for the ATCAS fuselage barrel have corresponding cost equations, it is important to discuss some key features to address in future updates. Section 5.2.3 will discuss some of the key process steps for fabrication and assembly cells that add significantly to total barrel costs.

Manufacturing trials performed to increase the cost database (producibility and time trials) should pursue information in ranges of design variables critical to the baseline concepts. Figure 5-19 helps to illustrate this focus with an ATCAS cost equation developed for drilling countersunk holes in graphite/epoxy parts. This equation is based on data available for a wide range of hole volumes; however, ATCAS predictions are dependent on the accuracy of correlations in the shaded region. Additional data may be collected for specific ATCAS design details in order to improve the accuracy of the current equation in this region. If differences are noted, the equation should be changed for ATCAS purposes. It is important to remember that the intent of such focus is not to constrain use of ATCAS technology in other products, but instead to improve cost prediction accuracy. As a result the design space considered in manufacturing trials to expand a database should be based on the feasibility of applying the technology to other potential products.

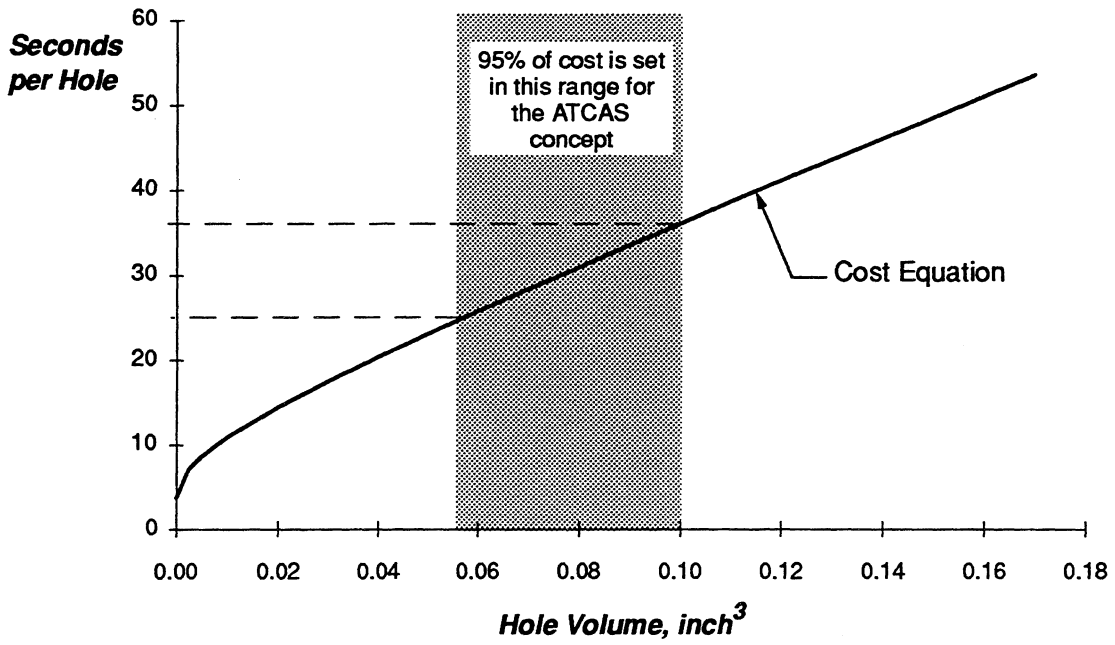

Figure 5-19. Hole volume critical to ATCAS predictions for drilling countersunk holes in graphite /epoxy parts.

Another issue crucial to future development is apparent in the illustrations given in Figures 5-20 and 5-21. Figure 5-20 shows processes that are related to a particular design length and perform the same task, but with different velocities, dynamic time constants, and setup times. Processes A and B appear optimum for part lengths less than and greater than 140 inches, respectively. Figure 5-21 illustrates the same processes as Figure 5-20 but the intersection between curves which distinguish an optimum process as a function of part length changes due to the specific labor rates. In this example, an automated process (B) operated at an increased velocity requires a workforce with higher labor rates. This occurs because greater skill levels are needed to perform an automated process and/or capital and facilities investments (burdening the labor) are amortized in the rates.

The current ACT groundrules, which lead to cost estimates based on constant wrap rates for recurring ($100/hr) and non-recurring ($75/hr) labor preclude the evaluation of issues illustrated in comparing Figures 5-20 and 5-21. Future efforts in cost analysis should not force constant labor rates that are independent of the process. The PCAD software created to support ATCAS cost analysis (ref. 55) has the necessary flexibility to allow the entry of different labor rates for each process step. As discussed in Section 4.3, equipment, tooling, and facilities should receive more attention in subsequent stages of development. Process times predicted from the current cost equations can provide a basis for the more rigorous cost assessments, including a detailed evaluation of the quantity of equipment and tools and the associated facilities floor space needed for production. Such evaluations are essential for minimizing capital costs and successful implementation of new technologies in future products.

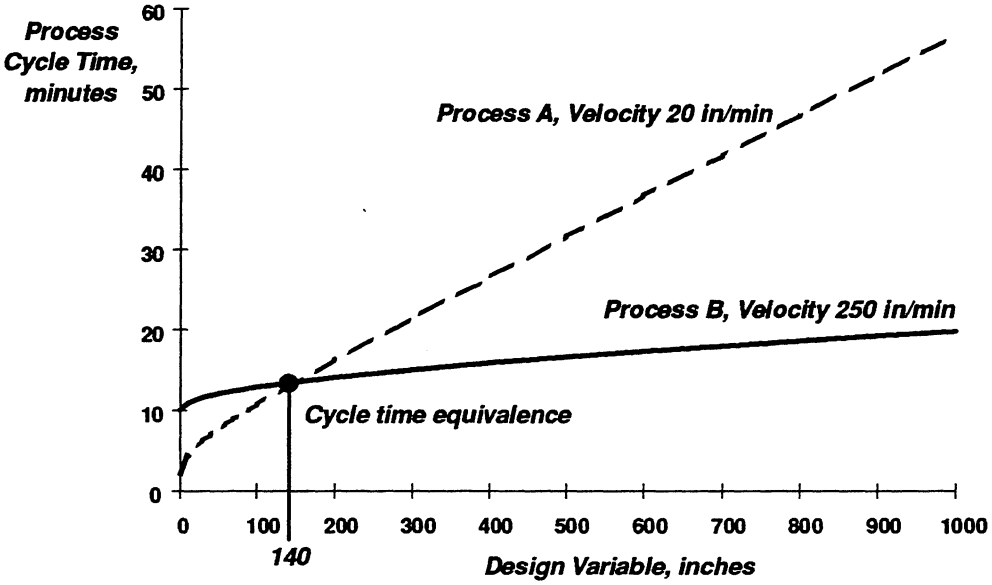

Figure 5-20. Optimum process changes as a function of the design.

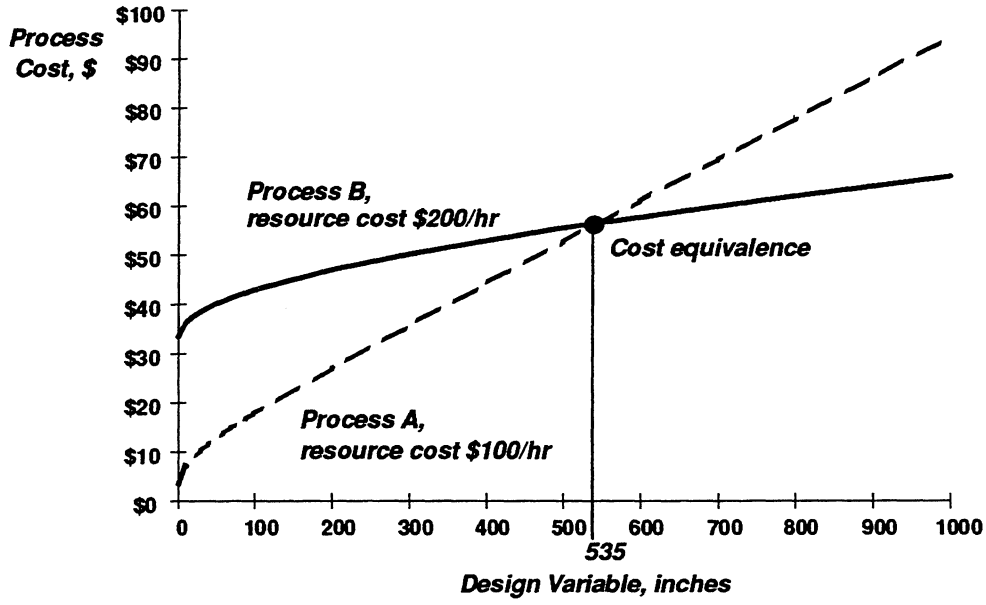

Figure 5-21. Importance of labor rates linked to required skill levels and resources (equipment and facilities).

5.2.3 Breakouts by Selected Process Cells

Figure 5-7 shows process cost centers for the ATCAS fuselage barrel. The first three (AFP, panel bond assembly, and braided/RTM) all relate to fabrication cells in the baseline factory (see Figure 5-2). These processes have received the most attention during Phases A and B of the ATCAS program.

A comparison of Figures 5-7 and 5-11 indicates that those processes contributing the most cost to the ATCAS fuselage barrel have a high labor content. Although the order is different, the top four cost centers are the same in both figures. This section will review key process steps and the equations used to predict labor costs for these four processes. The order of presentation will be given from highest to lowest labor content. Section 5.2.3.1 will discuss the critical fabrication cells of braided/RTM, panel bond assembly, and AFP. Section 5.2.3.4 will describe the fourth highest process cost center, barrel assembly. This cost center relates to assembly cells (see Figure 5-3).

5.2.3.1 Critical Fabrication Cells

Braided/Resin-Transfer-Molding Frame Fabrication. The braided/RTM process cell, illustrated in Figure 5-22, is used to fabricate composite fuselage frames. Predicted ATCAS costs for braided/RTM frames in the study section have been dominated by recurring labor (see Figure 5-7). As shown in Figure 5-11, the braided/RTM frame process has significantly more labor content than other processes, contributing to approximately 25% of the total labor costs. Section 4.2.4.2 summarized the ATCAS manufacturing trials that helped quantify the labor times for key braided/RTM process steps. Other discussions in this section indicate braid mandrel and RTM cure tooling costs can become significant, depending on frame part commonality and production rate.

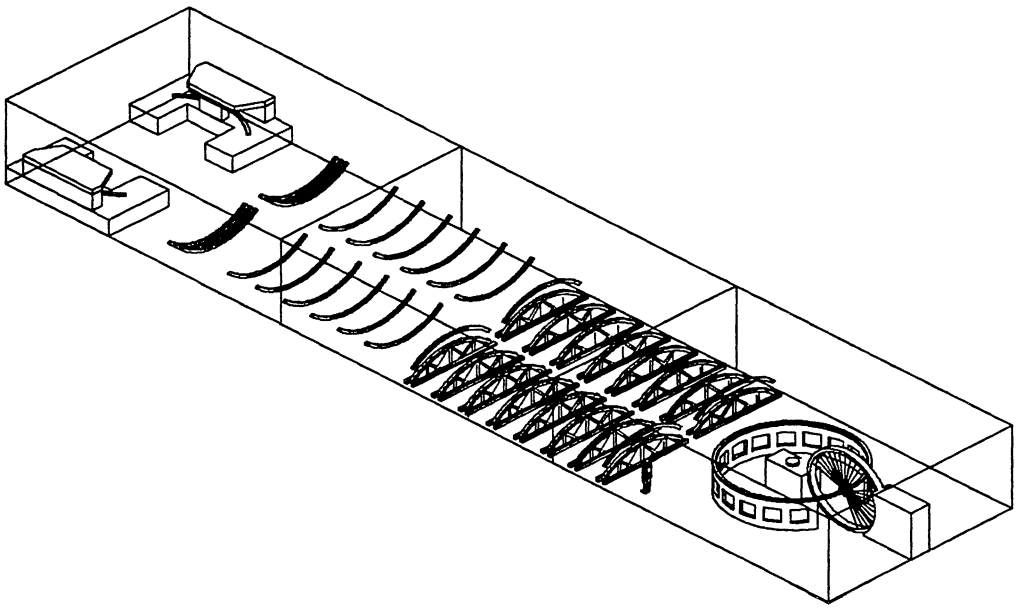

Figure 5-22. Process cell for braided/RTM frame fabrication.

Figure 5-23 shows labor content, in order of the highest to lowest costs, predicted using equations for braided/RTM process steps. This form of presentation helps to identify the most expensive process steps and/or most used methods for predicting labor costs. Hence, helping to focus manufacturing technology and cost method development efforts. Appendix H provides a brief description of the associated identification numbers. In the case of the 18 braided/RTM process steps listed in Figure 5-23, none of the equations are used more than once. Note that this is not the case for other processes (e.g., see AFP discussions below).

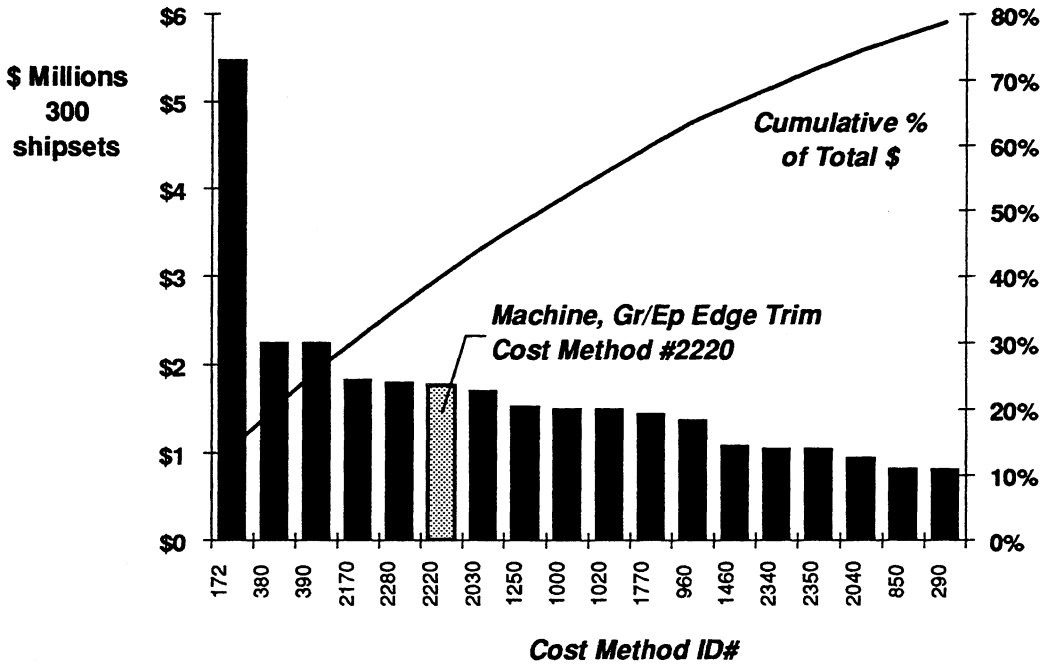

Figure 5-23. Cost methods used to predict labor cost components braided/RTM frame fabrication.

Figure 5-24 gives an alternative presentation of some of the same results as those shown in Figure 5-23. Note that Figure 5-24 sums costs to 100% of the total for that process cell, while Figure 5-23 only reaches about 80%. In order to further illustrate differences in the format used for the two figures, the cost method highlighted in both Figures 5-23 and 5-24 (i.e., number 2220) relates to an edge trim process step. Figure 5-24 groups this method with others associated with trim (i.e., including 2280, 2340, 2350 from Figure 5-23). All cost methods used for trim, automated or manual, depend on trim length variables (related to frame geometry) and lineal velocities that represent process parameters.

As shown in Figure 5-24, other key cost methods used to predict braided/RTM labor content can be catagorized as position, braid, remove, cure, setup, and transport tasks. Due to frame part geometry, most position and remove tasks depend on length variables (e.g., tool length or perimeter) and lineal velocities. The long frames needed for the wide

ATCAS quadrant panels and characteristics of an efficient braided/RTM process require that most position and remove tasks are hoist assisted. Braiding costs were dependent on fiber weight and the associated processing rate (lbs/min). Cure, setup and transport task times were simulated using constants. The only process steps related to part or tool areas were layup (e.g., manual placement of peel plies) and tool cleaning.

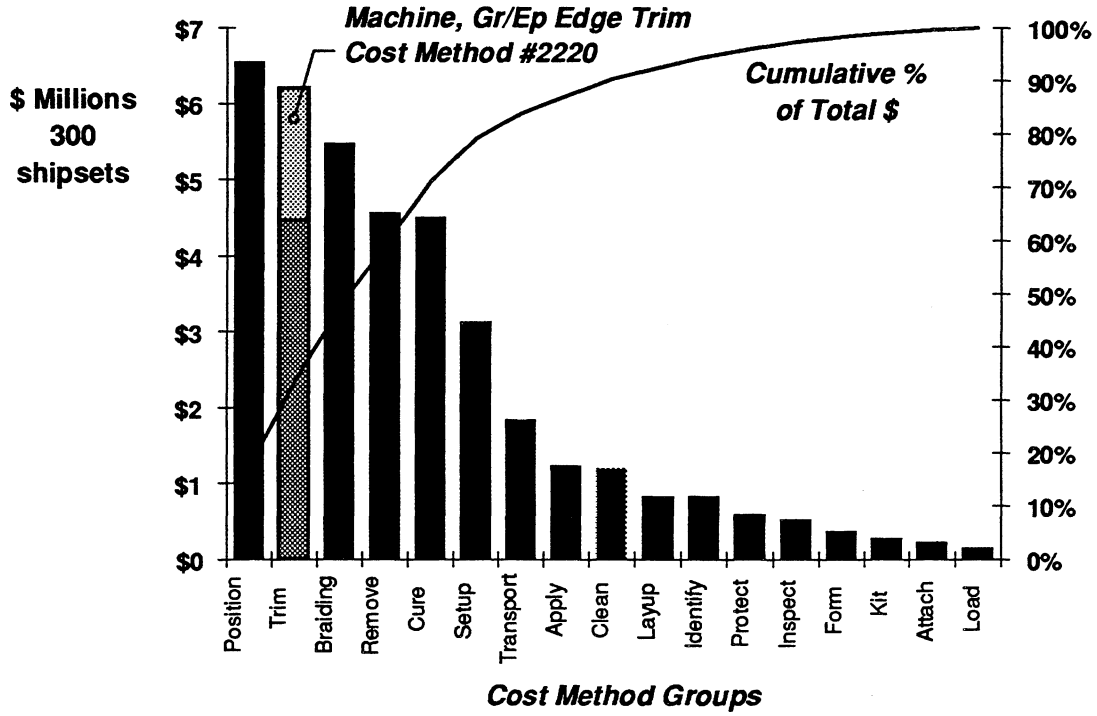

Figure 5-24. Critical braided/RTM frame fabrication labor cost components.

Quadrant Panel Bond Assembly. Predicted ATCAS costs for panel bond assembly have been dominated by recurring labor and non-recurring tooling (see Figure 5-7). The bond assembly process cells, illustrated in Figure 5-25 for a sandwich side quadrant, are used to position, bag, cure, and inspect composite fuselage skin panels. As shown in Figure 5-11, panel bond is the second most labor-intensive process type in the ATCAS factory. As a result, it has also received considerable attention in manufacturing trials performed to date. For example, Section 4.2.4.3 summarized the ATCAS trials that helped quantify the labor times for crown panel bond process steps.

Tooling costs for panel bond assembly include an OML cure tool, reusable bags, and tooling aids for bonded details. As discussed earlier, total tooling costs will invariably be linked to labor content. For example, efficient processes will maximize tool utilization by minimizing the time of labor tasks performed while the part is on the tool. Inefficient processes may require more tools to meet production rate.

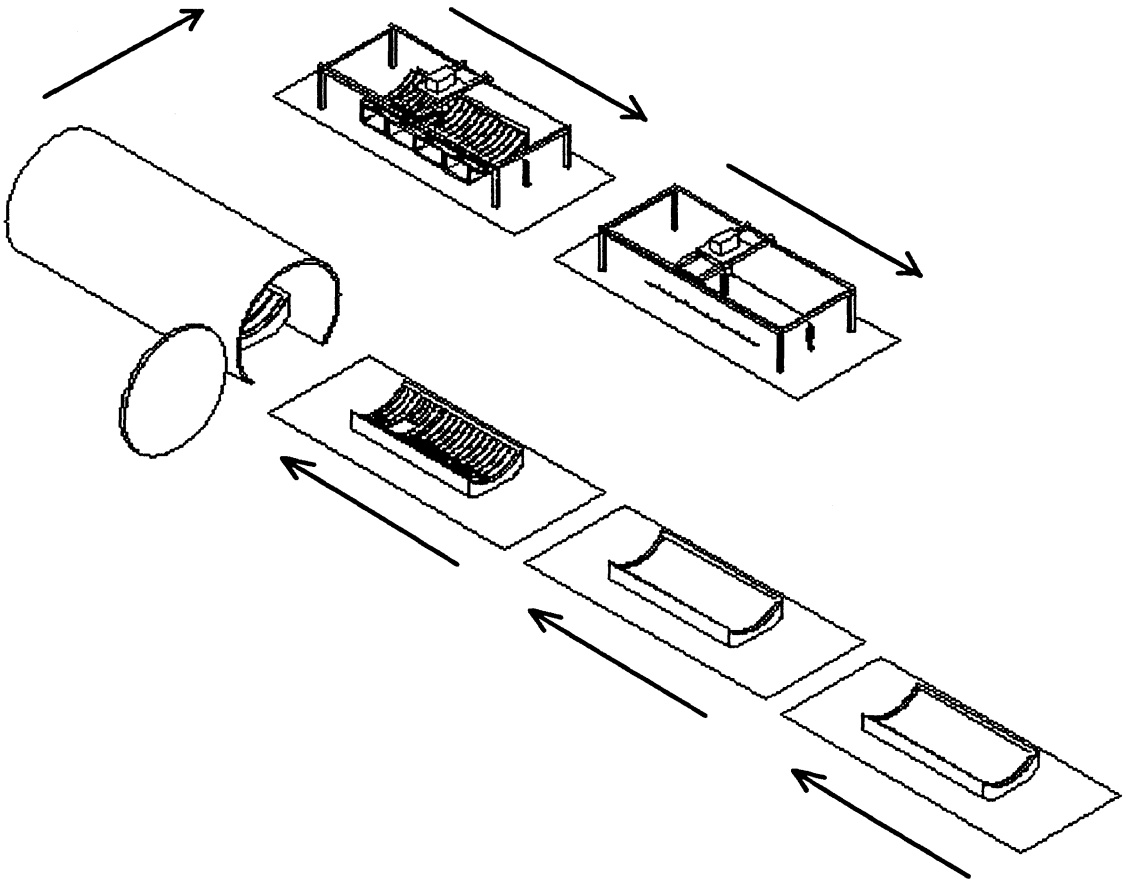

Figure 5-25. Process cells for panel bond assembly.

Figure 5-26 shows the most used cost methods for predicting process step labor costs in the panel bond assembly cells. Referring to Appendix H, most methods relate to manual positioning and removal tasks that depend on quadrant panel areas. Figure 5-27 confirms this dominance. The majority of positioning steps occur in preparing the panel for autoclave cure (i.e., positioning core and frame details, flexible IML cauls, and reusable bags). Due to the size and fragility of a bonded core blanket, positioning on the OML skin is hoist assisted. Most removal tasks occur after cure (i.e., removing bags and tooling aids from the IML surface and taking the cured panel off the OML cure tools). Due to the large area and weight of a cured quadrant panel, it is mechanically removed from the OML cure tool.

Figure 5-27 shows other process groups, adding with position and removal tasks, to set 90% of the panel bond labor costs include cured panel inspection, autoclave cure, tool cleaning, and part/tool transport. Inspection and cleaning steps generally depend on part area. Cure and transport tasks are normally automated or mechanically assisted and assumed to be constants.

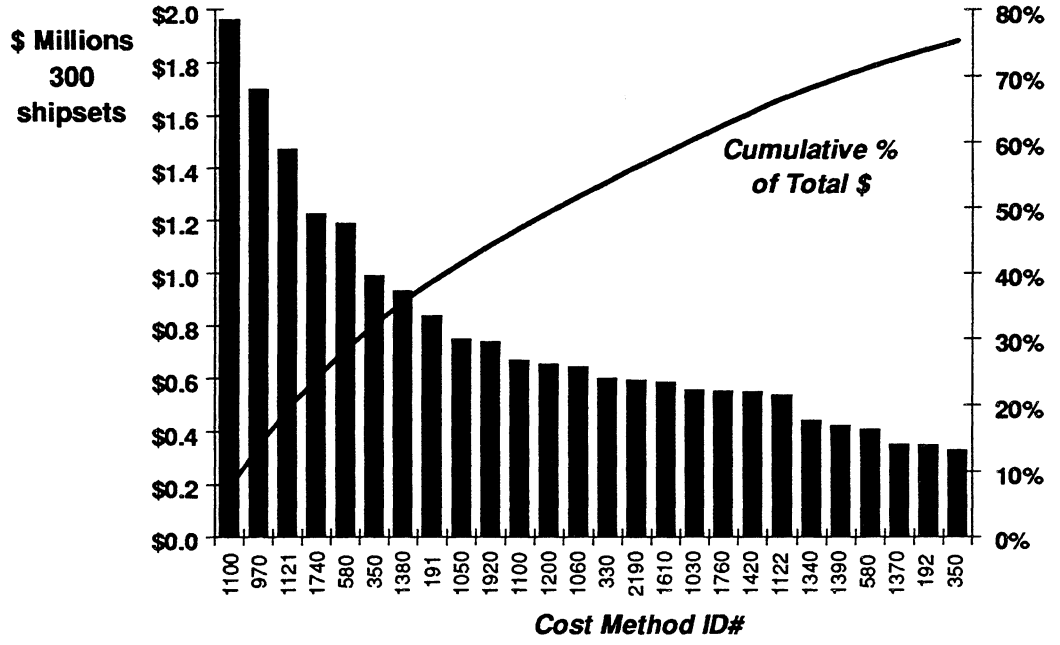

Figure 5-26. Cost methods used to predict panel bond assembly labor cost components.

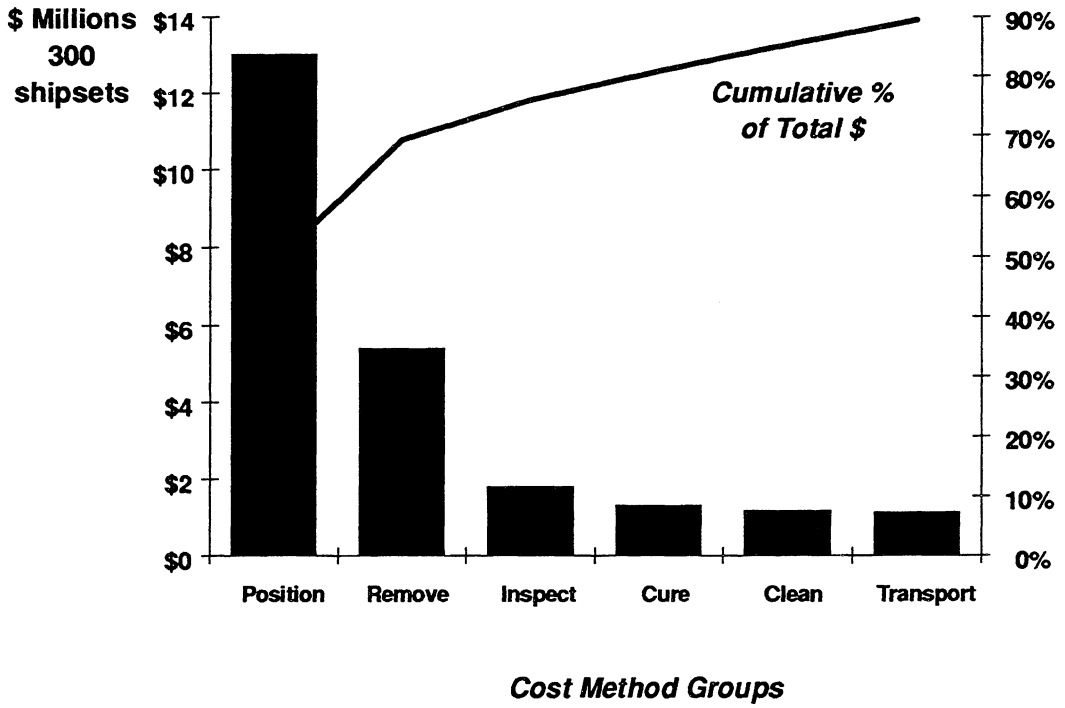

Figure 5-27. Critical panel bond labor cost components.

Automated Fiber Placement. Predicted ATCAS costs for AFP have been dominated by recurring material. The AFP process, illustrated in Figure 4-20, is used to laminate the composite fuselage skins which constitute most the weight of each quadrant. Numerous ATCAS studies evaluated quadrant skin designs which attacked the material cost center (refs. 1, 51, 62, 63). Blending software utilities developed to help select laminate layups, ply dropping schemes, and local padups were found to support practical design optimization (ref. 1). Trades including AFP recurring labor and material cost components indicate that design cost is generally dominated by the latter (see Section 4.2.3). However, these studies suggested that the extent of dominance may be tempered by limitations of current ACT groundrules which are based on constant labor rates and do not allow direct assessment of capital equipment costs.

Even with the current ACT groundrules, labor constitutes about 25% of costs occuring in the AFP process cell. Not all of these costs relate to the operation of an AFP machine. For example, manual layup is used for fabric plies and adhesive. Figure 5-28 shows the most used cost methods for predicting process step labor costs in the AFP cell. Appendix H provides a brief description of the associated identification numbers. Most methods relate to layup of: (i) prepreg tow using AFP, (ii) prepreg fabric, or (iii) film adhesive. The key design variable for all of these parameters relate to a part area. Figure 5-29 shows the dominance of layup tasks in total labor costs for the AFP process cell. Another labor-intensive AFP process step (number 920) is loading prepreg tow onto spools that dispense the material during layup. The key design variable in this case is prepreg weight.

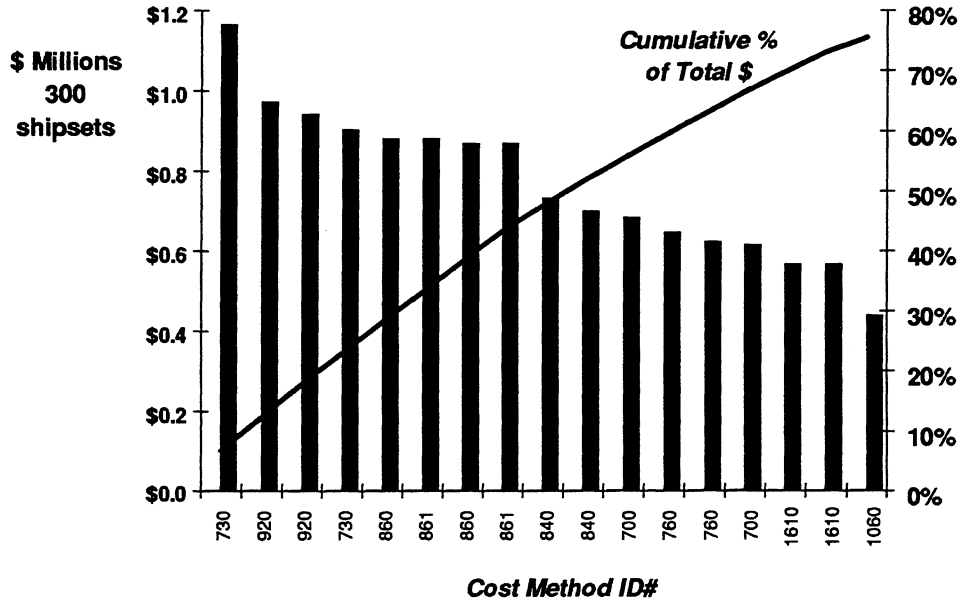

Figure 5-28. Cost methods used to predict AFP labor cost components.

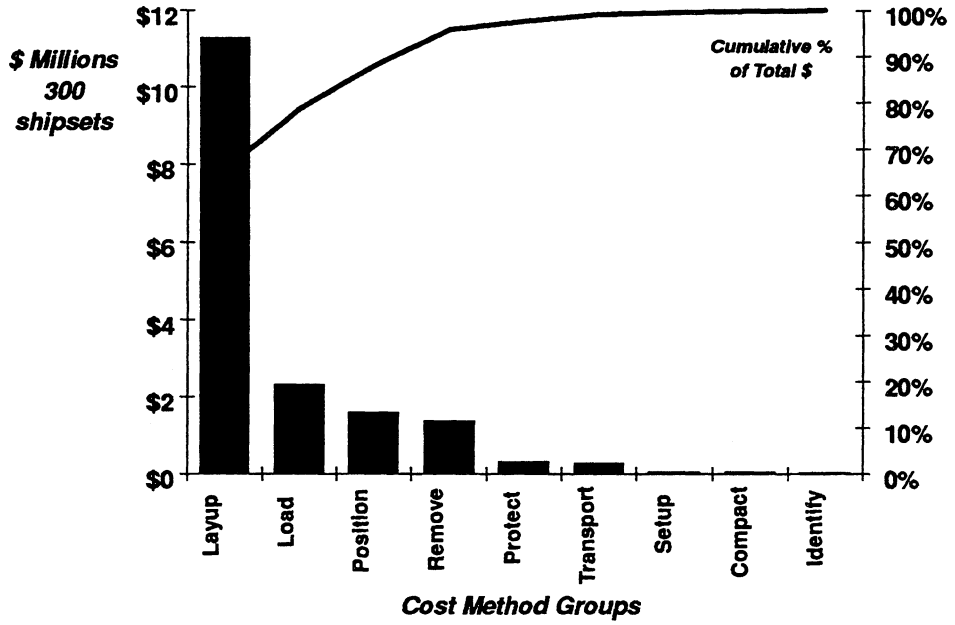

Figure 5-29. Critical AFP labor cost components.

Future cost evaluations of the AFP process cell will need to consider capital equipment and the associated maintenance, energy resources, and facilities floor space. A more detailed assessment of the AFP tools (e.g., layup mandrels) needed to make production rate should also be performed. Current cost trades suggest the layup of most plies should be stopped whenever structural requirements allow it, sacrificing layup efficiency (i.e., time at maximum speed) for reduced material costs. Other factors could change such trends. For example, an AFP machine may require more maintenance (down time) and/or longer setup times when operated to laminate skins with repeated ply add and drop details. An increase in the total number of AFP machines or layup tools needed for a factory producing such designs may change the total cost assessment. Other steps that interrupt the machine operation (e.g., manual fabric or adhesive layup) can also slow process flow, changing AFP equipment or tooling needs. This occurs as tooling and equipment resources are rendered idle by intermediate steps that delay the total process.

5.2.2.2 Critical Assembly Cells

Mechanical Assembly of the Fuselage Barrel. About 50% of the predicted ATCAS costs for fuselage barrel assembly is recurring labor (see Figure 5-7). Recurring material (i.e., fasteners and shims) and non-recurring tooling (assembly jigs) comprise approximately equal shares of the remaining 50%. Cells illustrated in Figure 5-3, with the exception of detail part pultrusion, and cargo and passenger floor grid assembly, were lumped under the label of barrel assembly in Figure 5-11. This category is the most labor-intensive of those in the barrel assembly portion of the ATCAS factory. Although rigorous assembly trials have not been performed in ATCAS to date, cured panel tolerances have received considerable attention due to their relationship with shimming costs. Note that shimming has a significant effect on barrel assembly labor, material, and tooling costs.

Figure 5-30 shows the most used cost methods for predicting process step labor costs in the barrel assembly cells. Lockbolt fastener installation (method 640), which is plotted as a sum of the all times required to install fasteners during barrel assembly, appears dominate. Current predictions assume each fastener is installed in a constant process time. This is effectively the same as assuming a constant setup time plus an average fastening rate for each fastener. The ATCAS model for fastener installation is a good example of the hierarchical nature of cost analyses, whereby the simulation can be simplified by a single constant for average time. Statistical treatment of data from total time trials seems appropriate in the case of fastener installation. This approach avoids quantifying more coefficients (e.g., see Figure 5-16) for short-duration, repetitious process steps.

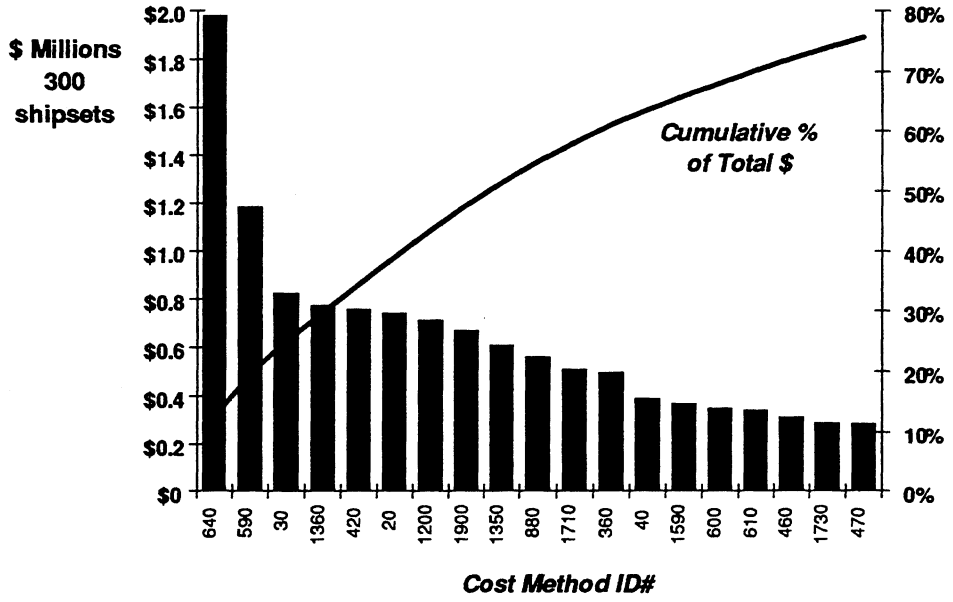

Figure 5-30. Cost methods used to predict labor cost components for full barrel assembly.

Other methods crucial to the total barrel assembly cost prediction can be determined by comparing identification numbers in Figure 5-30 with the associated descriptions in Appendix H. The resulting methods predict times for position, remove, inspect, shim (apply, fabricate, layup, and cure), and drill tasks. A dominance of methods to predict the times for these groups of cost methods is confimed by the graph shown in Figure 5-31.

Position and remove tasks again depend on variables that relate to part geometry (length or area). The associated process parameters are either lineal or areal velocites. Inspection tasks either depend on the interface geometry between parts which assemble (e.g., lineal velocities for the time to determine gap dimensions) or a constant for the time to inspect each hole or fastener. Most shim fabrication tasks relate to areal velocities which combine with assumed average liquid and solid shim areas per given interface area. Forces applied during process steps which aid in the shimming and subsequent installation tasks were related to a lineal velocity. Finally, hole drilling tasks are some of the few process steps

whose times depend on volumetric rates. In this case, the design variables are individual hole volumes.

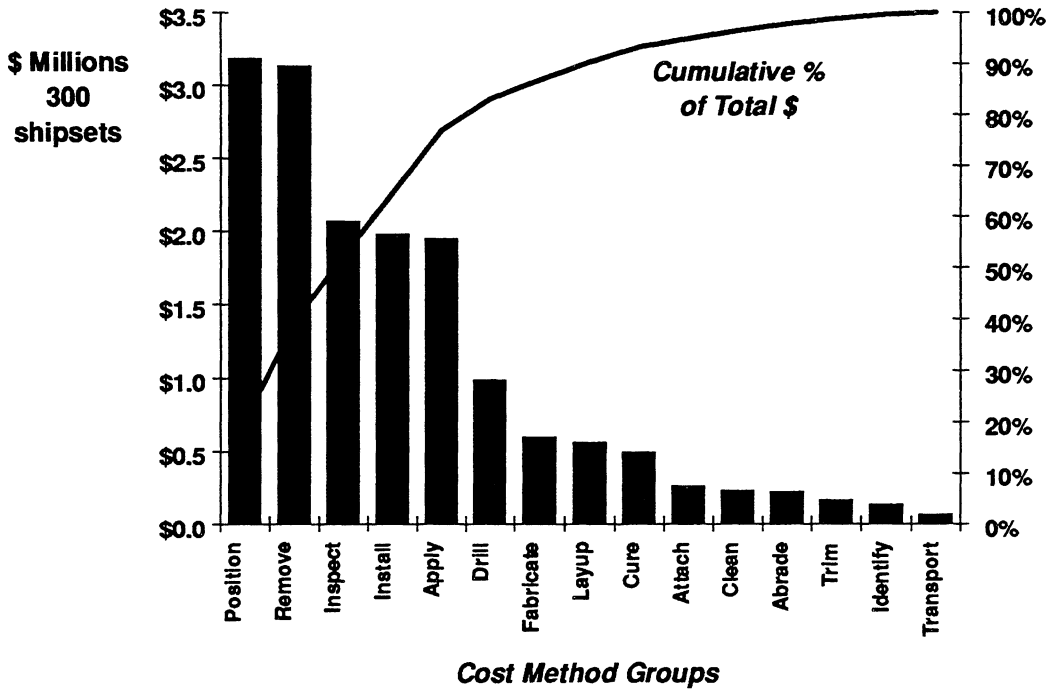

Figure 5-31. Critical full barrel assembly labor cost components.

6.0 CONCLUDING REMARKS

A framework has been established for design cost modeling in support of the development and implementation of new technology to manufactured products. The proposed framework enhances team efforts to support initial concept selection and analytical formulations which improve predictive accuracy during subsequent data collection and manufacturing improvement cycles. Current work has emphasized the importance of predicting the effects of design variables on process times and efficiencies as related to manufacturing costs. A theoretical framework is justified by the communication and educational benefits possible in linking physical principles to the tasks required to create and update design cost analyses.

The theoretical framework described consists of an analytical and physical foundation with recommended procedures for equation formulation, data collection, and methods to seek improvements in predictive accuracy. This framework is dependent on synthesis of the information collected by a design build team (DBT) during integrated technology development. The focus of examples demonstrating the framework has been on ATCAS composite technology for cost-effective transport fuselage structure. Much of the ATCAS design/manufacturing concepts selected to achieve cost and weight saving goals versus state-of-the-art aluminum construction have little or no production database. Such new technology applications justify the need for a theoretical framework.

Three main applications for a design cost model have been envisioned which include support to concept development, product development, and production. Each of these applications are summarized below.

(1) Concept development is primarily research oriented. *During the first application of new technology, design cost analyses can be used to select and help guide the development of design/manufacturing concepts which have potential value to future products.*

(2) During product development, the analyses should evolve to help define design configurations, manufacturing plans, tooling approaches, and factory layouts with optimum value to a specific company's product line. *The second application is crucial because the lower limit of production costs are strongly affected by DBT decisions made by the end of the product development stage (e.g., make or buy decisions and commitments to equipment, tooling, and facilities).*

(3) During production, a cost model and the supporting database should be at a level of accuracy that ensures compatibility of structural design and process details. *The third application is crucial in final DBT efforts to release designs that allow manufacturing efficiency in the selected factory and, hence, achieve the lower limit of production costs.*

An analytical basis was developed to predict size effects for extensive process steps (manual and automated), whose time depends on dynamic equations for motion over some region in space. A fundamental extensive equation form, which can be linked to first order dynamic theories or mass motion relationships, has found the most application to date.

Several approximations of this equation have found practical use in design cost analyses. These included a hyperbolic formulation that provided reasonable accuracy for the entire time and space domain, as well as square root and linear equation forms which were accurate for short and long duration process steps, respectively. More generalized equations for extensive processes were also presented. Applications of the additional degrees of freedom in these formulations should be physically justified on a need to simulate unique process traits rather than improved curve fits to data.

The "power law" curve that has been widely used for process-time estimating in industry was found to be another way to approximate the fundamental extensive equation form for relatively small part sizes. A power law may have a wider range of applicability for processes which change to become more efficient as the part size increases. However, it is difficult to interpret a physical basis in the coefficients for an equation which estimates changes to a process.

Analytical models were also developed for part-complexity scaling. These were based on the premise that parts having complex geometry are more difficult to manufacture. The two methods developed for complexity scaling employed a measure of the aggregate curvature of fibers that comprise the part. Several examples were presented to illustrate use of the theory. A combination of size- and complexity-scaling analyses yielded reasonable predictions of empirical databases for hand lay-up of composite parts. The benefit of using the hyperbolic equation over other approximations for size scaling was seen in comparing results for a wide range of part geometries. Future efforts will need to evaluate the merits of complexity scaling as applied to automated composite processes of interest (e.g., AFP, braiding, and NC machining). The approach taken in ATCAS has been to establish lower level process definition in which the part complexity is embedded in coefficients for multiple size-effect equations that sum to predict manufacturing time.

Other methods evaluated to support the framework included (1) models for process steps used in manual or mechanical material handling, (2) procedures to identify cost drivers, and (3) some simplifying analyses traditionally used for cost estimating. Two distinct classes of material handling tasks were considered: transport and positioning. The same equation form was found to be appropriate for both cases; however, coefficients were dependent on the specific task and whether it involved manual or mechanical operations. The recommended approach of focusing initial development efforts on cost drivers was justified by observing data trends in process-step times for fabrication and assembly methods of interest. In addition, the benefits and limitations of some simplifying analyses (e.g., learning curves and power laws) that have been empirically derived in industry were discussed. The assumed changes and process improvements implicit in historical data used to develop these analyses should be viewed with caution before applying them to new technology.

Procedures for applying the framework to specific structure were documented in Section 4, which starts with background leading to the ACT design cost model initiative, and ends with recommended stages of cost model development. Most recommendations were linked to ATCAS experiences in concept selection, critical process step identification,

initial model developments, correlation with data from manufacturing trials, and equation enhancements. Three stages of research, plus a fourth to complete product development, were envisioned to achieve the necessary production readiness to apply new technology to transport aircraft structure. Subsequent stages relate to applications and updates for design cost models that occur during production and product support.

To date, ATCAS is close to completing the second stage of cost model development for designs and processes of interest. In the first stage, rigorous cost and weight trades were performed to select a design family and associated manufacturing concepts with predicted value for future transport fuselage structure. During the course of ATCAS, these trade studies evolved to include the assessment of technical risk and development potential. In the second stage, more detailed assessments were performed, including manufacturing trials and structural evaluation at a subscale of sufficient size to address many issues. An example of the critical manufacturing steps and fuselage design space studied during the second stage was documented for the most labor-intensive process in the ATCAS factory, fabrication of braided/RTM circumferential frames. The third stage will address issues that require large-scale databases.

Several approaches for determining initial equation coefficients for new processes were documented, including data from manufacturing trials, comparisons with similar processes, dynamic models, and physical limits. Hand layup times for parts representative of the aerospace industry accurately predicted using areal velocities determined in laboratory experiments performed at MIT. These velocities also compared well with rates achieved by tasks common in other manufacturing industries (e.g., laying down carpet, putting up wallpaper). An example of a dynamic model and the initial equation coefficients developed for the AFP process used to laminate fuselage skins was presented. Trade studies performed with the model indicated the importance of process parameters and cost estimating groundrules in predicting manufacturing costs. Fabrication trials were performed to improve the accuracy of the coefficients in cost equations for the three new ATCAS processes with the highest labor content: braided/RTM frames, panel bond assembly, and AFP skins.

Section 5 of this document provided a detailed breakdown of cost components for the baseline composite fuselage barrel as predicted at the end of Phase B. Using ACT cost estimating groundrules, recurring labor was found to comprise 43% of the predicted costs, while the rest was found in recurring material (30%) and non-recurring tooling (27%). Design variables most critical to cost include part area, prepreg weight, and mechanical interface area. Labor cost breakouts by selected fabrication and assembly cells helped to isolate the critical manufacturing steps and associated cost equations. In this report, the four most labor intensive ATCAS processes were documented. Three were fabrication processes discussed in the previous paragraph and the fourth was full barrel assembly. Other processes were investigated using similar approaches.

Detailed assessment of labor cost components and coefficients from the associated equations used to predict process time provided physical insights to help guide future ATCAS developments. Approximately 200 cost equations were used for more than 1900

process steps to predict labor costs for the ATCAS baseline concept. Some of these equations became crucial due to the large number of times they were used (e.g., drilling and fastening), while others came from methods that were used for a small number of high labor content tasks (contributing to approximately 60% of the total labor costs). Plots of lineal and areal velocities were rank ordered in a manner consistent with the observed task difficulty. The importance of future effort to improve the cost analyses for assessments of differing labor rates for processes that require special skills was discussed.

Analyses to evaluate the synergistic interactions of process step times, equipment and tooling quantities, facilities, and overall factory flow must be supplemented by strong DBT support to solve these difficult cost problems. Pursuit of such solutions is motivated by their importance to the cost-effective implementation of advanced manufacturing and design technologies that add overall value to commercial aircraft.

7.0 REFERENCES

1) Mabson, G. E., Ilcewicz, L.B., Graesser, D.L., Metschan, S.L., Proctor, M.R., Tervo, D.K., Tuttle, M.E., and Zabinsky, Z.B., "Cost Optimization Software for Transport Aircraft Design Evaluation - Overview," NASA CR-4736, 1996.

2) Freeman, W.T., Ilcewicz, L.B., Swanson, G.D., and Gutowski, T.G., "Designers' Unified Cost Model," Proceedings 9th DoD/NASA/FAA Conference, Fibrous Composites in Structural Design, DOT/FAA/CT-92-25, Vol. II, Lake Tahoe, Nevada, Nov., 1991, pp. 601-620.

3) Freeman, W.T., Vosteen, L.F., and Siddiqi, S., "A Unified Approach for Composite Cost Reporting and Prediction in the ACT Program," First NASA Advanced Composites Technology Conference, NASA CP-3104, Part 1, 1991, pp. 357-369.

4) Ilcewicz, L. B., Walker, T.H., Willden, K.S., Swanson, G.D., Truslove, G., and Pfahl, C.L., "Application of a Design-Build-Team Approach to Low Cost and Weight Composite Fuselage Structure," NASA CR 4418, 1991.

5) Ilcewicz, L. B., Smith, P.J., Hanson, C.T., Walker, T.H., Metschan, S.L., Mabson, G.E., Willden, K.S., Flynn, B.W., Scholz, D.B., Polland, D.R., Fredrickson, H.G., and Olson, J.T., "Advanced Technology Composite Fuselage - Program Overview," NASA CR-4734, 1996.

6) Neoh, E. T., "Adaptive Framework for Estimating Fabrication Time of Advanced Composites Manufacturing Processes," Massachusetts Institute of Technology, PHD Dissertation, Department of Mechanical Engineering, Aug., 1995.

7) Barnes, R. M., Motion and Time Study: Design and Measurement of Work, 6th. edition, Wiley, 1968.

8) Currie, R. M., Simplified PMTS: Predetermined Motion Time Systems, A Manual for Practitioners and Trainers, British Institute of Management, London, 1963.

9) Karger, D. W., and Bayha, F.H., Engineered Work Measurement, 2nd. edition, Industrial Press, New York, 1966.

10) Konz, S., Work Design: Industrial Ergonomics, 2nd. edition, Publishing Horizons, Ohio, 1987.

11) Mundel, M.E., Motion and Time Study: Improving Productivity, 6th edition, Prentice-Hall, Englewood Cliffs, N.J., 1985.

12) Niebel, B.W., Motion and Time Study, 8th. edition, Irwin, Homewood, Illinois, 1988.

13) Northrop Corporation, "Advanced Composite Cost Estimating Manual (ACCEM)," AFFDL-TR-76-87, August 1976.

14) Ostwald, P.F., AM Cost Estimator, 4th Edition, Penton Publishing Inc., 1988.

15) Boothroyd, G., and Dewhurst, P., Product Design for Assembly, Boothroyd Dewhurst, Inc. 1991.

16) Harmon, B. and Arnold, S.A. "Cost Implications of Composite Materials in Military Airframes," Advanced Composite Materials: New Developments and Applications Conference Proceedings, Detriot, Michigan, Sept. 30 - Oct. 3, 1991.

17) Boothroyd, G., Dewhurst, P., and Knight, W., Product Design for Manufacturing and Assembly, Marcel Dekker, 1994.

18) Busch, J.V., "Primary Fabrication Methods and Costs in Polymer Processing for Automobile Application," M.S. Thesis, Department of Materials Science and Engineering, M.I.T., 1983.

19) Wright, T.P., "Factors Affecting the Costs of Airplanes," Articles and Addresses of Theodore P. Wright, Vol. 2, 1936, pp. 34 - 40.

20) Wright, T.P., "Airplane Production Efficiency: An Index for Measuring the Efficient Utilization of Manpower in the Production of Airplanes," Articles and Addresses of Theodore P. Wright, Vol. 2, 1943, pp. 223 - 249.

21) Fitts, P.M., and Posner, M.I., Human Performance, Basic Concepts in Psychology Series, Brooks/Cole Publishing Co., 1967.

22) Sheridan, T.B., and Ferrell, W.R., Man-Machine Systems: Information, Control, and Decision Models of Human Performance, M.I.T. Press, 1974.

23) Sanders M.S., and McCormick, E. J., Human Factors in Engineering and Design, 7th. edition, McGraw-Hill, 1993.

24) Chase, K.W., and Greenwood, W.H., "Design Issues in Mechanical Tolerance Analysis," *Manufacturing Review*, Vol. 1, No. 1, pp 50-59, March 1988.

25) Shannon, C.E., and Weaver, W., The Mathematical Theory of Communication, University of Illinois Press, Urbana, IL, 1949.

26) Suh, N.P., The Principles of Design, Oxford University Press, New York, NY, 1990.

27) Tam, A.S., A Deformation Model for the Forming of Aligned Fiber Composites, Ph.D. Thesis, Department of Mechanical Engineering, Massachusetts Institute of Technology, June 1990.

28) Tam A.S., and Gutowski, T. G., "The Kinematics for Forming Ideal Aligned Fiber Composites", *Composites Manufacturing*, Vol.1, No. 4, 1990.

29) Gonzalez-Zugasti, J., Computer Modeling of Advanced Composites Forming, M.S. Thesis, Department of Mechanical Engineering, Massachusetts Institute of Technology, September 1991.

30) Ching, W.C., A Model of Human Performance in Assembly Tasks, B.S. Thesis, Department of Mechanical Engineering, Massachusetts Institute of Technology, July 1993.

31) Goldman, J., and Hart, L.W., Jr., Information Theory and Industrial Learning, *Journal of Industrial Engineering*, September-October, 1965.

32) Muter, S., Cost Comparisons of Alternate Designs: An Information Based Model, M.S. Thesis, Department of Mechanical Engineering, Massachusetts Institute of Technology, June 1993.

33) Kreyszig, E., Differential Geometry, Dover, New York, 1991.

34) Stoker, J.J., Differential Geometry, Wiley-Interscience, New York, NY, 1969.

35) Struik, D.J., Lectures on Classical Differential Geometry, 2nd. Edition, Addison-Wesley, Reading, MA, 1961.

36) Kim, C.E., Composites Cost Modeling: Complexity, M.S. Thesis, Department of Mechanical Engineering, Massachusetts Institute of Technology, May 1993.

37) Tse, M., Design Cost Model for Advanced Composite Structures, M.S. Thesis, Department of Mechanical Engineering, Massachusetts Institute of Technology, September 1992.

38) Waters, T.R., Putz-Anderson, V., Garg A., and Fine, L.J., "Revised NIOSH Equation for the Design and Evaluation of Manual Lifting Tasks," *Ergonomics*, 1993, Vol. 36, No. 7, pp. 749 - 776.

39) Snook, S. H. and Ciriello, V. M., "The Design of Manual Handling Tasks: Revised Tables of Maximum Acceptable Weights and Forces," *Ergonomics*, 1991, Vol. 34, No. 9, pp. 1197 - 1213.

40) Kroemer, K., Kroemer, H., and Kroemer-Elbert, K., Ergonomics: How to Design for Ease and Efficiency, Prentice Hall, Englewood Cliffs, New Jersey, 1994.

41) Karnopp, D. and Rosenberg, R., System Dynamics: A Unified Approach, Wiley-Interscience, 1975.

42) Ogata, K., Modern Control Engineering, 2nd Edition, Prentice-Hall Publishing, Englewood Cliffs, NJ, 1990.

43) Ciriello, V. M., and Snook, S. H., "A Study of Size, Distance, Height, and Frequency Effects on Manual Handling Tasks," *Human Factors*, 1983, 25(5), 473-483.

44) Barkan, P., and Hinckley, C.M., "The Benefits and Limitations of Structured Design Methodologies," *Manufacturing Review*, Vol. 6, No. 3, p. 211-220, Sept. 1993.

45) Tanner, J.P., "The Learning Curve," *Production Engineering*, May, 1985, pp. 72-78.

46) Kivenko, K., "Predict Your Production Costs with Learning Curves," *Production Engineering*, August, 1977.

47) Dutton, J.M., Thomas, A., and Butler, J. E., "The History of Progress Functions as a Managerial Technology," *Business History Review*, 58 (Summer), President and Fellows of Harvard College, 1984.

48) Mabson, G.E., and Graesser, D.L., "Cost Optimization Software for Transport Aircraft Design Evaluation - User's Manual," NASA CR-4738, 1996.

49) Flynn, B., Morris, M., Metschan, S., Swanson, G., Smith, P., Griess, K., Schramm, M., Willden, K., and Humphrey, R.: "Global Cost and Weight Evaluation of Fuselage Keel Design Concepts," NASA CR 4541, December, 1993.

50) Polland, D.R., Finn, S.R., Griess, K.H., Hafenrichter, J.L., Hanson, C.T., Ilcewicz, L.B., Metschan, S.L., Scholz, D.S., and Smith, P.J., "Global Cost and Weight Evaluation of Fuselage Side Panel Design Concepts," NASA CR-4730, 1996.

51) Swanson, G.D., Ilcewicz, L.B., Walker, T.H., Graesser, D., Tuttle, M., and Zabinsky, Z., "Local Design Optimization for Transport Fuselage Crown Panels," in Proceedings of Ninth DoD/NASA/FAA Conf. on Fibrous Composites in Structural Design, Lake Tahoe, NV, DOT/FAA/CT-92-25, Vol. II, 1991, pp. 795-814.

52) Willden, K.S., Flynn, B.W., Gessel, M., Harris, C.G., Scholz, D.B., and Stawski, S., "Advanced Technology Composite Fuselage - Manufacturing," NASA CR-4735, 1996.

53) Scholz, D.B., Dost, E.F., Flynn, B.W., Ilcewicz, L.B., Lakes, R.S., Nelson, K.M., Sawicki, A.J., and Walker, T.H., "Advanced Technology Composite Fuselage - Materials and Processes," NASA CR-4731, 1996.

54) Metschan, S., Willden, K., Sharpless, G., and Andelman, R., "Cost Model Relationships Between Textile Manufacturing Processes and Design Details for Transport Fuselage Elements," Third NASA/DOD Advanced Composite Technology Conference, NASA CP-3178, 1992, pp. 323-340.

55) Proctor, M., Metschan, S., and Klein, H., Cost Optimization Software for Transport Aircraft Design Evaluation - Process Cost Analysis Database, CR-4739, 1996.

56) DeGarmo, E.P., Black, J.T., and Kohser, R.A., Materials and Processes in Manufacturing, 7th. edition, Macmillan Publishing Company, New York, 1988.

57) Kalpakjian, S., Manufacturing Engineering and Technology, 2nd ed., Addison-Wesley Publishing Co. 1992.

58) Schey, J.A., Introduction to Manufacturing Processes, 2nd. edition, McGraw-Hill, 1987.

59) Eagar, T.W., Processes of Joining Materials, Unpublished Manuscript, Department of Material Science and Engineering, Massachusetts Institute of Technology.

60) Cleveland, A.B., Means Man-Hour Standards, R.S. Means Co., Kingston, MA, 1983.

61) Neoh, E.T., Gutowski, T.G., and Dillon, G., "Framework for Estimating Fabrication Time of Advanced Composites Manufacturing Processes," *40th International SAMPE Symposium and Exhibition*, May, 1995.

62) Metschan, S.L., Graesser, D.L., Mabson, G.E., Proctor, M.R., Tervo, D.K., and Ilcewicz, L.B., "Manufacturing Data for COSTADE Analysis of Composite Fuselage Panels", Fifth NASA/DoD CP-3294, 1995, pp. 93-125.

63) Mabson, G.E., Flynn, B.W., Ilcewicz, L.B., and Graesser, D.L., "The Use of COSTADE in Developing Commercial Aircraft Fuselage Structures", AIAA-94-1492, Proceedings of 35th AIAA/ASME/ASCE/AHS/ASC SDM Conference, Hilton Head, SC, Apr. 18-20, 1994.

64) Metschan, S.L., Mabson, G.E., Swanson, G.D., Gessel, M.H., Humphrey, R.J., and Tervo, D.K., "Integration of Advanced Composite Manufacturing Trials Into a Design/Cost Database," Fourth NASA/DoD Advanced Composite Technology Conference, 1993.

APPENDIX A

CURVE FITTING FIRST-ORDER MODEL TO POWER LAW

This appendix outlines the procedure to estimate τ_d and v_o for the first order model based on the power law model in ACCEM (ref. 13). Obviously, the estimated values will depend on the curve fitting criteria. In order to standardize the results, we have established the following procedures. As an initial estimate, the following steps are recommended (with the results tabulated in Table A-1):

1) Estimate v_o using

$$v_o \equiv \frac{L_{max}^{1-r}}{rA} . \tag{A.1}$$

2) Estimate τ_d using

$$\tau_d \cong (0.63)^{\frac{r}{1-r}} A L_{max}^{r} = (0.63)^{\frac{r}{1-r}} t_{max} . \tag{A.2}$$

3) Estimate $L^* \cdot e$ with

$$L^* \cdot e = \tau_d v_o . \tag{A.3}$$

4) Check if $L^* \cdot e < L_{max}$ (Go to step 6 if $L^* \cdot e > L_{max}$).

5) If $L^* \cdot e < L_{max}$, repeat steps (1, 2 and 3) with L_{max} replaced by L where

$$L = \frac{L^* \cdot e + L_{max}}{2} . \tag{A.4}$$

6) If $L^* \cdot e > L_{max}$, then the process is always in the nonlinear regime; in which case, Equation A.7 should be used to determine the ratio τ_d/v_o. This will be illustrated by the "720 IPM" example below.

Process		3" Manual	12" Manual	360 IPM	720 IPM
Power Law Constants	A	0.0014	0.001454	0.00058	0.00063
	r	0.6018	0.8245	0.5716	0.4942
	L_{max} (in)	200	200	290	300
First Iteration	τ_d (hr)	0.017	0.013	0.008	0.007
	V_o (in/hr)	9788	2114	34227	57502
	$L^* \cdot e$	165.32	27.68	273.89	386.51
	$(L_{max} + L^* \cdot e)/2$	182.66	113.84	281.94	$L^* \cdot e > L_{max}$
Using $L = (L_{max} + L^* \cdot e)/2$	τ_d (hr)	0.016	0.008	0.008	**N/A**
	V_o (in/hr)	9441	1915	33817	
	New $L^* \cdot e$	150.98	15.75	266.28	

Table A-1. ***τ_d and v_o estimated using the quick estimation procedure.***

Note that steps (1) to (3) are based on the maximum length quoted for that particular process. In order not to place such a heavy emphasis on the limiting value quoted (which

might represent the limit of the process) it is recommended that an intermediate value between the first $L^* \cdot e$ estimated and L_{max} be used for the second iteration in step (5).

For cases where $L^* \cdot e < L_{max}$, the rough estimates obtained with the above method will be used as "educated guesses" for the next phase; where we place equal weight on all lengths and then use the "least square" criterion to improve on the estimates for t_d and v_o. This procedure is outlined below:

1) Calculate time, t, for each evenly spaced length, L, for $L_{min} \leq L \leq L_{max}$ using

$$t = AL^r \tag{A.5}$$

2) Use "least square" criteria, fit $L = f\ (\tau_d, v_o, t)$ as in equation (A.6):

$$L = v_o \left[t - \tau_d \left(1 - e^{-t/\tau_d} \right) \right] . \tag{A.6}$$

Note that because the first order model in Equation A.6 cannot be inverted for time, t, we ended up having to fit τ_d and v_o in the form of Equation A.6 to the data pairs generated using Equation A.5. This was done using the "user defined curve fit" in DeltaGraph® and the results are shown in Figures A-1 to A-4. As shown in Table A-2, the results obtained using the "least square" method are comparable to that from the quick estimates of Table A-1. The one exception is for the case of 720 IPM where $L^* \cdot e > L_{max}$.

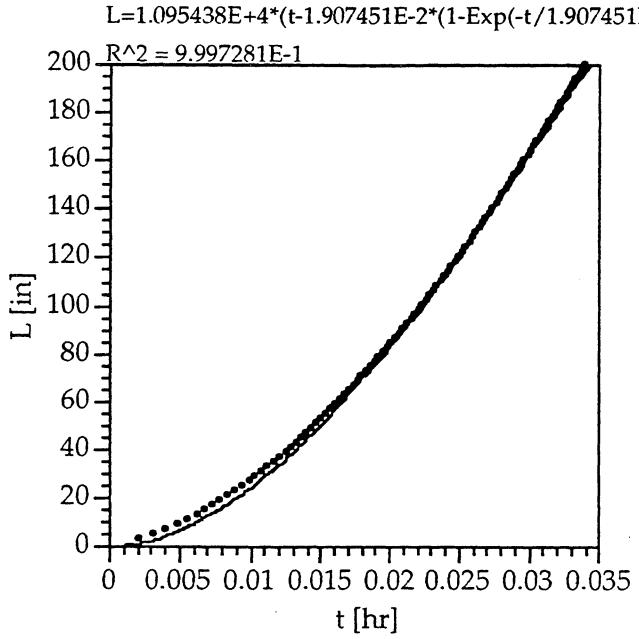

Figure A-1. Curve fit for 3 in. manual tape layup: $\tau_d = 0.0191$ hr, $v_o = 10950$ in/hr.

® DeltaGraph Professional version 2.03 by DeltaPoint Inc.

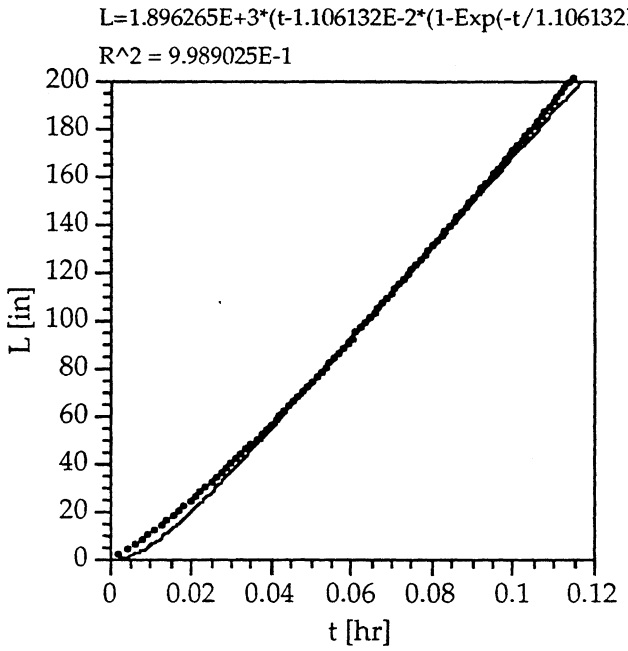

Figure A-2. Curve fit for 12 in. manual tape layup: τ_d = 0.0111 hr, v_o = 1896 in/hr.

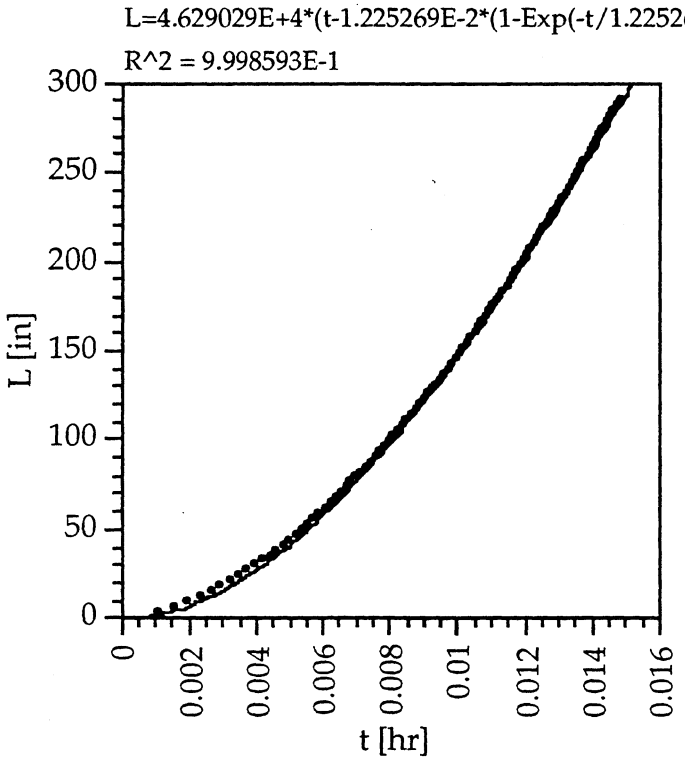

Figure A-3. Curve fit for 360 IPM: τ_d = 0.0123 hr, v_o = 46290 in/hr.

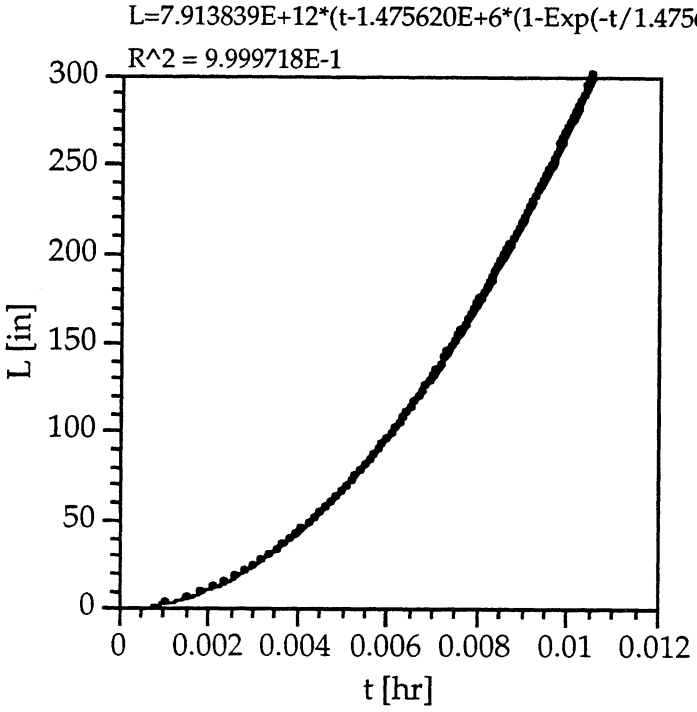

Figure A-4. Curve fit for 720 IPM: τ_d = 1.476E6 hr, v_o = 7.914E12 in/hr.

Process		3" Manual	12" Manual	360 IPM	720 IPM
Power Law Constants	A	0.0014	0.001454	0.00058	0.00063
	r	0.6018	0.8245	0.5716	0.4942
	L_{max} (in)	200	200	290	300
Using Rough Estimation	τ_d (hr)	0.016	0.008	0.008	**N/A**
	V_o (in/hr)	9441	1915	33817	**N/A**
	L* · e	150.98	15.75	266.28	L* · e > L_{max}
Using Least Square Fit	τ_d (hr)	0.0191	0.0111	0.0123	**N/A**
	V_o (in/hr)	10950	1896	46290	
	L* · e	209.145	21.0456	569.367	
	τ_d/V_o	1.7E-06	5.85E-06	2.7E-07	1.87E-07

Table A-2. τ_d and v_o estimated using the procedures outlined [1].

[1]Note that for 360IPM, v_o is much larger than 360 in/min = 21,600 in/hr. This suggests that the original data and/or curve fit from ACCEM may be in error.

As is evident from very high constants shown in Figure A-4, the "least square" method clearly resulted in absurd results as $L^* \cdot e > L_{max}$. In this case, the system entered a non-linear region and Equation A.7 proves more compatible with least squares analysis (see Figure A-5). The power law index of $r \approx 0.5$ also suggests Equation A.7 for this case.

$$t = \sqrt{\frac{2\tau_d L}{v_o}} \tag{A.7}$$

However, Equation A.7 will only give us the ratio τ_d/v_o. This example illustrates the fact that we have to be aware of the results from curve fitting procedures.

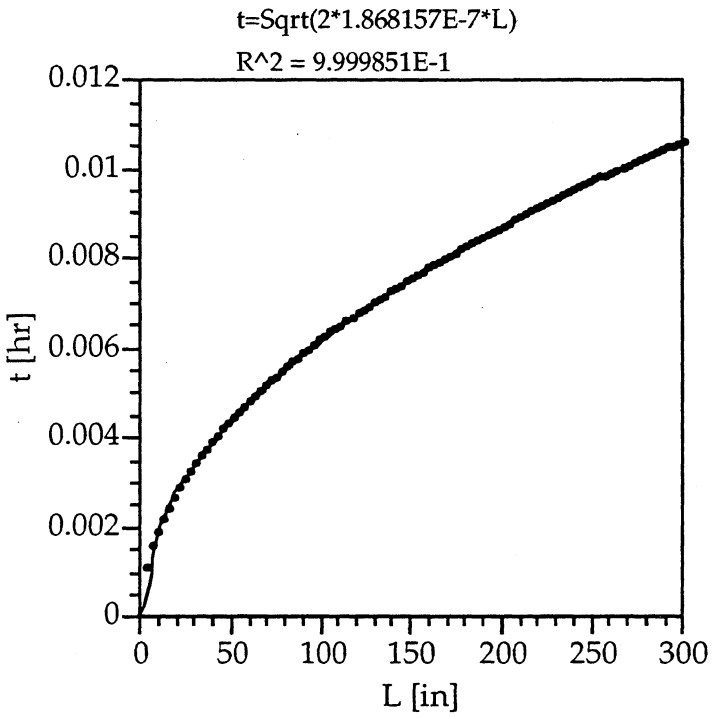

Figure A-5. Curve fit for 720 IPM: τ_d/v_o = 1.8682E-7 hr^2/in.

Figures A-6 to A-9 illustrate the difference between the rough estimate and the "least square" fit that utilizes Equation A.7. In all cases, the least square method, combined with the power law approximation, yield satisfactory results.

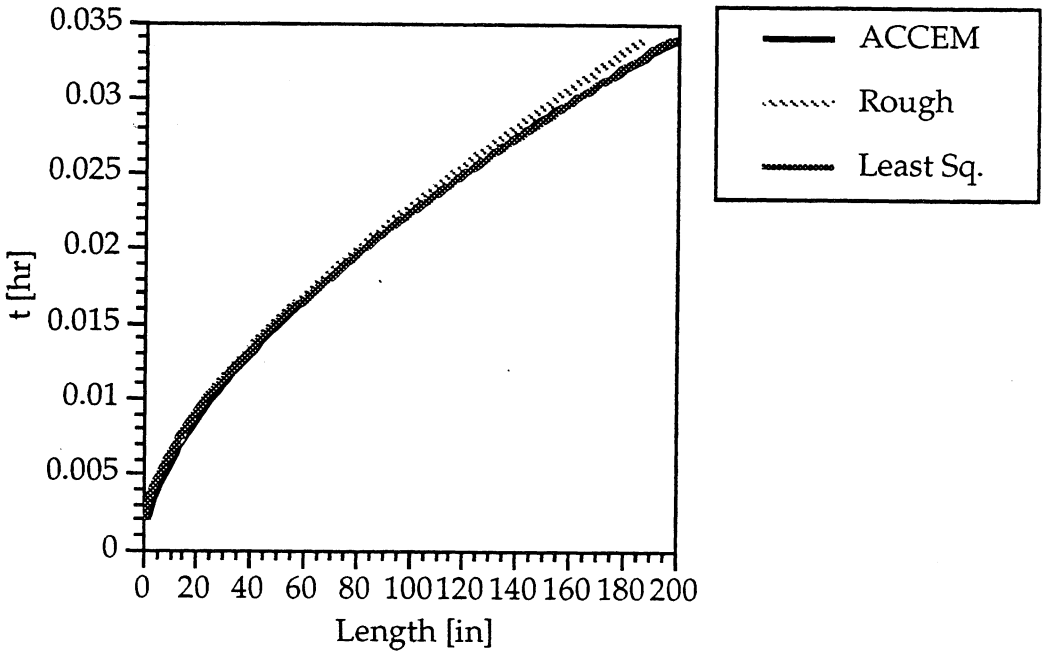

Figure A-6. Comparing fits for 3 in. manual tape layup process.

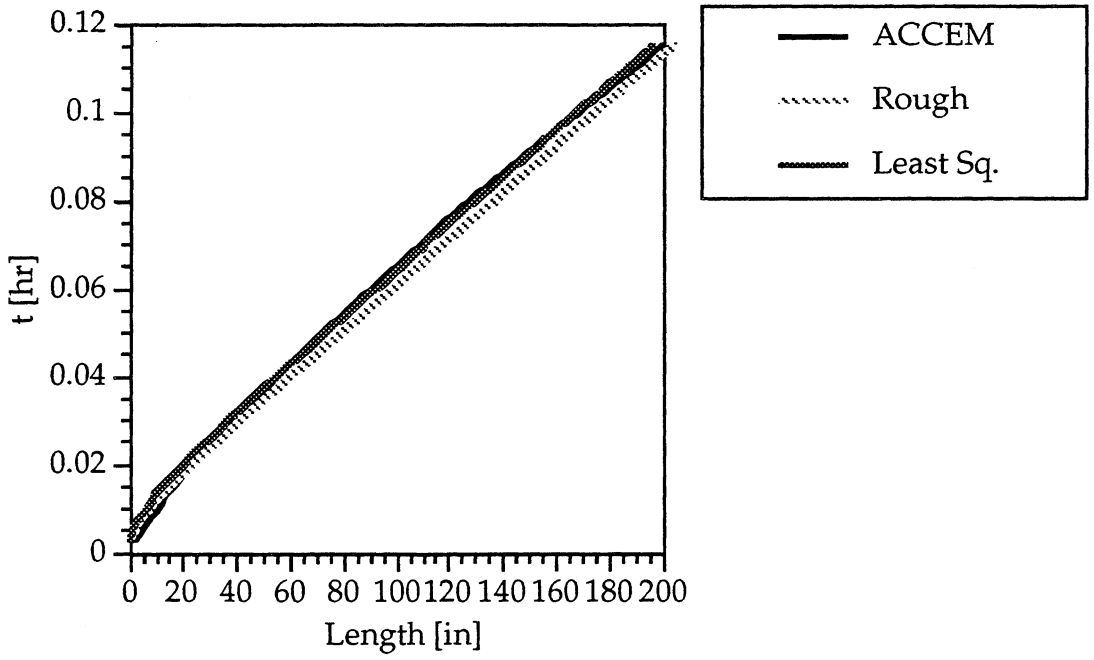

Figure A-7. Comparing fits for 12 in. manual tape layup process.

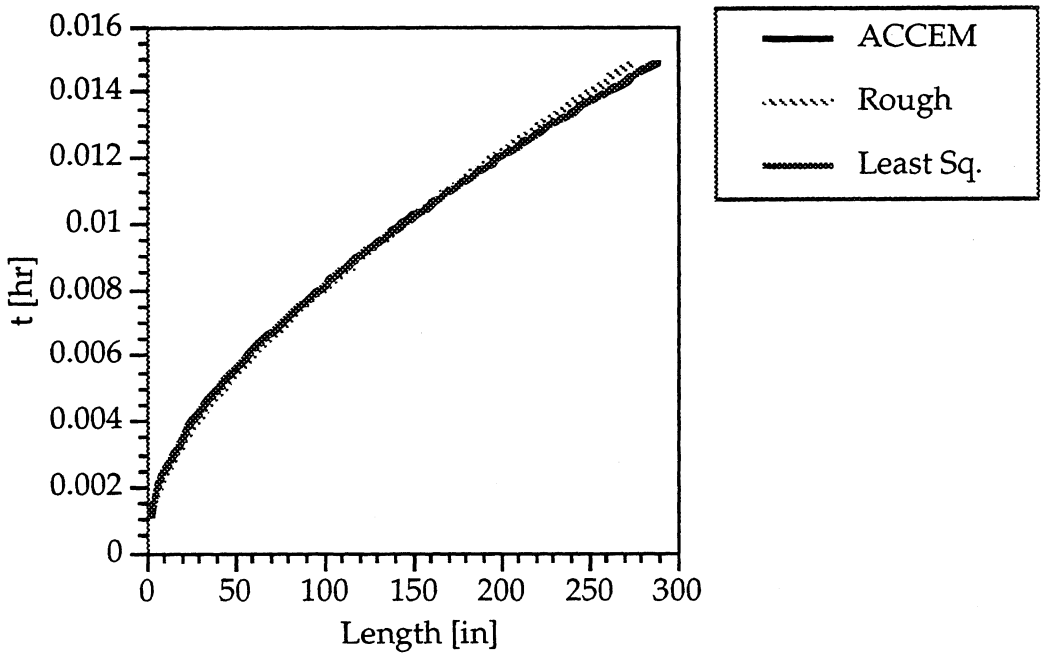

Figure A-8. Comparing fits for 360 IPM process.

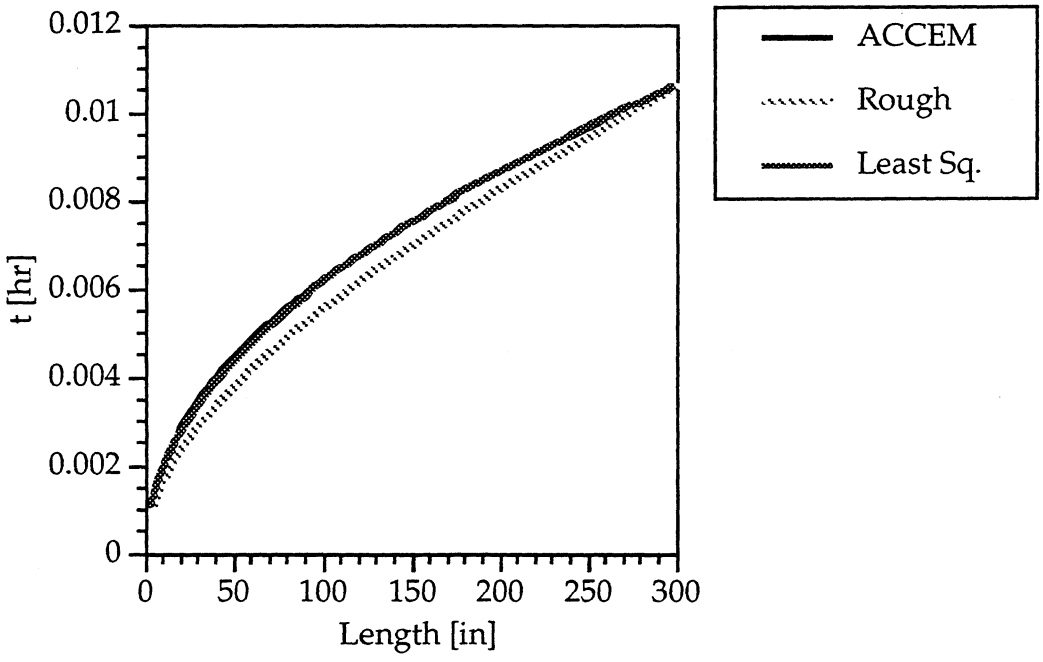

Figure A-9. Comparing fits for 720 IPM process.

APPENDIX B

EXAMPLE PLY DROP-OFF & ORIENTATION CALCULATIONS

This appendix illustrates the effects of ply drop-off, build-up, and orientation on the complexities of the laminate layup operation. Specific examples will be given to illustrate how these forms of complexities effect the average number of strips required per unit volume of the part.

Three special cases have been selected for examples. The first calculations will show effects of ply orientation on a constant cross-section beam. The next set of calculations will show effects of ply drop-offs for different ply orientations in a tapered beam (i.e., ply drop-offs in a single direction). Final calculations will show effects of ply drop-offs in two directions by contrasting a pyramid to a cube for a quasi-isotropic lay-up.

Below is a list of the general variables that are used throughout this appendix:

Average number of strips per layer, $\bar{n} = \frac{\bar{D}}{w}$ (B.1)

where, w = width of strip

and $\bar{D}$ = effective length across tape width.

Number of layers per part, $N = \frac{H}{h}$ (B.2)

where, H = part thickness,

and h = ply thickness.

Total number of strips per part $N_L = \bar{n} N = \frac{\bar{D} H}{w h}$ (B.3)

where, W = part width

and L = part length.

B.1 Effects of Lay-up Orientation On the Number of Strips Required

B.1.1 0° Lay-up

As a starting point, the effects of lay-up orientation on the number of strips required to lay-up a single rectangular layer must be calculated. For a 0° lay-up orientation as shown in Figure B-1, the number of strips required per layer is simply

$$n = \frac{W}{w} \tag{B.4}$$

thus

$$\bar{D} = W \tag{B.5}$$

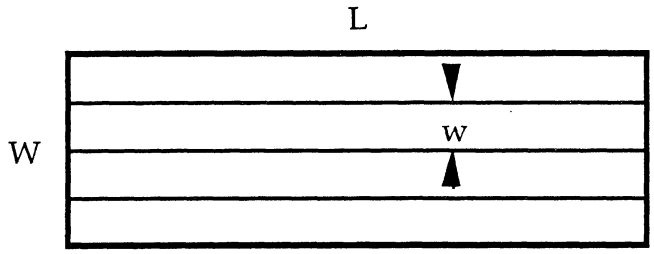

Figure B-1. Plan view of a 0° lay-up.

B.1.2 90° Lay-up

Similarly, for a 90° lay-up orientation as shown in Figure B-2, the number of strips required per layer is simply

$$n = \frac{L}{w} \tag{B.6}$$

thus

$$\overline{D} = L \tag{B.7}$$

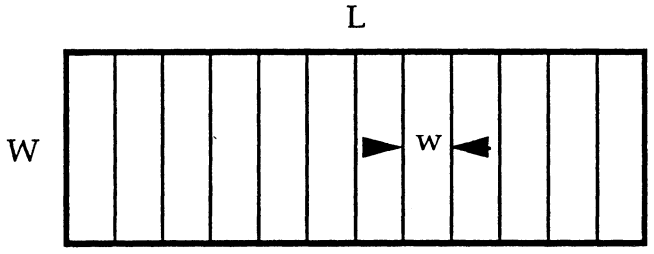

Figure B-2. Plan view of a 90° lay-up.

B.1.3 ±45° Lay-up

In general, a lay-up angle other than 0° and 90° needs more attention. Such cases can be divided further into two subcases, depending on whether the layup angle, Ψ, is larger than the critical angle, Ψ_{crit}, for the particular geometry. When $\Psi > \Psi_{crit}$, as shown in Figure B-3, the number of strips required per layer is

$$n = \frac{\left(L + \frac{W}{\tan \Psi}\right)}{\frac{w}{\sin \Psi}} \tag{B.8}$$

which simplifies to (for $\Psi = 45°$)

$$n = \frac{0.707\ (L + W)}{w} \tag{B.9}$$

Thus,

$$\overline{D} = 0.707\ (L + W) \tag{B.10}$$

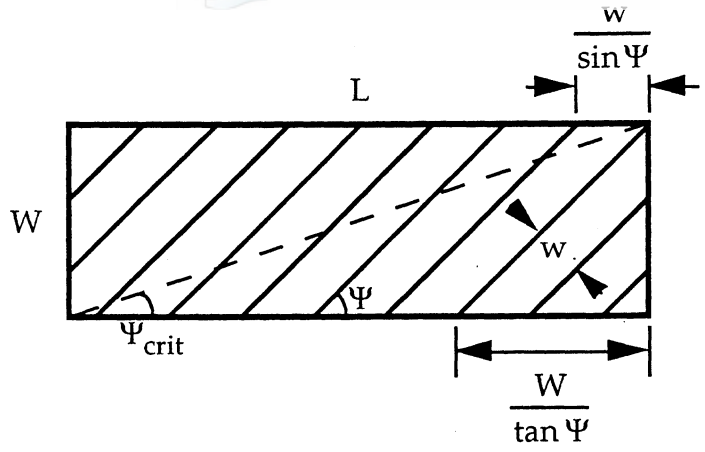

Figure B-3. Plan view of a 45° lay-up with $\Psi > \Psi_{crit}$.

On the other hand, when $\Psi < \Psi_{crit}$, as shown in Figure B-4, the number of strips required per layer is

$$n = \frac{(W + L \tan \Psi)}{\frac{w}{\cos \Psi}} \qquad \text{(B.11)}$$

which simplifies to (for $\Psi = 45°$)

$$n = \frac{0.707\ (W + L)}{w} \quad . \qquad \text{(B.12)}$$

Thus,

$$\overline{D} = 0.707\ (W + L) \quad . \qquad \text{(B.13)}$$

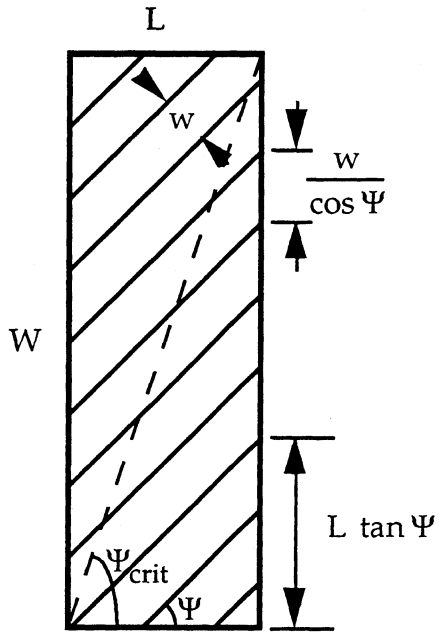

Figure B-4. Plan view of a 45° lay-up with $\Psi < \Psi_{crit}$.

B.2 Constant Cross Section Beam of Various Ply Orientations

For the constant cross section beam shown in Figure B-5, the part volume is given by

$$V = L\,W\,H \tag{B.14}$$

For $\Psi = 0°$, $\overline{D} = W$. Using Equations B.3 and B.14 yields

$$\boxed{\frac{N_L}{V} = \frac{1}{w\,h}\left(\frac{1}{L}\right)}\,. \tag{B.15}$$

Similarly, for $\Psi = 90°$, $\overline{D} = L$ and

$$\boxed{\frac{N_L}{V} = \frac{1}{w\,h}\left(\frac{1}{W}\right)}\,. \tag{B.16}$$

Finally, for $\Psi = \pm 45°$, $\overline{D} = 0.707\,(L + W)$ and

$$\boxed{\frac{N_L}{V} = \frac{1}{w\,h}\left(\frac{0.707\,(L + W)}{W\,L}\right)}\,. \tag{B.17}$$

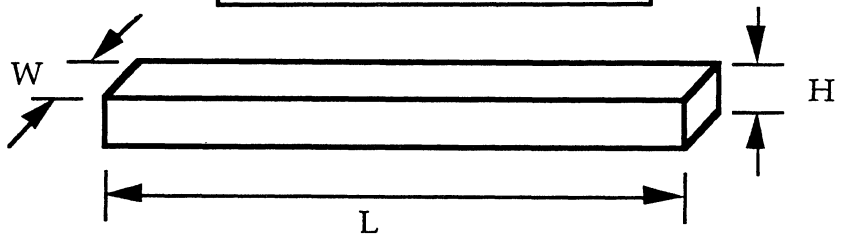

Figure B-5. Constant cross section beam

B.3 Effects of Ply Drop-off in One Dimension (Tapered Beam)

For the tapered beam shown in Figure B-6, the part volume is given by

$$V = L\,W\,H/2 \tag{B.18}$$

For $\Psi = 0°$, $\overline{D} = W$. Using Equations B.3 and B.18 yields

$$\boxed{\frac{N_L}{V} = \frac{1}{w\,h}\left(\frac{2}{L}\right)}\,. \tag{B.19}$$

Similarly, for $\Psi = 90°$, $\overline{D} = L/2$ and

$$\boxed{\frac{N_L}{V} = \frac{1}{w\,h}\left(\frac{1}{W}\right)}\,. \tag{B.20}$$

Finally, for $\Psi = \pm 45°$, $\overline{D} = 0.707\,(L/2 + W)$ and

$$\boxed{\frac{N_L}{V} = \frac{1}{w\,h}\left(\frac{1.414\left(L/2 + W\right)}{W\,L}\right)}\,. \tag{B.21}$$

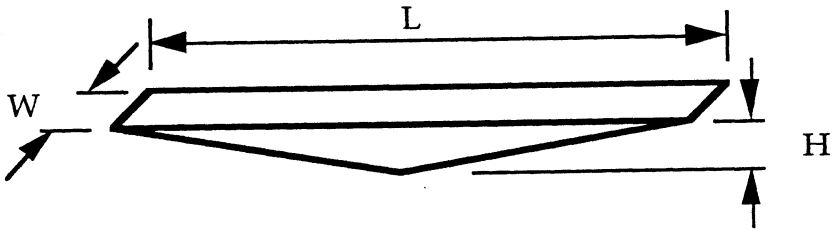

Figure B-6. Tapered beam illustrating ply drop-off in one direction

B.4 Effects of Ply Drop-off in Two Dimensions (Pyramid vs. Cube)

The effects of laminate ply drop-offs in two directions can be observed by comparing a cube to a pyramid. This comparison is simplified by assuming the same quasi-isotropic lay-up, $[0/90/\pm45]_{Ns}$ for both cases. For the cube shown in Figure B-7 (L = W = H), the part volume is $V = L^3$. The average number of strips per layer is given by

$$\bar{n} = \frac{1}{4}\left[\frac{W}{w} + \frac{L}{w} + \frac{1.414\ (L + W)}{w}\right] = \frac{1.207\ L}{w} \quad . \tag{B.22}$$

Therefore,

$$\boxed{\frac{N_L}{V} = \frac{1}{w\,h}\left(\frac{1.207}{L}\right)} \quad . \tag{B.23}$$

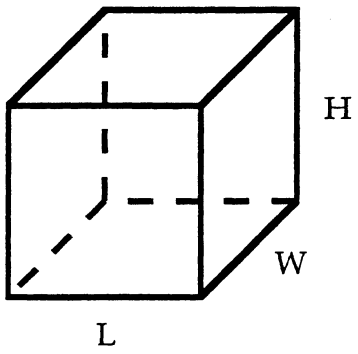

Figure B-7. Cube with quasi-isotropic lay-up $[0/90/\pm45]_{Ns}$.

Similarly, for the general case of a truncated pyramid shown in Figure B-8, the part voulme is given by

$$V = \frac{H}{6}\left(2\,L_1\,W_1 + L_1\,W_2 + L_2\,W_1 + 2\,L_2\,W_2\right) \tag{B.24}$$

Let $\bar{L} = \frac{L_1 + L_2}{2}$ and $\bar{W} = \frac{W_1 + W_2}{2}$, then the average number of strips per layer is given by

$$\bar{n} = \frac{1}{4}\left(\frac{\bar{W}}{w} + \frac{\bar{L}}{w} + \frac{1.414\,(\bar{L} + \bar{W})}{w}\right). \tag{B.25}$$

Therefore,

$$\bar{D} = 0.6035\,(\bar{L} + \bar{W}) \tag{B.26}$$

Subsequently, Equations B.3, B.24, and B.26 yield

$$\frac{N_L}{V} = \frac{1}{w\,h}\left(\frac{3.621\,(\bar{L} + \bar{W})}{2\,L_1\,W_1 + L_1\,W_2 + L_2\,W_1 + 2\,L_2\,W_2}\right). \tag{B.27}$$

Note that Equation B.27 is for the general case of a truncated pyramid. For a square base pyramid, $L_1 = W_1 = L$ and $L_2 = W_2 = 0$, Equation B.27 can be greatly simplified to give

$$\boxed{\frac{N_L}{V} = \frac{1}{w\,h}\left(\frac{1.811}{L}\right)}. \tag{B.28}$$

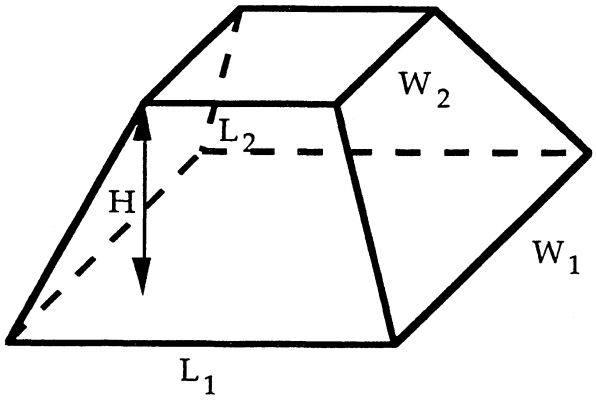

Figure B-8. Truncated pyramid with quasi-isotropic lay-up, $\mathbf{[0/90/\pm45]_{Ns}}$.

The relative complexity, expressed as the number of strips per unit volume of a part, gives a scaling measure for the effects of ply orientation and ply drop-off in laminate lay-up processes. A box was drawn around the equations obtained for this ratio at the end of each example analyzed in this appendix. Table 2-2 also lists these relative complexity factors.

APPENDIX C

CALCULATIONS OF THE ENCLOSED ANGLE θ FOR COMPLEX GEOMETRY

C.1 θ_n for Arbitrary Fiber Orientation and Out-of-Plane Bend Angle

The enclosed angle for a straight fiber when it is draped between two planes, as shown in Figure C-1, was derived by Tse (ref. 37). Let the angle between the two planes be α, and the angle between the tangent vector of the fiber and the line of intersection between the planes be Ψ. The deviation (β) of the two fiber segments on each plane is the angle swept when one fiber segment is placed on the first plane and the other segment is bent to lie flat on the second plane. The internal angle resulting form this motion is denoted by ϕ. If a perpendicular bisector is drawn between the two planes, it makes angles of $\phi/2$ between the fiber segments, and $\alpha/2$ normally between the plane surfaces. At an elevation c along the bisector, we can determine distances a in the plane of the bisector and the surface normal, and b in the plane of the bisector and the fiber's tangent vector.

Using this notation, we find that the following relationships hold.

$$c = a \cos\left(\frac{\alpha}{2}\right) . \tag{C.1}$$

for the plane, and

$$c = b \cos\left(\frac{\phi}{2}\right) . \tag{C.2}$$

for the fiber. In addition the fiber makes an angle along the plane:

$$b = \frac{a}{\sin(\Psi)} . \tag{C.3}$$

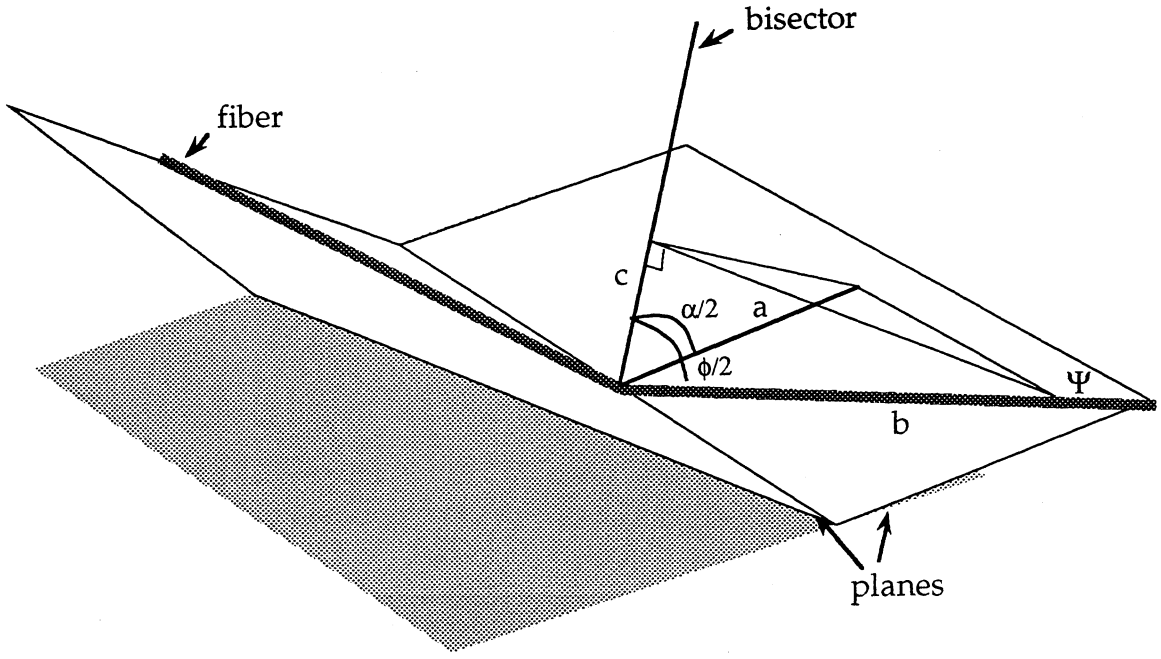

Figure C-1: Derivation of fiber deviation over two inclined planes for a general angle of attack, Ψ.

Using Equations C.1, C.2 and C.3, the expression for the fiber angle ϕ is

$$\cos\left(\frac{\phi}{2}\right) = \sin\Psi \cos\left(\frac{\alpha}{2}\right) .$$

$$\phi = 2\cos^{-1}\left[\sin\Psi \cos\left(\frac{\alpha}{2}\right)\right] . \qquad \text{(C.4)}$$

The fiber segment deviation is given by $\beta = \pi - \phi$ and since the enclosed angle $\theta_n = \beta$,

$$\theta_n = \pi - 2\cos^{-1}\left[\sin\Psi \cos\left(\frac{\alpha}{2}\right)\right] . \qquad \text{(C.5)}$$

Equation C.5 is used to calculate the enclosed angle, θ_n, for the out-of-plane bending of a fiber oriented at, Ψ, between two surfaces which are at an angle, α.

C.2 In-plane Enclosed Angle, θ_g, for Complex Geometry

The in-plane curvature, or geodesic curvature κ_g, and its attendant enclosed angle θ_g, was shown to be related to part curvature through the appropriate use of the Gauss Bonnet theorem (refs. 27, 28). In words, the Gauss Bonnet theorem relates the geodesic curvature for the piecewise line segments of an enclosed path *C* to the Gaussian or double curvature K, in the enclosed region *R*, and the angles of intersection θ_i. The Gauss Bonnet Theorem is expressed as Equation C.6

$$\int_C \kappa_g \, ds + \iint_R K \, dA = 2\pi - \sum \theta_i \quad , \qquad \text{(C.6)}$$

and is illustrated in Figure C-2.

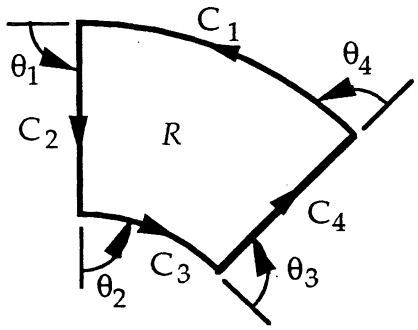

Figure C-2. The Gauss-Bonnet Theorem. The C_i are smooth curves enclosing a simply connected region* R *and θ_i are the exterior angles between the curves.

By choosing C_1 and C_3 to be fiber paths and C_2 and C_4 to be orthogonal geodesic paths, the exterior angles sum to 2π and the right hand side of Equation C.6 vanishes, therefore

$$\theta_g = \int_C \kappa_g \, ds = -\iint_R K \, dA \quad . \qquad \text{(C.7)}$$

Equation C.7 can be used to evaluate the in-plane enclosed angle θ_g for the double curvature parts in Sections C.2.1, C.2.2, C.2.3, and C.2.4 (ref. 27).

C.2.1 Hemisphere

For the hemisphere shown in Figure C-3, application of Equation C.7 yields

$$\boxed{\theta_g = \pi \sin \phi} \quad . \tag{C.8}$$

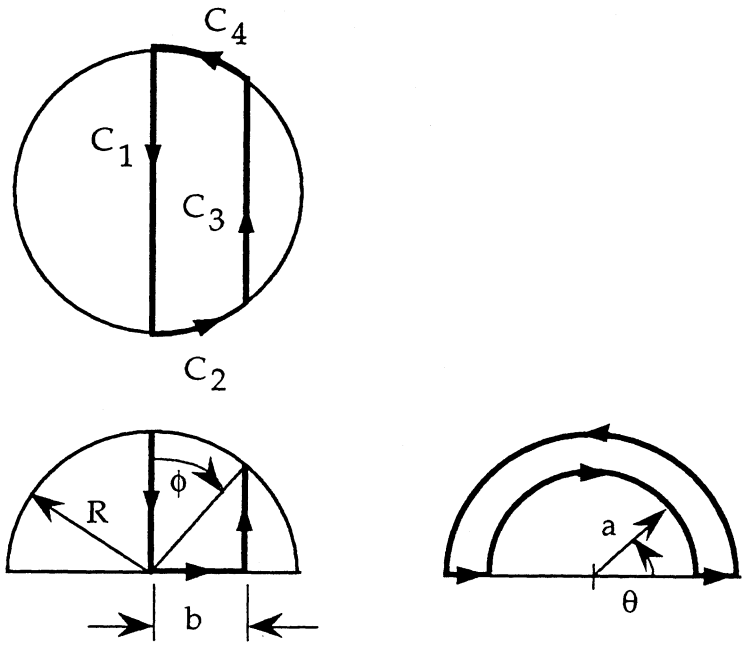

Figure C-3. In-plane enclosed angle θ_g calculation for a hemisphere.

C.2.2 Cone

Similarly, θ_g for the cone with the fiber path shown in Figure C.4b is

$$\boxed{\theta_g = 2\pi \sin \alpha} \quad . \tag{C.9}$$

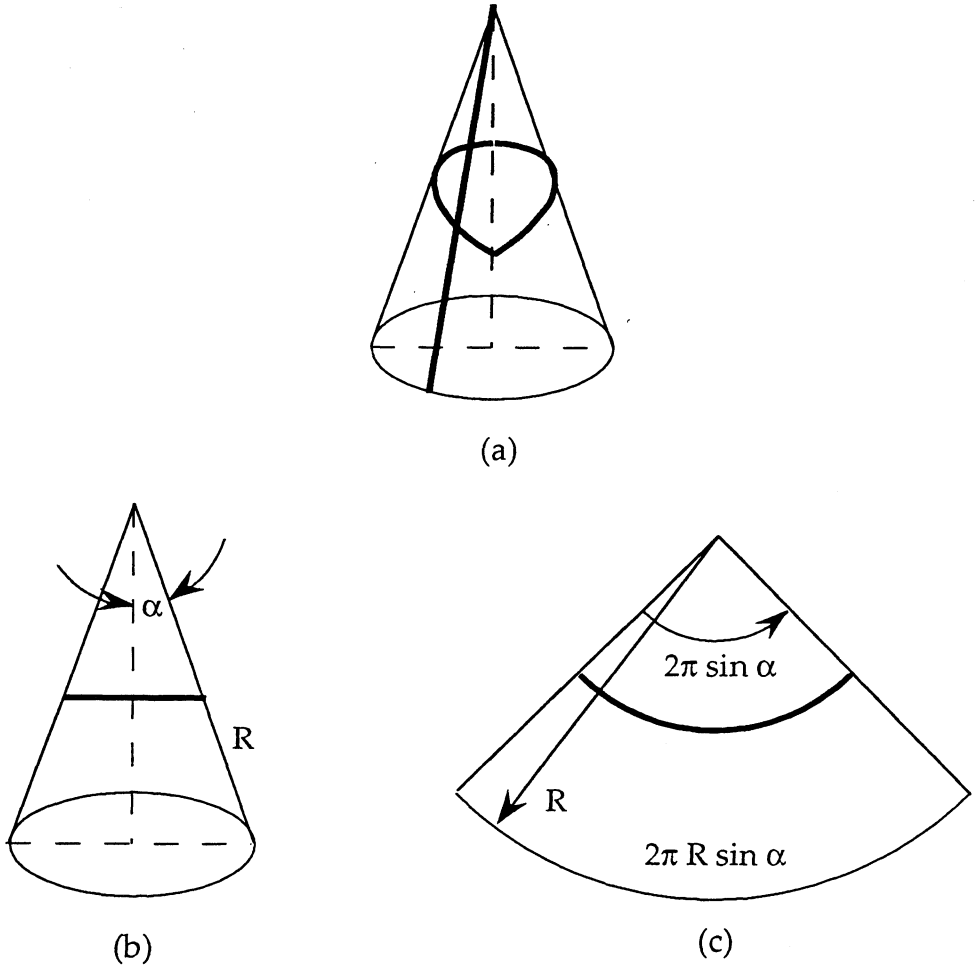

Figure C-4. In-plane enclosed angle θ_g for a cone.
(a) Geodesic paths may not be the desired paths.
(b) Circumferential fiber path on a cone with apex angle α.
(c) Unrolled surface of the cone showing circular fiber path.

C.2.3 C-channel with Joggle

For the joggle contour shown in Figure C-5, the maximum θ_g for the arbitrary fiber orientation Ψ is

$$\boxed{|\theta_g| = \alpha} \quad , \tag{C.10}$$

where α is the joggle angle. Note that two different θ_g distributions can be obtained depending on the initial fiber placement; as shown in Figures C.5b and C.5c. However, in both cases, the width of the band experiencing $|\theta_g|$, $w_{\theta g}$, is given by

$$w_{\theta g} = L_{joggle} \, |\sin(\Psi - \alpha)| \quad . \tag{C.11}$$

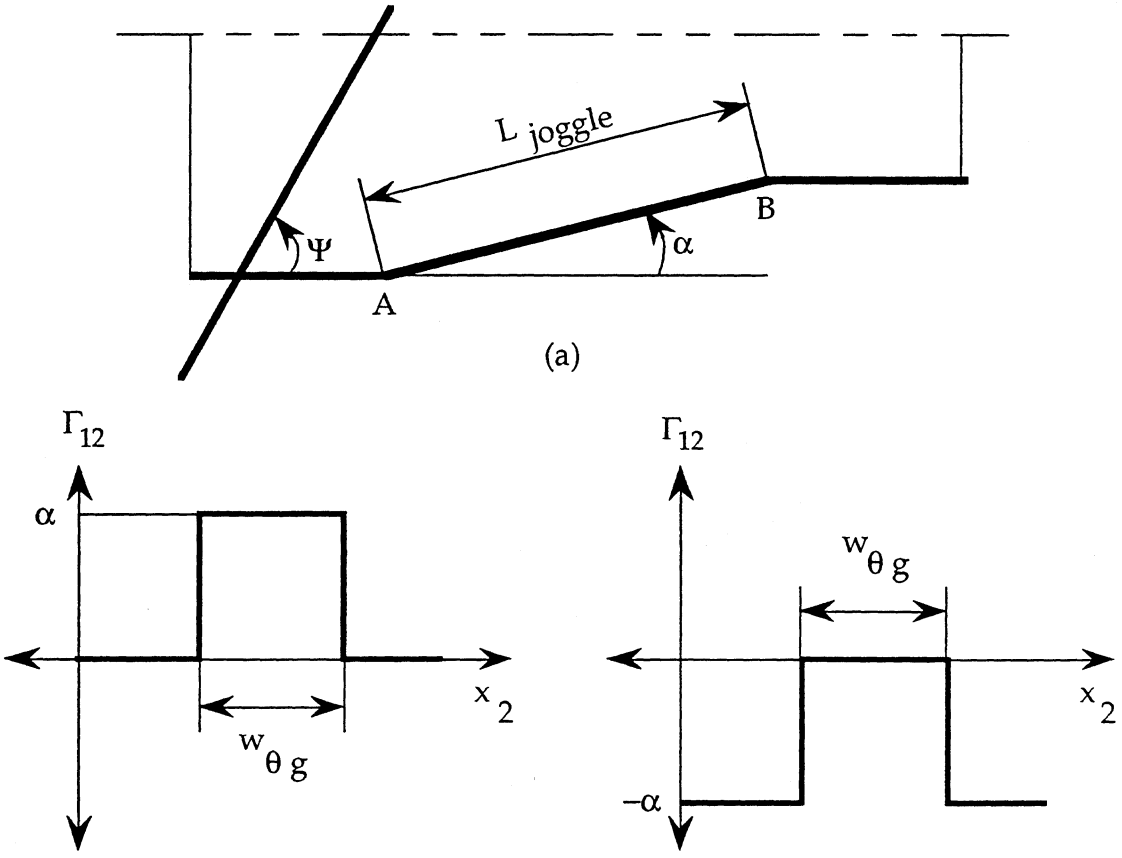

Figure C-5. In-plane shear (θ_g) calculation for a joggle contour.
(a) Dimension of the joggle.
(b) θ_g with initial fiber outside the joggle region.
(c) θ_g with initial fiber inside the flange region.

C.2.4 Curved C-channel

The maximum in-plane enclosed angle $\theta_{g,max}$ for the curved C-channel shown in Figure C-6 was calculated as

$$\boxed{\theta_{g,max} = \frac{\alpha}{2}} \quad . \tag{C.12}$$

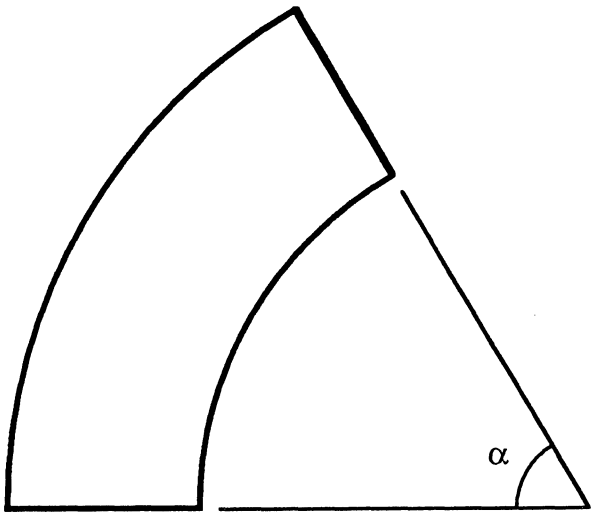

Figure C-6. Plan view of a curved C-channel with enclosing angle α.

C.3 Sample Calculations of $\bar{\theta}_g$, for Complex Geometry

In order to weigh the different regions of a part with different degrees of curvatures in a consistent manner, it is proposed that an area averaging technique be used to calculate the average in-plane enclosed angle as

$$\bar{\theta}_g = \frac{1}{A}\int \theta_g \cdot S \, dS_n. \tag{C.13}$$

Here A is the total area of the part, θ_g is the enclosed angle for a given fiber of length S, and S_n is the distance normal to the fiber direction (along the fiber width). In the following sub-section, calculations are illustrated for the lay-up orientation $\Psi = 0°$ for various complex geometric shapes. Note that θ_g for the bead stiffener and the box depends on the relative dimensions of the part; whereas θ_g for the hemisphere does not.

C.3.1 Bead

For the bead stiffener shown in Figure C-7, only material on the two surfaces bounded by L_1 on the bottom and L_2 on the top will experience any in plane curvature. The enclosed angle for this particular in-plane curvature derived in ref. 36 is given as

$$\theta_g = 4\beta_1 - \pi. \tag{C.14}$$

In this case, Equation C.13 simply reduces to

$$\bar{\theta}_g = \frac{1}{A}\int \theta_g \cdot S \, dS_n = \frac{1}{A}\theta_g A_{affected}. \tag{C.15}$$

Since

$$A_{affected} = (L_1 + L_2)\, H \tag{C.16}$$

and

$$A = (L_1 + L_2 + W_1 + W_2)\, H + L_2 W_2 \quad . \tag{C.17}$$

Therefore

$$\bar{\theta}_g = \frac{(4\beta_1 - \pi)(L_1 + L_2)H}{(L_1 + L_2 + W_1 + W_2)H + L_2 W_2} \quad . \tag{C.18}$$

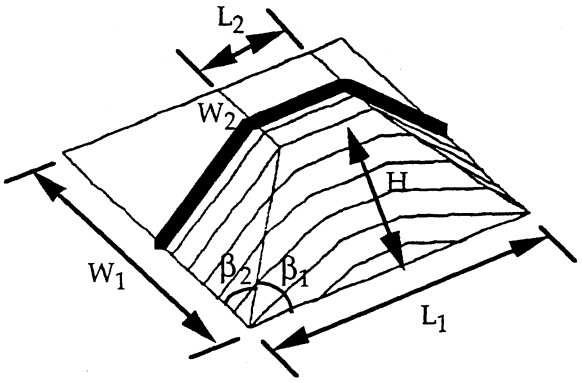

Figure C-7. Bead stiffener with the fiber mapping used in calculation.

C.3.2 Box

Similar to the case of a bead, only material on the two surfaces bounded by the sides L and H shown in Figure C-8 will experience the in-plane curvature with an enclosed angle of

$$\theta_g = \pi. \tag{C.19}$$

Again, in this case, Equation C.13 simply reduces to

$$\bar{\theta}_g = \frac{1}{A}\int \theta_g \cdot S \, dS_n = \frac{1}{A}\,\theta_g \, A_{affected}. \tag{C.20}$$

Since

$$A_{affected} = 2LH \tag{C.21}$$

and

$$A = LW + 2LH + 2WH \quad . \tag{C.22}$$

Therefore

$$\boxed{\bar{\theta}_g = \frac{2\pi LH}{LW + 2LH + 2WH}}. \tag{C.23}$$

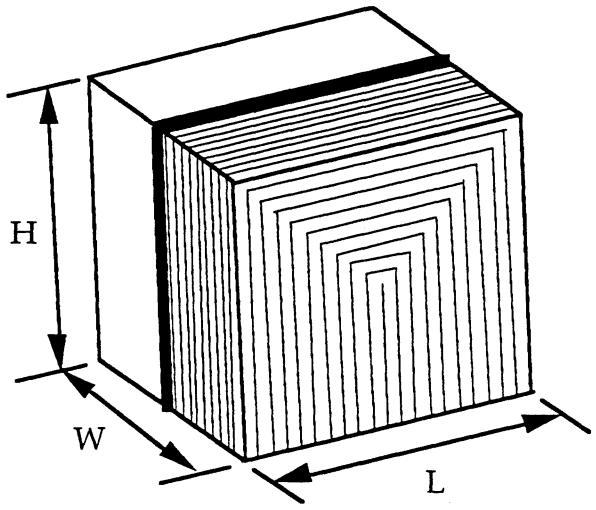

Figure C-8. Box with the fiber mapping used in calculation.

C.3.3 Hemisphere

For the hemisphere shown in Figure C-9, Section C.2.1 Equation C.8 gives the enclosed angle as

$$\theta_g = \pi \sin\phi. \tag{C.24}$$

Knowing the area as

$$A = 2\pi R^2 \ , \tag{C.25}$$

and considering only one half of the hemisphere due to symmetry, integrating Equation C.13 yields

$$\boxed{\bar{\theta}_g = \frac{\pi}{2}} \ . \tag{C.26}$$

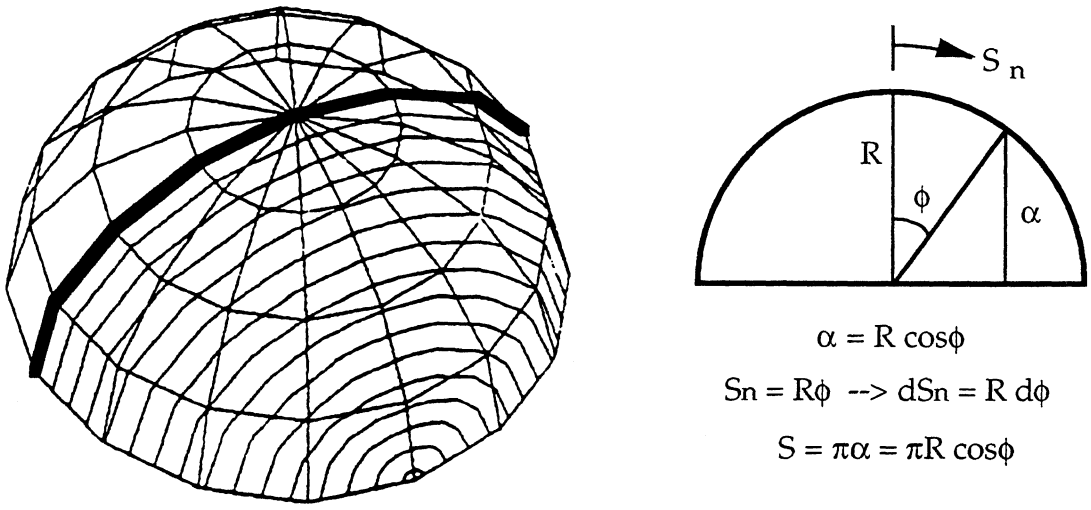

Figure C-9. Hemisphere with the fiber mapping used in calculation.

C.4 Sample Calculations of the Relative Complexity

This section illustrates how to calculate the relative complexity of a given part. For example, consider a part shown in Figure C-10 which has straight bends (simple and complex), a curved bend (stretch flange), and a bead feature on the top surface.

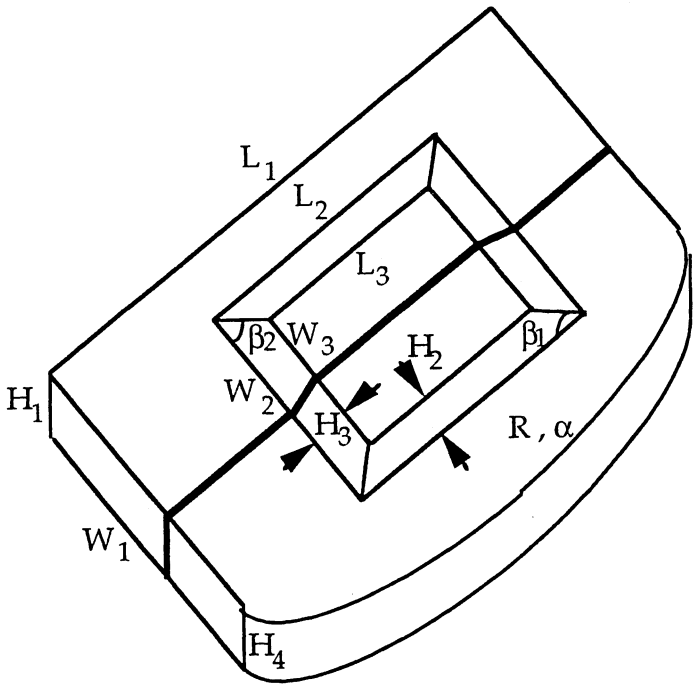

Figure C-10. Example complex part with different types of bends (in-plane and out-of-plane) and features. Note that the bottom surface is open.

Since the bottom surface is open, the total area, A_{total}, for the part shown in Figure C-10 is

$$A_{total} = L_1 H_1 + (L_1 W_1 - L_2 W_2) + L_3 W_3 + H_2\left(\frac{L_2 + L_3}{2}\right) + H_3\left(\frac{W_2 + W_3}{2}\right) + 2 W_1 H_1 + \frac{\alpha R^2}{2} + \alpha R H_4 \quad \text{(C.27)}$$

and the perimeter of the part is

$$P = L_1 + 2 W_1 + R\alpha. \quad \text{(C.28)}$$

If we define the complexity of a feature, relative to a flat laminate, as the enclosed angle of the fibers (in-plane or out-of-plane) weighted by the area (or length) ratio of the effected area (or length) to that of the total area (or perimeter), the complexities due to the features depicted can be summarized as:

Out of plane bends:

$$\bar{\theta}_n = \frac{\pi}{2} \frac{(L_1 + 2W_1 + R\alpha)}{P} \quad \text{(C.29)}$$

Average in-plane bends:

Bead:
$$\bar{\theta}_{g,bead} = \frac{\left[(4\beta_1 - \pi)(L_2 + L_3) H_2 + (4\beta_2 - \pi)(W_2 + W_3) H_3\right]}{2 A_{total}} \quad (C.30)$$

Stretch flange:
$$\bar{\theta}_{g,flange} = \frac{\alpha^2 R H_4}{2 A_{total}} \quad (C.31)$$

$^3/_4$ Box:
$$\bar{\theta}_{g,box} = \frac{\pi (L_1 H_1 + 2W_1 H_1)}{3 A_{total}}. \quad (C.32)$$

Therefore, the time constant for the manufacturing process including the effects due to the various features (enclosed angles) is expressed as

$$\tau = \tau_o + \sum_{j=1}^{N_e} b_j \bar{\theta}_j, \quad (C.33)$$

where θ_j corresponds to Equations C.29 to C.32. The coefficient b_j specifies the time per radian for the appropriate enclosed angle and N_e corresponds to the number of types of enclosed angles which need to be summed (in this case $N_e = 4$).

Note that the major assumption in the above calculation is that the effects of interaction between features is ignored. In addition, the bead's contribution to the out-of-plane bending from Equation C.29 is assumed to be negligible.

APPENDIX D

DESIGN FAMILIES USED FOR ATCAS

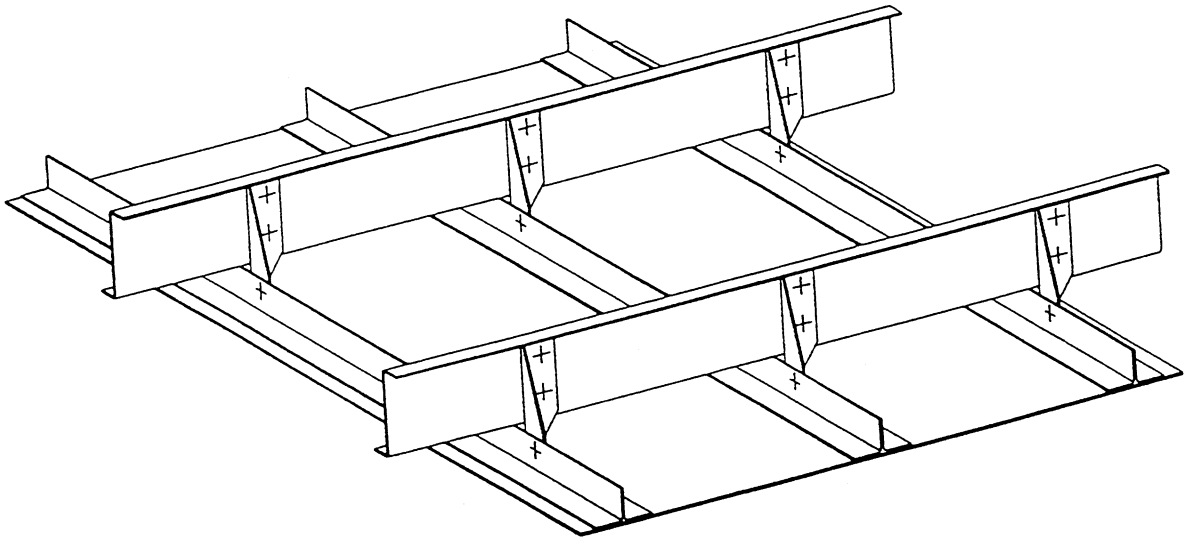

Family A: Skin-Stringer-Frame (Mechanically Fastened Stringers and Frames)

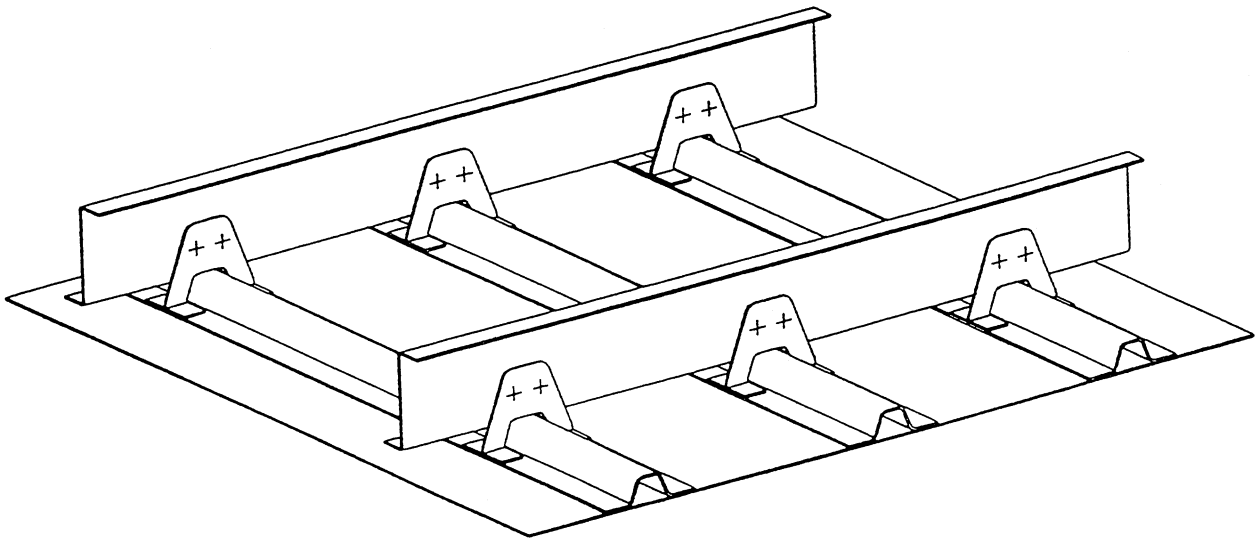

Family B: Skin-Stringer-Frame (Bonded Stringers)

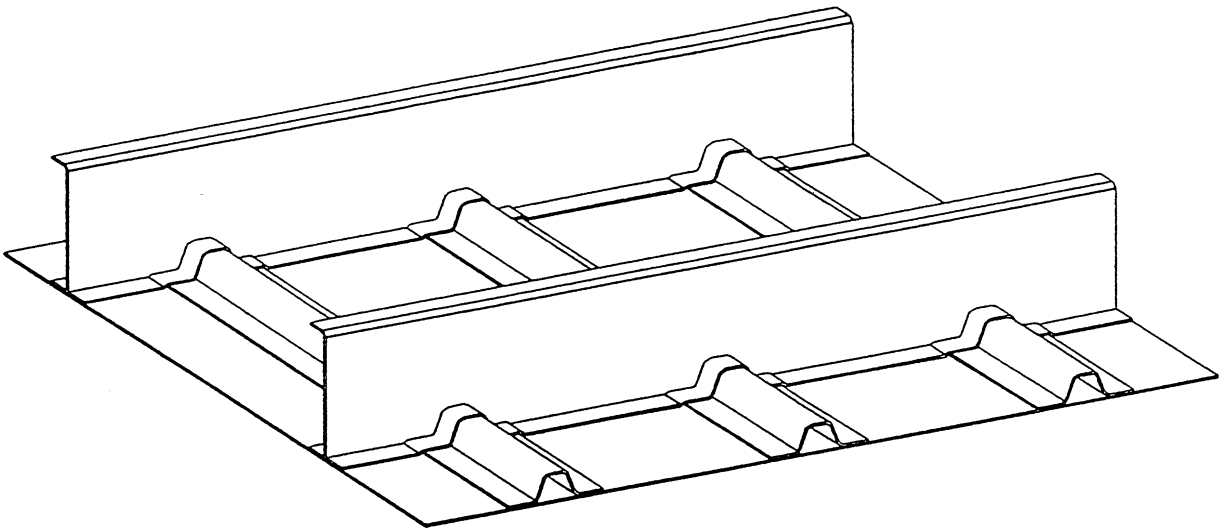

Family C: Skin-Stringer-Frame (Bonded Stringers and Frames)

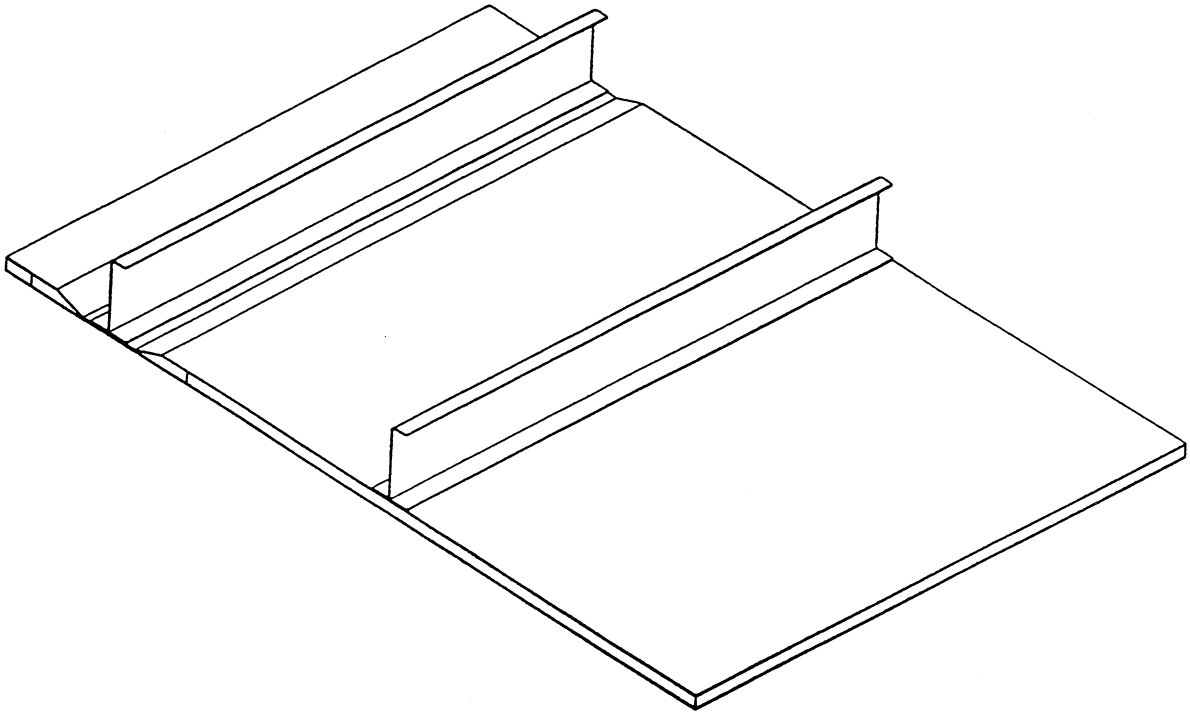

Family D: Sandwich

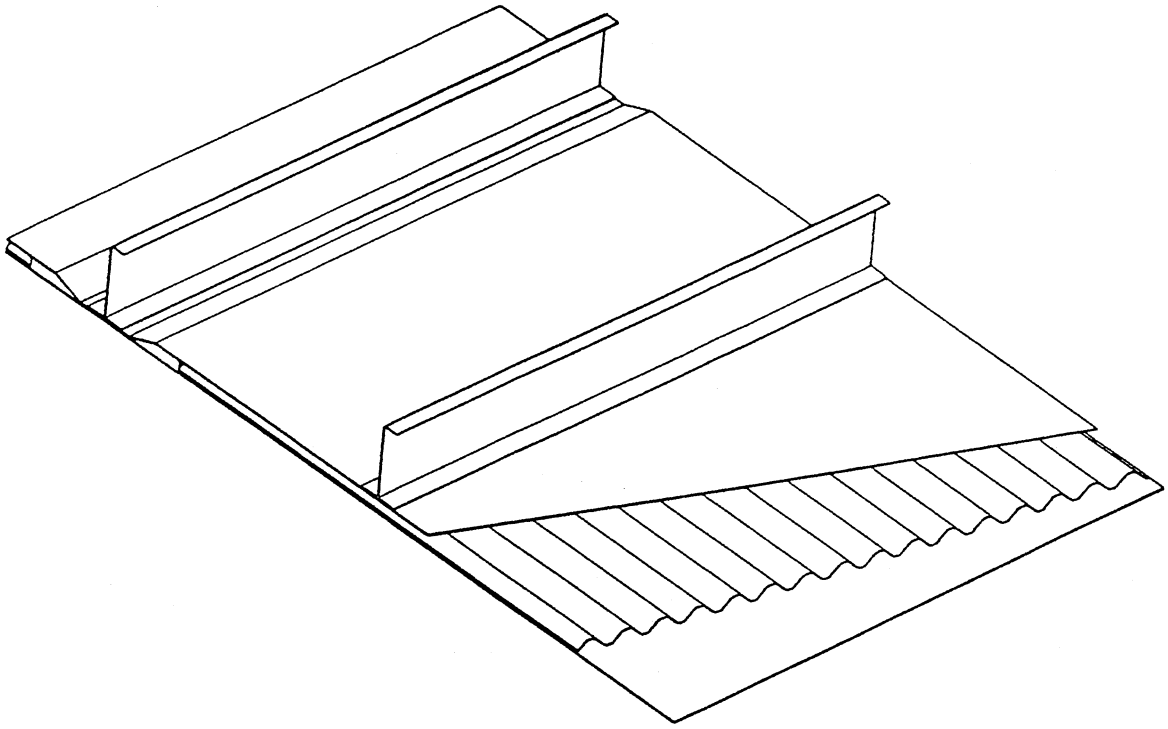

Family E: Corrugated

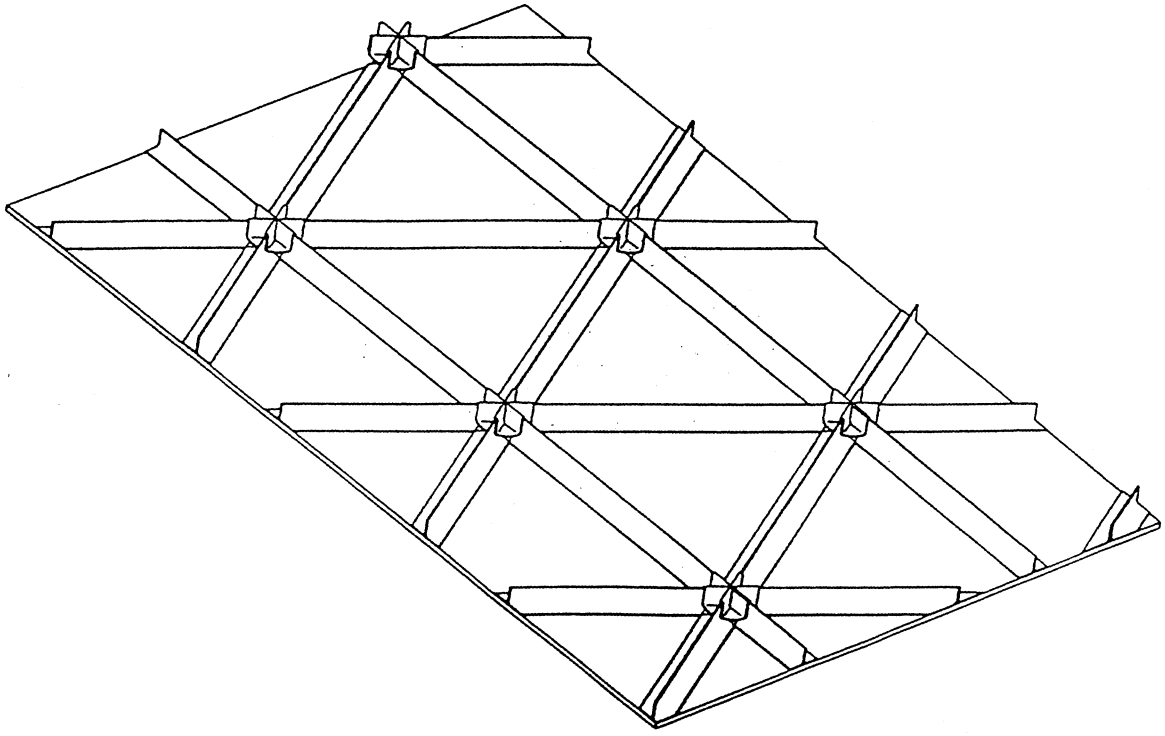

Family F: Geodesic

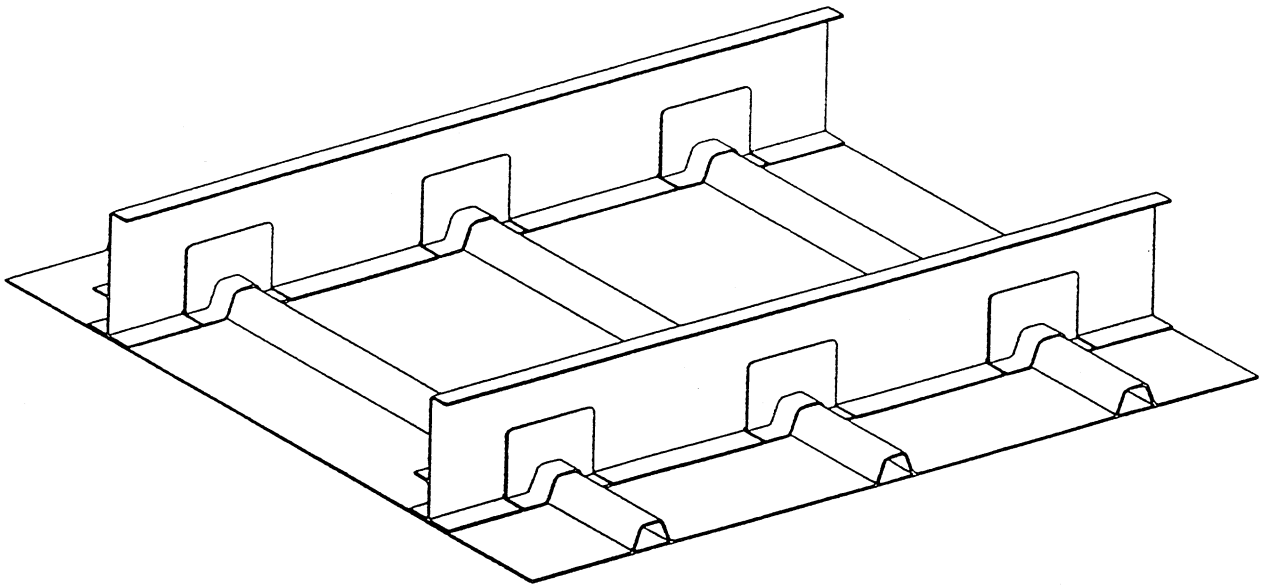

Family G: Integrally Stiffened Skins

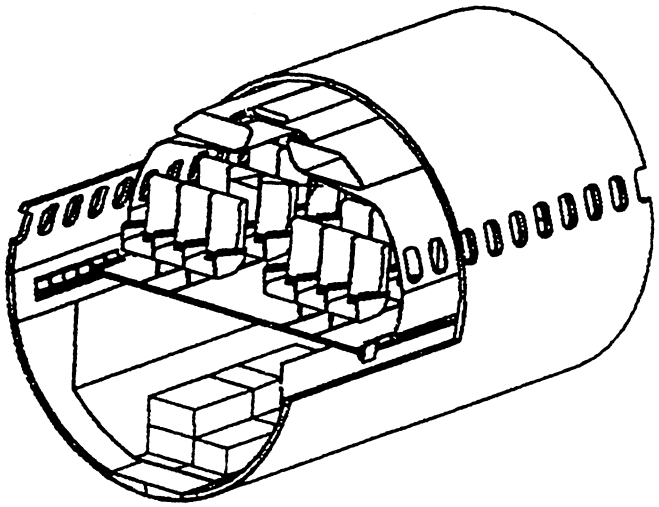

Family H: Continuous 360°

APPENDIX E

ATCAS DESIGN AND PROCESS CONSIDERATIONS FOR BRAIDED/RTM TRANSPORT FUSELAGE FRAMES

E.1 Fuselage Frame Design Considerations

A good physical understanding of the overall design configuration is fundamental to establishing reliable cost relationships between various process and structural details. The first step is to quantify the viable range in key design features for a given product. Shown in Figure E-1, is a typical widebody subsonic transport. Figure E-2 represents a skin/stringer/frame layout of a typical widebody commercial transport aircraft. This diagram is produced by essentially splitting the fuselage tube at the lower centerline and unrolling it into a flat pattern. Note that there is not necessarily a splice at the lower centerline.

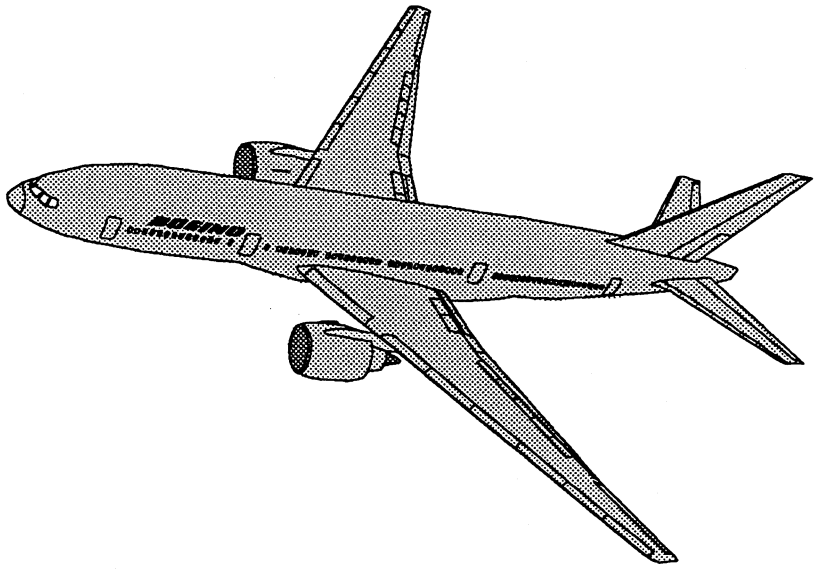

Figure E-1. Typical widebody commercial transport.

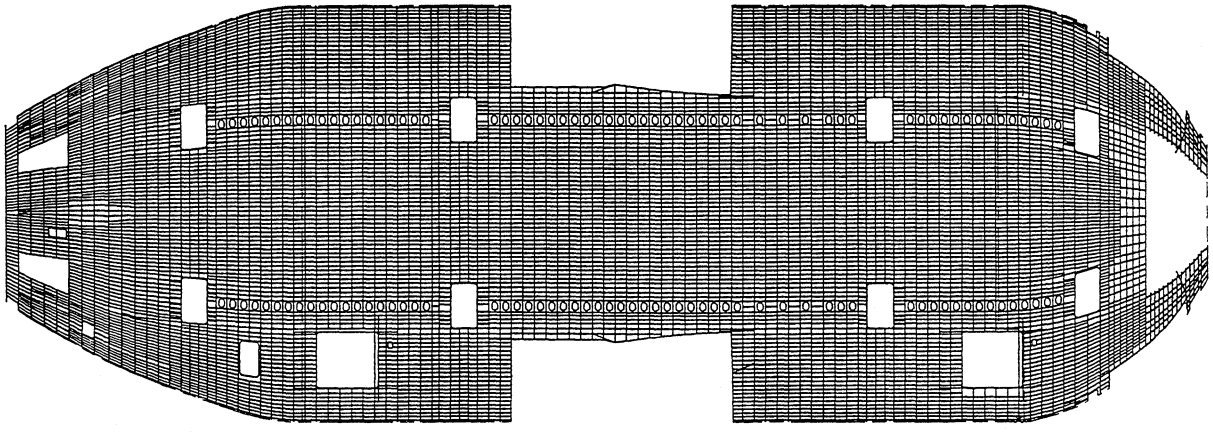

Figure E-2. Skin/stringer/frame layout.

At the start of ATCAS, numerous DBT meetings were held to determine the processes best suited for different fuselage elements. Potential cost savings were seen in using a particular braided/RTM process for some of the circumferential frames. Figure E-3 shows the frames which were candidates for this process. As seen by comparing this figure with Figure E-2, all the fuselage frames aft of the rear pressure bulkhead and in the cockpit area were removed from consideration. The frames aft of the rear pressure bulkhead are in a non-pressurized area of the airplane and have fundamentally different design drivers. The ATCAS DBT also felt that frames in the cockpit area should be fabricated using a different method due to very complex shape interactions between skin, stringer, and frame.

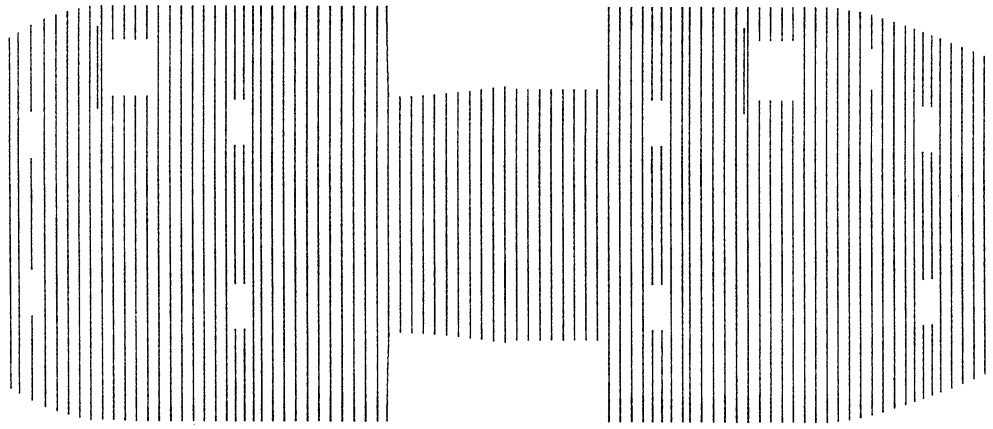

Figure E-3. Fuselage frame members.

Figure E-4 shows the fuselage frames considered in early ATCAS cost model development with a particular braided/RTM process (ref. 54). In comparison to Figure E-3, additional frames at bulkheads and near door cutouts were removed. Design of the main and auxiliary frames that surround door cutouts is strongly influenced by unique structural details and fundamentally different load patterns and damage criteria. Although braided/RTM processes are still candidates for these frames, it is reasonable to assume that different optimal design and process steps will result (note that an ATCAS subcontract with the Northrop Corporation was established to develop the processes for door frames, see ref. 52). All major fuselage frame bulkheads, which again have fundamentally different requirements from most other frames, were also removed for purposes of the current discussions.

The fuselage frames in Figure E-4 were grouped by two key design features; curvature and length. The frame length was dictated by manufacturing breaks and cutout locations. Manufacturing breaks were assumed to be the same as the ATCAS quadrant approach shown in Figure E-5 (ref. 5).

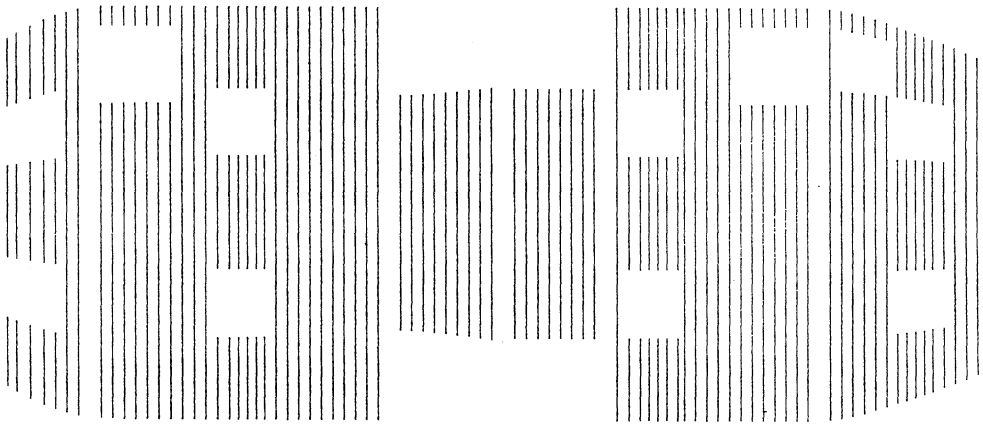

Figure E-4. Fuselage frames considered in ref. 54.

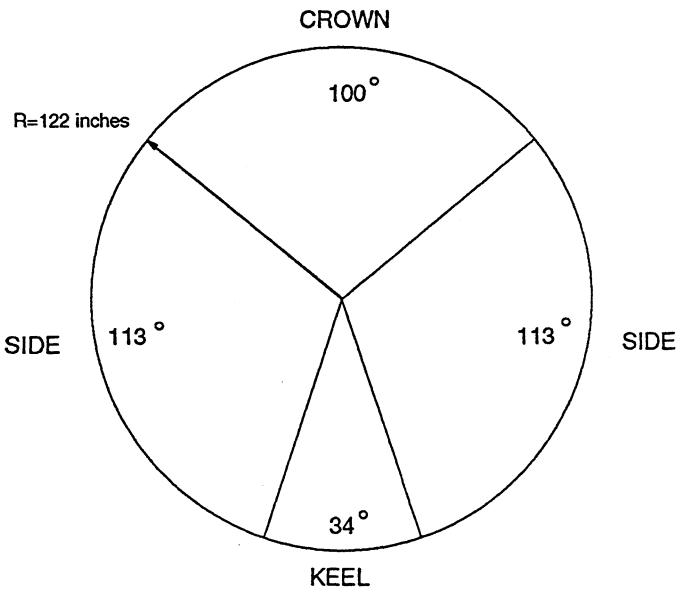

Figure E-5. ATCAS fuselage manufacturing breaks.

Frame curvature was defined to be either constant or non-constant. Figure E-6 shows eight different frame design groups that were distinguished by length and curvature. Some groups include frames with similar lengths and constant curvatures. Other design groups consist of frames with similar lengths and non-constant curvatures.

Fuselage frame groups were further sub-divided by another key design feature, gage. Depending on the application, composites have traditionally saved 10 to 40% weight over metal. The ability to tailor frame gage for varying loads will be important in maintaining this margin. Unfortunately, this introduces additional variation in the frame design.

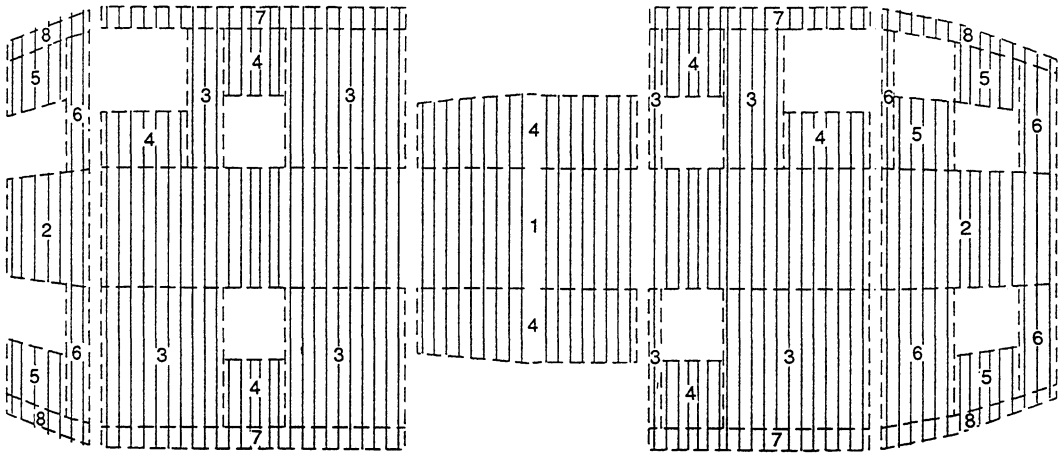

Figure E-6. Frame design groups with similar length & curvature.

Loads and moments were analyzed to approximate gage variations within frame groups, yielding sub-groups categorized by curvature, length, and gage. Variations around the fuselage circumference and along its length were considered. Figure E-7 shows load and moment variations around the fuselage circumference at a typical frame station. Figure E-8 plots frame loads along the length of the fuselage for the same circumferential point in the crown. This plot shows little change in these loads after station 1580.

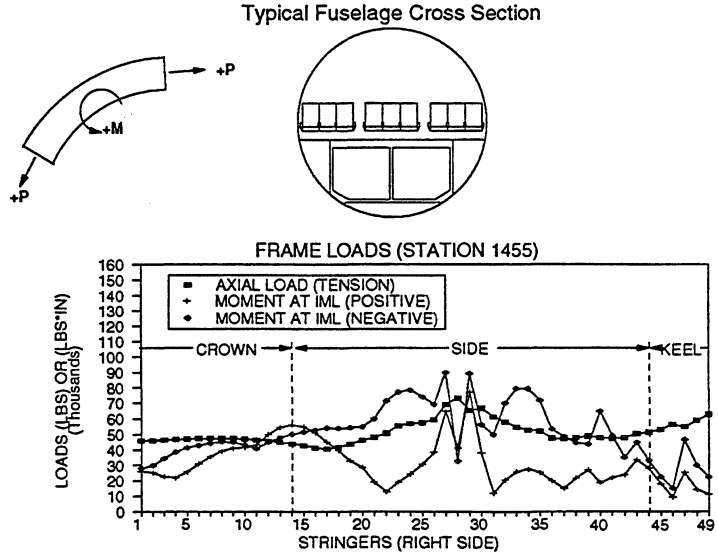

Figure E-7. Frame fuselage loads at Station 1455.

A total of nineteen design groups were categorized by curvature, length, and gage. The locations of these design groups are shown in Figures E-9. The resulting 319 frames per airplane have an average length and area of 155 inches and 1.0 in^2, respectively. Using the

ACT cost estimating ground rules of 5 airplane/month over 5 years this results in 3350 lbs of graphite/epoxy per airplane or 210,000 lbs/year.

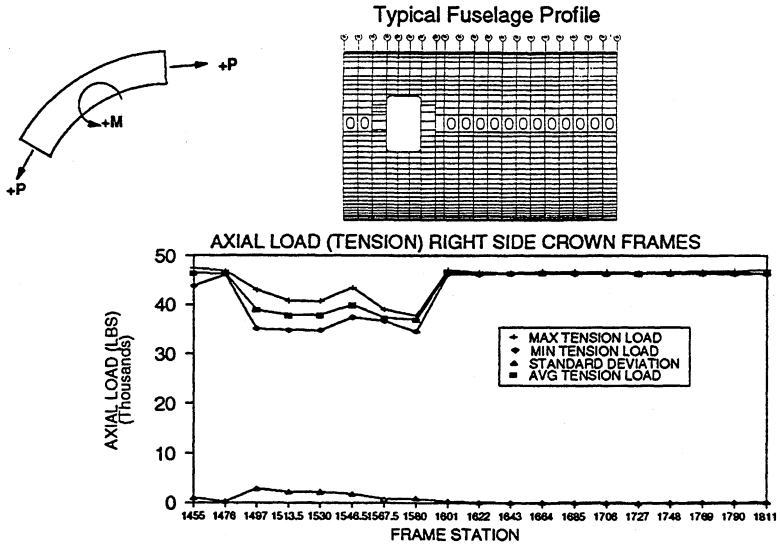

Figure E-8. Fuselage frame load variations by station.

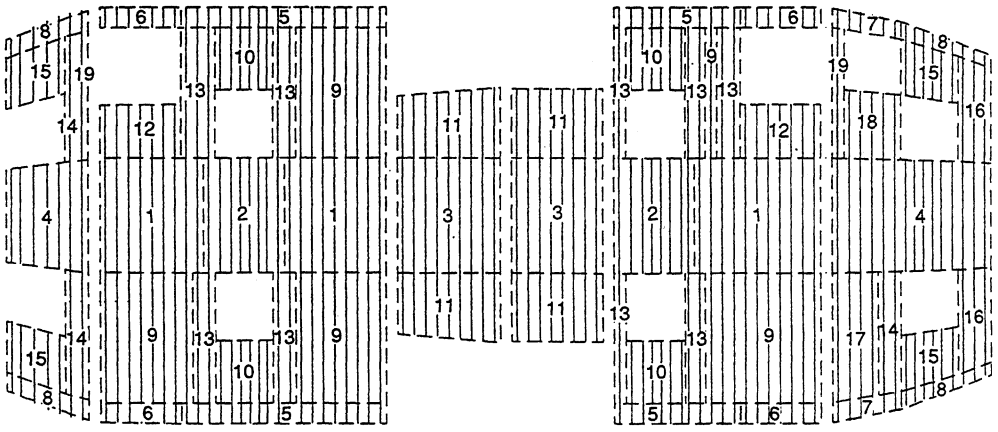

Figure E-9. Frame design groups by length, curvature, and gage

Other key design features are the material form and constituents. For purposes of this discussion, the triaxial, 2D-braided, AS4[1]/1895[2] material was assumed the baseline

---

1 AS4 is a graphite fiber system produced by Hercules, Inc.

2 1895 is an epoxy resin system that was produced by Shell

material. Other materials and preforming techniques could be evaluated but such analysis would require material cost, process definition, and producibility data.

E.2 Fuselage Frame Process Considerations

An understanding of process capabilities and sensitivities is essential to evaluating the effect of design features on cost. The 2D-braided/RTM process cell which was originally modeled for ATCAS is shown in Figure E-10 (refs. 52 and 54). Each process step shown in the figure was modeled with an equation which described cost as a function of the key design features and processing parameters.

The braided/RTM process cell layout shown in Figure E-10 was designed to efficiently produce frame groups having common structural features. For example, smaller frames are cut from longer segments (i.e., batched) to help equalize handling requirements. This allows the material handling system to be designed to handle similar size frame blanks.

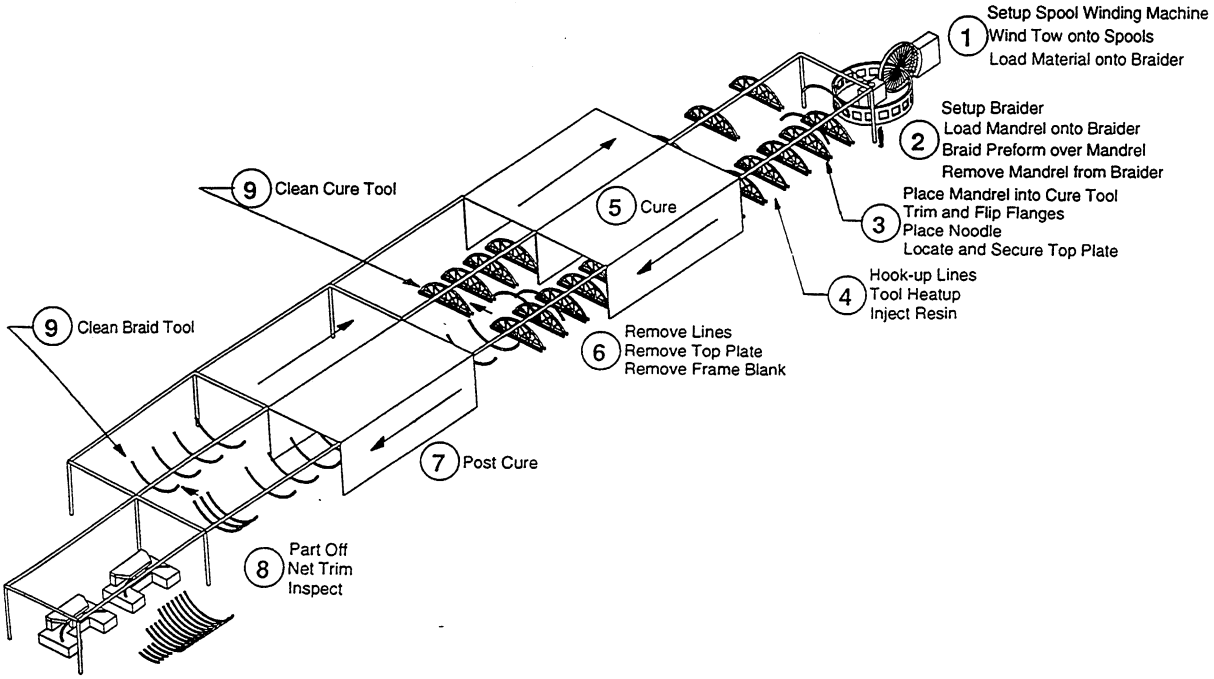

Figure E-10. Braid/RTM fuselage frame process cell used by ATCAS.

An "assembly-line" process sequence, similar to that found in the automotive industry, also helps to reduce cost. Low commercial aircraft production rates and less part commonality have not encouraged such production schemes in past applications. Current aircraft production is striving for manufacturing flexibility, part commonality, and grouping of similar process steps to significantly improve costs. In the process cell shown in Figure E-10, the part type specific portion of the process comes in braiding the correct preform

to matched braiding and cure tools. After these steps are accomplished the differences between one frame and the next becomes transparent to the process.

Another area of importance to the cost of braid/RTM processes are the interactions between tooling approaches and the design. For example, state-of-the-art metal frames have structural detail variations that increase the number of design groups shown in Figure E-9. Minor design differences that lead to unique RTM tools for each frame could yield high non-recurring tooling costs and eliminate the braided/RTM process as a candidate for commercial transport applications. A cost effective solution is dependent on integration of the tool and frame designs to achieve efficient process flow.

The braiding mandrel follows the part through most of the process cycle shown in Figure E-10. The cure tool on the other hand, bypasses the post cure cycle and would have an inherently higher utilization rate. It would follow that more braiding mandrels would be required to support the production rate. Therefore, gage variations for different frames could be tailored into the braiding mandrel shown in Figure E-11. This would allow datum cure tools to be baselined and fabricated early in a production program. The braiding mandrel could then be fabricated once the frame design was finalized. Additionally, tool design should incorporate shim areas such that slight variations between frame details can be incorporated, allowing higher utilization rates and reduced tooling costs for a greater number of parts.

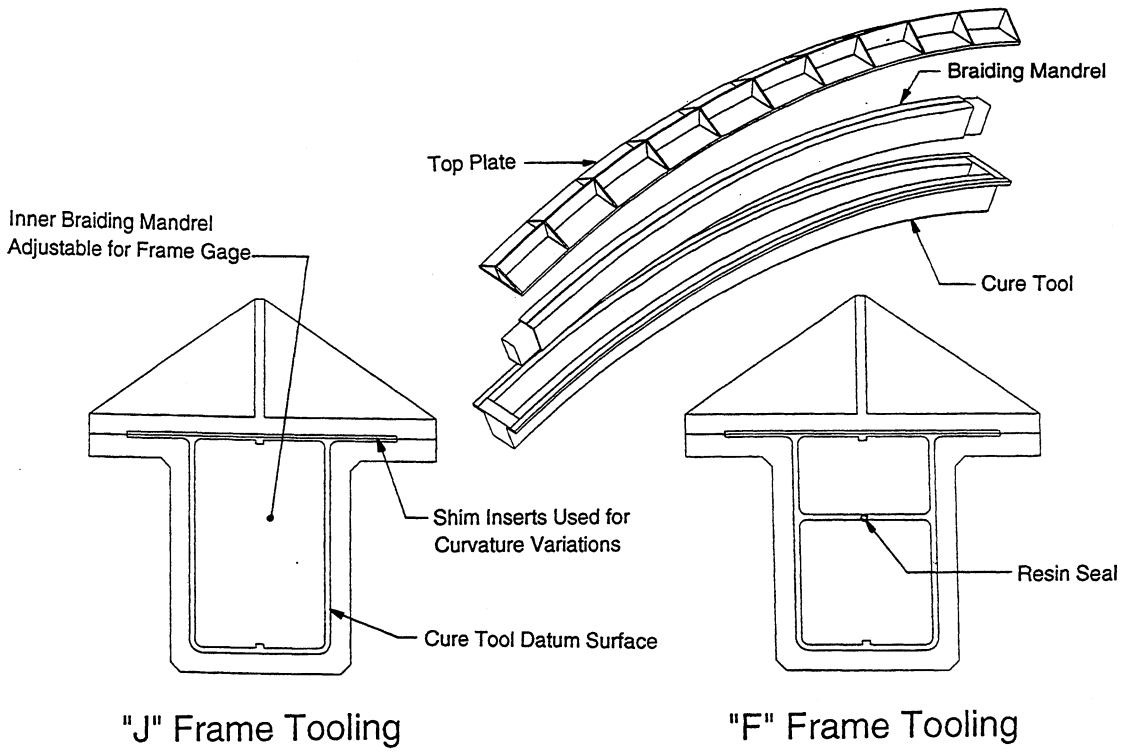

Figure E-11. Braided/RTM tooling approach for fuselage frames.

APPENDIX F

EXAMPLES OF PHYSICAL LIMITS TO PROCESS PARAMETERS FOR DESIGN COST MODELS

F.1 Example of the Physical Limits for Machining

The two principle rate limiting phenomena in rough machining are power availability and tool life; assuming that tool and workpiece deflection, and vibration are not the central issues. As discussed in refs. 56-58, the available power in a metal cutting machine can set a limit on the material removal rate (MRR) in rough machining; primarily in terms of the depth of cut. Specifically, the material removal rate under power limiting condition is

$$MRR = \frac{\eta \, Power}{E} \tag{F.1}$$

where η is efficiency of the machine tool (usually $0.7 \leq \eta \leq 0.8$) and E is specific cutting energy of the workpiece (defined as the energy consumed in removing a unit volume of material). Tables of specific energies for different materials are available in refs 56-58.

Assuming that the machine has sufficient cutting power, the material removal rate is then often chosen based on economic considerations. Since tool replacement or rework not only costs money but also leads to machine down time, the specific issue is tool life. Tool life considerations usually limit material removal rate in terms of the cutting speed, as long as the cutting forces are not so high as to cause catastrophic failure of the tool or workpiece. Taylor's tool wear equation for flank wear is

$$v_{cut} = \frac{C}{T^n} \tag{F.2}$$

where v_{cut} = cutting speed [ft/min]
T = tool life [min]
C = constant representing cutting speed for tool life of 1 minute
n = exponent which depends mostly on tool material.
(e.g., 0.08-0.2 for HSS, 0.2-0.5 for carbides, and 0.5-0.7 for ceramics).

Therefore, one has to trade machining time, in terms of v_{cut}, with the cost of tool changes when choosing the optimum cutting speed; as elaborated in more detail in refs. 56-58.

F.2 Example of the Physical Limits for Welding

From Eagar's manuscript (ref. 59), the two rate limiting mechanisms in fusion welding can be summarized as i) heat input, for low power density welding processes, and ii) control of heat location, for very high power density welding processes. As shown in Figure F-1, the power density for all welding processes lie between about 10^3 to 10^6 watts/cm^2. Specifically, below 400 watts/cm^2, heat is conducted away as fast as it is introduced; and thus no melting and fusion welding occurs. On the other end of the spectrum, very high power density in excess of 10^6 watts/cm^2, such as from lasers or electron beams, causes vaporization of most metals within a few micro-seconds; resulting in cuts instead of welds.

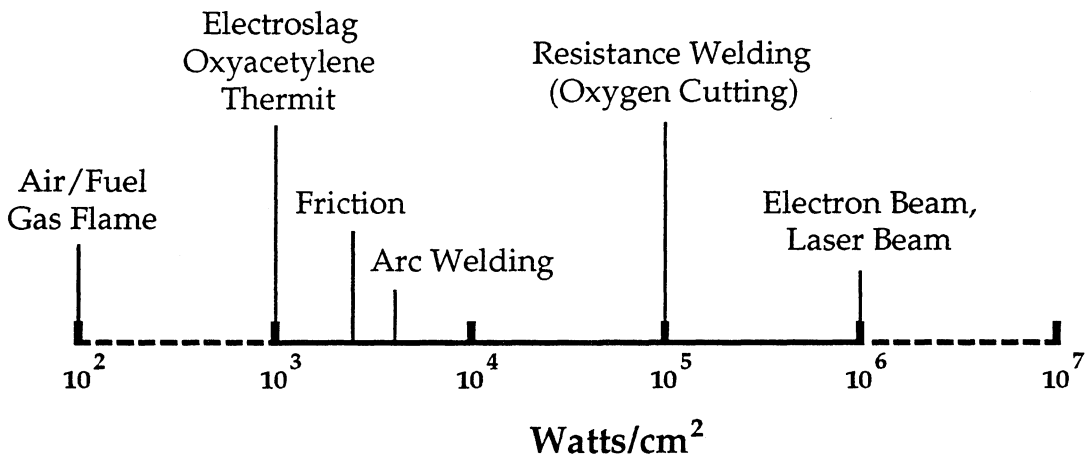

Figure F-1. Spectrum of practical heat intensities used in fusion welding (ref. 59).

Welding heat source interaction times from ref. 59 are shown in Figure F-2. Materials with a high thermal diffusivity, such as copper and aluminum, would lie near the top of the band shown in the figure. Steels, nickel alloys or titanium would lie in the middle of the band. Uranium and ceramics, with very low thermal diffusivities, would lie near the bottom of the band.

The maximum weld travel velocity, v_{max}, is defined as

$$v_{max} = \frac{\text{Heat Source Diameter}}{\text{Interaction Time}}. \qquad \text{(F.3)}$$

Figures F-1, F-2, and F-3 provide the necessary heat intensity and relationships for determining the interaction time and heat source diameter. These are needed to calculate v_{max} (plotted as the bottom band of Figure F-3). For example, oxyacetylene welding with heat intensity in the order of 10^3 W/cm^3 has an interaction time of about 25 seconds and v_{max} of about 0.1 cm/sec. The slow rate for processes with such a low heat source intensity is controlled by heat flow. This slow rate makes such processes suitable for beginners.

On the other hand, faster response time and greater skills are required to control the more rapid processes with high heat source intensity. For example, laser and electron beam welding with heat intensity in the order of 10^6 W/cm^3 has an interaction time of about 25 micro-seconds and v_{max} in the order of 10^3 cm/sec. This clearly makes controlling the pool of a high heat intensity laser and electron beam welding beyond the capability of humans. Thus, these processes must be automated in order to be controlled. Given that the positioning accuracy must be in the order of the heat source diameter, and the control frequency must be higher than the ratio of travel velocity/heat source diameter; the high travel speed and narrow weld zone make seam tracking of such processes difficult. In fact

for the laser and electron beam welding example, the controller and hardware need to have positioning accuracy better than 0.4 cm at a frequency higher than 25 KHz.

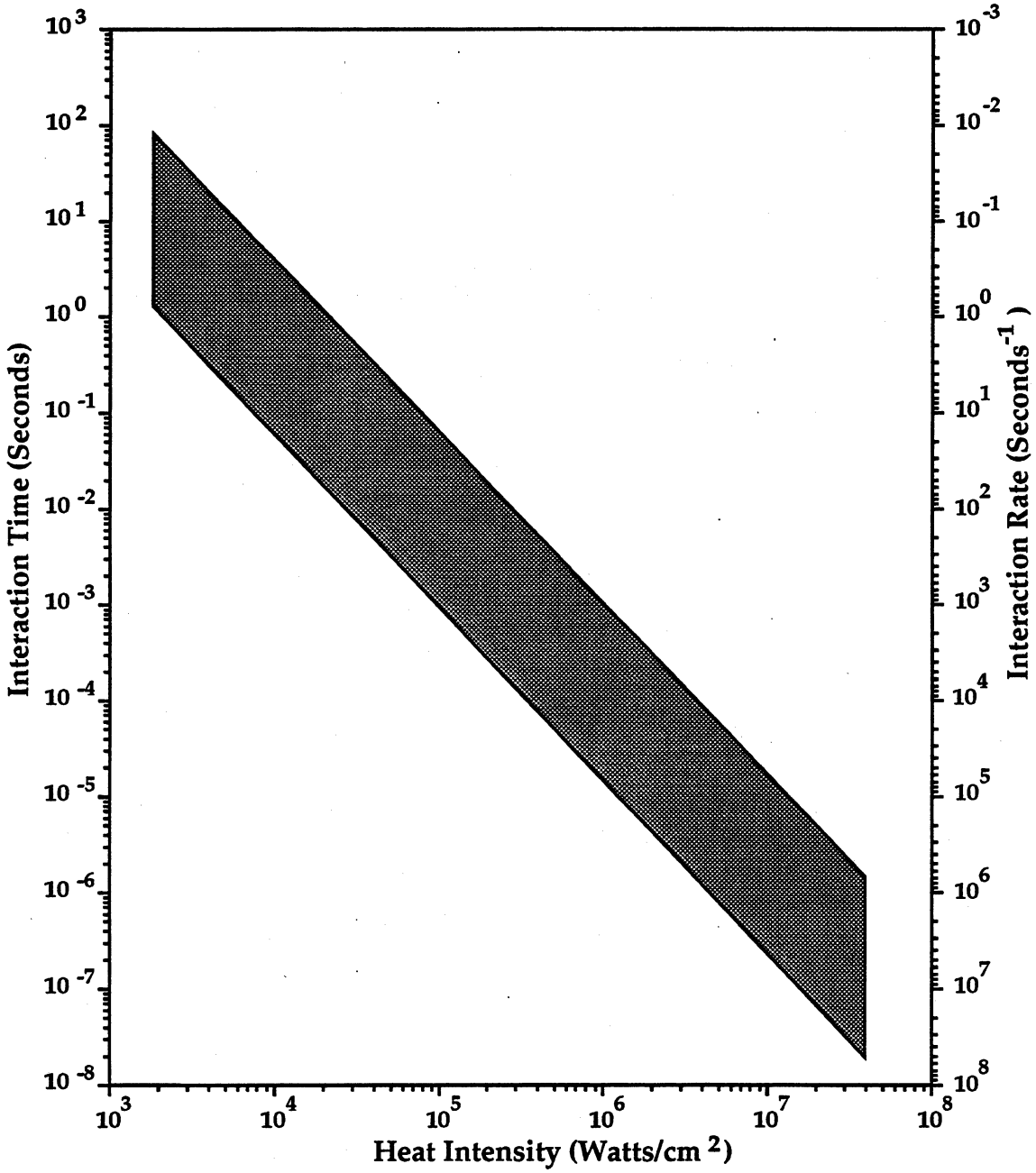

Figure F-2. Typical weld pool heat source interaction times as a function of source heat intensity (from ref. 59).

Therefore, depending on the intensity of the heat source used, the rate for welding processes can be determined by heat transfer (for low heat intensities) or the dynamics of the controller and hardware (for high heat intensities). In the latter case, one can resort to dynamic models as described in Section 2.2 to model the process.

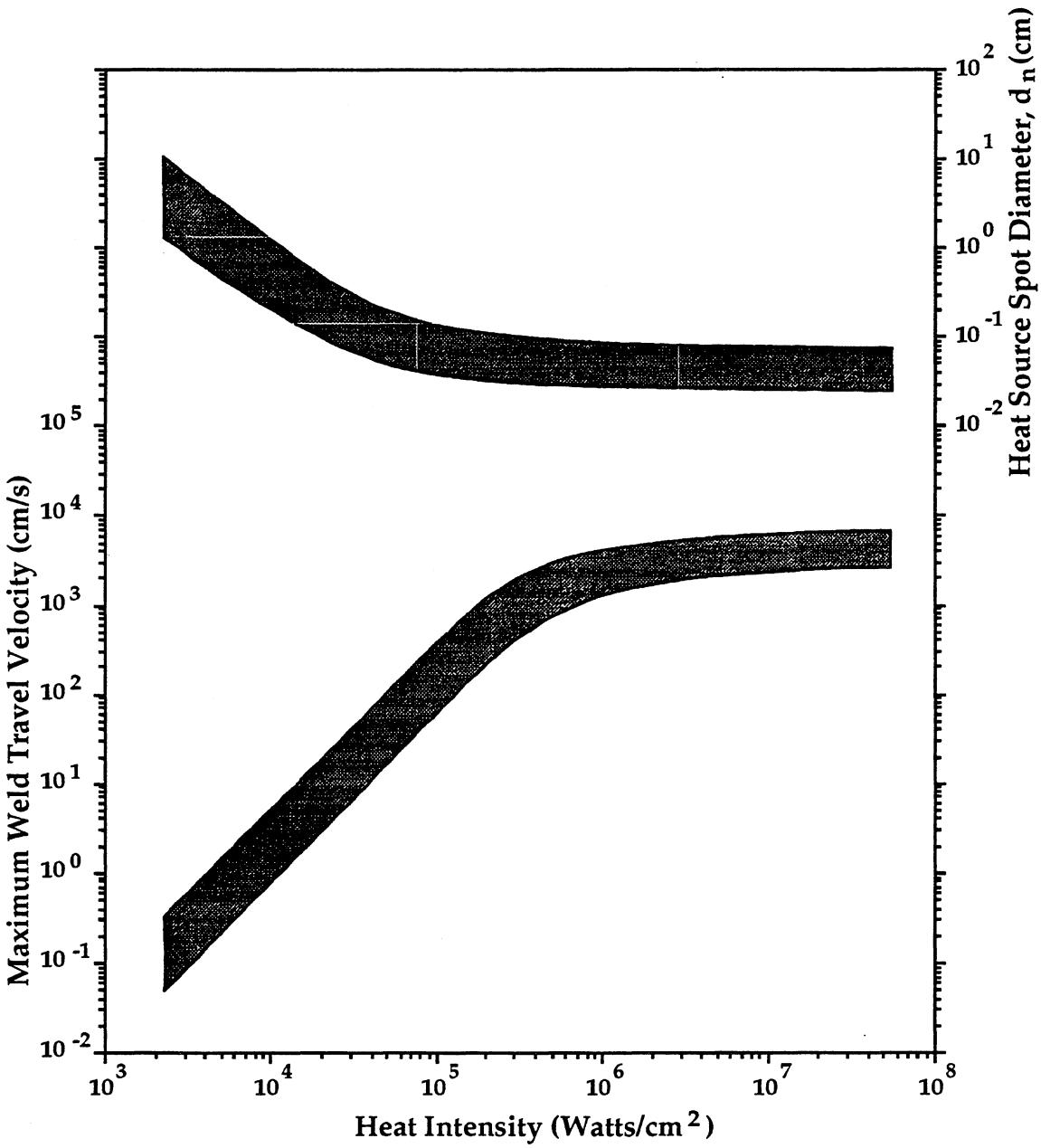

Figure F-3. ***Maximum weld travel velocity as a function of source heat intensity based upon typical heat source spot diameters (from ref. 59).***

APPENDIX G

MASTER CHARTS FOR PROCESS PARAMETERS: LINEAL AND AREAL VELOCITIES AND VOLUMETRIC RATES

Figures G-1, G-2, and G-3 show the medians and the ranges of processing rates for given classes of processes. Variation in processing methods used within a given category yield some wide ranges. This can be attributed to factors such as level of automation and design/process complexity. Note that some categories in Figures G-1, G-2, and G-3 are derived from the ATCAS process-step equations of Appendix H; many of which represent new and evolving composite processes. In addition, some categories with very small or no ranges have not been studied to the same level of detail as those plotted with relatively large ranges.

The information compiled in Figures G-1, G-2, and G-3 is based on data collected to date. As shown in moving from left to right along the horizontal axes in each figure, the rates (median) decrease as the processes get harder. This is consistent with general observation. For example, Figure G-2 shows that spreading humus peat is faster than painting, which in turn is faster than abrading surfaces. Another example from Figure G-2 shows that the construction time standards published in ref. 60 for laying down carpet and putting up wallpaper correspond to the analogous composite processes for laying up prepreg. Similarly, tool cleaning can be compared to cleaning walls; and applying adhesive is similar to painting walls.

While the general trends of velocities in Master Charts make physical sense, other process parameters are currently more difficult to initially quantify through comparisons with similar processes. For example, another process parameter, the dynamic time constant (τ), for the fundamental extensive equation form (see Section 2.2.2) is not as easily derived from published data. This is because available references often quote the time required for a certain task as a function of setup time and the process rate (refs. 14 and 60). Values for τ have not been tabulated, and are probably absorbed into either setup time or the process rate listed in the published tables. If the proposed theoretical framework for design cost modeling is adopted, one should be able to organize values for τ into similar Master Charts as the ones for steady state velocities and volumetric rates shown in Figures G-1, G-2, and G-3. Variations associated with part complexity and process automation should also become more evident as a theoretical framework is applied over time.

Figure G-1: Master chart for lineal velocities, V_O, of different processes from various fields of manufacturing.

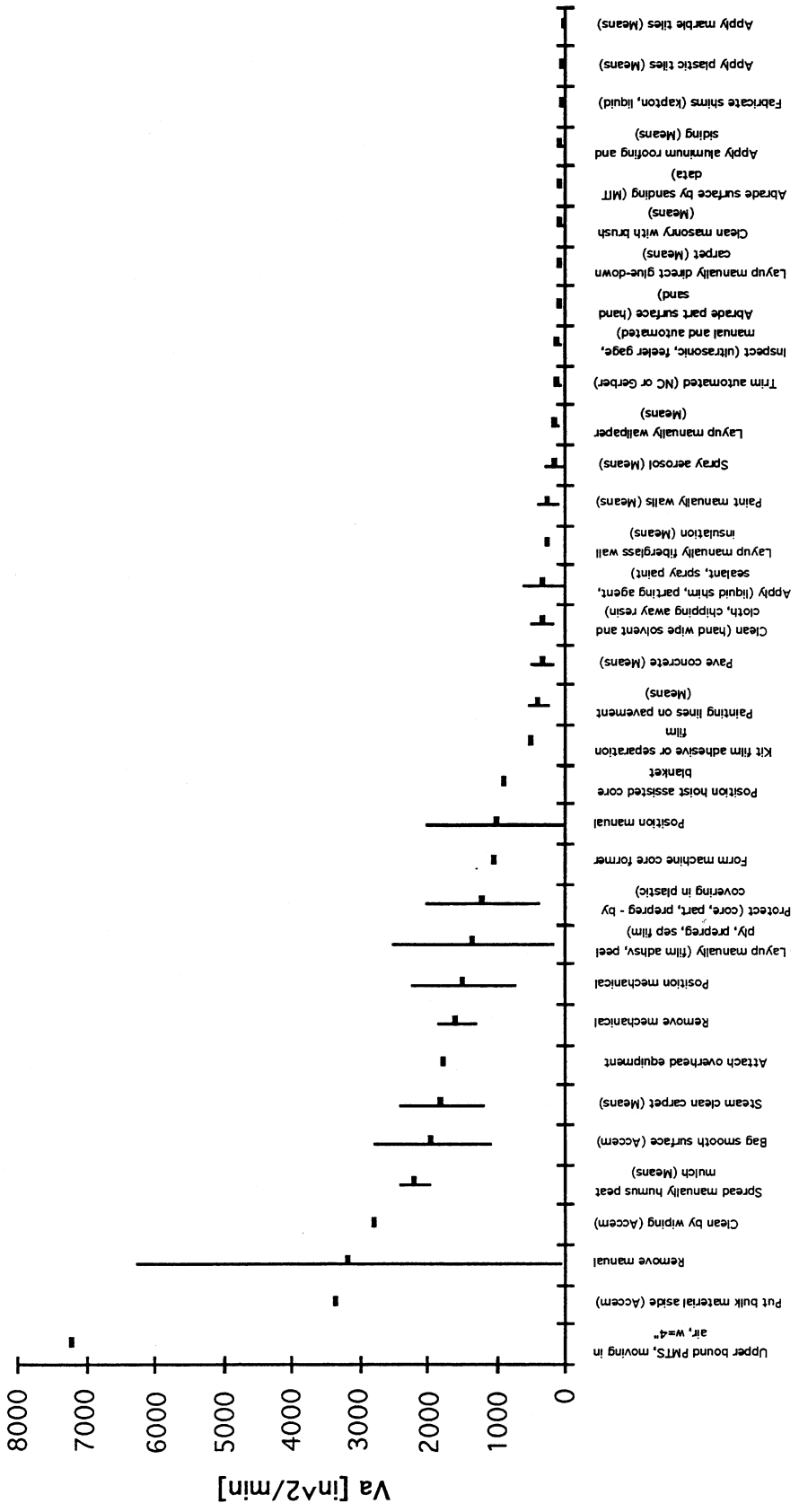

Figure G-2. Master Chart for areal velocities, V_a, of different processes from various fields of manufacturing.

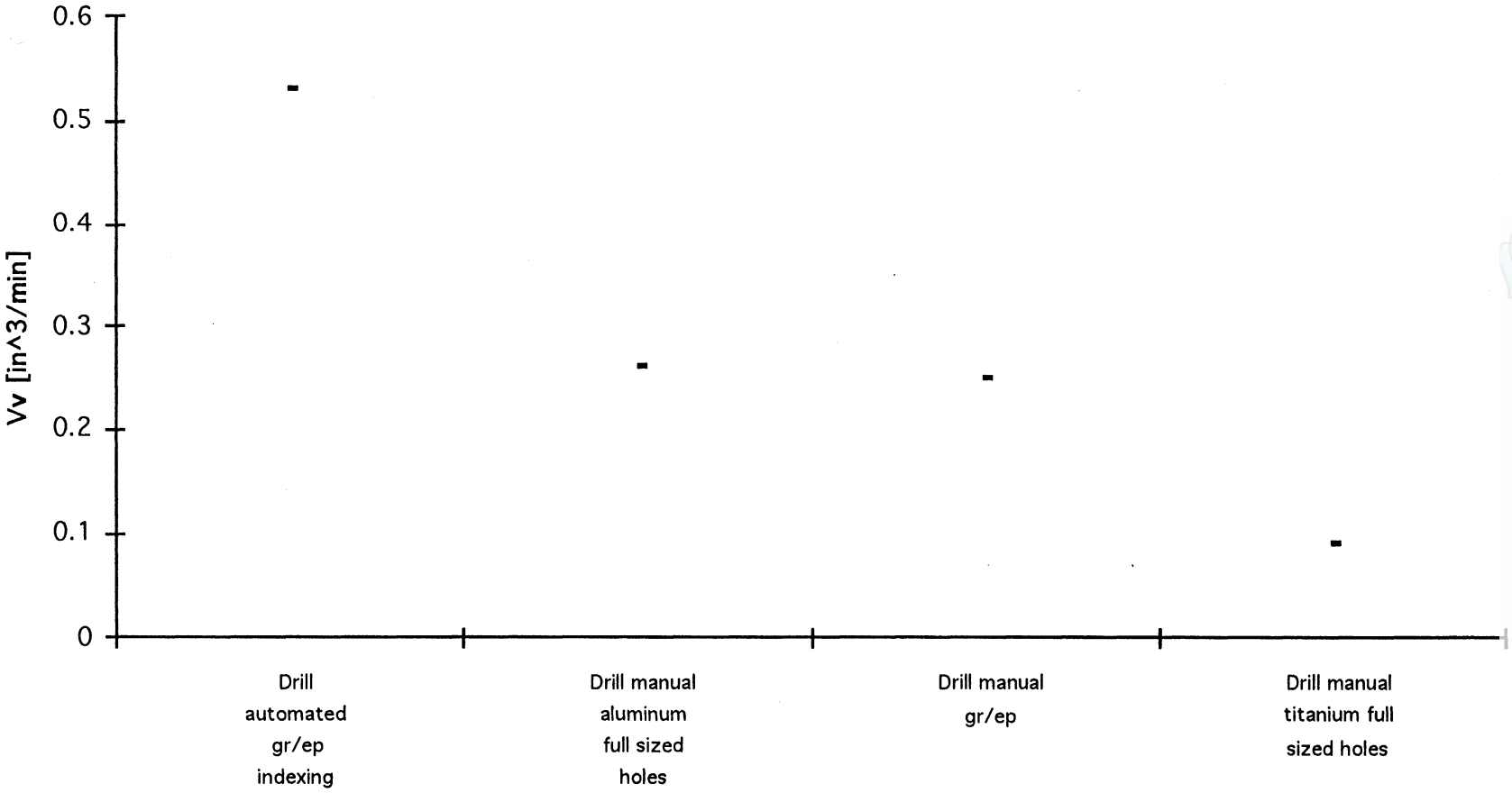

Figure G-3. Master chart for volumetric rates, V_v, of different processes from various fields of manufacturing.

APPENDIX H

ATCAS PROCESS-STEP COST TABLES

The following tables group the process steps in two ways. Table H-1 lists the methods by the type of scaling: linear, areal, volume, weight, and constant times. Table H-2 simply lists all the processes alphabetically. In both tables, the extensive variable is identified.

ID #	Cost Method Description	Variable Desc.	Units
20	Apply clamping force clamps	interface length	in/min
30	Apply clamping force straps	interface length	in/min
90	Attach lines resin injection RTM mold	injection mold length	in/min
130	Attach lines thermocouple cure	part perimeter	in/min
110	Attach lines thermocouple RTM mold	injection mold length	in/min
150	Attach lines vacuum cure	part perimeter	in/min
140	Attach lines vacuum RTM mold	injection mold length	in/min
210	Clean tool form die pultrusion	section trace	in/min
320	Compact vacuum core	bag perimeter	in/min
330	Compact vacuum prepreg charge nylon	bag perimeter	in/min
500	Form machine prepreg charge roller form	charge length	in/min
520	Form manual dry preform	preform length	in/min
530	Identify interface area	interface perimeter	in/min
560	Inspect automated dimensionally	interface perimeter	in/min
571	Inspect automated ultrasonic frames	part length	in/min
570	Inspect automated ultrasonic inline	part length	in/min
590	Inspect manual feeler gage interface gaps	interface perimeter	in/min
680	Kit parts	part length	in/min
681	Kit parts frames	part length	in/min
960	Position hoist assisted mandrel braiding	tool length	in/min
1010	Position hoist assisted part into transport tool	part length	in/min
1000	Position hoist assisted part NC trim equip.	part length	in/min
1020	Position hoist assisted part onto ultrsonic equip.	part length	in/min
990	Position hoist assisted part with indexing holes	part length	in/min
1040	Position manual airweave	part perimeter	in/min
1130	Position manual foaming adhesive	part perimeter	in/min
1155	Position manual form die core	tool length	in/min
1161	Position manual form die female stringer	tool length	in/min
1150	Position manual form die skin	tool length	in/min
1160	Position manual form die stringer	tool length	in/min
1170	Position manual heat lamps	interface length	in/min
1210	Position manual part	part length	in/min
1200	Position manual part into assembly jig	part length	in/min
1230	Position manual prepreg charge roller transfer	charge length	in/min
1240	Position manual radius filler	filler length	in/min
1250	Position manual RTM mold lid	tool lid perimeter	in/min
1260	Position manual RTM mold seal	seal length	in/min
1270	Position manual thermocouples	part perimeter	in/min
1450	Pultrude resin shell 1895	pultrusion length	in/min
1460	Remove hoist assisted mandrel braiding	tool length	in/min
1470	Remove hoist assisted part from NC trim equip.	part length	in/min
1480	Remove hoist assisted part from ultrasonic equip.	part length	in/min
1500	Remove lines resin injection RTM mold	injection mold length	in/min
1540	Remove lines thermocouple cure	part perimeter	in/min
1520	Remove lines thermocouple RTM mold	injection mold length	in/min
1560	Remove lines vacuum cure	bag perimeter	in/min
1550	Remove lines vacuum RTM mold	injection mold length	in/min
1570	Remove manual airweave airweave	part perimeter	in/min

Table H-1. Cost methods grouped according to variable type

ID #	Cost Method Description	Variable Desc.	Units
1590	Remove manual clamp	interface length	in/min
1610	Remove manual compaction bag	bag perimeter	in/min
1675	Remove manual form die	tool length	in/min
1685	Remove manual form die female stringer	tool length	in/min
1670	Remove manual form die skin	tool length	in/min
1680	Remove manual form die stringer	tool length	in/min
1690	Remove manual heat lamps	interface length	in/min
1710	Remove manual liquid shim squeezeout	interface perimeter	in/min
1730	Remove manual part from assembly jig	part length	in/min
1770	Remove manual RTM mold lid	tool lid perimeter	in/min
1780	Remove manual RTM mold seal	seal length	in/min
1790	Remove manual sealant squeezeout	interface perimeter	in/min
1810	Remove manual strap	interface length	in/min
2210	Trim automated edge core slab	core length	in/min
2220	Trim automated edge gr/ep	trim length	in/min
2230	Trim automated edge laminate/charge	trim length	in/min
2240	Trim automated edge single ply	trim length	in/min
2300	Trim manual edge adhesive strips	strip length	in/min
2270	Trim manual edge dry preform	trim length	in/min
2280	Trim manual edge gr/ep	trim length	in/min
2290	Trim manual edge prepreg charge	trim length	in/min
2330	Trim manual edge sacrificial shim strips	strip length	in/min
2310	Trim manual edge separation film sheets	separation film per.	in/min
2320	Trim manual edge separation film strips	strip length	in/min
2340	Trim manual gr/ep deburr	trim length	in/min
2350	Trim manual gr/ep deflash	trim length	in/min
10	Abrade part surface	interface area	in^2/min
15	Abrade part surface liquid shim	interface area	in^2/min
40	Apply liquid shim	interface area	in^2/min
50	Apply parting agent core bonding assembly jig	tool area	in^2/min
51	Apply parting agent form die	tool area	in^2/min
53	Apply parting agent mandrel braiding	tool area	in^2/min
52	Apply parting agent OML cure tool	tool area	in^2/min
54	Apply parting agent resin transfer mold	tool area	in^2/min
60	Apply sealant	interface area	in^2/min
70	Apply spray paint	sprayed area	in^2/min
160	Attach overhead equip.	part area	in^2/min
180	Clean part	interface area	in^2/min
185	Clean part liquid shim	interface area	in^2/min
190	Clean tool flexible caul	caul area	in^2/min
191	Clean tool flexible caul core	caul area	in^2/min
192	Clean tool flexible caul stringer	caul area	in^2/min
200	Clean tool form die core	tool area	in^2/min
230	Clean tool form die stringer	tool area	in^2/min
240	Clean tool layup cure core	tool area	in^2/min
241	Clean tool layup cure panel	tool area	in^2/min
250	Clean tool layup cure stringer	tool area	in^2/min

Table H-1. Cost methods grouped according to variable type (cont.)

ID #	Cost Method Description	Variable Desc.	Units
260	Clean tool mandrel braiding	tool area	in^2/min
270	Clean tool mandrel silicone	tool area	in^2/min
280	Clean tool prepreg storage	tool area	in^2/min
290	Clean tool RTM mold	tool area	in^2/min
242	Clean tool winding mandrel skin	tool area	in^2/min
460	Fabricate kapton shims	interface area	in^2/min
470	Fabricate liquid shims	interface area	in^2/min
480	Form machine core former	core area	in^2/min
580	Inspect automated ultrasonic panel	part area	in^2/min
620	Inspect manual visually cure liquid shim	interface area	in^2/min
670	Kit film adhesive	film adhesive area	in^2/min
690	Kit seperation film	film adhesive area	in^2/min
700	Layup automated ATP prepreg tow 0 degree	ply area 0	in^2/min
710	Layup automated ATP prepreg tow 15 degree	ply area 15	in^2/min
720	Layup automated ATP prepreg tow 30 degree	ply area 30	in^2/min
730	Layup automated ATP prepreg tow 45 degree	ply area 45	in^2/min
740	Layup automated ATP prepreg tow 60 degree	ply area 60	in^2/min
750	Layup automated ATP prepreg tow 75 degree	ply area 75	in^2/min
760	Layup automated ATP prepreg tow 90 degree	ply area 90	in^2/min
770	Layup automated CTLM 6" prepreg tape 0 degree	ply area 0	in^2/min
780	Layup automated CTLM 6" prepreg tape 15 degree	ply area 15	in^2/min
790	Layup automated CTLM 6" prepreg tape 30 degree	ply area 30	in^2/min
800	Layup automated CTLM 6" prepreg tape 45 degree	ply area 45	in^2/min
810	Layup automated CTLM 6" prepreg tape 60 degree	ply area 60	in^2/min
820	Layup automated CTLM 6" prepreg tape 75 degree	ply area 75	in^2/min
830	Layup automated CTLM 6" prepreg tape 90 degree	ply area 90	in^2/min
840	Layup manual film adhesive	film adhesive area	in^2/min
845	Layup manual film adhesive strips	film adhesive area	in^2/min
851	Layup manual peel ply sheets	peel ply area	in^2/min
850	Layup manual peel ply strips	peel ply area	in^2/min
860	Layup manual prepreg fabric IML	fabric area	in^2/min
861	Layup manual prepreg fabric OML	fabric area	in^2/min
870	Layup manual sacrificial shim material	sacrifical shim area	in^2/min
885	Layup manual seperation film	separation film area	in^2/min
880	Layup manual seperation film liquid shim	separation film area	in^2/min
970	Position hoist assisted core blanket	core blanket area	in^2/min
1050	Position manual assembly jig	tool area	in^2/min
1060	Position manual compaction bag	bag area	in^2/min
1070	Position manual core potting	potting area	in^2/min
1090	Position manual core slab on cure tool	core area	in^2/min
1100	Position manual cure bag	bag area	in^2/min
1120	Position manual flexible caul	caul area	in^2/min
1121	Position manual flexible caul core	caul area	in^2/min
1122	Position manual flexible caul stringer	caul area	in^2/min
1180	Position manual kapton shims	interface area	in^2/min
1190	Position manual mylar template	template area	in^2/min
1220	Position manual prepreg charge	charge area	in^2/min
1350	Position mechanical panel into assembly jig	part area	in^2/min

Table H-1. Cost methods grouped according to variable type (cont.)

ID #	Cost Method Description	Variable Desc.	Units
1380	Position mechanical panel into transport tool	part area	in^2/min
1370	Position mechanical panel NC trim equip.	part area	in^2/min
1390	Position mechanical panel onto ultrasonic equip.	part area	in^2/min
1360	Position mechanical panel with indexing holes	part area	in^2/min
1400	Protect core blanket	core blanket area	in^2/min
1410	Protect core slab	total core area	in^2/min
1420	Protect panel	part area	in^2/min
1430	Protect part	part area	in^2/min
1440	Protect prepreg charge	part area	in^2/min
1435	Protect skin	part area	in^2/min
1630	Remove manual cure bag	bag area	in^2/min
1581	Remove manual drill plate	tool area	in^2/min
1650	Remove manual flexible caul	caul area	in^2/min
1651	Remove manual flexible caul core	caul area	in^2/min
1652	Remove manual flexible caul stringer	caul area	in^2/min
1582	Remove manual floor assembly jig	tool area	in^2/min
1720	Remove manual mylar template	template area	in^2/min
1580	Remove manual panel bond assembly jig	tool area	in^2/min
1740	Remove manual peel ply	peel ply area	in^2/min
1760	Remove manual protection panel	protection film area	in^2/min
1750	Remove manual protection part	protection area	in^2/min
1800	Remove manual separation film	separation film area	in^2/min
1820	Remove manual tool attachments	part area	in^2/min
1900	Remove mechanical panel from assembly jig	part area	in^2/min
1920	Remove mechanical panel from transport tool	part area	in^2/min
2250	Trim automated surface core	core area	in^2/min
2251	Trim automated surface core blanket	core blanket area	in^2/min
2252	Trim automated surface core edge	core edge area	in^2/min
2260	Trim automated surface sacrificial material	interface area	in^2/min
400	Drill automated gr/ep holes c/t indexing holes	hole volume	in^3/min
410	Drill manual aluminum holes	hole volume	in^3/min
420	Drill manual gr/ep countersunk holes	hole volume	in^3/min
425	Drill manual gr/ep countersunk holes c/t clecos	hole volume	in^3/min
430	Drill manual gr/ep holes	hole volume	in^3/min
435	Drill manual gr/ep holes c/t clecos	hole volume	in^3/min
437	Drill manual gr/ep holes c/t indexing holes	hole volume	in^3/min
440	Drill manual gr/ep pilot holes	hole volume	in^3/min
450	Drill manual titanium full sized holes	hole volume	in^3/min
170	Braiding 2D triaxial inner section	fiber weight	lb/min
171	Braiding 2D triaxial outer section	fiber weight	lb/min
172	Braiding 2D triaxial overwrap section	fiber weight	lb/min
890	Load dry fiber spool braiding equip.	preform fiber weight	lb/min
910	Load prepreg tape rolls CTLM	prepreg weight	lb/min
920	Load prepreg tow spools ATP	prepreg weight	lb/min
930	Load two part resin injection equip.	resin weight	lb/min

Table H-1. Cost methods grouped according to variable type (cont.)

ID #	Cost Method Description	Variable Desc.	Units
80	Apply vacuum	constant	min
100	Attach lines resin injection pultrusion die	constant	min
120	Attach lines thermocouple pultrusion die	constant	min
220	Clean tool form die roller	constant	min
300	Close autoclave	constant	min
310	Close oven	constant	min
340	Compact vacuum prepreg charge silicone	constant	min
350	Cure autoclave	constant	min
360	Cure liquid shim	constant	min
370	Cure oven	constant	min
380	Cure RTM cure cycle shell 1895	constant	min
390	Cure RTM postcure	constant	min
490	Form machine prepreg charge hot drape	constant	min
510	Form machine prepreg charge stringer form die	constant	min
540	Identify part	constant	min
550	Identify required items	constant	min
600	Inspect manual visually fasteners	constant	min
610	Inspect manual visually holes	constant	min
615	Inspect manual visually holes c/t clecos	constant	min
617	Inspect manual visually holes c/t indexing holes	constant	min
630	Install fasteners clecos	constant	min
631	Install fasteners clecos holes c/t clecos	constant	min
632	Install fasteners clecos holes c/t indexing holes	constant	min
640	Install fasteners lockbolts	constant	min
645	Install fasteners lockbolts holes c/t clecos	constant	min
647	Install fasteners lockbolts holes c/t indexing holes	constant	min
650	Install fasteners torqued	constant	min
660	Kit core	constant	min
900	Load dry woven preform pultrusion equip.	constant	min
940	Open autoclave	constant	min
950	Open oven	constant	min
980	Position hoist assisted core block	constant	min
1030	Position hoist assisted winding tool	constant	min
1080	Position manual core slab into forming equip.	constant	min
1110	Position manual drill template	constant	min
1140	Position manual form die pultrusion	constant	min
1280	Position mechanical floor grid into assembly jig	constant	min
1290	Position mechanical floor grid NC trim equip.	constant	min
1300	Position mechanical full barrel into floor assy. jig	constant	min
1320	Position mechanical full barrel into transport tool	constant	min
1310	Position mechanical full barrel NC trim equip.	constant	min
1330	Position mechanical full barrel onto ultra-sonic equip.	constant	min
1340	Position mechanical layup cure tool	constant	min
1490	Remove hoist assisted winding tool	constant	min
1510	Remove lines resin injection pultrusion die	constant	min
1530	Remove lines thermocouple pultrusion die	constant	min
1600	Remove manual clecos	constant	min
1605	Remove manual clecos c/t indexing holes	constant	min

Table H-1: Cost methods grouped according to variable type (cont.)

ID #	Cost Method Description	Variable Desc.	Units
1620	Remove manual core	constant	min
1640	Remove manual drill template	constant	min
1660	Remove manual form die pultrusion	constant	min
1700	Remove manual IML core blanket tool	constant	min
1830	Remove mechanical floor grid from assembly jig	constant	min
1840	Remove mechanical floor grid from NC trim equip.	constant	min
1850	Remove mechanical full barrel from NC trim equip.	constant	min
1860	Remove mechanical full barrel from transport tool	constant	min
1870	Remove mechanical full barrel from ultrasonic equip.	constant	min
1880	Remove mechanical full barrel from winding tool	constant	min
1890	Remove mechanical layup cure tool	constant	min
1910	Remove mechanical panel from NC trim equip.	constant	min
1930	Remove mechanical panel from ultrasonic equip.	constant	min
1940	Setup machine advanced tow placement	constant	min
1950	Setup machine braiding	constant	min
1960	Setup machine core	constant	min
1970	Setup machine core surface machining	constant	min
1980	Setup machine core trim	constant	min
1990	Setup machine CTLM	constant	min
2000	Setup machine hot drape forming	constant	min
2010	Setup machine inline trim	constant	min
2020	Setup machine inspection inline ultrasonic	constant	min
2030	Setup machine inspection ultrasonic	constant	min
2040	Setup machine NC trim	constant	min
2050	Setup machine oven	constant	min
2060	Setup machine prepreg trim	constant	min
2070	Setup machine pultrusion	constant	min
2080	Setup machine resin injection	constant	min
2090	Setup machine roller forming	constant	min
2100	Setup tool assembly jig	constant	min
2110	Setup tool transport	constant	min
2120	Transport part floor grid	constant	min
2130	Transport part panel	constant	min
2140	Transport tool assembly jig	constant	min
2150	Transport tool core storage	constant	min
2160	Transport tool layup cure	constant	min
2170	Transport tool part storage	constant	min
2180	Transport tool prepreg storage	constant	min
2190	Transport tool transport	constant	min
2200	Transport tool winding	constant	min

Table H-1. Cost methods grouped according to variable type (cont.)

ID #	Cost Method Description	Variable Desc.	Units
10	Abrade part surface	interface area	in^2/min
15	Abrade part surface liquid shim	interface area	in^2/min
20	Apply clamping force clamps	interface length	in/min
30	Apply clamping force straps	interface length	in/min
40	Apply liquid shim	interface area	in^2/min
50	Apply parting agent core bonding assembly jig	tool area	in^2/min
51	Apply parting agent form die	tool area	in^2/min
53	Apply parting agent mandrel braiding	tool area	in^2/min
52	Apply parting agent OML cure tool	tool area	in^2/min
54	Apply parting agent resin transfer mold	tool area	in^2/min
60	Apply sealant	interface area	in^2/min
70	Apply spray paint	sprayed area	in^2/min
80	Apply vacuum	constant	min
100	Attach lines resin injection pultrusion die	constant	min
90	Attach lines resin injection RTM mold	injection mold length	in/min
130	Attach lines thermocouple cure	part perimeter	in/min
120	Attach lines thermocouple pultrusion die	constant	min
110	Attach lines thermocouple RTM mold	injection mold length	in/min
150	Attach lines vacuum cure	part perimeter	in/min
140	Attach lines vacuum RTM mold	injection mold length	in/min
160	Attach overhead equip.	part area	in^2/min
170	Braiding 2D triaxial inner section	fiber weight	lb/min
171	Braiding 2D triaxial outer section	fiber weight	lb/min
172	Braiding 2D triaxial overwrap section	fiber weight	lb/min
180	Clean part	interface area	in^2/min
185	Clean part liquid shim	interface area	in^2/min
190	Clean tool flexible caul	caul area	in^2/min
191	Clean tool flexible caul core	caul area	in^2/min
192	Clean tool flexible caul stringer	caul area	in^2/min
200	Clean tool form die core	tool area	in^2/min
210	Clean tool form die pultrusion	section trace	in/min
220	Clean tool form die roller	constant	min
230	Clean tool form die stringer	tool area	in^2/min
240	Clean tool layup cure core	tool area	in^2/min
241	Clean tool layup cure panel	tool area	in^2/min
250	Clean tool layup cure stringer	tool area	in^2/min
260	Clean tool mandrel braiding	tool area	in^2/min
270	Clean tool mandrel silicone	tool area	in^2/min
280	Clean tool prepreg storage	tool area	in^2/min
290	Clean tool RTM mold	tool area	in^2/min
242	Clean tool winding mandrel skin	tool area	in^2/min
300	Close autoclave	constant	min
310	Close oven	constant	min
320	Compact vacuum core	bag perimeter	in/min
330	Compact vacuum prepreg charge nylon	bag perimeter	in/min
340	Compact vacuum prepreg charge silicone	constant	min
350	Cure autoclave	constant	min
360	Cure liquid shim	constant	min

Table H-2. Cost methods listed alphabetically.

ID #	Cost Method Description	Variable Desc.	Units
370	Cure oven	constant	min
380	Cure RTM cure cycle shell 1895	constant	min
390	Cure RTM postcure	constant	min
400	Drill automated gr/ep holes c/t indexing holes	hole volume	in^3/min
410	Drill manual aluminum holes	hole volume	in^3/min
420	Drill manual gr/ep countersunk holes	hole volume	in^3/min
425	Drill manual gr/ep countersunk holes c/t clecos	hole volume	in^3/min
430	Drill manual gr/ep holes	hole volume	in^3/min
435	Drill manual gr/ep holes c/t clecos	hole volume	in^3/min
437	Drill manual gr/ep holes c/t indexing holes	hole volume	in^3/min
440	Drill manual gr/ep pilot holes	hole volume	in^3/min
450	Drill manual titanium full sized holes	hole volume	in^3/min
460	Fabricate kapton shims	interface area	in^2/min
470	Fabricate liquid shims	interface area	in^2/min
480	Form machine core former	core area	in^2/min
490	Form machine prepreg charge hot drape	constant	min
500	Form machine prepreg charge roller form	charge length	in/min
510	Form machine prepreg charge stringer form die	constant	min
520	Form manual dry preform	preform length	in/min
530	Identify interface area	interface perimeter	in/min
540	Identify part	constant	min
550	Identify required items	constant	min
560	Inspect automated dimensionally	interface perimeter	in/min
571	Inspect automated ultrasonic frames	part length	in/min
570	Inspect automated ultrasonic inline	part length	in/min
580	Inspect automated ultrasonic panel	part area	in^2/min
590	Inspect manual feeler gage interface gaps	interface perimeter	in/min
620	Inspect manual visually cure liquid shim	interface area	in^2/min
600	Inspect manual visually fasteners	constant	min
610	Inspect manual visually holes	constant	min
615	Inspect manual visually holes c/t clecos	constant	min
617	Inspect manual visually holes c/t indexing holes	constant	min
630	Install fasteners clecos	constant	min
631	Install fasteners clecos holes c/t clecos	constant	min
632	Install fasteners clecos holes c/t indexing holes	constant	min
640	Install fasteners lockbolts	constant	min
645	Install fasteners lockbolts holes c/t clecos	constant	min
647	Install fasteners lockbolts holes c/t indexing holes	constant	min
650	Install fasteners torqued	constant	min
660	Kit core	constant	min
670	Kit film adhesive	film adhesive area	in^2/min
680	Kit parts	part length	in/min
681	Kit parts frames	part length	in/min
690	Kit seperation film	film adhesive area	in^2/min
700	Layup automated ATP prepreg tow 0 degree	ply area 0	in^2/min
710	Layup automated ATP prepreg tow 15 degree	ply area 15	in^2/min
720	Layup automated ATP prepreg tow 30 degree	ply area 30	in^2/min
730	Layup automated ATP prepreg tow 45 degree	ply area 45	in^2/min

Table H-2. Cost methods listed alphabetically (cont.).

ID #	Cost Method Description	Variable Desc.	Units
740	Layup automated ATP prepreg tow 60 degree	ply area 60	in^2/min
750	Layup automated ATP prepreg tow 75 degree	ply area 75	in^2/min
760	Layup automated ATP prepreg tow 90 degree	ply area 90	in^2/min
770	Layup automated CTLM 6" prepreg tape 0 degree	ply area 0	in^2/min
780	Layup automated CTLM 6" prepreg tape 15 degree	ply area 15	in^2/min
790	Layup automated CTLM 6" prepreg tape 30 degree	ply area 30	in^2/min
800	Layup automated CTLM 6" prepreg tape 45 degree	ply area 45	in^2/min
810	Layup automated CTLM 6" prepreg tape 60 degree	ply area 60	in^2/min
820	Layup automated CTLM 6" prepreg tape 75 degree	ply area 75	in^2/min
830	Layup automated CTLM 6" prepreg tape 90 degree	ply area 90	in^2/min
840	Layup manual film adhesive	film adhesive area	in^2/min
845	Layup manual film adhesive strips	film adhesive area	in^2/min
851	Layup manual peel ply sheets	peel ply area	in^2/min
850	Layup manual peel ply strips	peel ply area	in^2/min
860	Layup manual prepreg fabric IML	fabric area	in^2/min
861	Layup manual prepreg fabric OML	fabric area	in^2/min
870	Layup manual sacrificial shim material	sacrifical shim area	in^2/min
885	Layup manual seperation film	separation film area	in^2/min
880	Layup manual seperation film liquid shim	separation film area	in^2/min
890	Load dry fiber spool braiding equip.	preform fiber weight	lb/min
900	Load dry woven preform pultrusion equip.	constant	min
910	Load prepreg tape rolls CTLM	prepreg weight	lb/min
920	Load prepreg tow spools ATP	prepreg weight	lb/min
930	Load two part resin injection equip.	resin weight	lb/min
940	Open autoclave	constant	min
950	Open oven	constant	min
970	Position hoist assisted core blanket	core blanket area	in^2/min
980	Position hoist assisted core block	constant	min
960	Position hoist assisted mandrel braiding	tool length	in/min
1010	Position hoist assisted part into transport tool	part length	in/min
1000	Position hoist assisted part NC trim equip.	part length	in/min
1020	Position hoist assisted part onto ultrsonic equip.	part length	in/min
990	Position hoist assisted part with indexing holes	part length	in/min
1030	Position hoist assisted winding tool	constant	min
1040	Position manual airweave	part perimeter	in/min
1050	Position manual assembly jig	tool area	in^2/min
1060	Position manual compaction bag	bag area	in^2/min
1070	Position manual core potting	potting area	in^2/min
1080	Position manual core slab into forming equip.	constant	min
1090	Position manual core slab on cure tool	core area	in^2/min
1100	Position manual cure bag	bag area	in^2/min
1110	Position manual drill template	constant	min
1120	Position manual flexible caul	caul area	in^2/min
1121	Position manual flexible caul core	caul area	in^2/min
1122	Position manual flexible caul stringer	caul area	in^2/min
1130	Position manual foaming adhesive	part perimeter	in/min
1155	Position manual form die core	tool length	in/min
1161	Position manual form die female stringer	tool length	in/min

Table H-2. Cost methods listed alphabetically (cont.).

ID #	Cost Method Description	Variable Desc.	Units
1140	Position manual form die pultrusion	constant	min
1150	Position manual form die skin	tool length	in/min
1160	Position manual form die stringer	tool length	in/min
1170	Position manual heat lamps	interface length	in/min
1180	Position manual kapton shims	interface area	in^2/min
1190	Position manual mylar template	template area	in^2/min
1210	Position manual part	part length	in/min
1200	Position manual part into assembly jig	part length	in/min
1220	Position manual prepreg charge	charge area	in^2/min
1230	Position manual prepreg charge roller transfer	charge length	in/min
1240	Position manual radius filler	filler length	in/min
1250	Position manual RTM mold lid	tool lid perimeter	in/min
1260	Position manual RTM mold seal	seal length	in/min
1270	Position manual thermocouples	part perimeter	in/min
1280	Position mechanical floor grid into assembly jig	constant	min
1290	Position mechanical floor grid NC trim equip.	constant	min
1300	Position mechanical full barrel into floor assembly jig	constant	min
1320	Position mechanical full barrel into transport tool	constant	min
1310	Position mechanical full barrel NC trim equip.	constant	min
1330	Position mechanical full barrel onto ultra-sonic equip.	constant	min
1340	Position mechanical layup cure tool	constant	min
1350	Position mechanical panel into assembly jig	part area	in^2/min
1380	Position mechanical panel into transport tool	part area	in^2/min
1370	Position mechanical panel NC trim equip.	part area	in^2/min
1390	Position mechanical panel onto ultrasonic equip.	part area	in^2/min
1360	Position mechanical panel with indexing holes	part area	in^2/min
1400	Protect core blanket	core blanket area	in^2/min
1410	Protect core slab	total core area	in^2/min
1420	Protect panel	part area	in^2/min
1430	Protect part	part area	in^2/min
1440	Protect prepreg charge	part area	in^2/min
1435	Protect skin	part area	in^2/min
1450	Pultrude resin shell 1895	pultrusion length	in/min
1460	Remove hoist assisted mandrel braiding	tool length	in/min
1470	Remove hoist assisted part from NC trim equip.	part length	in/min
1480	Remove hoist assisted part from ultrasonic equip.	part length	in/min
1490	Remove hoist assisted winding tool	constant	min
1510	Remove lines resin injection pultrusion die	constant	min
1500	Remove lines resin injection RTM mold	injection mold length	in/min
1540	Remove lines thermocouple cure	part perimeter	in/min
1530	Remove lines thermocouple pultrusion die	constant	min
1520	Remove lines thermocouple RTM mold	injection mold length	in/min
1560	Remove lines vacuum cure	bag perimeter	in/min
1550	Remove lines vacuum RTM mold	injection mold length	in/min
1570	Remove manual airweave airweave	part perimeter	in/min
1590	Remove manual clamp	interface length	in/min
1600	Remove manual clecos	constant	min
1605	Remove manual clecos c/t indexing holes	constant	min

Table H-2. Cost methods listed alphabetically (cont.).

ID #	Cost Method Description	Variable Desc.	Units
1610	Remove manual compaction bag	bag perimeter	in/min
1620	Remove manual core	constant	min
1630	Remove manual cure bag	bag area	in^2/min
1581	Remove manual drill plate	tool area	in^2/min
1640	Remove manual drill template	constant	min
1650	Remove manual flexible caul	caul area	in^2/min
1651	Remove manual flexible caul core	caul area	in^2/min
1652	Remove manual flexible caul stringer	caul area	in^2/min
1582	Remove manual floor assembly jig	tool area	in^2/min
1675	Remove manual form die	tool length	in/min
1685	Remove manual form die female stringer	tool length	in/min
1660	Remove manual form die pultrusion	constant	min
1670	Remove manual form die skin	tool length	in/min
1680	Remove manual form die stringer	tool length	in/min
1690	Remove manual heat lamps	interface length	in/min
1700	Remove manual IML core blanket tool	constant	min
1710	Remove manual liquid shim squeezeout	interface perimeter	in/min
1720	Remove manual mylar template	template area	in^2/min
1580	Remove manual panel bond assembly jig	tool area	in^2/min
1730	Remove manual part from assembly jig	part length	in/min
1740	Remove manual peel ply	peel ply area	in^2/min
1760	Remove manual protection panel	protection film area	in^2/min
1750	Remove manual protection part	protection area	in^2/min
1770	Remove manual RTM mold lid	tool lid perimeter	in/min
1780	Remove manual RTM mold seal	seal length	in/min
1790	Remove manual sealant squeezeout	interface perimeter	in/min
1800	Remove manual separation film	separation film area	in^2/min
1810	Remove manual strap	interface length	in/min
1820	Remove manual tool attachments	part area	in^2/min
1830	Remove mechanical floor grid from assembly jig	constant	min
1840	Remove mechanical floor grid from NC trim equip.	constant	min
1850	Remove mechanical full barrel from NC trim equip.	constant	min
1860	Remove mechanical full barrel from transport tool	constant	min
1870	Remove mechanical full barrel from ultrasonic equip.	constant	min
1880	Remove mechanical full barrel from winding tool	constant	min
1890	Remove mechanical layup cure tool	constant	min
1900	Remove mechanical panel from assembly jig	part area	in^2/min
1910	Remove mechanical panel from NC trim equip.	constant	min
1920	Remove mechanical panel from transport tool	part area	in^2/min
1930	Remove mechanical panel from ultrasonic equip.	constant	min
1940	Setup machine advanced tow placement	constant	min
1950	Setup machine braiding	constant	min
1960	Setup machine core	constant	min
1970	Setup machine core surface machining	constant	min
1980	Setup machine core trim	constant	min
1990	Setup machine CTLM	constant	min
2000	Setup machine hot drape forming	constant	min
2010	Setup machine inline trim	constant	min

Table H-2. Cost methods listed alphabetically (cont.).

ID #	Cost Method Description	Variable Desc.	Units
2020	Setup machine inspection inline ultrasonic	constant	min
2030	Setup machine inspection ultrasonic	constant	min
2040	Setup machine NC trim	constant	min
2050	Setup machine oven	constant	min
2060	Setup machine prepreg trim	constant	min
2070	Setup machine pultrusion	constant	min
2080	Setup machine resin injection	constant	min
2090	Setup machine roller forming	constant	min
2100	Setup tool assembly jig	constant	min
2110	Setup tool transport	constant	min
2120	Transport part floor grid	constant	min
2130	Transport part panel	constant	min
2140	Transport tool assembly jig	constant	min
2150	Transport tool core storage	constant	min
2160	Transport tool layup cure	constant	min
2170	Transport tool part storage	constant	min
2180	Transport tool prepreg storage	constant	min
2190	Transport tool transport	constant	min
2200	Transport tool winding	constant	min
2210	Trim automated edge core slab	core length	in/min
2220	Trim automated edge gr/ep	trim length	in/min
2230	Trim automated edge laminate/charge	trim length	in/min
2240	Trim automated edge single ply	trim length	in/min
2250	Trim automated surface core	core area	in^2/min
2251	Trim automated surface core blanket	core blanket area	in^2/min
2252	Trim automated surface core edge	core edge area	in^2/min
2260	Trim automated surface sacrificial material	interface area	in^2/min
2300	Trim manual edge adhesive strips	strip length	in/min
2270	Trim manual edge dry preform	trim length	in/min
2280	Trim manual edge gr/ep	trim length	in/min
2290	Trim manual edge prepreg charge	trim length	in/min
2330	Trim manual edge sacrificial shim strips	strip length	in/min
2310	Trim manual edge separation film sheets	separation film per.	in/min
2320	Trim manual edge separation film strips	strip length	in/min
2340	Trim manual gr/ep deburr	trim length	in/min
2350	Trim manual gr/ep deflash	trim length	in/min

Table H-2. Cost methods listed alphabetically (cont.).

REPORT DOCUMENTATION PAGE

Form Approved
OMB No. 0704-0188

1. AGENCY USE ONLY *(Leave Blank)*	2. REPORT DATE	3. REPORT TYPE AND DATES COVERED
	August 1996	Contractor Report

4. TITLE AND SUBTITLE
Cost Optimization Software for Transport Aircraft Design Evaluation (COSTADE) - Design Cost Methods

5. FUNDING NUMBERS
C NAS1-18889
C NAS1-20013 (Task 2)
WU 510-02-13-01

6. AUTHOR(S)
L.B. Ilcewicz, G.E. Mabson, S.L. Metschan, G.D. Swanson, M.R. Proctor, D.K. Tervo, H.G. Fredrikson, T.G. Gutowski, E.T. Neoh, and K.C. Polgar

7. PERFORMING ORGANIZATION NAME(S) AND ADDRESS(ES)
The Boeing Company
P.O. Box 3707
Seattle, WA 98124-2207

8. PERFORMING ORGANIZATION REPORT NUMBER

9. SPONSORING / MONITORING AGENCY NAME(S) AND ADDRESS(ES)
National Aeronautics and Space Administration
Langley Research Center
Hampton, VA 23681-0001

10. SPONSORING / MONITORING AGENCY REPORT NUMBER
NASA CR-4737

11. SUPPLEMENTARY NOTES
Langley Technical Monitor: W.T. Freeman, Jr.

12a. DISTRIBUTION / AVAILABILITY STATEMENT
[redacted] Unclassified - Unlimited
Subject Category 24

12b. DISTRIBUTION CODE

13. ABSTRACT *(Maximum 200 words)*

Cost Optimization Software for Transport Aircraft Design Evaluation (COSTADE) is being developed as a tool to support design build teams in their efforts to achieve cost effective and feasible commercial aircraft composite fuselage structure. COSTADE is a multi-disciplinary evaluation and optimization tool that includes cost, weight, design, stress, and manufacturing modules. Fabrication costs are included early in the structural development process allowing the identification of cost-weight sensitivities. The use of this tool also reduces engineering development costs by shortening design cycle times and by providing improved starting points for more detailed evaluations.

This report documents a theoretical framework for design cost analyses and guidelines to support such team efforts have been developed in the Advanced Technology Composite Aircraft Structures (ATCAS) program.

14. SUBJECT TERMS	15. NUMBER OF PAGES
Advanced Composite Technology Program; Cost Model; Cost Prediction	244
	16. PRICE CODE

17. SECURITY CLASSIFICATION OF REPORT	18. SECURITY CLASSIFICATION OF THIS PAGE	19. SECURITY CLASSIFICATION OF ABSTRACT	20. LIMITATION OF ABSTRACT
Unclassified	Unclassified	Unclassified	